SC

# TRIPLET DERIVED RADICAL PAIRS IN MICELLES: DECAY KINETICS AND MAGNETIC FIELD EFFECTS.

by

Christopher Evans

A thesis

presented to the University of Ottawa

in partial fulfillment of the degree of

Ph.D.

in

Chemistry

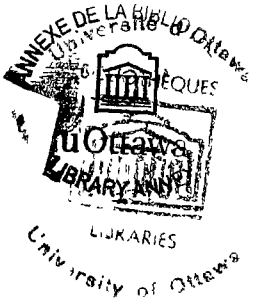

ACKNOWLEDGEMENTS

I would like to express my sincere appreciation to my thesis advisor, Dr. J.C. (Tito) Scaiano, for his seemingly inexhaustible reserves of enthusiasm, patience, encouragement and insight as well as for on going financial support. I would also like to thank the past and present members of Tito's group who have without fail been men and women of good humour. In particular I would like to thank Drs. D. Weir, W.G. McGimpsey, L.J. Johnston, and R.W. Redmond as well as Mr. S.E. Sugamori. Thanks also to Dr. K.U. Ingold for helpful discussions as well for support in other areas. Dr. H Casal should also be recognized for making the FTIR measurements and for useful discussions relating to the nature of micelles.

I would also like to express my gratitude to the members of my family on both sides of the Atlantic for the ongoing care and warmth which they have offered over the years. Finally, this thesis would not have reached an end if I had not had the good fortune to be married to Halla and to be the father of Fjóla.

TABLE OF CONTENTS

LIST OF TABLES

LIST OF FIGURES

## CHARTS AND SCHEMES

## ABSTRACT

This thesis presents a detailed laser flash photolysis study of the kinetic behaviour of two triplet–derived radical pairs in homogeneous solution and in micellar media. The systems chosen for examination were ketyl–aryloxyl radical pairs formed via hydrogen abstraction from Vitamin E (EOH) and related phenols by the $n\pi^*$ triplet of butyrophenone (BUP), and thiophene–methyl viologen (MV) radical cation pairs formed upon electron transfer from triplet terthienyls to the MV ground state.

As a preliminary study the reactivity of EOH towards various ketone triplets and free radicals in organic solvents was measured. It was found that ketone triplets abstract hydrogen from EOH with rate constants approaching the diffusion controlled limit and that this reaction generates radicals with quantum yields approaching 1.0. It was concluded that the most suitable ketone triplet for use in the micellar systems was that of BUP. This was largely due to the fact that the lifetime of triplet BUP is limited to ≤ 100ns by intramolecular reaction. The latter reaction thus becomes a "clock" for the hydrogen abstraction reaction. The use of such a "clock" technique for the generation of radical pairs in micelles is a unique and very efficient way of obtaining the radical pairs of interest.

Photolysis of phenols plus BUP in micelles leads to radical pairs the decay kinetics of which can be readily observed at the $\lambda_{max}$ of the phenoxyl radical. The phenoxyl decay is due to two competing processes; exit of radicals form the micelle and geminate reaction. Independent values of the rate constants for both processes were obtained as were values of the fraction of radical pairs which underwent exit. Large magnetic field effects on kgem and on the escape fraction were observed and could be attributed to inhibition of hyperfine coupling at low fields and of spin relaxation at higher fields. For the EOH/BUP system in SDS the geminate rate constant ($k_{gem}$) was $2.0 \times 10^6 s^{-1}$ while the exit rate constant (k–) was $0.77 \times 10^6 s^{-1}$, both at zero magnetic field. These rate constants were found to be inversely related to

micellar size. Arrhenius data indicates that k– reflects the kinetics of the exit of the ketyl radical from the micelle into the bulk water phase.

The Arrhenius data relating to $k_{gem}$ indicates that practically all the variation of this rate constant with temperature is due to changes in micellar volume with temperature. The value of Ea for the EOH/BUP pair based on $k_{gem}$ in the absence of added electrolytes is only about 1kcal/mol which is comparable with activation energies obtained for triplet biradicals, the lifetimes of which are controlled by intersystem crossing. On the other hand the observed variation of $k_{gem}$ with micellar volume combined with the observed magnetic field effect cannot be explained either in terms of any of the conventional intersystem crossing mechanisms or in terms of a solely diffusion controlled process. We have offered an alternative explanation in which the triplet–derived radical pair undergoes hyperfine coupling induced spin state mixing so that one must view a "triplet" radical pair as being predominantly triplet but with a degree of singlet character. Thus the value of $k_{gem}$ should be related to the product of the frequency of intramicellar radical reencounter with the degree of singlet character.

The radical cation pairs studied can be generated in homogeneous solution by diffusion controlled electron transfer from thiophene triplets to acceptors such as tetracyanoethylene and MV. The thiophene radical cations absorb in the 540 to 550nm region with large extinction coefficients (~ $10^4$ $M^{-1}cm^{-1}$). Direct electron transfer to oxygen is very inefficient. The radical cation pairs can be generated in micelles by electron transfer from the triplet thiophenes to MV. For these systems $k_{gem}$ ~$4x10^6s^{-1}$ and k– ~$0.2x10^6s^{-1}$ at zero field in SDS. $k_{gem}$ and escape fraction are subject to large magnetic field effects. $k_{gem}$ and k– are inversely related to micellar size. We therefore view the the radical pairs as being of mixed spin state rather than being pure triplet. Finally, substitution of the thiophene with Br increases the zero field value of $k_{gem}$ and also suppressed the magnetic field effect on the exit fraction.

## COPYRIGHT INFORMATION

The following figures in this thesis have been reproduced from earlier publications:

| | |
|---|---|
| Figure 1.1 | Copyright, 1985, Academic Press. |
| Figure 1.2 | Copyright, 1981, Elsevier Science Publishers B.V. |
| Figure 1.3 | Copyright, 1984, Academic Press. |
| Figure 1.4 | Copyright, 1984, Academic Press. |
| Figure 1.5 | Copyright, 1982, American Chemical Society. |

The author wishes to express his appreciation to the copyright holders for permission to make use of the figures noted.

## LIST OF ABBREVIATIONS

| | |
|---|---|
| a | electronic–nuclear hyperfine coupling constant. |
| αB | α–bithienyl. |
| AOT | Aerosol OT [sodium bis(2–ethylhexyl)sulfosuccinate]. |
| ArOH | a phenol. |
| αT | α–terthienyl. |
| BHT | 2,6–di–t–butyl–4–methylphenol. |
| BOOB | di–t–butylperoxide. |
| BrαT | monobromo–α–terthienyl. |
| BTK | butyrophenone ketyl radical. |
| BUP | n–butyrophenone. |
| CDBA | cetyldimethylbenzylammonium chloride. |
| CHD | 1,4–cyclohexadiene or 1,4–cyclohexadienyl. |
| cmc | critical micelle concentration. |
| cmt | critical micelle temperature. |
| CNαT | cyano–α–terthienyl. |
| CRM | 6–hydroxy–2,2,5,7,8–pentamethylchroman. |
| CT | charge transfer. |
| CTAB | cetyltrimethylammonium bromide. |
| CTAC | cetyltrimethylammonium chloride. |
| 35D | 3,5–dimethylphenol. |
| DBK | dibenzylketone. |
| DPE | diphenylethylene. |
| DTAB | dodecyltrimethylammonium bromide. |
| Ea | activation energy. |
| EO• | vitamin E phenoxyl radical. |
| EOH | vitamin E. |
| ESR | electron spin resonance. |
| $f_S$ | fraction of singlet character. |

| | |
|---|---|
| $f_T$ | fraction of triplet character. |
| FTIR | Fourier transform infrared spectroscopy. |
| FUR | 2,3–dihydro–5–hydroxy–2,2,4,6,7–pentamethylbenzofuran. |
| g | electronic g–factor. |
| G | Gauss. |
| $\Delta G^{\neq}$ | free energy of activation. |
| H | Hamiltonian or magnetic field strength. |
| $H_0$, $H_Z$ | magnetic field strength. |
| Hd | field at which T_/S become degenerate. |
| $H_{1/2}$ | half–field value. |
| $\Delta H^{\neq}$ | enthalpy of activation. |
| hfc | hyperfine coupling. |
| I | nuclear spin angular momentum vector. |
| $I_0$ | incident intensity of monitoring beam or unquenched fluorescence intensity. |
| $I_Q$ | fluorescence intensity in the presence of a quencher. |
| J | electronic exchange integral. |
| K | equilibrium constant for association of a quencher with the micellar pseudo–phase. |
| k+ | entrance rate constant. |
| k– | exit rate constant. |
| $k_{AHF}$ | anisotropic hyperfine coupling rate constant. |
| $k_{diff}$ | intramicellar diffusion controlled rate constant. |
| $k_e$ | intramicellar frequency of radical encounter. |
| $k_{gem}$ | geminate decay rate constant. |
| $k_{obs}$ | observed rate constant. |
| $k_R$, $k_{R'}$, $k_{rel}$ | spin relaxation rate constants. |
| $k_{SO}$ | g–tensor anisotropy rate constant. |
| $k_{SR}$ | spin–rotation rate constant. |
| LFP | laser flash photolysis. |

| | |
|---|---|
| MCA | multichannel analyzer. |
| MV | methyl viologen. |
| N | mean micellar aggregation number. |
| $n_Q$ | mean occupation number. |
| NRCC | National Research Council, Canada. |
| $\Delta$O.D. | change in optical density. |
| OMA | optical multichannel analyzer. |
| PMAP | p–methoxyacetophenone. |
| PMT | photomultiplier tube. |
| r | mean hydrodynamic radius of a micelle or radius of the water pool in a reversed micelle. |
| S | singlet spin state of a radical pair. |
| $\Delta S^{\neq}$ | entropy of activation. |
| SDS | sodium dodecyl sulfate. |
| SDecS | sodium decyl sulfate. |
| SOC | spin–orbit coupling. |
| SOMO | singly occupied molecular orbital. |
| SOS | sodium octyl sulfate. |
| T | a terthienyl or the absolute temperature. |
| $T_{\pm}$, $T_0$ | triplet spin states of a radical pair. |
| $\tau_C$ | rotational correlation time. |
| TAC | time-to-amplitude converter. |
| t–BuO$^{\bullet}$ | tert–butoxyl radical. |
| TCNE | tetracyanoethylene. |
| top OD | maximum observed optical density change. |
| Trolox | 6–hydroxy–2,5,7,8–tetramethylchroman–2–carboxylic acid. |
| XH | xanthene. |
| XO | xanthone. |

# CHAPTER 1. INTRODUCTION.

## 1.1 Preliminaries.

Chemists are most familiar with reactions which take place in homogeneous environments. In nature such reactions are less common than in the laboratory, with many processes occurring at surfaces [1] or in the presence of binding substrates as in the case of natural waters [2]. Perhaps the most distinctive feature of the chemistry of living systems is that much of it occurs within a constrained, or organized, environment. For example, in photosynthetic plants solar photons are captured by an array of chlorophyll molecules which are embedded in protein. The efficiency of energy transfer from these light-harvesting molecules to those special chlorophyll molecules which are involved in the chemical act of photosynthesis is extremely high–on the order of 95% [3]. This great efficiency arises mainly from the fact that the antenna chlorophylls are "organized" by the protein molecules to be at the optimum separation and orientation relative to each other to facilitate energy transfer at the expense of other deactivation pathways.

Generally, the outcome of a chemical reaction carried out in an organized system can be quite different from the outcome of the same reaction carried out in a homogeneous organic solvent [4]. Of particular interest in this respect is the effect of solubilization of organic reagents in micelles on the reactivity of these reagents. Micellar environments can influence reactivity through enhanced cage effects, high microviscosity of the micellar pseudo–phase, localization of reagents and so–called pre–orientational effects [5]. The control over chemical reactivity provided by micellar solutions has found application in micellar catalysis [6], emulsion polymerization [7] and in attempts to improve the efficiency of photoredox conversion of solar energy [4]. Micelles have also been of interest because they are among the simpler self–aggregating micro assemblies which include vesicles and biological membranes [8].

For these reasons micelles and their properties have been the subject of intense study for a number of decades.

One subfield of research into the influence of micelles on chemical behaviour has been the study of magnetic field effects on the kinetics and product ratios of micellized triplet radical pairs. One of the better known examples of this phenomenon cn be found in the work by Turro's group [9] on unsymmetrically substituted dibenzylketones (DBK). Photolysis of these substrates in micellar solution leads mainly to three different diphenylethanes. Of these, some fraction are formed via intramicellar recombination of the triplet radical pairs generated upon cleavage of the $n\pi^*$ DBK triplet state. For the DBK parent compound about 33% of the products are due to intramicellar reaction in the Earth's magnetic field while at 13kG applied field this fraction is reduced to only 16%! As we shall see, this remarkable result can be explained in terms of a competition between two processes leading to the decay of the intermediate triplet radical pair. These processes are geminate reaction of the pair (which requires access to the singlet surface) and diffusional separation of the radical partners. Furthermore this competition arises directly from the details of micellar structure.

Descriptions of and attempts to understand magnetic field effects on the chemistry of radical pairs have lead to a substantial body of literature on the subject. This has been augmented by several attempts at developing technological applications of magnetic field effects. In particular patents have been filed for an enhanced isotope enrichment process as well as an improved emulsion polymerization technique [10]. Although this body of work has lead to a fairly detailed understanding of magnetic field effects there are some areas which have been explored less fully. For example, very few reports on systems involving radicals centered on atoms other than carbon or involving radical ions have been published. It is the investigation of these and other issues via a study of the behaviour of two triplet

radical pair systems in the absence and presence of applied magnetic fields which is the main topic of this thesis. The radical pairs examined in this study are the phenoxyl–ketyl pair formed upon hydrogen abstraction from phenols by an $n\pi^*$ ketone triplet state and the radical cation pair formed upon electron transfer from the triplet state of a thiophene trimer, α–terthienyl, to a suitable electron acceptor. Neither of these systems have been studied before.

## 1.2 The Nature and Properties of Micelles.

Perhaps the most distinctive property of micelles is their ability to solubilize organic reagents which would otherwise not be soluble in an aqueous medium. To understand how this happens one must have a suitable picture of micellar structure. There is a vast literature on this subject and only a brief overview will be presented here.

Micelles are microscopic assemblies of amphiphillic molecules known as surfactants. They may be classified, along with bilayers, vesicles and biological membranes, as association colloids [11]. That is to say that micelles form spontaneously in an aqueous environment due to self association of the surfactant molecules. There is a large body of data indicating that surfactants self associate, most of it dealing with the concept of the critical micelle concentration (cmc).

Below a certain narrow concentration range, called the cmc, surfactant molecules behave as simple electrolytes [12]. At the cmc there is an abrupt change in solution behaviour. This change is reflected in a wide variety of solution properties including viscosity, solubilization of reagents, osmotic pressure, conductivity, surface tension, magnetic resonance and fluorescent probe behaviour [13]. Above the cmc these properties change in such a way as to indicate that there is extensive association of the surfactant molecules into larger assemblies. At still higher overall

concentration, the free surfactant concentration remains more–or–less constant at the cmc while the number of micelles increases [14].

There are several different categories of micelles according to the nature of the surfactant molecules from which they are constructed [6]. Surfactant molecules consist of a hydrocarbon chain and a polar or ionic head group. Surfactants are classified as anionic, cationic, zwitterionic or non–ionic depending on the type of head group they carry. Much of the literature dealing with micelle structure [13] and with the influence of micelles on chemical reactivity [4, 6] has been concerned with ionic micelles.

At low micelle concentration, at room temperature and in the absence of additives ionic micelles are essentially spherical [13, 14]. Under these conditions the hydrodynamic radius of sodium dodecylsulfate (SDS) micelles has been estimated to be on the order of 20 to 25Å [15, 16] by quasielastic light scattering. The mean aggregation number (N), that is the average number of surfactant molecules per micelle, of SDS under these conditions is close to 60 [4, 6]. It is micelles of this type that the two most widely recognized models of micellar structure seek to describe.

The Hartley model [17] and the Dill–Flory model [18] of micelle structure share a number of common features. Both describe an anionic micelle as a region of hydrocarbon material surrounded by a spherical electrical double layer consisting of the hydrated anionic head groups and their counterions in the aqueous phase (Figure 1.1). In addition, both models recognize that the hydrocarbon interior is disordered, i.e. it is liquid like. The main difference between the two descriptions is that the Hartley model views the hydrocarbon tails as sticks (all trans conformation) while the Dill–Flory model suggests that neighboring segments in a chain may have a local gauche conformation with respect to one another (i.e. the tail is kinked). The latter formulation is believed to reflect more realistically the packing of hydrocarbon chains at the center of the micelle [14, 19] and is also consistent with the observation that there is some contact of the upper portions (i.e. near the head group) of the

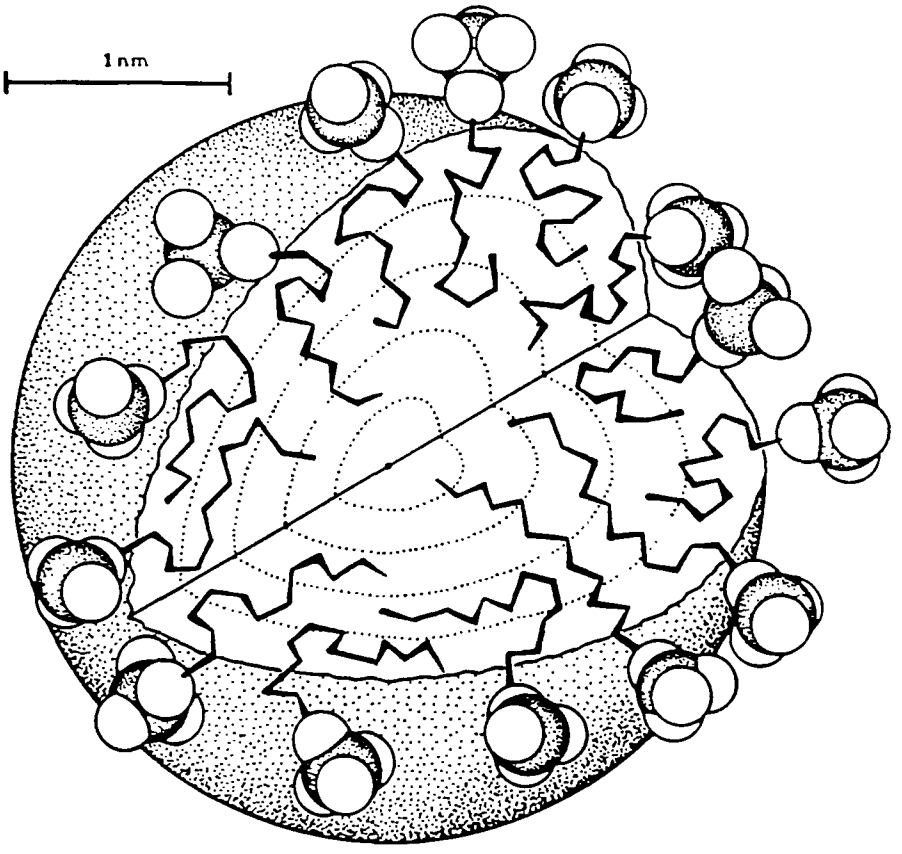


Figure 1.1. A sodium dodecylsulfate micelle drawn to scale. From reference [11].

hydrocarbon chains with the aqueous phase [5]. The question then arises as to how oil–like the interior actually is. Some authors suggest that there is substantial water penetration of the hydrocarbon core [19, 20] but it seems that the most widely held view is that the interior is essentially a liquid hydrocarbon [4, 8, 13, 21]. Recent calculations by Klein indicate that while the inner core of sodium octanoate micelles are devoid of water, there is considerable water penetration of the outer region of the core [22]. Recent FTIR measurements of ketones in sodium octanoate provide experimental evidence for this view [23]. On the other hand, vibronic band intensity ratios in pyrene fluorescence suggesting that SDS polarity is comparable to that of ethanol [24, 25] may reflect in part solubilization of the probe at sites near the micellar surface [4]. So at present the solvent characteristics of the micellar core are not firmly established. Leaving the issue of water penetration aside, it is this fact of micelle structure, that there is an inside (hydrocarbon) and an outside (water phase), that permits solubilization of hydrophobic reagents. In this sense the micelle can be thought of as a microreactor. This simple picture will permit us to understand many of the effects which micellization has on chemical reactivity.

The conditions under which surfactant monomers will aggregate to form micelles and the forces that favour the aggregation process are now well recognized. Before closing this section we will consider these issues. The discussion will follow that presented by Tanford [8] and Israelachvili [11].

The activity of an aggregate of aggregation number N in an ideal surfactant solution at equilibrium is given by

$$X_N = N\left\{ X_1 \exp\left[ \frac{\left(\mu_1^0 - \mu_N^0\right)}{kT} \right] \right\}^N \qquad (1.1)$$

where $X_1$ is the activity of isolated monomer, $\mu^0_1$ is the standard free energy of interaction of an isolated monomer with its environment and $\mu^0_N$ is the standard free energy of interaction of a monomer in an aggregate consisting of N monomers. This simply tells us that the concentration of an aggregate of aggregation number N is exponentially related to the difference in free energy of a monomer free in the aqueous environment and that of the same monomer in the aggregate. It is also clear that $X_N$ achieves a significant value only when $\mu^0_N < \mu^0_1$ for some value or values of N. This is the thermodynamic condition for self association and it is achieved when $\mu^0_N$ decreases progressively as N increases or when $\mu^0_N$ has a minimum value at some finite N. In the former case aggregation continues until the monomers have formed an assembly with $N \rightarrow \infty$ (this corresponds to a true phase separation) while in the latter case structures of finite size, such as micelles, are formed. It is the detailed variation of $\mu^0_N$ with N, then, which determines the mean size and the degree of polydispersity of the aggregate.

The relationship between $\mu^0_N$ and N is governed by the dimensionality of the aggregate [11]. For example, for simple infinite structures this relationship takes the form

$$\mu^0_N = \mu^0_\infty + \frac{\alpha kT}{N^P} \qquad (1.2)$$

where $\mu^0_\infty$ is the bulk free energy of a molecule in an infinite aggregate, $\alpha$ is a positive constant which depends on the magnitude of intermolecular interactions and P is a factor that depends only on the dimensions of the aggregate. P = 1 for rods, 1/2 for disks and 1/3 for spheres. The key point is simply that $\mu^0_N$ decreases as N increases in a way that is governed by the shape of the aggregate formed.

These thermodynamic considerations reveal the necessary requirement for self association but gives no information about the driving force for micellization at a molecular level. Furthermore, what are the molecular factors that cause ionic micelles to grow only to a finite size and to achieve a characteristic shape?

Micelles grow to a finite size because the self association of amphiphiles is governed by a balance between two opposing forces [8]. There is a repulsive interaction between monomers due to ionic head group repulsion, steric crowding of head groups, chain interactions and the hydrophilicity of the head group which is very complex. This interaction opposes self association. Counteracting this repulsive force is an attractive one due largely to the so called hydrophobic interaction [11].

The term hydrophobic interaction refers to the unusually strong attraction between non–polar molecules in water; often stronger than in free space. This attraction is largely an entropic effect and can be rationalized in terms of the well known hydrophobic effect [8, 11, 26]. When hydrophobic molecules are placed in contact with water the partial charges of the water molecules which face the non–polar solute are no longer available for hydrogen bonding. This is energetically unfavorable so the water molecules rearrange so as to maximize the total number of hydrogen bonds formed. The net effect of this is that a cavity is created in which the non–polar molecule sits. This process is associated with a decrease in entropy. Dispersion forces are not important in this context since the dispersion interaction between water and hydrocarbon is nearly the same as that between water molecules[11]. The increased attraction between non–polar solutes in water arises simply because fewer molecules of water must be ordered in order to contain two hydrophobic species in a single cavity than in two separate cavities. Thus the decrease in entropy for two non–polar molecules in a single water cavity is less than that for two separate solute molecules. It is this entropically driven attractive interaction which is the molecular basis for self association.

When the two opposing forces noted above are in balance, $\mu^0_N$ will achieve a minimum value. The surface area , a, occupied by monomer head groups when $\mu^0_N$ obtains this minimum value is called the optimum area per head group ,$a_0$. The expression for $\mu^0_N$ written in terms of $a_0$, a and $\gamma$, the interfacial free energy per unit area, is [11]

$$\mu_N^0 = 2\gamma a_0 + \frac{\gamma}{a}(a - a_0) \qquad (1.3)$$

which is the equation of a parabola. Thus $\mu^0_N$ increases (i.e. disfavors micellization) when a is greater than or less than $a_0$. Thus the concept of balanced opposing forces leads directly to the conclusion that surfactants should associate into aggregates of finite size; those for which $a \approx a_0$.

The packing of the surfactant monomers in the micelle is also important in determining size and shape. For given values of $a_0$, the hydrocarbon chain volume, v, and the maximum effective alkyl chain length, $l_c$, there are many possible sizes and shapes all of which will have roughly the same $\mu^0_N$. However, of these many structures entropy will favour that unique structure with the lowest aggregation number. Larger structures are unfavorable because they require that more monomers be ordered and smaller structures are energetically unfavorable because $a > a_0$. This fact is reflected in the observation that, for spherical micelles, there is a unique aggregation number for a given set of experimental conditions.

In summary we have seen that the balance between opposing forces at the molecular level leads to self association of amphiphiles into micelles of finite size and reasonably well defined structure. The resulting micelle structure can be approximately described as a spherical pool of liquid hydrocarbon enclosed by an electrical double layer. It is this compartmental nature which gives micelles one of

their most distinctive characteristics–the ability to solubilize hydrophobic reagents in aqueous media.

## 1.3 Cages and Super Cages in Radical Chemistry.

### 1.3.1 Radicals, cages and the radical pair concept.

Thermal or photolytic homolysis of a bond leads to formation of two molecular fragments each bearing one unpaired electron.

$$ACH_2CH_2B \longrightarrow A^{\bullet} + BCH_2CH_2^{\bullet} \qquad (1.4)$$

These species are known as radicals and they are generally very reactive [27]. Radicals can be formed by other types of reactions as well; hydrogen abstraction by an excited ketone for example [28].

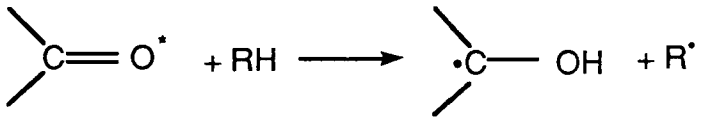

(1.5)

Once formed radicals can undergo a variety of reactions with other radicals and molecules. Reactions of radicals with molecules always generate a new radical center and such events are typical propagation steps in free radical polymerization [7]. The reaction of one radical with another generates a stable molecular species via either recombination (equation 1.6) or disproportionation (equation 1.7).

$$A^{\bullet} + {}^{\bullet}CH_2CH_2B \longrightarrow ACH_2CH_2B \qquad (1.6)$$

$$A^{\bullet} + {}^{\bullet}CH_2CH_2B \longrightarrow AH + CH_2{=}CHB \qquad (1.7)$$

These would be typical termination steps in a chain reaction. Disproportionation is generally somewhat slower than recombination for alkyl radicals [29] being most important for tertiary radicals since the reaction depends on the presence of β–hydrogens [30].

Since each radical contains an unpaired electron, termination of neutral radicals can proceed with a very low activation barrier [29] if no restrictive conditions pertain. Such restrictive conditions can be the presence of large groups near the radical center which may inhibit the close approach of the unpaired electrons necessary to bring about termination [31] or electron spin based restrictions which might inhibit formation of closed shell (i.e. singlet) molecular products. Because of their low activation energies radical recombinations generally proceed in solution with rate constants approaching diffusion control ($10^9$ to $10^{10}$ $M^{-1}s^{-1}$) at room temperature [27].

When a molecule undergoes homolysis in solution the resulting pair of radicals will be held together briefly by collision with the surrounding solvent. When the radical pair is in this solvent cage, the radical partners (spin permitting) are more likely to react with each other than with any other species in the solution. This statement may be taken as a working definition of the solvent cage [32]. Since the existence of the cage is dictated by collisions between the radical fragments and solvent molecules the cage should be prolonged in a more dense (or viscous) solvent. For typical organic solvents at room temperature the duration of the cage is on the order of $10^{-11}$ to $10^{-10}$s [33–35]. Since in the absence of spin or other restrictions the rate of recombination of radicals is comparable to the duration of the cage, some fraction of the initially formed radical pairs will undergo reaction within the cage. These radicals will therefore not be available to react with other species in the bulk solution. This "in cage" reaction is known as geminate reaction and phenomena that arise from this behaviour are called cage effects [33, 36, 37]. That cage effects do

occur, that is the reduction of *free* radical yields due to in cage reaction, has been amply demonstrated experimentally [35, 38].

The model currently used to describe cage effects is that given by Noyes[33, 34] building on the earlier proposals of Rabinowich [36, 37]. As shown in Scheme 1.1 there are three possible forms of in cage reaction following homolysis of A–B: (a) recombination of the primary pairs which have never separated: (b) recombination of secondary pairs which have separated to some extent and then returned; (c) recombination of free radicals which have separated fully and recombine in a random manner. Primary and secondary recombinations can only give rise to products involving fragments from the original starting materials and the sum of these two processes are what we have referred to as geminate reactions in order to distinguish them from random reactions that may lead to the same product. For our purposes it will not be necessary to make a distinction between primary and secondary geminate processes–only between geminate and non–geminate events. While random reactions of free radicals do take place in a solvent cage (forming so called diffusion radical pairs), such reactions are not considered geminate.

Two free (i.e. non–geminate) radicals randomly distributed in terms of space are each in a doublet spin state. Free radicals are said to have uncorrelated spins [39]. That is the electrons do not have a "memory" for the phase relation they had to one another when homolysis took place. Geminate radical pairs are said to have correlated spins [39]. Such radical pairs can be described as being in an overall singlet or triplet spin state depending on whether the two radical electron spins are paired or unpaired, respectively. The nature of the overall spin state of a spin correlated radical pair will depend on the spin state of the precursor molecule(s) from which the radical pair is formed. This is a direct consequence of Wigner's spin conservation rule [40] which states that the total electron spin of a reacting system is maintained in any elementary step. This means that a correlated radical pair formed

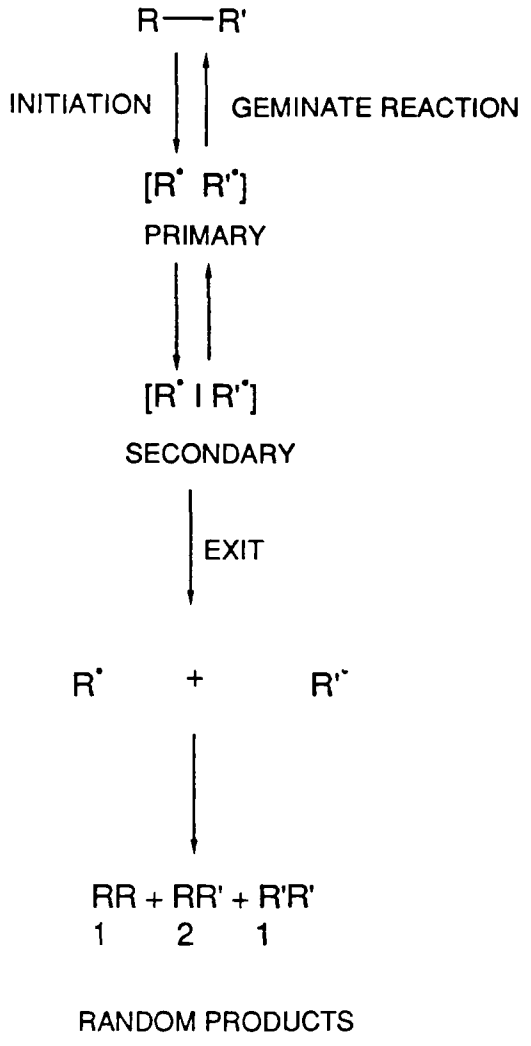
R—R'
INITIATION
GEMINATE REACTION
[R• R'•]
PRIMARY
[R• | R'•]
SECONDARY
EXIT
R•
+
R'•
RR + RR' + R'R'
1 2 1
RANDOM PRODUCTS

Scheme 1.1.

by, say, reaction of a ketone triplet with a hydrogen donor (reaction 1.5) will have an overall triplet spin state.

The spin state of a radical pair can have a profound effect on the chemical behaviour of the pair. Recombination of a singlet radical pair to form ground state molecular products is spin allowed [28]. This means that recombination of a singlet radical pair may well be competitive with, or faster than, escape of the pair from the solvent cage. In other words, for a singlet radical pair there may be a significant cage effect. For example, 55% of singlet ethyl pairs undergo geminate reaction in decalin at $30^0$C [30]. By contrast, the geminate reaction of triplet radical pairs in homogeneous solution is expected to be negligible. Direct reaction of a triplet radical pair to give ground state (i.e. singlet) products is spin forbidden [28] and can only occur after intersystem crossing (intersystem crossing) of the triplet pair to the singlet. Triplet–singlet intersystem crossing is a relatively slow process in general with rate constants on the order $10^6$ to $10^8 s^{-1}$ for triplet biradicals [41–43] in homogeneous solution at room temperature. There is little probability that such a slow process can compete with exit from the solvent cage which occurs on the order of $10^{10}$ $s^{-1}$ or faster. [32] Thus the majority of triplet radical pairs formed in homogeneous solution are expected to exit the solvent cage prior to undergoing intersystem crossing. As a result cage reaction is unimportant for triplet radical pairs under these conditions. This expectation is borne out by experiment. For example, the yields of free radicals formed upon separation of triplet thionine radical–light atom substituted aniline radical cation pairs generated in methanol have been reported to be close to 1.0 [44]. A second example is that of the photodecarbonylation of substituted dibenzyl ketones which proceeds via a triplet radical pair [45–47]. The cross coupling products of this reaction in homogeneous solution are formed in the ratios expected for random recombination of uncorrelated radicals [28, 47]. In both of these systems the cage

effect is therefore close to zero. This type of behaviour can be dramatically altered by carrying out reactions involving triplet radical pairs in micellar solution.

### 1.3.2 Micelles as "supercages".

As indicated previously, one of the distinctive features of micelles is their compartment–like nature. This structural characteristic makes them suitable for solubilization of the types of organic reagents which can lead to the formation of radicals. Furthermore, once formed hydrophobic radicals will tend to remain associated with the micellar environment. If a hydrophobic radical pair is formed within a micelle it will remain within its restricted space until one or both partners exit into the bulk aqueous phase. Thus, micelles can be thought of as cages for hydrophobic radical pairs in aqueous solution [4, 5, 9, 39, 48].

The analogy between solvent cage and micellar cage is not a complete one. There are two important differences [39]: (1) while the volume of the solvent cage is essentially the same as that of the encounter radical pair, the volume of a micellar cage is sufficient to allow geminate pair separations on the order of tens of Ångstroms; (2) while the duration of the solvent cage for a non–viscous organic liquid at room temperature is on the order of $10^{-10}$ s, the micellar residence time for a molecule of 6 or more carbon atoms will be $\geq 10^{-6}$s [49, 50]. Thus the micelles act as "supercages" in the sense that they prolong the cage lifetime [48]. While the importance of the former factor will become apparent later let us now consider the effect of micellar residence time on radical pair reactivity.

In micellar solution triplet radical pairs maintain their geminate character much longer than in the solvent cages of homogeneous systems. In fact the rate of escape from the micellar supercage may be comparable to, rather than faster than, the rate of intersystem crossing in the triplet radical pair. Diffusion of the individual radical partners of the triplet radical pair "within a micelle" is generally believed to be faster

than intersystem crossing [51–58]. In micellar solutions, therefore, a significant fraction of triplet born radical pairs may undergo intersystem crossing while still maintaining their geminate character. Once the transformation into a singlet radical pair is complete rapid spin–allowed reaction to give closed shell products can occur. While in homogeneous solution cage effects on the reactivity of triplet radical pairs are rather low (≤ 10%) compartmentalization of the triplet pair in a micelle leads to cage effects ranging between 30 and 100% [39]. It is the competition between intersystem crossing and exit processes imposed upon the triplet radical pair by micellization that leads to this remarkable change in behaviour.

A number of studies clearly show that the cage effect on triplet radical pairs in micelles is substantially greater than that in homogeneous solution. For example α cleavage of triplet deoxybenzoin in acetonitrile gives benzaldehyde and dicumyl as the major products with only minor amounts of the cage products α–methylstyrene and benzil being formed [59, 60]. In CTAC micelles the situation is reversed with the major products being α–methylstyrene and benzil [59, 60]. In the micellar system intersystem crossing followed by geminate disproportionation is competitive with separation of the triplet radical pair initially formed in this reaction. Similar effects of micellization have been reported on the photolysis of phenyladamantyl ketone [61], benzylphenyl acetone [4] and 2,4–diphenylpenta–3–ones [62]. Better known examples of this micellar "supercage" effect are those involving the photoreduction of benzophenone and the photolysis of dibenzyl ketones.

As indicated earlier the cage effect on the photodecarbonylation of dibenzyl ketone (DBK) in homogeneous solution (reaction 1.8) is close to zero. This is also true of unsymmetrically substituted dibenzylketones which we will abbreviate as ACOB. Here A and B are benzyl fragments with different substitution patterns.In aqueous solutions of CTAC the cage effect on the photolysis of ACOB is quite different. For DBK itself the cage effect has been reported to be between 33 and

50%[48, 63] while for unsymmetric DBKs it is as high or even higher [48]. Furthermore, this increase in cage effect occurs sharply at the cmc of CTAC indicating that it is closely associated with the formation of the micelles.

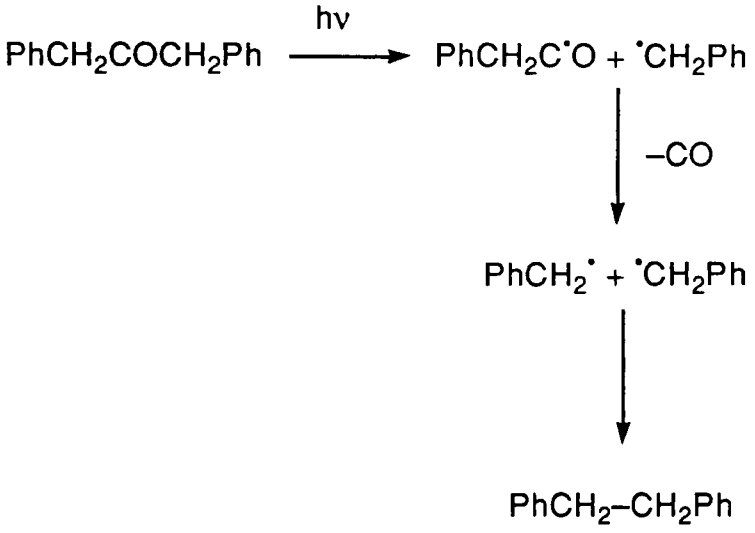


(1.8)

Since for all the DBK derivatives studied the cage effect is less than 100% some fraction of the radical pairs are subject to exit processes. These exiting free radicals will recombine randomly in the bulk phase and form diphenylethanes (DPE). That this is so has been verified by scavenging the exiting radicals with Cu(II) [48, 64]. In these experiments the yield of DPE drops rapidly and then levels off with increasing copper concentration while the disappearence of DBK is independent of the cupric ion concentration. The leveling off of the DPE yield is due to the fraction of triplet benzyl radical pairs confined to the micelles and therefore not subject to quenching by Cu(II). This technique has been used as one method to estimate the degree of geminate reaction (i.e. the cage effect) in the DBK systems. The data suggest that about 1/3 of all the DPE formed during the photolysis of DBK in CTAC is due to geminate recombination of the benzyl radicals. These product studies are consistent with the view that the micelles serve to maintain the geminate character of

the triplet benzyl pair for a sufficiently long time so that intersystem crossing may occur. The singlet radical pair can then undergo rapid reaction to give in cage products AB. Loss of geminate character due to escape competes with the intersystem crossing process causing the cage effect to be less than 100%.

The influence of micellization on the kinetic behaviour of triplet radical pairs is perhaps best illustrated by the work that has been done on the photoreduction of benzophenone in micellar solution. The photoreduction of the triplet state of benzophenone by hydrogen donors ,RH, (reaction 1.9) is one of the most carefully studied photochemical reactions [28].

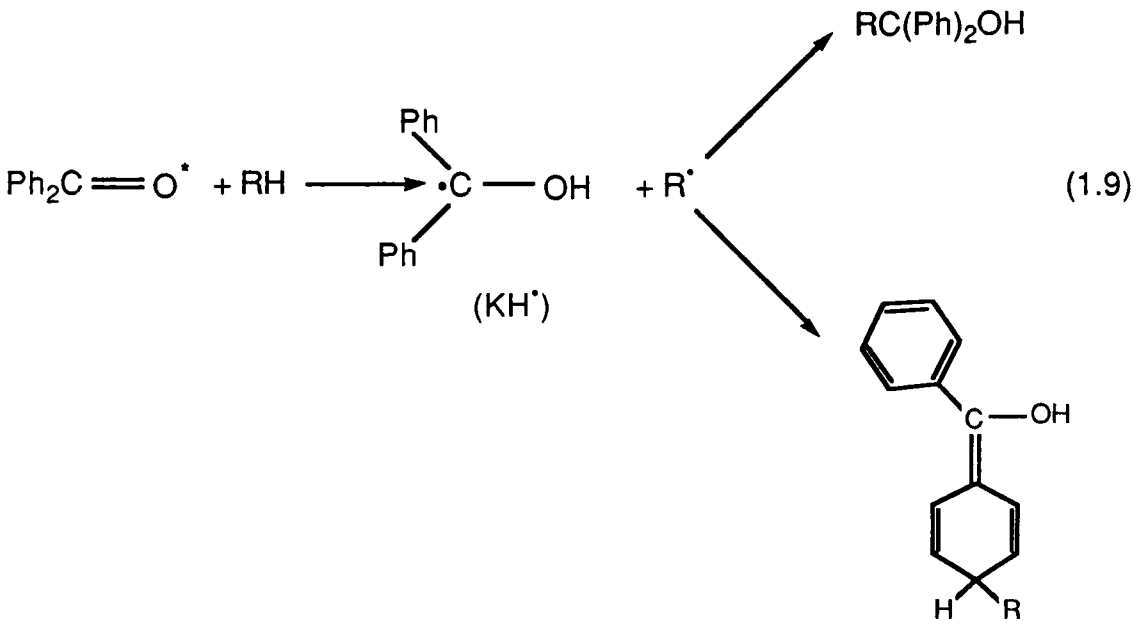


(1.9)

In homogeneous solution the reaction yields pinacols as the major product along with the minor para–coupling, or light absorbing transient, product [65, 66]. As shown in equation 1.9 the reaction proceeds via the intermediacy of the benzophenone ketyl radical, KH•, and the radical, R•, resulting from hydrogen abstraction from the hydrogen donor. The initially formed radical pair will be a triplet because of spin conservation. The same reaction mechanism applies in micellar solutions [54, 55].

The transient kinetics of benzophenone in SDS have been examined in the absence [51, 52, 67, 68] and presence [54, 55, 69] of added hydrogen donors; 1,4–cyclohexadiene in particular. In order to obtain reliable kinetic data on the decay of micellized triplet radical pairs it is essential that the pair be formed in a time much shorter than its geminate lifetime. The concurrent formation and decay of the radical pair of interest makes the study of its kinetics quite complex and the resulting data unreliable. In the absence of added hydrogen donor the formation of the triplet radical pair in the benzophenone/SDS system can take as long as 300ns [53–55]. In the presence of 1,4–cyclohexadiene the triplet state reactivity becomes enhanced to the extent that reaction 1.9 becomes essentially instantaneous on the time scale over which the triplet radical pair decays.

Figure 1.2 shows a transient absorption decay trace obtained at 545nm after nitrogen laser excitation of a solution of benzophenone and 1,4–cyclohexadiene in SDS [54, 55]. Under these conditions and at this wavelength the only species observed is $KH^{\bullet}$. Note that the formation of the ketyl is instantaneous. The system decays in a biphasic manner with a rapid initial decay followed by a residual absorption which is much longer lived. The observed decay characteristics can be interpreted in terms of the model shown Scheme 1.2 [54, 55]. The initial fast decay, $k_{obs}$, can be fit to a first order kinetic expression. $k_{obs}$ corresponds to processes that result in decay of the geminate triplet radical pair, i.e., geminate reaction and exit, and [54,55]

$$k_{obs} = k_{gem} + k- \qquad (1.10)$$

where $k_{gem}$ represents the rate constant for geminate reaction of the triplet radical pair which is believed to be intersystem crossing controlled. k– is the sum the rate constants for all processes which destroy the geminate nature of the pair. The long

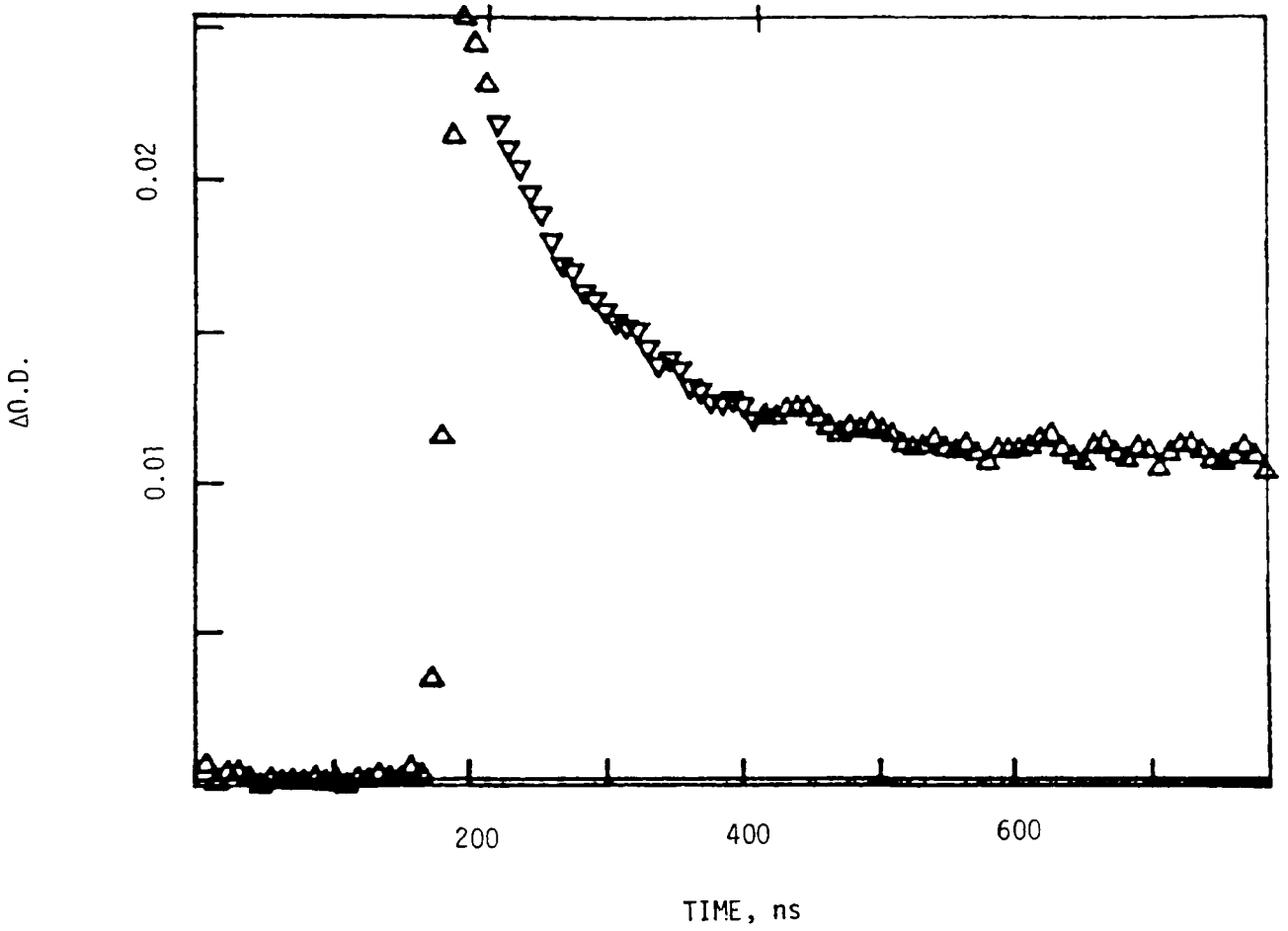


Figure 1.2. Transient absorption decay monitored at 545nm for benzophenone in 0.22M SDS with 0.032M 1,4–cyclohexadiene. H = 0G. From reference [54].

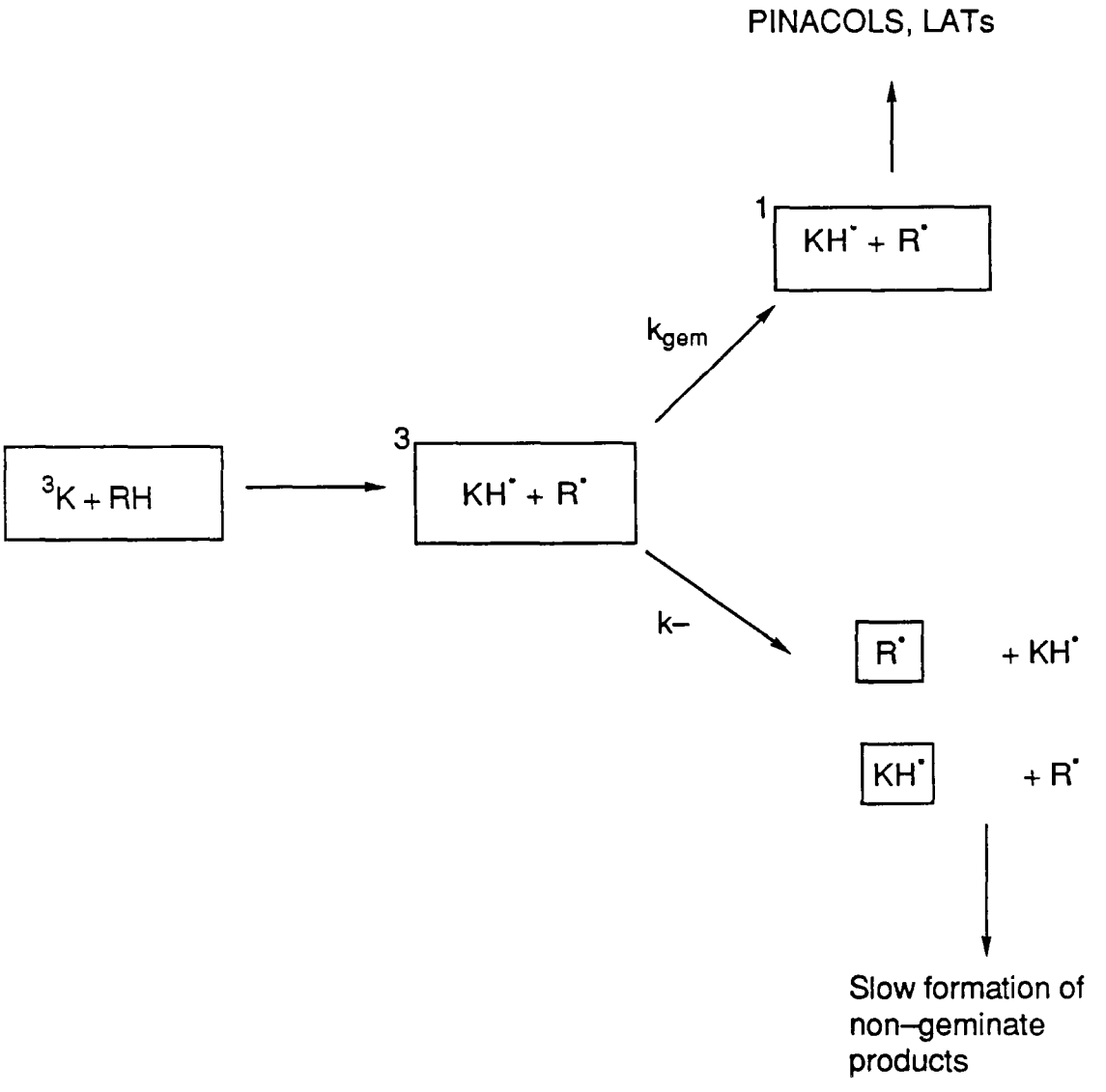
PINACOLS, LATs
1
KH• + R•
kgem
3
3K + RH
KH• + R•
k–
R•
+ KH•
KH•
+ R•
Slow formation of
non–geminate
products

Scheme 1.2

lived absorption corresponds to that fraction of pairs which undergo exit from the micelle. This residual optical density (ΔO.D.) is related to the escape fraction, or %escape, by

$$\% \text{ Escape} = 100\left(\frac{\text{Residual } \Delta\text{O.D.}}{\text{Total } \Delta\text{O.D.}}\right) = 100\left(\frac{k-}{(k_{gem} + k-)}\right) \qquad (1.11)$$

By fitting the fast component and determining the %escape it is possible to obtain separate values of $k_{gem}$ and k– from equations 10 and 11. Equation 1.11 illustrates a second reason why rapid radical pair formation is desireable. Concurrent formation and deacy of the triplet radical pair will distort the value of total, i.e. initial, ΔO.D. and therefore lead to erroneous values of the rate constants. Finally one should note that in general the analysis just presented can only place an upper limit on k– Interference from fluorescence and geminate reaction products that absorb at the detection wavelength may serve to decrease the total ΔO.D. and increase the residual ΔO.D., respectively.

For the benzophenone/SDS/cyclohexadiene system under conditions of rapid radical pair generation $k_{gem} = 5.8 \times 10^6 s^{-1}$ and $k- = 4.4 \times 10^6 s^{-1}$ in the Earth's magnetic field [54, 55]. Once again these results are consistent with the model of the micelle as a supercage. The value of the exit rate constant verifies that the duration of the cage is indeed quite long compared to homogeneous solution. Also the observed value of %escape indicates that about 53% of the triplet radical pair decay is geminate in character.

Transient kinetic studies have also been carried out on the DBK system in CTAC [56, 70]. In this case the chromophore monitored is the benzyl radical formed in reaction 1.8. In homogeneous solution benzyl radicals decay by second order kinetics over time scales of tens of μs [71]. In surfactant solutions the observed decay

of the benzyl radical absorption is biphasic as was the case in the benzophenone system. The fast component may be fit to first order kinetics and was found to have an observed rate constant of $k_{obs} = 2.5x10^6 s^{-1}$ in the Earth's magnetic field. The slow component decays with a rate constant of $2.1x10^5 s^{-1}$ The authors of this paper assigned the fast component to the decay of the spin correlated benzyl radical pair and the slow component to the decay of the escaping pairs. Furthermore the fast decay accounts for only 47% of the initially formed benzyl radicals. The remaining 53% are those that exit the micellar environment. The value of 47% is consistent with estimates of the DBK cage effect based on yields of final products. Finally it is worth noting that this work assumes that the rate of triplet benzyl radical pair formation is very rapid. Recent evidence has suggested that in fact this may not be so for the DBK systems. In fact the decarbonylation step which leads to the benzyl radical pair (reaction 1.8) may require as long as 200 ns [72, 73].

We have seen that micellization can lead to profound effects on the chemical and kinetic behaviour of triplet radical pairs. These effects arise directly from the fact that the micelles hold the radical pair together for sufficiently long times that $k_{gem}$ and k– become comparable. As we shall see, when $k_{gem} \approx$ k– the kinetic behaviour of, and product distribution arising from, a triplet radical pair can often be dramatically altered by the application of moderate magnetic fields. Since the rates of triplet radical pair intersystem crossing and exit are often comparable in micelles, many of the reports of magnetic field effects on radical pairs have dealt with systems in surfactant solutions.

## 1.4 Magnetic Field Effects on the Behaviour of Triplet Radical Pairs.

### 1.4.1 Background.

Reports of the influence of applied magnetic fields on chemical reactivity can be traced back to the early years of this century (see reviews by Atkins and

Buchachenko for early examples [74, 75]). With a few exceptions many of the early examples were subsequently shown to be spurious. However over the last 15 years or so a large body of experimental data has shown conclusively that magnetic fields can in fact have a marked effect on chemical behaviour. By far the largest part of this data is concerned with field effects on radical pairs. The most pronounced effects are observed when there is some force causing the pair to maintain its geminate character for relatively long periods of time. These forces can be the barrier to diffusion imposed by the micelle–water interface or electrostatic attraction, hydrogen–bonding or high solvent viscosity in homogeneous solvents.

What is the source of these magnetic field effects? In the following section we shall present a theoretical framework for understanding the influence of external fields on the behaviour of spin correlated radical pairs. As it turns out, magnetic field effects arise because of the impact of the applied field on the radical pair intersystem crossing processes.

### 1.4.2 Mechanisms of radical pair intersystem crossing and the source of magnetic field effects.

As was implied in section 1.3.1 the probability of radical recombination depends on steric factors and the spin state of the radical pair. In addition it depends on the probability of re–encounter of the geminate partners since recombination is a contact process [32]. Since steric and reencounter factors should be the same for a given radical pair regardless of its overall spin configuration we need only consider the details of the radical pair spin state to describe the recombination probability in a given case. That is, we must concern ourselves with radical pair intersystem crossing.

The ultimate source of magnetic field effects on radical pair chemistry is the inhibition or enhancement of radical pair intersystem crossing in the presence of an external magnetic field. In order to understand how a magnetic field influences

intersystem crossing one must have some insight into the mechanisms of radical pair intersystem crossing in the absence of an applied field. It is the purpose of this section to present the most important intersystem crossing mechanisms and to indicate how changing the field strength may alter their effectiveness.

Upon homolysis of a molecule AB to give radical fragments $A^{\bullet}$ and $B^{\bullet}$ the unpaired electrons can have correlated spins corresponding to an overall singlet or triplet spin state. Since each unpaired electron can have two possible spin orientations, $\alpha$ or $\beta$, relative to an applied magnetic field, there are in fact one singlet and three triplet spin configurations possible [28, 32, 74, 76]. This is shown schematically in Figure 1.3. In the Figure the spin of each electron is represented by a vector ,$\alpha$ or $\beta$, which precesses around the direction of the applied field, $H_z$. In the singlet radical pair (denoted S) one electron is $\alpha$ and the other is $\beta$. In addition the components of these vectors perpendicular to $H_z$ are 180° out of phase so that the sum of these components equals zero. Two of the triplet states have the spin vectors orientated as $\alpha\alpha$ ($T_+$) or $\beta\beta$ ($T_-$). The third ,$T_o$, is $\alpha\beta$ as was the S state. However in the $T_o$ case $\alpha$ and $\beta$ are in phase so that their components perpendicular to $H_z$ add up to 1.

From the simple vectorial representation of Figure 1.3 it is clear that $T_o$ <–> S interconversions require a rephasing of the spin vectors while for $T_\pm$ <–> S a spin flip must occur. In the absence of perturbations singlet–triplet transitions are forbidden[28,32, 74, 76]. Describing intersystem crossing mechanisms therefore reduces to indentifying perturbations which can lead to spin rephasing and spin flips. It is the interactions between the unpaired electrons and internal or external magnetic fields which provides the required perturbations.

An isolated electron spin has a magnetic moment associated with it. It is through this magnetic moment that the spinning electron interacts with other external

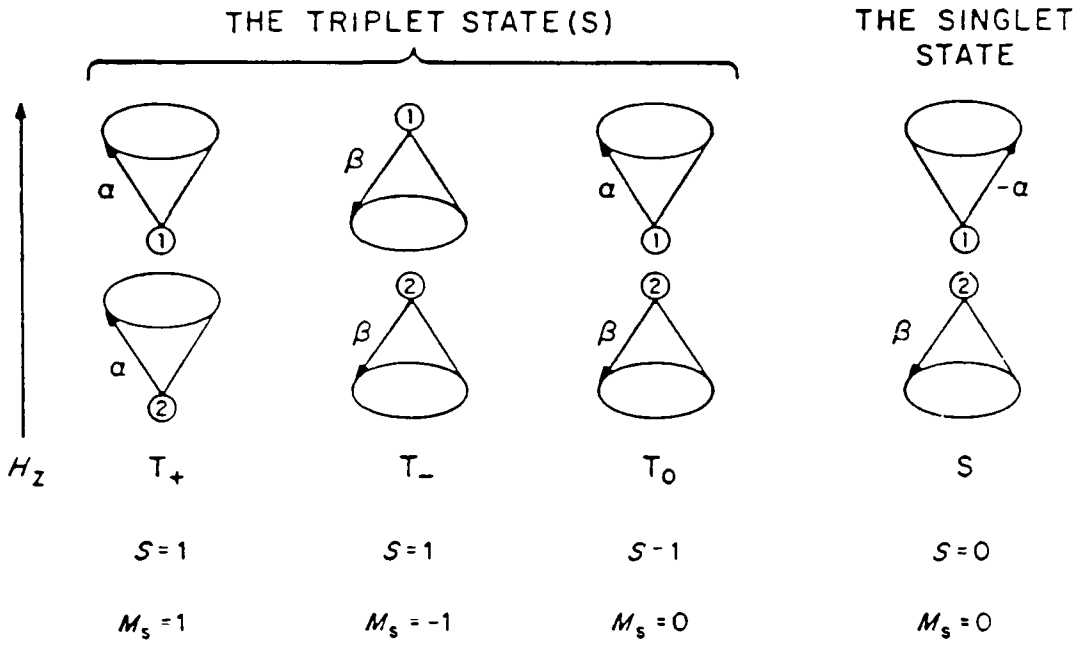


Figure 1.3. Vector model of the singlet and triplet states of a radical pair. From reference [76].

or local fields. The interaction energies ,E, can in principle be derived from the operation of a suitable Hamiltonian , H, on spin wavefunctions Φ. [77]

$$H\Phi = E\Phi \qquad (1.12)$$

H is called the spin Hamiltonian and it consists of several terms each representing a particular type of magnetic interaction of the unpaired electron spin. In particular, the interactions normally considered important [77] are the Zeeman interaction, isotropic electron–nuclear hyperfine coupling (hfc), so called dipolar interactions and other anisotropic effects such as spin–rotational coupling.

$$H = H_Z + H_{hfc} + H_{an} \qquad (1.13)$$

Strictly speaking equation 1.13 should also include a term relating to the Zeeman effect on the nuclear spins but since this interaction is nearly 700 times weaker than the electronic Zeeman effect it is generally ignored [77] in discussions of systems in fluid solution.

Since spinning magnetic nuclei like $^1H$ also generate magnetic fields there can be a classical dipolar coupling between the magnetic moments of the unpaired electron and the nuclei which is analogous to the interaction between bar magnets. This interaction is anisotropic in nature and can in fact lead to spin interconversions in radical pairs. However in solutions of moderate viscosity (~ 1cP) the rate of spin interconversion via this mechanism is in the range of $10^{-5}$s for an ideal situation where there is perfect energy matching between the interconverting states [32]. As we shall see this is somewhat slow compared to experimental reports of the rates of radical pair intersystem crossing. In addition this and other anisotropic effects (vide infra) are influenced by the rate of radical tumbling in solution. They are generally

considered to be averaged to zero with time [77]. As a result anisotropic effects have often been discounted as possible sources of radical pair intersystem crossing [32]. We will leave aside the discussion of interactions of this type for the time being.

In discussing the behaviour of radical pairs each term in equation 1.13 must be applied to each radical center. Furthermore radical pairs are subject to another effect that is not relevant in the case of isolated electron spins–the exchange interaction. The electron exchange interaction arises from the requirement that electrons be indistinguishable [78]. It is the source of the energy gap between singlet and triplet states in molecules, biradicals and radical pairs and it also couples the spins of the two electrons which define the spin states of these various species [28]. Thus equation 1.13 becomes

$$H = (H_{Z1} + H_{Z2}) + (H_{hfc1} + H_{hfc2}) + H_{ex} \qquad (1.14)$$

where the indices 1 and 2 refer to the two radical centers of the radical pair. Written out in full equation 1.14 becomes

$$H = (g_1 s_1 + g_2 s_2)H_0 + s_1\left(\sum_j a_j I_j\right) + s_2\left(\sum_k a_k I_k\right) - J(1/2 + 2s_1 s_2) \qquad (1.15)$$

where $g_1$, $g_2$ are the electron g factors for each radical, $\beta$ is the Bohr magneton, $H_0$ is the applied field strength, $s_1$ and $s_2$ the spin angular momentum vectors of the two unpaired electrons, $a_j$ and $a_k$ are the hfc coupling constants and $I_j$, $I_k$ are the nuclear spin angular momentum vectors. The sums are over nuclei j for radical 1 and over nuclei k for radical 2 which couple with the unpaired electron spin on the given radical. J is the electronic exchange integral. The electronic exchange energy, which is related to the value of J, decreases exponentially with interradical distance.

According to the conventional view, for separations at which radical pair intersystem crossing typically takes place J≈0. So we will drop the exchange term from equation 1.15 and consider only the Zeeman and hfc terms. As we shall see in Chapter 4 this approach is perhaps oversimplified.

If a radical pair is initially formed in, say, a singlet spin state, no S <–> $T_0$ intersystem crossing will occur as long as the frequencies of precession of the two electrons do not change. That is the difference in precessional frequencies, $\Delta\omega$, remains zero. The value of $\Delta\omega$ will come directly from the solution of equation 1.12, using Hamiltonian 1.15, since E =h$\Delta\omega$. For Zeeman and isotropic hfc interactions

$$\Delta\omega \cong (\Delta g \beta h H_Z) + \left( \sum_j a_j I_j - \sum_k a_k I_k \right) \qquad (1.16)$$

The rate constant for intersystem crossing, $k_{gem}$, is directly related to $\Delta\omega$. From equation 1.16 we can deduce that there are at least two mechanisms for radical pair S <–> $T_0$ interconversion; the $\Delta g$ mechanism and the hfc mechanism. Of these the latter appears to be the most commonly observed (see Chapter 2). In fact, prior to 1984 nearly all magnetic field effects in micellar solution were explained in terms of the hfc mechanism.

If $A^\bullet$ and $B^\bullet$ are are not the same radical they will have different g values so that $\Delta g$ in equation 1.16 will be non–zero. When this is so the rate of precession of the electron spin of $A^\bullet$ about an applied field will differ from that of $B^\bullet$ so that their original singlet relationship will be lost. Eventually S will rephase into $T_0$ and, after another period of time, $T_0$ will rephase back into S. This so called $\Delta g$ mechanism serves only to induce S <–> $T_0$ interconversions and is only feasible in the presence of an external field. For carbon centered radicals $\Delta g \sim 10^{-3}$ so in the Earth's magnetic field (~1G) the rate of S <–> $T_0$ intersystem crossing due to the $\Delta g$ mechanism will only be

about $10^3$–$10^4$ $s^{-1}$. In a strong field of $10^5$G the rate constant will be on the order of $10^8$–$10^9 s^{-1}$ if S and $T_0$ are degenerate or nearly so.

How does S <–> $T_0$ intersystem crossing occur in radical pairs for which $\Delta g$ = 0? Now the local field experienced by the unpaired electrons will be due to the magnetic field generated by nearby nuclear spins as well as by any applied fields. In the absence of applied fields and at radical separations for which the approximation J~0 holds, the dominant magnetic interaction is the isotropic hfc. Hfc can induce radical pair intersystem crossing in two different ways. In Figure 1.4a we can see how hfc causes S <–> $T_0$. The field in the z direction, $H_z$, due to the coupling nuclei generates a magnetic "torque" on the precessing spin vectors which are initially in the S state. From equation 1.16 we see that the rate of hfc induced S <–> $T_0$ will be related to

$$\Delta\omega \cong \sum_j a_j I_j - \sum_k a_k I_k \qquad (1.17)$$

Even for identical radicals, in which $a_j = a_k$, we can expect $\Delta\omega \neq 0$ if the nuclear spin states, $I_j$ and $I_k$, are different. In other words the two electron spins will almost certainly experience different magnetic torque and the initial phase relationship will be lost. This is true even when there is no external field.

Hfc can also lead to S <–> $T_\pm$ interconversions. This is illustrated in Figure 1.4b. Here the electron spins of radicals 1 and 2 are coupled to nuclear spins which provide magnetic fields in the x and y directions. The latter fields provide a magnetic "torque" which induces $T_\pm$ <–> S interconversions. In these transitions the overall spin angular momentum is conserved since the electronic spin flips are accompanied by nuclear spin flips.

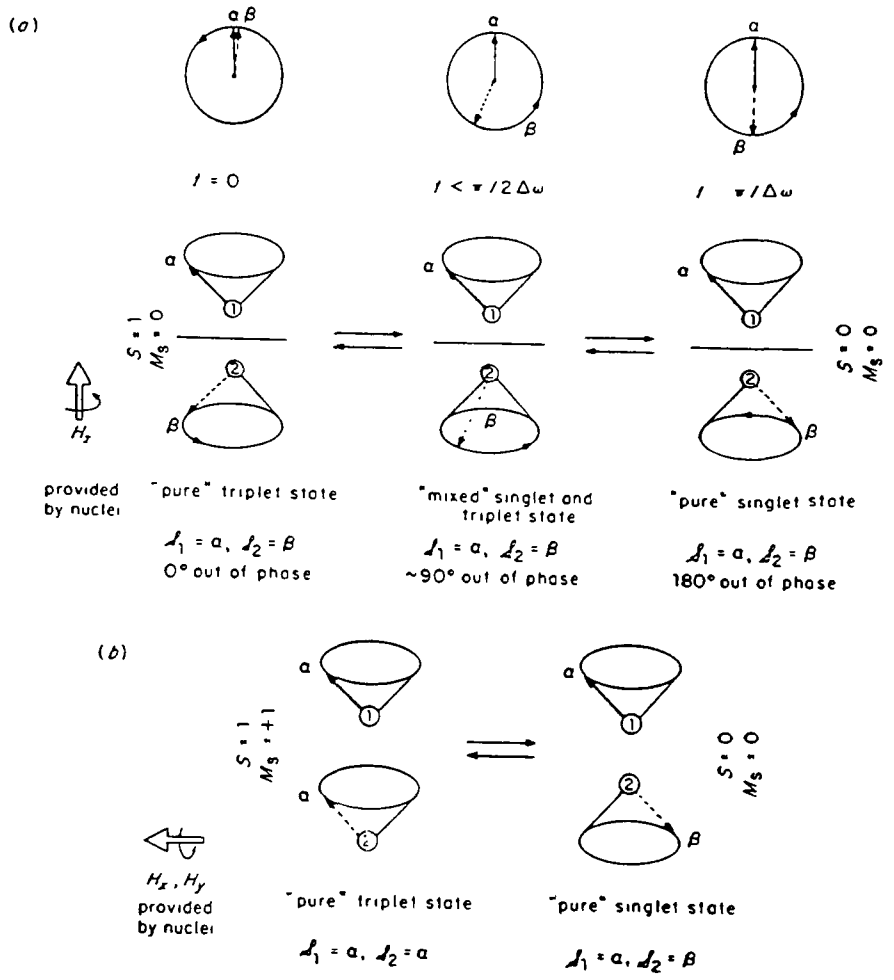


Figure 1.4. (a) A spin clock and vectorial representation of the $T_0$ <–> S intersystem crossing mechanism in radical pairs. (b) A vectorial representation of a $T_+$ <–> S intersystem crossing showing the required changes in electron spin. Taken from reference [76].

We have now identified two radical pair intersystem crossing mechanisms. How can application of an external magnetic field interfere with these processes and result in magnetic field effects on radical pair behaviour? To answer this question we will consider the hfc mechanism first.

In general the rate constant for intersystem crossing in a radical pair can be described by a "golden rule" expression such as 18 [76]

$$k_{ISC} \cong \frac{\langle TIHIS \rangle^2}{h\,\Delta E} \qquad (1.18)$$

where <TIHIS> is the matrix element for interconversion between the triplet and singlet radical pair as mediated by the spin Hamiltonian, H. $\Delta E$ is the energy gap between the T and S states. Here we are following the conventional view that $k_{gem}$ is intersystem crossing controlled. Figure 1.5 shows the dependence of this energy gap on radical pair separation which in turn depends on the variation of J with radical separation. At small separations J is large compared to the hfc coupling energy and $\Delta E$ is also large. At larger separations (on the order of 6 to 10Å) J~0 and therefore $\Delta E \sim 0$. In the absence of an external field $T_{\pm}$ and $T_0$ are degenerate with one another and, when J~0, with S as well.Thus at radical separations on the order of 10Å hfc will contribute extensively to $k_{gem}$. In the presence of an external field $T_{\pm}$ are split from $T_0$ by $\pm(g_1 + g_2)\beta H_0/2$ as shown in the Figure. At fields about one order of magnitude greater than the hfc (i.e., at fields of about 1kG) the energy gap between $T_{\pm}$ and S becomes larger than the hfc energy. Hfc is then no longer sufficient to cause spin flips between $T_{\pm}$ and S and the contribution of hfc to $k_{gem}$ between these states will become small. $k_{gem}$ for $T_0$ <–> S remains unaffected. Thus in the high field limit intersystem crossing from $T_{\pm}$ to S will no longer be effective and the overall efficiency of intersystem crossing will be reduced. From the foregoing it is evident that the hfc

mechanism will lead to magnetic field effects only in fields which are less than about 1kG. The implication is that products derived from geminate recombination following hfc mediated intersystem crossing of a triplet radical pair are less likely to form in a high magnetic field. Another way of expressing this is to say that the yield of non–cage products (i.e., those formed by radicals that have escaped the micellar or solvent cage) will increase in a high field at the expense of cage products. This is shown schematically in Figure 1.6a. The same type of behaviour should be evident in time resolved studies. The residual absorption (Figure 1.2) due to triplet radical pairs which undergo escape should increase when a magnetic field is applied. All of these effects arise directly from the fact that the degeneracy between two out of three triplet sublevels and S is lost at fields ≤1kG when intersystem crossing is a hfc process.

At this point it should be re–emphasized that it is of key importance to the hfc explanation of magnetic field effects that the radicals be able to separate to the point that J –> 0. It is within this context that the larger volume of micellar cages compared to that of solvent cages (see section 1.3.2) becomes significant. Micelles can not only keep the radicals in spatial proximity long enough for intersystem crossing to take place but they also allow enough spatial separation that J~0.

While the hfc intersystem crossing mechanism is the most common there are some instances where intersystem crossing occurs in radical pairs where $J \neq 0$. In these cases hfc cannot bring about intersystem crossing at zero field. However if an external field is applied the Zeeman splitting may result in a degeneracy at some particular field value. This is also shown in Figure 1.5. Here the system has a singlet ground state and at the field value $H_d$ $T_-$ becomes degenerate with S. At $H_d$ hfc mediated intersystem crossing can occur. This mechanism is known as the level crossing mechanism and it too leads to magnetic fields effects. In particular at fields below and above $H_d$ $\Delta E$ will be large and intersystem crossing will be unimportant. At $H_d$ intersystem crossing will be effective. For a triplet radical pair there will thus be a

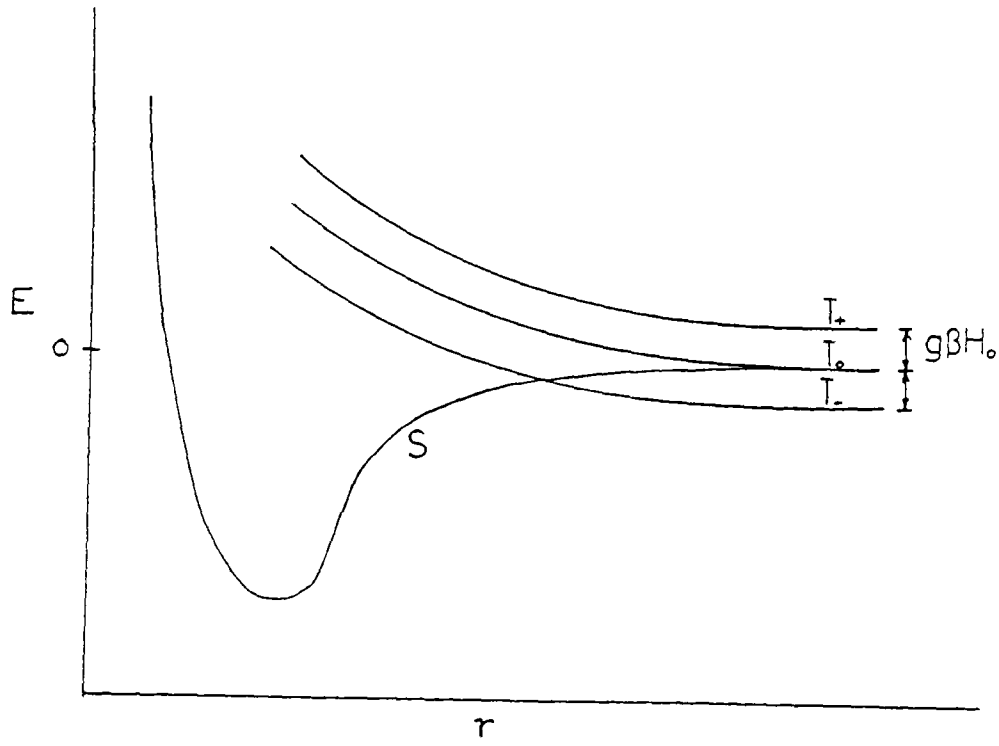


Figure 1.5. Potential energy surface for a radical pair in a strong magnetic field showing the splitting of the $T_+$, $T_-$ and $T_0$ levels. From reference [99].

a) Hyperfine coupling mechanism.

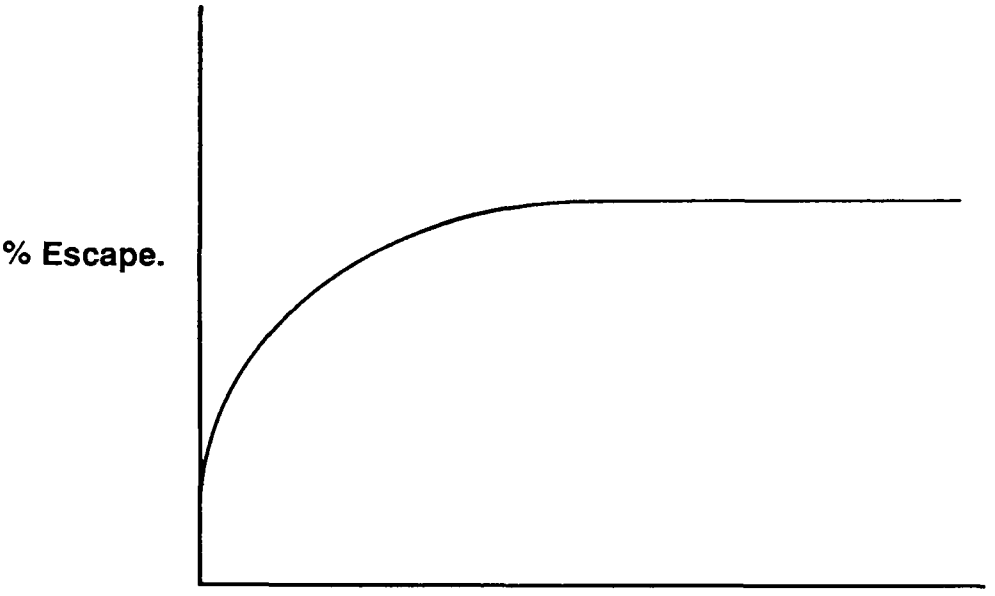


b) Level crossing mechanism.

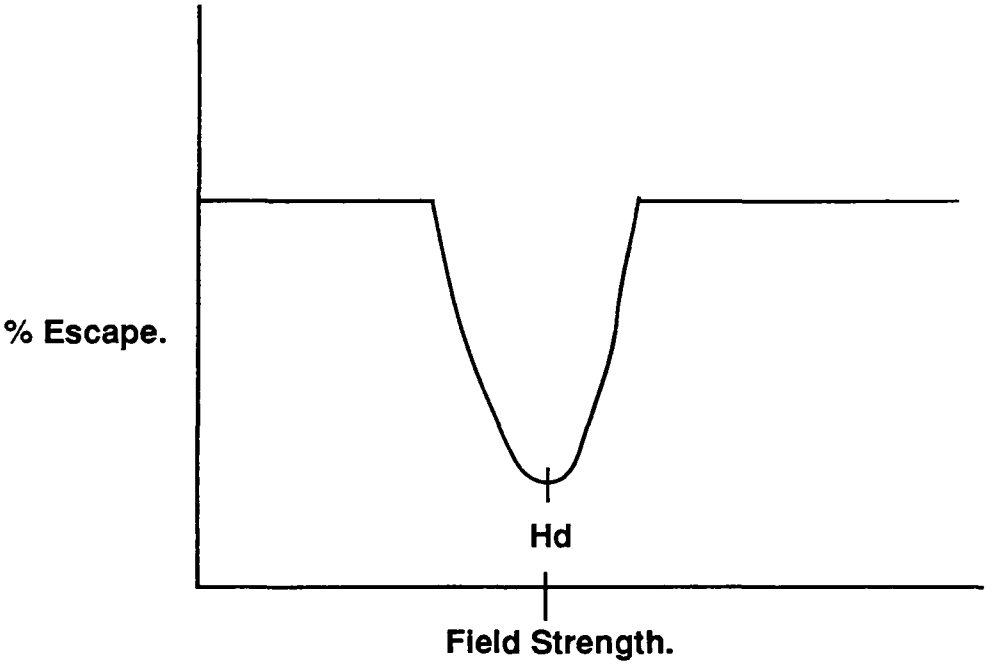


Figure 1.6. Expected behaviour of escape product yield as a function of applied field strength. After reference [83].

narrow range of fields centered on $H_d$ at which substantial amounts of in cage products can form. Above or below this range little cage product will be found (Figure 1.6b).

Magnetic field effects can also arise due to the $\Delta g$ mechanism. For a triplet radical pair for which this process dominates $k_{gem}$ should increase linearly with increasing field strength as indicated by the first term in equation 1.16. The portion of in cage product should also increase linearly with increasing field strength. While $k_{gem}$ for the hfc process is $10^7$–$10^8 s^{-1}$ in the Earth's field [75], the rate constant for $\Delta g$ induced intersystem crossing is much smaller. Thus the contribution of the $\Delta g$ mechanism to magnetic field effects is likely to become important only at very high fields (~10kG).

Let us now consider the anisotropic contribution to the spin Hamiltonian. Radical pair intersystem crossing mediated by anisotropic effects is known as the spin, or paramagnetic, relaxation mechanism. Although considered to be of minimal importance by many authors [32, 48, 55, 59, 76, 79–81], this mechanism has been invoked extensively by Hayashi's group [82–88] and occasionally by others [44, 89, 90]. For example, to explain the magnetic field dependence of triplet radical pair behaviour at fields above those at which isotropic hfc is expected to saturate[52,53,82].

The spin relaxation model originally proposed by Hayashi [83, 84], building on the earlier work of Brocklehurst [91], begins by assuming a separated radical pair (J~0). So at zero field $T_{\pm}$, $T_0$ and S are degenerate. At high field the Zeeman effect splits $T_{\pm}$ and the degeneracy of these states with the other two is lost. Hayashi proposed that even at fields as high as 10kG $T_{\pm}$ <–> $T_0$ and $T_{\pm}$ <–> S interconversions are possible due to the anisotropic interactions. At zero field intersystem crossing is due to isotropic hfc. As shown in Figure 1.7 these high field interconversions proceed with rate constants $k_R$ and $k_{R'}$ for $T_{\pm}$ <–> $T_0$ and $T_{\pm}$ <–> S,

(a) Zero field.

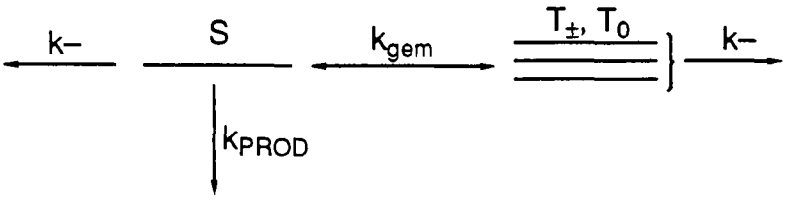


(b) High field.

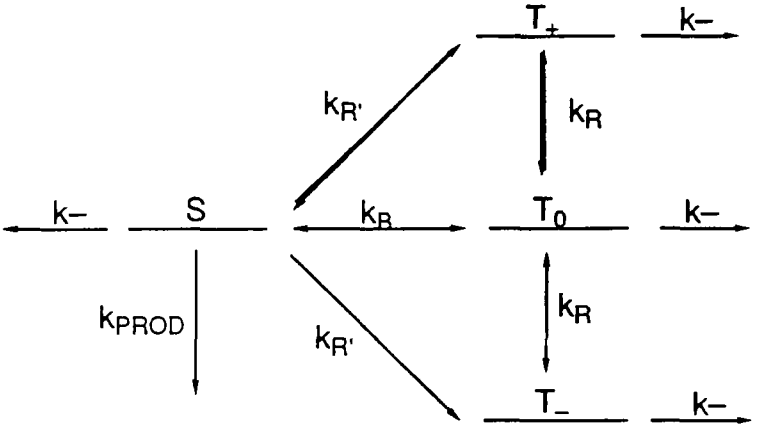


Figure 1.7. Kinetic scheme for a radical pair that is subject to spin relaxation.

respectively. The high field $T_o$ <–> S rate constant, $k_B$, will be equal to, or greater than, the zero field rate constant, $k_{gem}$, because of the difference in g values of the two radicals. According to Hayashi's analysis, most of the magnetic field effect will be due to the difference in rate constants $k_B - k_{gem} + 2k_R$. According to Hayashi $k_R$, a rate constant dependent on the magnitude of anisotropic interactions, is less sensitive to magnetic fields than the $k_B - k_{gem}$ term so that spin relaxation induced transitions are feasible even up to rather high values of $H_z$.

Relaxation between electronic spin states of a radical pair in fluid solution can arise because of random time dependent modulation of the local magnetic field experienced by the unpaired electrons [32, 77, 92]. This random modulation occurs because of the tumbling of the radicals in solution. In particular, as a radical tumbles the magnetic interactions that it induces in a nearby radical will fluctuate. This occurs because the tumbling induces random fluctuations in the g–tensor anisotropy [77, 92], the anisotropic hfc interaction and the spin–rotational coupling interaction [93]. To understand this, consider the g–tensor anisotropy. The g factor of an unpaired electron is a measure of the spin–orbit coupling of that electron [77] and it determines the magnitude of the spin magnetic moment of the electron. Thus the g factor in part determines the extent of the electron's interaction with magnetic fields. The g factor normally measured in a solution ESR experiment is the isotropic, or time averaged, g factor [77]. This is the average value of the g–tensor diagonal for a randomly tumbling radical. At a given instant the g–tensor of a radical is in fact anisotropic. According to the relaxation model the random motion of this anisotropy contributes to $T_{\pm}$ <–> $T_o$,S interconversions at high fields. In the terminology of the vector description of electron spins, the fluctuating anisotropic magnetic field caused by the g–tensor anisotropy of one of the radicals provides a magnetic torque on the x and y components of the spin vector of the other radical. Similar arguments can be made for the hfc anisotropy. Spin–rotational coupling also contributes to spin relaxation. Spin–rotational coupling

arises because the rotation (tumbling) of a paramagnetic species generates a magnetic field which can couple with the spin magnetic moment of the unpaired electron.

We can now write the relaxation rate constants, $k_{rel}$ and $k_{rel}'$, as a sum of various contributions. For example

$$k_{rel} = k_{AHF} + k_{SO} + k_{SR} \qquad (1.20)$$

where $k_{SO}$ is the spin–orbit (g–tensor anisotropy) term, $k_{SR}$ is the spin–rotation term and $k_{AHF}$ is the anisotropic hfc term. The former terms are related to spin–orbit coulping effects. Application of an external magnetic fields influences these rate constants in different ways: $k_{SO}$ increases with increasing field; $k_{AHF}$ decreases with increasing field; $k_{SR}$ does not depend on the field strength [32, 92, 93]. Furthermore, all three rate constants depend on the so called rotational correlation time, $\tau_C$, which in turn depends on the viscosity of the medium in which the radicals are tumbling. $\tau_C$ increases as the solvent becomes more viscous. In a non–viscous solvent ($\eta$ ~1cP) $\tau_C \sim 10^{-11}$s so, at zero field, tumbling is so fast that anisotropic effects are averaged out. Only at rather high fields ($10^3$ to $10^5$G) [32] will the interplay of the field and tumbling dependencies of $k_{SO}$ and $k_{AHF}$ give these rate constants significant values for carbon centered radicals.

In terms of its expected effect on the extent of cage reaction, the relaxation mechanism should show behaviour similar to that of the hfc mechanism. That is, for a triplet radical pair, the cage effect should decrease smoothly as the field strength increases ($\Delta E$ increases). The difference is that $T_{\pm}$ <–> S transitions will be shut off (i.e., the effect will saturate) at field much larger than those associated with hfc processes.

We have now identified the most important intersystem crossing mechanisms for triplet radical pairs and seen how application of external magnetic fields can interfere with these processes. It is the net influence of the perturbation of radical pair intersystem crossing by external fields that is the ultimate source of magnetic field effects.

## 1.5 Purpose of the Thesis.

Research on the effects of magnetic fields on the behaviour of radical pairs has been carried out for about 15 years. In that time the major themes of this area of radical chemistry seem to have been elucidated. In particular models are available to explain why external fields can influence the product yields and kinetics of reactions which proceed through the intermediacy of radical pairs. It is thus possible to predict under what conditions one might expect to see a magnetic field effect on a chemical reaction. In spite of this insight there are are some areas which remain relatively unexplored.

Most of the radical pair systems studied have involved carbon centered radicals. Only in the past few years have reports of systems containing heavy atoms started to appear. The effects of heavy atom substitution on radical pair behaviour are still unclear. For example, some authors report that heavy atoms have no influence on radical pair kinetics but do affect product yields. Others suggest that heavy atoms affect both yields and kinetics (see Chapter 2).

The effects of changes in micellar structure have also received scant attention. In other words, can changes in the microenvironment experienced by the radical pair influence its reactivity and, if so, in what manner? A related question arises from recent reports by Turro [94] and Steiner [44], as well as earlier reports by Hayashi [83], who have questioned the widely held belief that intersystem crossing controls the decay of triplet radical pairs in the absence of applied fields. These authors suggest

that diffusion rather than intersystem crossing may be rate controlling in some cases. Studying the kinetics of a triplet radical pair under conditions where the diffusion characteristics change may help decide this question.

Finally the majority of magnetic field effect studies on the behaviour of triplet radical pairs in micellar solution have involved neutral pairs. The number of reports investigating radical ion pair systems are relatively few. Of these most are concerned with radical cation–radical anion pairs while a few have examined the characteristics of a neutral radical–radical cation pair. To the best of our knowledge none examine radical ion pairs containing like–charged species.

With these issues in mind we have undertaken a study of two different radical pair systems. The first is the neutral radical pair formed upon hydrogen abstraction from phenols, ArOH, by the n–butyrophenone $n\pi^*$ triplet state, $PhCOC_3H_7^*$,

$$PhCOC_3H_7^* + ArOH \longrightarrow 3[PhC^{\bullet}(OH)C_3H_7 , ArO^{\bullet}] \qquad (1.21)$$

The second system involves the triplet radical cation pair formed via photoinduced electron transfer from the triplet state of α–terthienyl (αT) to methylviologen ($MV^{+2}$). This process is summarized in reaction 1.22. In these two reactions the square brackets refer to the solvent or to the micellar cage. They will be used to represent cage throughout this thesis with the exception of also being used to represent concentration. However the meaning should be clear from the context in any given instance.

$$\alpha T^* + MV^{+2} \longrightarrow \alpha T^{+\bullet} + MV^{+\bullet} \qquad (1.22)$$

The structures of αT and $MV^{+2}$ are given below.

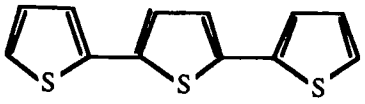

αT

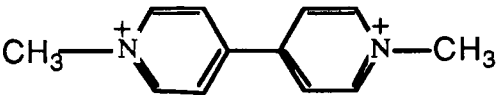

$MV^{+2}$

At the outset of this research project it was hoped that a detailed kinetic study of these radical pair systems, both in homogeneous and micellar solutions, would help clarify or expand the understanding of some of the areas of radical pair chemistry noted above. The results of these studies are the main topic of this thesis.

# CHAPTER 2. A SURVEY OF MAGNETIC FIELD EFFECTS ON RADICAL PAIR CHEMISTRY.

## 2.1 General comments.

The first reliable reports of magnetic field effects on radical pair reactivity appeared in 1973 [95, 96]. Since that time a large body of literature has developed. Studies have investigated the influence of fields on singlet and triplet neutral radical and radical ion pairs both in homogeneous and heterogeneous environments. These investigations have made use of products studies and time resolved techniques. One report has appeared relating to the kinetics of a singlet radical pair in reversed micelles [97]. Reviews of the earlier literature (pre–1980), especially in homogeneous solution, are available [32, 74–76]. Turro has written several reviews covering primarily his own work on the behavior of micellized triplet radical pairs [39, 98–100] as well as that of other workers [9, 76]. Several reviews have also appeared summarizing the work of Tanimoto and Itoh [81], Hayashi [101, 102] and other Japanese workers [103] on magnetic field effects involving triplet pairs in homogeneous and micellar solution. Field effect experiments with a biological flavor have been summarized by Schulten [104, 105]. Finally, a very comprehensive review of magnetic field and isotope effects covering reactions in the gas, liquid and solid phases as well as in micelles has appeared recently. [106]

Since 1980 homogeneous solution work has followed several different paths. Steiner's group has investigated weak magnetic field effects on the thionine radical–substituted aniline radical cation system in polar solvents [107–109] and attributed their findings to intersystem crossing in a proposed triplet exciplex. Weller and coworkers have examined the influence of fields on the yield of triplet pyrene formed via electron transfer quenching of pyrene singlet by amines [79, 110–112] while in related studies

the magnetic field modulation of the pyrene–amine exciplex fluorescence was monitored [112, 113]. All of these latter systems exhibit modest magnetic field effects (5 to 15%) in polar solvents and all were interpreted in terms of the hfc mechanism.

The product yields afforded by thermal and photodecomposition [114] of peroxides in alkane solvents have been reported to be weakly magnetic field dependent. These effects were assigned to the hfc and $\Delta g$ mechanisms, respectively.

Hata and coworkers have published several studies of magnetic field effects on the product yields arising from photolysis of isoquinoline–N–oxides and 4–methyl–2–quioline carbonitrile in alcohols [115–118]. Their results were explained in terms of a $T_+$ –> S level crossing process.

Finally Levin, Kuz'min and Bagdasar'yan [89, 119–124] have studied external field effects on the product yield and kinetics of the photoreduction of carbonyl triplets in viscous solvents. At low fields the observed effects were assigned to the hfc process while at high fields spin–relaxation, possibly dominated by spin–orbit coupling, was invoked. In one report the decarbonylation of DBK in glycerol was examined and the observed magnetic field effect was attributed to hfc. We will consider homogeneous systems in no further detail.

In this chapter we will present examples from the post–1979 literature of magnetic field effects on radical pair reactivity which have been interpreted in terms of the intersystem crossing mechanisms discussed in section 1.4.2. The emphasis will be on triplet radical and radical ion pair behavior in micelles examined by time resolved techniques. Magnetic isotope effects will not be covered and neither will magnetic field effects on triplet biradical reactivity. The magnetic field modulated behavior of these species, which are closely analogous to triplet radical pairs, has been reviewed very recently by Doubleday and Turro [125].

## 2.2 Heterogeneous systems.

The vast majority of radical pair magnetic field effects reported in heterogeneous environments have been in micellar systems. Several exceptions exist. In particular there have been a number of studies of the influence of external fileds on the radical ion pair formed upon photochemical electron transfer in the photosynthetic reaction center [126–130]. Recombination of a radical ion pair at the interface of a bilayer membrane has also been reported to be magnetic field sensitive[131]. Certain polymer systems also exhibit magnetic field effects [132–135] as does dibenzylketone in Nafion membranes [136]. Finally, there have been several examinations of magnetic field modulation of the products formed upon photolysis of aromatic ketones adsorbed on porous surfaces such as silica. This work has been reviewed recently [137].

Micelles have been popular microreactors for use in magnetic field studies for a number of reasons. Not only do they readily solubilize most organic reagents, they also provide a confining environment which permits competition between geminate reaction (typically taken to be intersystem crossing controlled in the literature) and exit of the radical pair. Micelles are also sufficiently voluminous that intramicellar diffusion can lead to radical pair separations at which the exchange interaction becomes very small. The driving force for the separation process is the diffusional motion of the individual radicals. Finally, micelles tend to dramatically enhance the degree of the magnetic field effects observed. This occurs because of the barrier to exit presented by the micelle–water interface. A larger fraction of triplet radical pairs will undergo geminate reaction rather than exit in micelles as compared to homogeneous solution.

It is the purpose of this section to review the literature relating to magnetic field effects on micellized triplet radical pairs. In order to make this examination more manageable the literature will be divided into three subsections: neutral radical pairs containing no heavy atoms; heavy atom systems; systems involving radical ions.

2.2.1. Neutral radical pairs containing no heavy atoms.

Perhaps the most widely known example of magnetic field effects on the behavior of radical pairs in a micellar environment is the work of Turro on substituted DBKs. As we have seen in section 1.3.2, photolysis of an unsymmetric DBK, ACOB, leads to products AA, AB, BB in 1:2:1 ratios in homogeneous solution. This corresponds to no cage effect. In cetyltrimethylammonium chloride (CTAC) the % cage reaction leading to AB is between 35 and 50% in the Earth's magnetic field. The situation is much different at higher magnetic fields. Table 2.1 presents selected data from Turro's work on substituted DBKs in CTAC. In every case the extent of the cage reaction, as judged by the yield of in cage products, was decreased in the presence of an applied field. In these systems the field effect saturated by about 500G ($H_{1/2}$ ~ 200G for DBK itself). These results were interpreted in the context of the hfc mechanism [48] and of Scheme 2.1. After decarbonylation of the initially formed benzoyl–benzyl triplet radical pair, a benzyl pair is formed. This can either intersystem cross to the singlet and ultimately yield the geminate product AB, or it can undergo exit processes to give radicals which recombine randomly. The magnetic field causes Zeeman splitting of the triplet sublevels of the benzyl radical pair thus enhancing exit and reducing the yield of AB.

A magnetic field effect on the recombination kinetics of the benzyl radical pair/micelle system has also been reported [56].

Table 2.1. Benzyl radical pair geminate recombination efficiency (cage effect) as measured in 0.05M CTAC[a].

| Ketone | %Cage Effect | |
|---|---|---|
| | 0 G | 13 kG |
| DBK | 31±1 | 16±1 |
| 4–MeDBK | 52±1 | 31±1 |
| 4–ClDBK | 52±1 | 30±0.6 |
| 4,4'–diMeDBK | 59±1 | 31±2 |

a) Data from reference [56].

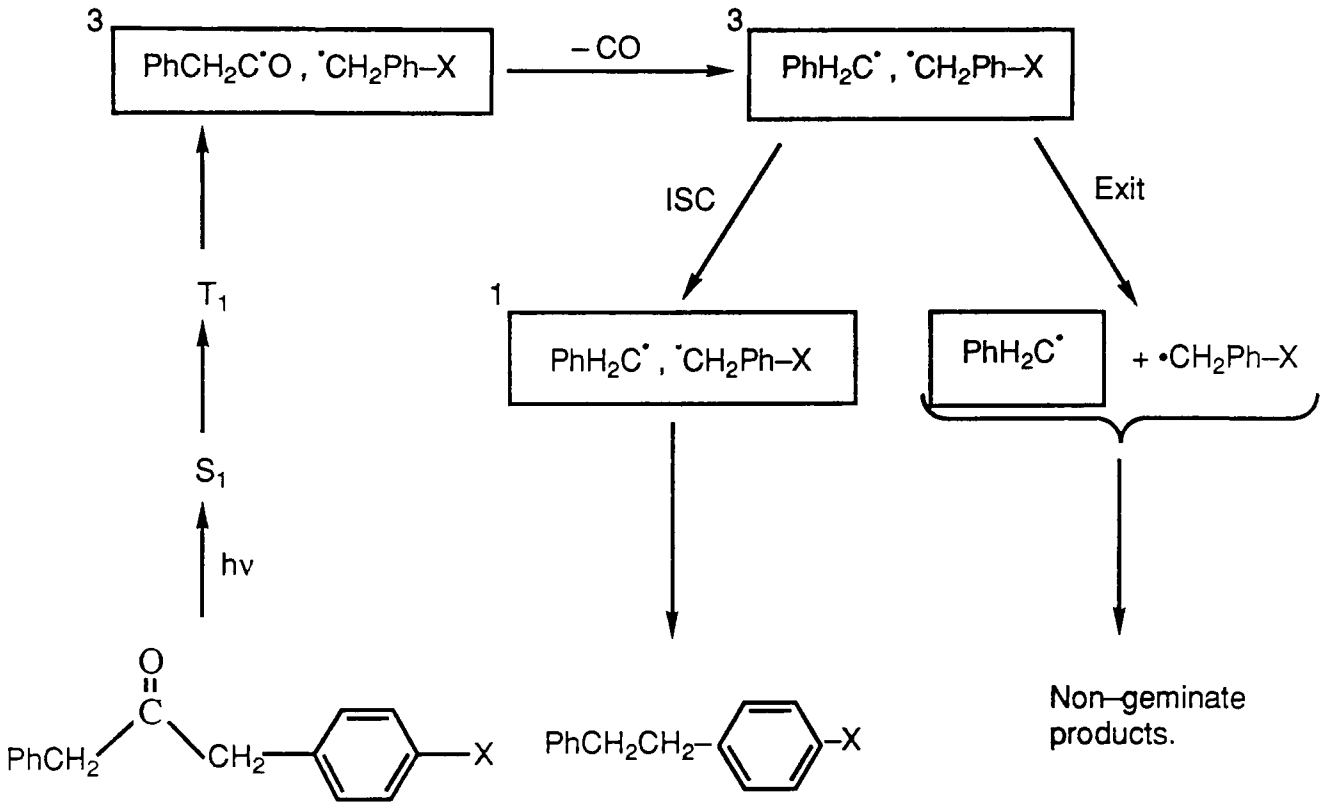
3
PhCH2C•O , •CH2Ph–X
– CO
3
PhH2C• , •CH2Ph–X
ISC
Exit
T1
1
PhH2C• , •CH2Ph–X
PhH2C•
+ •CH2Ph–X
S1
hv
O
C
PhCH2
CH2
X
PhCH2CH2–
–X
Non–geminate
products.

Scheme 2.1.

In particular, the observed decay of the benzyl radical absorption at 320nm in CTAC is biphasic as measured by laser flash photolysis. The observed rate constant for the fast decay component was found to be magnetic field dependent decreasing from $2.5x10^6s^{-1}$ at zero field to $1.4x10^6s_{-1}$ at 400G. The slow decay component was field independent. Furthermore, the fraction of the total benzyl signal represented by the slow component increased markedly at high fields. The kinetic effect was interpreted as a decrease in the rate of benzyl triplet radical pair intersystem crossing although the rate constant measured was not $k_{gem}$ but rather $k_{obs} = k_{gem} + k-$. The increased contribution from the slow decay process reflects the increased amount of exit from the micellar cage. These results are also consistent with Scheme 2.1.

In addition to their DBK work, Turro's group has reported magnetic field effects on other ketone systems. For example diastereomeric 2,4–diphenylpentan–3–ones exhibit a significant field effect on product yields in CTAC and SDS [62] due to the intermediacy of $PhCH_3CHC^{\bullet}O/PhCH_3HC^{\bullet}$ and $PhCH_3HC^{\bullet}/PhCH_3HC^{\bullet}$ radical pairs. The yield of the isomerized product was field dependent and based on its concentration the cage effect for this system in CTAC dropped from 71% at zero field to 52% at 3kG. A similar decrease was observed in SDS. These results were explained in terms of a scheme resembling Scheme 2.1 and in terms of the hfc mechanism.

Photofragmentation reactions have also revealed a magnetic field dependence in micellar media. Triplet deoxybenzoin underwent α–cleavage to give a geminate benzyl–cumyl triplet radical pair. In CTAC and SDS the %cage decreased when a field was applied. This was judged by the yields of the in cage products [56]. The effect saturated by 400G ($H_{1/2}$ ~ 120G) and thus it to was assigned to a hfc process.

Turro's group has also reported magnetic field effects on the emulsion polymerization of styrene using DBK as a photochemical initiator [10, 59, 138–140] The molecular weight of the product polystyrene increased by a factor of 5 on increasing

the field strength from zero to 1kG. The effect reached half its saturation value at about 300G which was taken to indicate the importance of hfc.

In contrast to Turro's work which has focussed mainly on product studies, that of the Hayashi group has been concerned with the effects of magnetic fields on radical pair kinetics. The early work of this group examined the photochemistry of DBK, benzophenone and substituted benzophenones in SDS [51–53, 67, 82, 101]. We will consider the benzophenone results in some detail. No magnetic field effects were observed with these ketones in the presence of hydrogen donors in homogeneous solvent.

Solutions of benzophenone ($1x10^{-3}$M) in 0.08M SDS were irradiated with 5ns pulses of a Nd:YAG laser emitting at 266nm. The time dependence of the transient absorption intensity was measured at both 325 and 525nm. The kinetic behavior was interpreted in the context of the following scheme

$$K \xrightarrow{h\nu,\ ISC} {}^3K^{\bullet} \qquad (2.1a)$$

$${}^3K^{\bullet} + RH \longrightarrow {}^3[KH^{\bullet}, R^{\bullet}] \qquad (2.1b)$$

$${}^3[KH^{\bullet}, R^{\bullet}] \longrightarrow {}^1[KH^{\bullet}, R^{\bullet}] \qquad (2.1c)$$

$${}^{3,1}[KH^{\bullet}, R^{\bullet}] \longrightarrow KH^{\bullet} + R^{\bullet} \qquad (2.1d)$$

$${}^1[KH^{\bullet}, R^{\bullet}] \longrightarrow \text{Geminate Products} \qquad (2.1e)$$

where RH is the surfactant., K represents benzophenone, $KH^{\bullet}$ is the benzophenone ketyl and $R^{\bullet}$ is the surfactant radical. At 325nm the extinction coefficient of ${}^3K^{\bullet}$ and $KH^{\bullet}$ are both significant with that of the latter being larger. At 525nm the situation is reversed. At 325nm in SDS a triphasic kinetic trace was observed. An initial growth period of about 150ns duration was followed by a rapid decay which was followed by a long lived component that was practically constant on the time scale of the experiment (about 5μs). The growth at 325nm was attributed to formation of the triplet

radical pair, $^3[KH^\bullet , R^\bullet]$, via reaction 2.1b. The rapid decay was assigned to decay of the triplet radical pair via reactions 2.1c and 2.1d while the long lived component was associated with the escape of the ketyl radical from the micellar environment (2.1d). Because of the complex triphasic behavior at 325nm all quantitative kinetic results were obtained at the longer wavelength.

At 525nm no growth was observed. The rapid initial decay could be fit to a first order kinetic expression yielding rate constant $k_{obs} = 2.82x10^6 s^{-1}$ at zero field. This decreased to $1.89x10^6 s^{-1}$ at 700G. The fast component was assigned to the decay of the triplet radical pair as before and the slow component to the decay of escaping ketyl radicals. In the initial report of this work [53] the decay of the triplet radical pair was concluded to be intersystem crossing controlled but in a later paper diffusion was said to be the rate limiting factor [83]. In addition the %escape increased from 40% at zero field to nearly 70% at 700G with no sign of saturation. In fact the magnetic field effect on this system was later reported to not saturate until close to 10kG [83]. In light of these results, Hayashi et al. have invoked the spin–relaxation mechanism to explain their observations [53, 83, 84]

Hayashi's benzophenone results have been criticized by Scaiano [54, 55] who points out that even at 525nm the kinetics of the benzophenone/SDS system are complicated by extensive overlap of the $^3K^*$ and $KH^\bullet$ signals both in time and in wavelength. Using kinetic data obtained at 540nm (the $\lambda_{max}$ of $KH^\bullet$) and 600nm (a wavelength where $KH^\bullet$ is transparent but $^3K^*$ is not) Scaiano was able to deconvolute the kinetic behavior of $KH^\bullet$ from that of $^3K^*$ for the benzophenone/SDS system [55]. This showed that while $KH^\bullet$ is formed in good yield, it is also formed over a rather long period of time (~0.5μs) which is consistent with Hayashi's own observations at 325nm. In addition the triplet lifetime under these conditions was about 320ns. Since the triplet absorbs significantly at 525nm, where Hayashi was attempting to monitor the ketyl, it is clear that the triplet will make a substantial contribution to the absorption observed at

this latter wavelength. Thus not only will the decay kinetics of the radical pair be distorted by the slow formation of the pair but the triplet optical density at 525nm can be expected to contribute to the apparent %escape resulting in a too large value of this quantity. These considerations lead one to the conclusion that Hayashi's rate constants must be viewed with some skepticism in this case.

Hayashi's DBK results [53, 67] were qualitatively similar to those of Turro. Although the observed rate constant for the fast component decreased with increasing field strength the authors did not report values of $k_{gem}$. The % escape, based on the measured yield of escaping benzyl radical monitored at 320nm, was found to follow a typical hfc pattern. The effect saturated at about 150G.

Hayashi's group has also reported magnetic field effects on the kinetic behavior of the triplet radical pair formed via hydrogen abstraction from SDS by the triplet states of naphthoquinones [85, 86, 141]. As was the case with the benzophenone system the observed magnetic field effects did not saturate until rather high fields (~10kG) had been obtained. The value of $k_{obs}$ was $4.7 \times 10^6 s^{-1}$ at zero field for 1,4–naphthoquinone and $4.1 \times 10^6 s^{-1}$ for 2–methyl–1,4–naphthoquinone. At 13.4kG the values were $0.5 \times 10^6$ and $0.6 \times 10^6 s^{-1}$, respectively. The zero field rate constants were concluded to reflect a combination of diffusion controlled formation of products (i.e., intersystem crossing faster than diffusion) and exit. The results were interpreted within the context of the spin–relaxation model. Finally, as was the case with the benzophenone/SDS system, it is not clear that the formation of the triplet radical pair was rapid compared to its rate of decay.

Scaiano and coworkers have also examined the behavior of micellized triplet radical pairs formed via photoreduction of triplet ketones–benzophenones in particular[54, 55, 69]. Nitrogen laser excitation of SDS or CTAC solutions of $1.6 \times 10^{-3}$ M benzophenone and 0.032M 1,4–cyclohexadiene led to a readily detected transient absorption at 540nm due to the benzophenone ketyl. As we saw in Chapter 1 the

kinetic analysis of this group permitted the zero field observed rate constant of the fast decay component to be separated into rate constants representing the two radical pair decay pathways; geminate recombination ($k_{gem}$), and exit (k–). The same analysis applies at high fields.

Using this approach Scaiano et al. have reported field effects on the decay of the triplet benzophenone ketyl–cyclohexadienyl (KH–CHD) radical pair in SDS and several other surfactants. These effects had saturated by 1kG in the case of SDS and by 2kG in the cases of CTAC and CTAB. $H_{1/2}$ ~ 400G in both CTAC and CTAB. The data were interpreted in terms of the hfc mechanism. Some representative data are given in Table 2.2.

The data of Table 2.2 are indicative of several things. First of all the increase in % escape at high field reflects the increased importance of radical escape from the micellar super cage at high fields. The value of k– in SDS is very close to the exit rate constants for 1,3–cyclohexadiene and benzene from the same micelle. Thus the k– values suggest that the bulk of the exiting radicals are of the cyclohexadienyl type.

The $k_{gem}$ values in SDS and CTAC agree with intersystem crossing rate constants reported for triplet biradicals containing similar radical centers. In addition $k_{obs}$ is essentially the same at zero and 2kG. Since k– should be field independent $k_{gem}$ must also have the same value at zero and 2kG. This was interpreted as reflecting complete shut off of $T_{\pm}$ –> S intersystem crossing at about 2kG while $T_0$ –> S intersystem crossing remains unaffected. This is consistent with hfc being the source of the observed magnetic field effects since at the moderate fields required for this mechanism to be effective the $\Delta g$ mechanism, which would change the rate of $T_0$ –> S, should be unimportant.

Another interesting point is that the $k_{gem}$ and k– values in SDS and DTAC were substantially larger than in the more voluminous CTAC and CTAB. A similar effect has been reported by Ulrich and Steiner for the triplet thionine radical–aniline radical

cation pair in reverse micelles [142]. This data suggests that there may be a relationship between these rate constants and the spatial properties of the micelle.

Data from Turro's group also indicates that there may be a relationship between micellar dimension and radical pair behavior. They have reported a positive correlation between the DBK cage effect and the alkyl chain length of sodium–n–alkyl sulfate micelles [48, 143]. In addition k– for benzyl radicals decreased as micellar volume increased [143]. These results were interpreted to mean that in large micelles the escape efficiency is reduced and/or the rate of geminate reaction is enhanced which in turn leads to an increased cage effect.

In a variation of their studies of the benzophenone/1,4–CHD system, Scaiano et al. have reported magnetic field effects on the decay kinetics of the $Ph_2HC^{\bullet}$–CHD triplet radical pair [69]. In this case the pair was formed via hydrogen abstraction from the diene by triplet diphenylcarbene following 308nm irradiation of diphenyldiazomethane in an oil in water microemulsion. The observation of a large field effect here provided direct evidence for the triplet nature of the radical pair and, by spin conservation, for the triplet nature of the carbene.

Fendler and coworkers have also reported a unique variation on the triplet benzophenone/cyclohexadiene in organized systems theme [144, 145]. The reaction was carried out in vesicles containing $Fe_3O_4$ particles. Variation of the concentration of these particles was shown to be equivalent to the variation of an external magnetic field. The escape fraction could be increased from 55% in the absence of the magnetic particles to a maximum of 86% in the presence of $Fe_3O_4$.

Tanimoto and Itoh have also investigated the behavior of a number of triplet radical pairs generated in micellar media upon photoreduction of carbonyl triplets by

Table 2.2. Kinetic and escape data for the benzophenone ketyl–cyclohexadienyl triplet radical pair in various micelles.[a]

| Surfactant | H kG | kgem $x10^6\ s^{-1}$ | k– | % escape |
|---|---|---|---|---|
| SDS | 0 | 5.8 | 4.4 | 43 |
| | 2 | | | 73 |
| CTAC | 0 | 1.4 | 1.9 | 55 |
| | 2 | | | 81 |
| CTAB | 0 | 0.9 | 1.3 | 61 |
| | 2 | | | 83 |
| DTAB | 0 | 10.1 | 4.9 | 33 |
| | 2 | | | 60 |

(a) Data from [54, 55].

hydrogen donor additives. Most of this work was done using laser flash transient absorption and it has been recently reviewed [81]. The magnetic field effects observed with each of the twenty individual systems studied by this group have been attributed to the hfc mechanism. Here we will restrict ourselves to a detailed examination of only one of these systems–the photoreduction of xanthone (XO) by xanthene (XH) in SDS [58, 146, 147].

Upon irradiation of XO in the presence of XH in SDS the xanthone ketyl (XOH)–9–xanthenyl (X) triplet radical pair is formed. The in cage product is the adduct of these radicals, XOH–X, while the escape processes can lead to regeneration of the XO and XH as well as the dimers $X_2$ and $(XOH)_2$. The relative quantum yield of XO disappearance was measured and found to decrease by about 25% between zero and 1kG. Over the same field range the in cage photoadduct yield was found to drop by about 10% while the dimer yields increased. At high fields escape is enhanced and so is regeneration of XO. This results in an apparent decrease in the quantum yield of XO loss as well as in an increase in the amount of dimer formed. Similarly intersystem crossing is inhibited at high field leading to a reduction in the yield of XOH–X.

Upon 337nm irradiation of $5x10^{-5}$M XO in SDS in the presence of $1x10^{-3}$M XH a transient absorption signal is observed at 345nm which can be attributed to X. The decay of this signal is magnetic field dependent. At zero field it was biphasic. The decay data was analyzed in terms of a scheme similar to that of Scheme 1.2. The observed fast decay rate constant was separated into $k_{gem}$ and k– using Scaiano's technique. At zero field $k_{gem} = 1.4x10^6 s^{-1}$ while at 640G $k_{gem} = 0.4x10^6 s^{-1}$. k–, which was field independent, was found to be $0.2x10^6 s^{-1}$. The magnetic field effect on $k_{gem}$ saturated by ~600G while the variation of the disappearance quantum yield of XO saturated by ~500G. Thus, the observed effects were attributed to the hfc mechanism. It should be noted that the X transient absorption signals reported in this study [146] clearly show a growth period. While at zero field X decays with an observed lifetime of

about 590ns the formation of X requires nearly 200ns to reach completion. This leads to unreliable estimates of % escape and therefore of $k_{gem}$ and k–.

Levin's and Kuz'min's group has also studied the photoreduction of carbonyl triplets in micellar solution [148–152] using laser flash photolysis. In these studies simple phenols were used as hydrogen donors while the carbonyl compound was either a 1,4–quinone or a benzophenone. In all cases the concentration of hydrogen donor was adjusted so that the triplet carbonyl lifetime was ≤ 10ns. For systems containing no heavy atoms the % escape at zero field did not exceed 30% but no high field values for this quantity were reported. The authors observed decay rate constants on the order of $1–6x10^6 s^{-1}$ at zero field based on the transient decay of either the phenoxyl or ketyl radical absorption. The observed zero field rate constants were interpreted as being diffusion controlled. The most pronounced magnetic field effects on the observed kinetics occurred between zero and 1kG but the observed rate constant continued to decrease with field strength up to 3kG. These results were interpreted in terms of a combined hfc (at low field) and spin–relaxation (at high field) process. When heavy atoms were included spin–orbit coupling effects were hypothesized (*vide infra*).

The effects of variation in micellar size were also studied by this group [149, 151]. Micellar volume was adjusted either by adding NaCl or by changing the alkyl chain length of the surfactant. The radical pair studied was the 1,4–benzosemiquinone/4–phenylphenoxyl pair. The observed zero field decay rate constant in SDS decreased with increasing NaCl concentrations between zero and 0.5M. At 0.5M there was a change of slope and the rate constant became independent of salt concentration.This was interpreted in terms of growth of the micelle with added salt. As the salt concentration increases the frequency of radical reencounter was said to decrease because of the increased micellar volume. Since the rate constant is taken to be diffusion controlled it also decreases.

The zero field recombination rate constants were observed to decrease with increasing surfactant alkyl chain length. This was also attributed to a reduction in radical reencounter in the larger micelles. These latter results agree qualitatively with those of Scaiano [54, 55] and Steiner [142].

It is worthwhile noting at this point that Levin's and Kuz'min's data [148–152] is open to some criticism. In particular the rate constants they call the recombination rate constants are in fact values of $k_{obs}$. That is they take $k_{gem} + k-$ as a value for $k_{gem}$ alone. This would be acceptable if the % escape were very small since it would indicate that escape processes make a negligible contribution to radical pair decay. However the authors clearly state that "the fraction of radicals going into the [aqueous] volume does not exceed 30%, and that $k_{obs}$ is thus basically determined by the value of $k_{rec}$.". $k_{rec}$ is their symbol for the recombination rate constant.

We have now examined in some detail data relating to magnetic field effects on the decay of neutral triplet radical pairs containing no heavy atoms. The majority of these systems involve a ketyl radical as one partner of the radical pair and the geminate recombination rate constants observed generally fall between $1x10^6$ and $6x10^6 s^{-1}$. In spite of the similarities of their results a number of conflicting views have come out of these studies.

While many of the results have been interpreted in terms of the hfc mechanism (i.e., Turro's, Scaiano's, Tanimoto's and Itoh's data representing some 25 distinct systems) it is clear that there is not a consensus as to the origin of field effects in systems of this type. In addition some authors contend that the zero field value of $k_{gem}$ is intersystem crossing controlled (see also reviews by Atkins [74] and Buchachenko[75]) while others hold that it is diffusion controlled. Finally, it seems that there are several cases in which conclusions based on kinetic data are open to criticism either because the rate of radical pair formation is too slow or because the reported rate constants are

values of $k_{obs}$ rather than of $k_{gem}$. We will leave these points unresolved and now examine triplet radical pairs containing heavy atoms.

2.2.2. Systems involving heavy atoms.

In an interesting extension of their naphthoquinone work Hayashi et al. have measured the kinetics and escape characteristics of this system in the presence of lanthanide ions [86]. The exit fraction at high field decreased as the concentration of paramagnetic ion increased. No effect on the zero field radical pair kinetics was observed up to 2mM ion. This external heavy atom effect was attributed to enhanced rates of $T_{\pm} \rightarrow T_0$ relaxation in the presence of the lanthanides. Turro [153] has reported corresponding behavior on the high field cage effect for DBK in the presence of lanthanides.

Kuz'min and Levin have examined the effect of $O_2$ and nitroxyl radicals on the kinetics of the 2,6–diphenyl–1,4–benzosemiquinone/4–phenylphenoxyl pair in SDS[150]. The observed rate constant ($k_{obs}$) increased with increasing concentration of paramagnetic species up to a certain point after which the rate constant no longer varied. At this quencher concentration $k_{obs}$ was also found to be field independent. These results were also explained in terms of enhanced spin–relaxation between triplet sublevels at high fields.

Systems involving internal heavy atoms have been examined by Hayashi and coworkers [87, 88, 154]. Germyl–ketyl triplet radical pairs formed via hydrogen abstraction from triethylgermane by xanthone in SDS are subject to weak magnetic field effects [154]. The decay kinetics were monitored by laser flash photolysis. For fields between zero and 10kG the value of $k_{obs}$ decreased only slightly (by a factor of 1.09) for the xanthone system. The escape fractions were also rather insensitive to the field strength. The % escape increased from 18% at zero field to 23% at 10kG. When acetophenone was used no magnetic field effects were observed. One should

compare these results with those reported for the benzophenone/SDS system mentioned previously. The reduction of the magnetic field effect in the case of the germyl system was again attributed to enhanced spin–relaxation in the presence of the heavy atom. It is worth noting, however, that the data presented in this paper clearly shows that the requirement of rapid radical pair formation is not fulfilled.

Similar, very modest magnetic field effects are observed for benzoylmethyl–benzenesulfonyl and 2,4,6–trimethyl–diphenylphosphonyl triplet radical pairs in SDS [87, 88].

A reduction in the effects of a magnetic field on the escape fraction of DBK has been reported when the ketone is substituted with bromine [48, 155]. The cage effect for 4–ClDBK in SDS was found to be 52±3%, 31±1% and 37±1% at zero, 13.5 and 145kG, respectively. The corresponding cage effects for 4–BrDBK at the same field strengths were 58±4%, 58±4% and 57±1%. The trend in the 4–ClDBK data was interpreted in terms of the $\Delta g$ mechanism. The increase in the %exit at very high fields reflects enhanced intersystem crossing due to the relatively large $\Delta g$ value of the benzyl/4–chlorobenzyl pair. In spite of a $\Delta g$ value which is nearly 4 times that of the 4–ClDBK system, 4–BrDBK shows no magnetic field effect at all. Spin–orbit coupling dominated intersystem crossing was invoked to explain this result.

Levin and Kuz'min have also examined internal heavy atom effects on triplet radical pairs in micelles [151, 152, 156]. Three systems were studied: benzophenones with 4–phenylphenol; 2,6–diphenyl–1,4–benzoquinone with 4–phenylphenol; benzophenones with 4–phenylanilines. In the latter case irradiation led initially to a triplet ketyl radical anion–aniline radical cation pair. These experiments were carried out in the presence of 0.01N HCl so that rapid protonation of the ketyl anion to give the neutral ketyl is favoured. The systems were studied using laser flash photolysis and values of $k_{obs}$ rather than of $k_{gem}$ were reported.

Applied fields reduced the value of $k_{obs}$ from that measured at zero field. In both benzophenone systems substitution with Cl or Br increases the zero field value of $k_{obs}$ and decreases the magnitude of the magnetic field effect on the rate constant compared to the light atom systems. These changes are most pronounced with the bromo–systems. The authors explain these effects as follows. At zero field $k_{obs} \sim k_{gem}$ and $k_{gem}$ is diffusion controlled. Thus $k_{gem} = k_{diff}/4$ where $k_{diff}$ is the diffusion controlled rate constant in the micellar environment. The increase in $k_{obs}$ upon heavy atom substitution is suggested to reflect a spin–orbit coupling (SOC) induced intersystem crossing channel which is open to radical pairs which are at separations corresponding to a (triplet) collision complex. The rate constant for geminate recombination at zero field now includes a term incorporating the probability of successful T –> S intersystem crossing in the collision complex, $P_{TS}$. So, $k_{gem} = (k_{diff}/4 + 3/4P_{TS})$. In the absence of heavy atoms substantial magnetic field effects on $k_{gem}$ arise because of the inhibition of hfc mediated T± –> S intersystem crossing at low fields and reduction of spin–relaxation rates at high fields. Levin and Kuz'min propose that, at high fields, the SOC rate constant for T –> S intersystem crossing in the collision complex is substantially higher than the relaxation rate constant in the radical pair for systems containing heavy atoms. Furthermore the rate of SOC transitions should be rather insensitive to applied fields because of the large exchange interaction in the collision complex. Thus light atom systems, for which collision complex SOC induced intersystem crossing is not important, will exhibit large magnetic field effects while heavy atom systems, in which SOC induced intersystem crossing is more likely, will not. Put another way, $P_{TS}$ is not a function of the field strength while the relaxation rate constants are. The authors are therefore proposing that intersystem crossing of collision complexes (or contact radical pairs) plays an important, perhaps dominant, role in heavy atom systems. This is a major departure

from the conventional view of magnetic field effects which tries to interpret the behavior of such systems in terms of true radical pairs (i.e., J–>0).

Steiner et al. [44] have also examined heavy atom effects in micellar solution using laser flash photolysis. The system was the triplet pair formed via electron transfer from halogen substituted anilines to triplet thionine in reverse micelles of cetyldimethylbenzylammonium chloride (CBDA) in benzene. At zero field the observed rate constant was found to be independent of the halogen atom substituent. As expected, bromo–substitution reduced the magnetic field effect on $k_{obs}$. For example, $k_{obs}$ was $3x10^6s^{-1}$, $3.1x10^6s^{-1}$ and $3.4x10^6s^{-1}$ for aniline, m– and p–bromoaniline, respectively, at zero field. At 10kG the observed values for the same three compounds were $0.94x10^6$, $2.1x10^6$ and $3.4x10^6s^{-1}$. In contrast to the bromo–systems the magnetic field effects for p–fluoro– and p–chloroaniline were as large as that for aniline itself. For those systems where % escape was a function of field strength, the magnetic field effect saturated only at fields close to 10kG.

The authors interpreted their results in terms of the relaxation mechanism for radical pairs. In particular, heavy atom substitution enhances the rate of $T_{\pm}$ –> $T_0$, S interconversion at high field thereby suppressing the magnetic field effect on the escape fraction.

We have seen that heavy atom substitution can have dramatic effects on the behavior of micellized triplet radical pairs, particularly at high fields. It is not necessary that the radical electron be localized on the heavy atom to observe such effects. Most of the heavy atom effects reported have been explained in terms of enhanced spin–relaxation due to some unspecified influence of the heavy atom. In addition one group has suggested that SOC is important in a hypothetical collision complex. From this it can be seen that understanding of the effects of heavy atoms on triplet radical pair reactivity is not well understood.

2.2.3. Systems involving radical ions.

There have been relatively few reports of magnetic field effects on systems involving radical ions in micellar solution. Of these we have already touched briefly on the work of Steiner's group and that of Levin and Kuz'min while discussing heavy atom effects. These systems, as well as all the other systems involving micellized radical ion pairs that have appeared in the literature to 1988, are summarized in Table 2.3. It is clear that studies of radical ion pair kinetics in micelles in the presence and absence of magnetic fields is a relatively unexplored area. In addition, there are no examples of a case where both radicals are of the same sign and therefore are both bound to the micellar surface if the micelle carries the opposite charge.

2.2.4. Summary.

Our review of the literature has identified several important points. There are two major schools of thought when it comes to explaining magnetic field effects on the behavior of triplet radical pairs in micelles. These are the hfc school and the spin–relaxation school. While proponents of the hfc mechanism generally hold that geminate recombination is intersystem crossing controlled at zero field, the spin–relaxation group believes that $k_{gem}$ is diffusion controlled in the absence of an applied field. Studies of heavy atom systems have also failed to lead to a consensus of interpretation. While essentially all authors who have studied heavy atom systems reach the conclusion that spin–relaxation is important they often fail to provide more than a phenomenological explanation of their results. In the two cases where a more detailed rationalization is available the proposed models are quite different.

Finally it should be noted that in several cases the kinetic data reported are subject to criticism either because of a failure to take the escape fraction into account or because the rapid formation of the radical pair was not ensured. These failings may in part be the cause of some of the conflicting views in the literature on this subject.

Table 2.3. Magnetic field effects on micellized pairs involving radical ions.

| Acceptor | Donor | Surfactant | Type of Study | Reference |
|---|---|---|---|---|
| Duroquinone ($T_1$) | Diphenyl aniline | SDS | Escape yield | 157 |
| Acetophenone ($T_1$) | Diphenyl aniline | SDS | Kinetics | 158 |
| 2,5–diphenyl benzoquinone ($T_1$) | 4–phenyl aniline | SDS | Kinetics | 148 |
| Thionine ($T_1$) | Aniline | CDBA/$C_6H_6$ | Escape yield<br>Kinetics | 159<br>142 |
| Thionine ($T_1$) | Halo–anilines | CDBA/$C_6H_6$ | Kinetics | 44 |
| Oxonine ($S_1$) | TMPDA[a] | AOT/isooctane | Kinetics | 97 |
| Pyrene ($S_1$) | DMA[b] | SDS | Kinetics | 160 |

(a) N.N'–tetramethyl–p–phenylenediamine.

(b) N,N'–dimethylaniline.

# CHAPTER 3. EXPERIMENTAL.

## 3.1. Instrumentation.

This section will focus primarily on a description of the laser flash photolysis (LFP) system used at the National Research Council of Canada's Sussex Drive laboratories. In addition a brief description of the single photon counting instrument that was used for a few experiments will be presented. Other, more familiar instruments such as the fluorimeter will not be described in detail.

### 3.1.1 The single photon counting instrument.

The system used consisted of components from Photochemical Research Associates (PRA). The excitation source was a low pressure (~0.5 atm) hydrogen lamp (PRA 510B). Lamp triggering was provided by supplying 6kV to one of the lamp's tungsten electrodes through a charging resistor and grounding the other electrode through a HY–2 gating thyratron. The thyratron grid was pulsed at 31kHz. The electrode gap was about 2mm providing a lamp decay profile of about 2ns. The lamp decay profile largely determines the time response limits of the instrument.

Photons from the lamp were converted into electrical signal by the lamp photomultiplier tube (PMT) which is built into the lamp housing. This configuration does away with the need for a beam splitter. The output signal from the lamp PMT was directed into the input of a PRA 1718, 100MHz discriminator which then transmitted a "start" signal to the PRA 1701 time–to–amplitude converter (TAC). The start pulse from the discriminator is generally passed through a delay stage before entering the TAC to ensure that the TAC is operating in its linear range. This start pulse effectively signalled the TAC to initiate its constant ramp voltage sweep.

The remainder of the lamp radiation was directed through an iris and onto the slit of the excitation monochromator (PRA 1280). The latter selected the excitation wavelength (± 2nm). The exciting wavelength so selected then irradiated the sample. Sample emission was collected at $90^0$ relative to the direction of the excitation beam. The emission wavelength(s) detected could be set by use of suitable band pass or cut–off filters. Photons emitted by the sample were focussed on the emission PMT which was housed in, and cooled by, the PRA 1551 thermoelectric refrigeration unit. This cooling system provided improved signal–to–noise by reducing the dark counts at the emission PMT.

The "raw" emission PMT output signal was now transmitted to the TAC via a variable bias amplifier and an adjustable delay stage. These latter components ensured that the entire time scale of the emission decay was observed. The first emitted photon detected by the emission PMT acted as a "stop" prompt terminating the voltage sweep of the TAC. The TAC then output a voltage of an amplitude which is proportional to the time between the start and stop pulses and hence to the temporal emission characteristics of the sample. Thus the TAC voltage ramp is really the heart of the single photon timing experiment.

The TAC output voltage amplitude was next fed into the TN–7200 multichannel analyzer unit (MCA). The analog/digital converter of the MCA converted the TAC voltage signal to a number of clock cycles. Different numbers of clock cycles were assigned different address locations in the MCA memory. When a particular address was generated one event (i.e., one "photon count") was added to the total number of events in that location. By numerous repetitions of this process a histogram of the number of photons emitted at a given time after sample excitation was built up. This histogram is essentially a plot of emission intensity as a function of time.

3.1.2. The laser flash photolysis system.

The LFP system in use at the NRCC consists in fact of two separate systems. One of these, the optical multichannel analyzer (OMA) system, is used exclusively for obtaining transient absorption or luminescence spectra. The other system, which we will call the kinetic system, is used primarily to determine the transient kinetics of reaction intermediates either by absorption or, less frequently, by luminescence detection. The kinetic system can also be used to obtain transient spectra although the procedure is more tedious than is the case with the OMA system. A schematic diagram of the overall system is given in Figure 3.1. In addition to the two nitrogen lasers and the excimer laser indicated, dye laser excitation capabilities are also available.

The kinetic system essentially consists of an excitation source (laser), a monitoring lamp, a monochromator plus PMT detection system and a data capture/processing system. The OMA system consists of an excitation source (laser), a monitoring lamp, a spectrograph, the OMA itself and a data collection/processing system. Both systems are equipped with a series of lenses, filters, mirrors and shutters.

The principle behind LFP is fairly simple and we will consider the kinetic experiment as an illustration. A solution containing a substrate, typically an organic molecule, is irradiated with a nanosecond laser pulse. This results in a relatively high concentration of excited states and/or other transient intermediate species (radicals, for example). Upon excitation the monitoring beam from the lamp is absorbed by the transient according to the Beer–Lambert law. This attenuates the intensity of the monitoring beam and this attenuation is measured by the PMT. The data from a LFP kinetic experiment thus consists of the incident intensity of the monitoring beam, $I_o$, and a set of a few hundred voltage signals as a function of time. These voltage signals are converted to optical density (O.D.) by the relation [161]

$$\Delta O.D. = -\log\left(1 - \frac{Signal}{I_o}\right) \qquad (3.1)$$

Figure 3.2 shows a typical kinetic trace obtained in these studies.

Equation 3.1 illustrates an important difference between transient absorption and conventional ground to excited state absorption. In the former case the concentration and extinction coefficient of the absorbing species are generally not known so only the difference in optical density ($\Delta$O.D.) between the starting materials (substrate) and the transient may be measured. Thus, at monitoring wavelengths where the extinction coefficient of the substrate is larger than that of the transient, a negative signal (bleaching) will be obtained.

We will now give a more detailed description of the kinetic and OMA systems as used in this study. Information relating to the kinetic system is available in the literature 162, 163.

3.1.2.1. The kinetic system.

*The excitation source:*

The samples were excited with the pulses (337.1nm, ~8ns, $\leq$ 10mJ/pulse) from a Molectron UV–24 nitrogen laser. There were in fact two such lasers arranged in "piggy–back" fashion. The upper nitrogen laser was used only for OMA experiments. Less frequently samples were irradiated with the pulses (308nm, ~5ns, up to 80mJ/pulse) from a Lumonics TE860–2 excimer laser operating with Xe–HCl–He mixtures. The pulses were concentrated (but not focussed) on the samples by a combination of spherical and cylindrical lenses as indicated in Figure 3.1. The lasers were pulsed at 1 or 2 Hz. Shutters were placed before the lasers in order to allow continuous pulsing of the lasers without irradiation of the sample with each shot. This regular pulsing leads to very reproducible pulse energies.

*The monitoring/detection system:*

The monitoring system consists of three key elements: a pulsed 200W Xenon lamp with vertical electrodes; a high intensity PRA–B204 monochromator; an RCA–

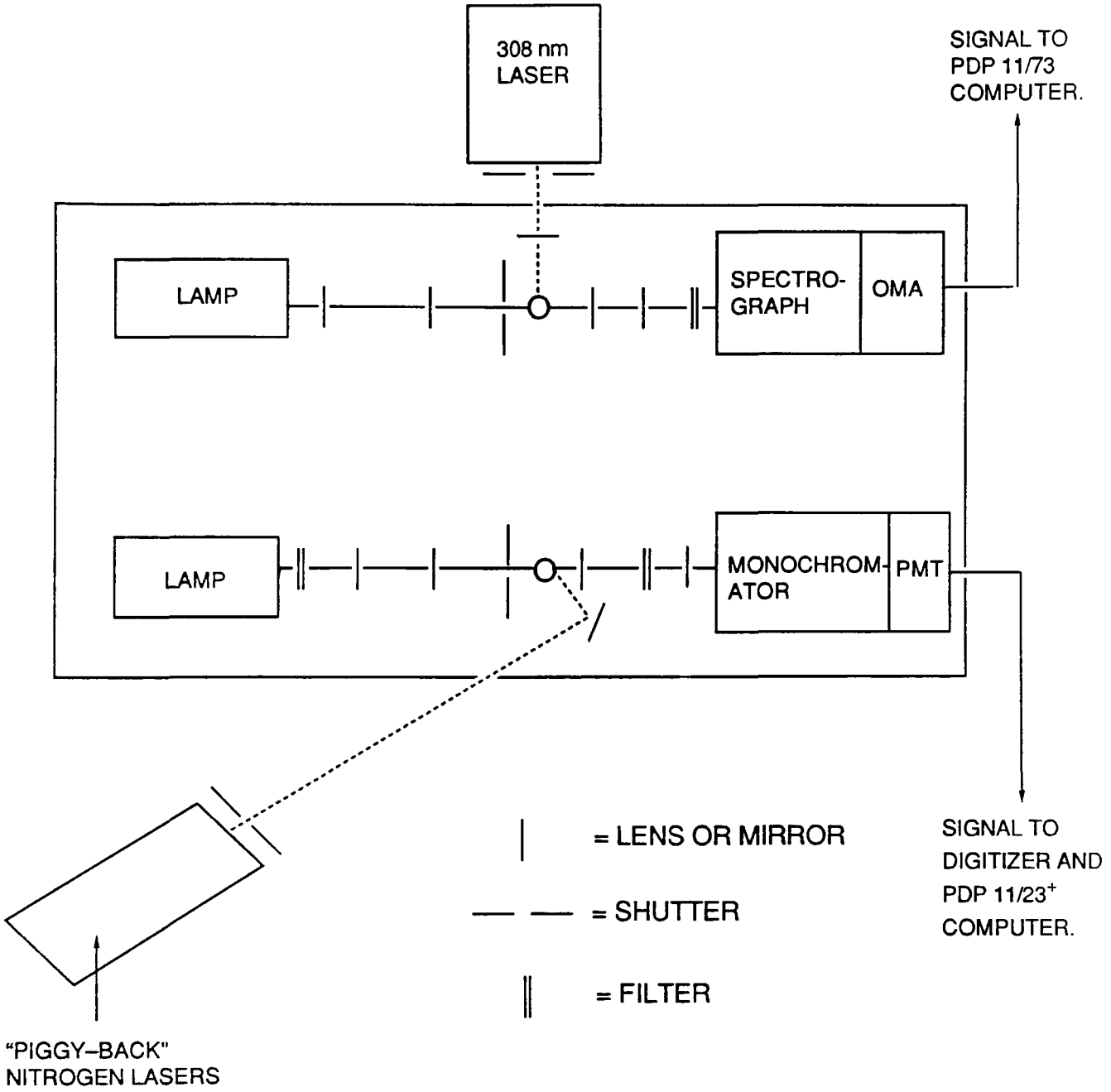


Figure 3.1. Schematic diagram of the NRCC laser flash photolysis system. Filters may be placed in front of lasers if desired.

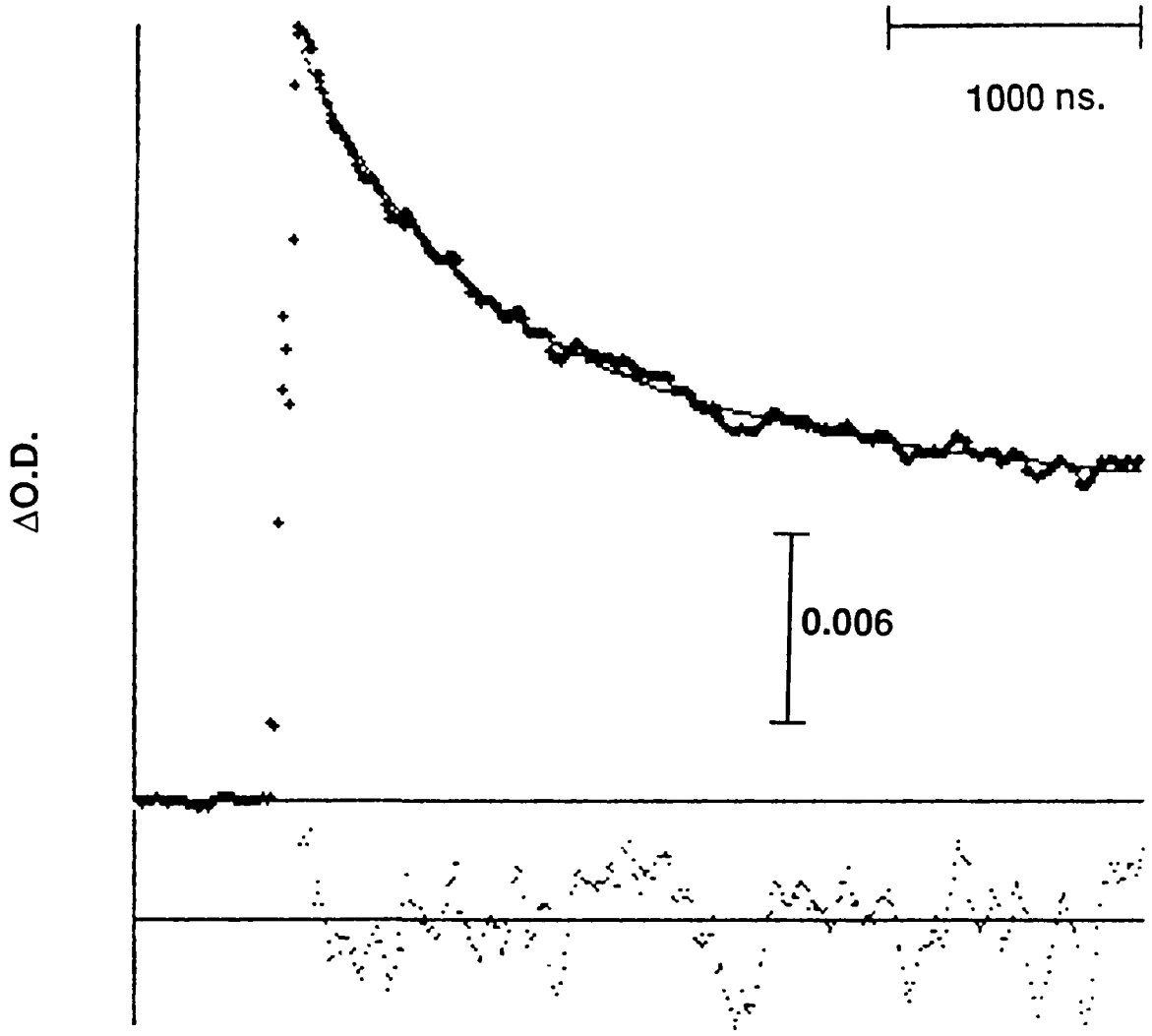


Figure 3.2. Transient decay trace (at 425nm) and fit for $1.5 \times 10^{-3}$M Vitamin E + 0.021M butyrophenone in 0.15M SDS at a magnetic field strength of 1.5kG. The insert shows a plot of the residuals of the fit. Top ΔO,D. = 0.022.

4840 PMT which operates on six dynodes. The PMT was typically terminated into a 93Ω load resistor. The monitoring beam was focussed onto the sample and the transmitted light focussed onto the monochromator slit. The system included cut–off filters to eliminate second order effects in the monochromator and a shutter to minimize irradiation of the sample by the monitoring beam.

The excimer laser beam entered the sample at right angles to the monitoring beam (Figure 3.1). The excimer beam could be directed into either the kinetic or OMA sample holder simply by placing an optical wedge in the laser's path. The angle between the nitrogen laser beam and the monitoring beam was small (~$19^0$). This arrangement gives a higher signal/noise [164] and is well suited for use with lower power excitation sources. In addition this configuration allowed one to change the excitation wavelength without altering the optical set–up.

*Data capture, processing, storage and experimental control:*

PMT output was captured by a R7912–Tektronix transient digitizer containing 4K local memory. A Tektronix 607 storage oscilloscope displayed each trace stored by the digitizer. The digitizer memory was read by a PDP $11/23^+$ computer via a CP–4100/CP bus Tektronix interface. As indicated earlier the raw data is voltage signal as a function of time. The computer converted this to ΔO.D. versus time (equation 3.1) and then stored the data. The decay traces could be transferred to a floppy disk if desired. The computer could recall the data and fit it to either first or second order kinetics. Hard copy facilities were also provided by the computer.

Transient decay signals were typically acquired using 10 (occasionally 20) laser shots per decay. Only five shots per decay were used to generate transient spectra using the kinetic system (vide infra). This form of data acquisition provides better signal/noise because of the averaging effect.

Another technique employed to improve data quality was the use of correction shots. The correction was either of the "background" type or of the "fluorescence" type.

Background correction took care of noise originating in the laser and Xenon lamp, as well as baseline drift due to changes in $I_0$. This was generally applied at longer time scales (≥ 2μs/division). The fluorescence correction compensated for sample fluorescence (at time scales < 2μs/division) as well as any photon source other than the monitoring beam, such as scattered light. These corrections were introduced by alternating signal and correction laser shots. This approach, combined with the averaging technique permits reliable detection of even quite weak absorption signals (ΔO.D. ~ 0.01). As such R7912 detection of absorption is more sensitive than OMA detection since in the latter case corrections are not collected on alternating shots. Rather, a group of correction shots are collected, averaged and the "average correction" applied to an average absorption signal derived from a series of laser shots collected independently of the correction shots.

In addition to its role in data acquisition, processing and storage the computer was also important in controlling the experiment. The computer signaled the opening of the shutters, activated the lamp pulses, controlled the movement of the cut–off filters as well as neutral density filters used to attenuate the laser dose.

*Time sequence of events:*

Figure 3.3 shows a plot of PMT output versus time for the period from one second before to one second after a particular laser pulse. The first event is the opening of the shutter in front of the monochromator which allows some light in. Next the monitoring lamp is pulsed, increasing the intensity of the light reaching the monochromator by about 50 times. The interface analog/digital converter reads and converts the PMT output (this corresponds to $I_0$) and then detection starts. Shortly after this the laser fires and the important signal is seen represented in the diagram by the small square. This corresponds to a decay trace of the sort shown in Figure 3.2. Finally, an electric switch dumps the charges on the lamp capacitors producing the spike shown, then the shutter closes ready for the next pulse.

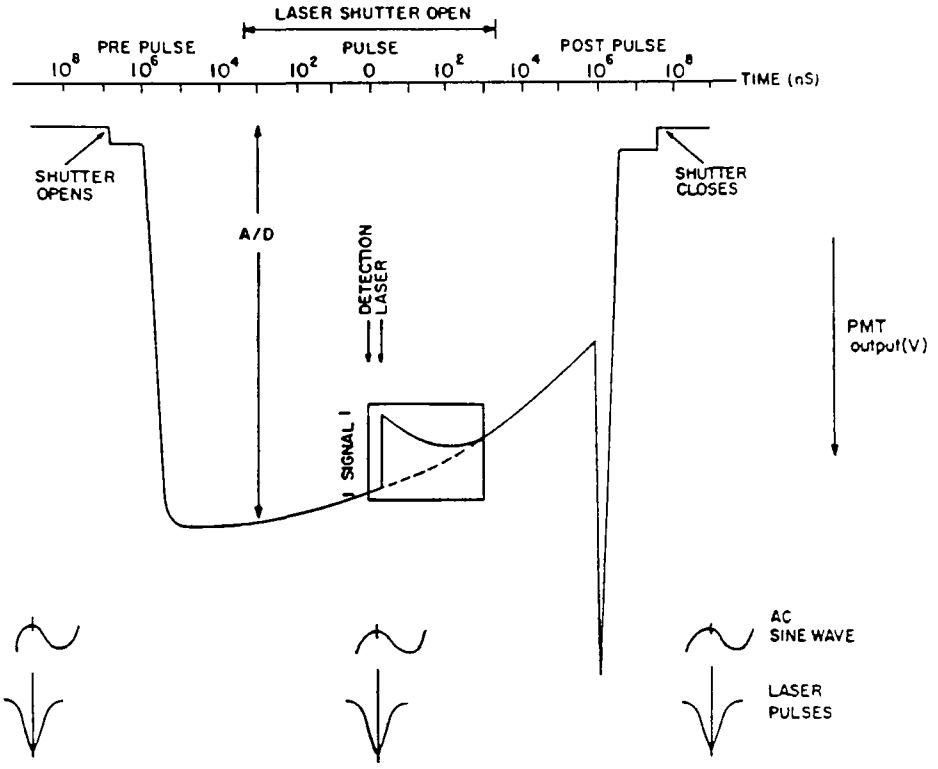


Figure 3.3. Time sequence of events in the kinetic laser flash photolysis experiment.

*Transient spectra:*

Although most transient spectra obtained in this study were recorded with the OMA system, there were a few instances where the signal strength was so low that R7912 detection was required. Transient absorption spectra can be built up with the kinetic system by acquiring a transient kinetic trace at several different wavelengths and plotting the ΔO.D. for each as a function of monitoring wavelength. With the NRCC system such measurements can in fact be made at several different delay times after excitation. Since ΔO.D. is measured, the transient spectrum is in fact a difference spectrum and shows the difference between the absorption spectrum of the substrate and that of the transient.This is also true of OMA spectra.

In order to record such a point–by–point transient spectrum it is important that the $I_0$ value be similar at each wavelength. If not the intensity ratios at different wavelengths will be unreliable. The NRCC system deals with this problem by having a programmable PMT power supply. The user indicates via a computer command the PMT output voltage which he/she desires.Typically the ΔO.D. at a given wavelength is an average of 3 to 5 shots. If the PMT output ($I_0$) after the first shot is not at the desired level the computer signals the PMT power supply to provide a more appropriate voltage to the PMT for the next shot. The computer bases the amount of additional supply voltage needed on the intensity of the monitoring beam from the previous shot. Since $I_0$ can fluctuate from shot–to–shot at a given wavelength and from wavelength–to–wavelength, standardization of the $I_0$ value in this way is critical. The computer also runs the monochromator stepper motor. All of these features are very useful for automatic recording of transient spectra.

3.1.2.2 The OMA system.

The OMA in use at the NRCC is a gated intensified E.G.&G. Series III model.

*The excitation source:*

This was essentially the same as for the kinetic system.

*The monitoring system:*

This too was similar to that used in the kinetic system. The monitoring beam for transient absorption studies was provided by a C.W. 150W Xenon lamp. This lamp could be pulsed if needed but was not used in pulse mode in the present study. As in the kinetic system, the monitoring beam was focussed onto the sample and the transmitted light focussed onto the slit of the spectrograph (vide infra). Filters and shutters were controlled by the computer–a PDP 11/73 in this case.

*The detection system:*

The detection system is the heart of the OMA. An OMA consists of several components.[165] In order to obtain spectrally resolved data the transmitted monitoring radiation was dispersed with a Jarrel–Ash MonSpec 27 spectrograph with a 600 grooves/inch grating blazed at 500nm. This spectrograph was of the Czerny–Turner type. The spectrograph was equipped with slits of various widths but the 200μm slit was most commonly employed in the present study. Spectral resolution of about ± 2nm was possible.

Subsequent to the spectrograph was the detector. The detector was an E.G.&.G. Model 1420–1024 cooled, intensified silicon photodiode array detector. The detector, which could be gated, had an array size of 1024 elements and was sensitive in the blue region of the spectrum. Gating was achieved by applying a high voltage (~200V on top of 2800V) across a microchannel plate intensifier, resulting in intensification for 700 diodes, for a specified period of time (the gate open time). The gate was activated by the third detection component–the high voltage pulse generator. In the NRCC system the E.G.&G. Model 1302 fast pulser was used. The gate width was typically 20ns although other values were available.

The output of the detector is essentially a set of voltage signals (ultimately ΔO.D.) as a function of array channel (essentially of wavelength). This set of 1024

channels and voltage signals was fed into another important OMA component–the detector controller (E.G.&G. Model 1463). This latter device scanned and digitized the output signal of the photodiode array. It also allowed one to select data from some fraction of the total number of array channels rather than collecting the entire set of points. Typically, the nearly 700 intensified points available were grouped in sets of four so that the output spectra generally consisted of 174 data points.

The controller output was transmitted to an E.G.&G. Model 1461 interface. The interface collected the detector output and stored it in its own memory until it could be read by the PDP 11/73. The 1461 also allowed the external computer to control the data acquisition process.

*Outline of the OMA experiment:*

The combination of spectrograph and OMA detection permits one, at least in principle, to collect an entire transient absorption spectrum with a single laser shot. In practice a number of such are averaged to give the final version of the spectrum stored by the computer. With the NRCC system it was possible to generate an absorption spectrum after a single "cycle". A cycle consisted of the following: 10 background shots for which both the laser and monitoring beam shutters were closed; 10 lamp profile shots for which the laser shutter was closed but the monitoring shutter was open; 10 signal shots for which both laser and lamp shutters were open; 10 luminescence shots for which only the laser irradiated the sample. Light entering the spectrograph during each of these phases of the cycle were dispersed onto the OMA's diode array, converted to analogue and then digitized output signal and temporarily stored in the interface. The background, lamp and luminescence data were subtracted from the total signal data leaving the desired transient absorption signal which was then transmitted to, and stored by, the PDP 11/73 computer. Thus a given transient spectrum was the average of 10 laser shots. The computer also provided data display and hard copy facilities.

The background and luminescence shots can be considered as corrections in the sense that they provide a way of eliminating extraneous photon sources (sample fluorescence, stray light, etc.) from the net photolysis data (that is lamp and lamp plus laser). Since the monitoring lamp runs continuously it is subject to little intensity fluctuation and what little fluctuation may occur is averaged out by obtaining 10 lamp profiles. Thus a reasonably reliable $I_0$ value is provided.

For strongly absorbing transients ($\Delta$O.D. ~ 0.1) it is generally sufficient to collect one or two cycles. For moderately absorbing transients ($\Delta$O.D. ~ 0.05) signal/noise can be improved by collecting numerous cycles provided the sample is photostable. The computer allows display of the transient spectrum after each cycle if desired so one can easily monitor the quality of the data as one performs the experiment. In the case of very weakly absorbing transients ($\Delta$O.D. ~ 0.01 to 0.02) the R7912 detected point–by–point approach to gathering spectra is preferable to the OMA due to the greater sensitivity of the former.

A final important feature of the OMA system is that the gate can be delayed in time from the end of the laser pulse up to 1ms after the laser pulse in steps of 10ns. This allows collection of transient spectra at different times after the laser fires and can be particularly useful if more than one species is present. The gate delay is provided by a home built delay unit.

## 3.2. Reagents.

### 3.2.1. Phenols and thiophenes.

Chart 3.1 shows the structures of the phenols examined and gives the abbreviations used. 3,5–Dimethylphenol, 35D, (Eastman–Kodak) was purified by recrystallization from hexane. (2R, 4'R, 8'R)–$\alpha$–Tocopherol, EOH, (Eastman–Kodak) was a high purity product ($\geq$ 99%) and was used as received. In a few experiments a slightly less pure EOH was used (Aldrich, 98%). 2,6–Di–tert–butyl–4–methylphenol,

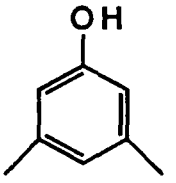


(35D)

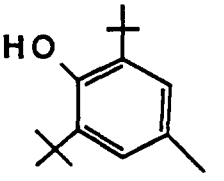


(BHT)

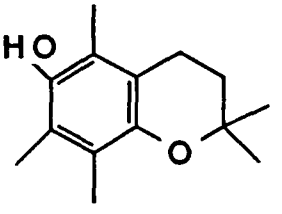


(CRM)

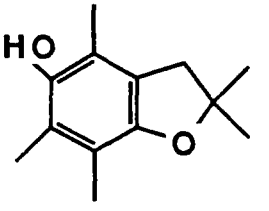


(FUR)

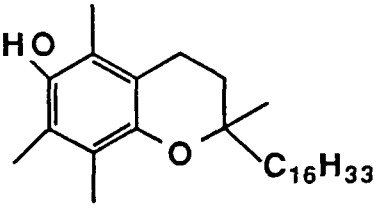


(EOH)

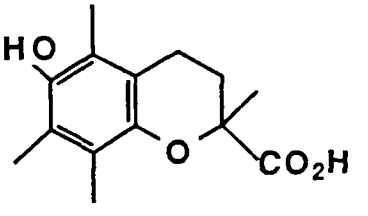


(TROLOX)

**Chart 3.1.**

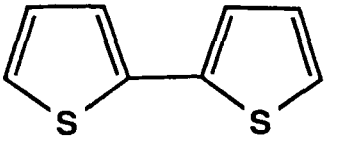

αB

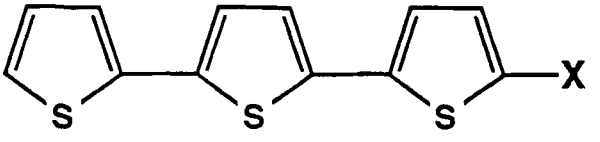

X = H, αT
X = CN, CN αT
X = Br, Br αT

**Chart 3.2.**

BHT, (Aldrich) and 6–hydroxy–2,5,7,8–tetramethylchroman–2–carboxylic acid, Trolox, (BDH) were also used as received. The compounds CRM and FUR (see Chart 3.1) were prepared by L. Hughes according to published procedures [166, 167] and were kindly donated by Dr. K.U. Ingold.

The structures and abbreviations of the thiophenes used are presented in Chart 3.2. α–Terthienyl, αT, the synthesis of which has been reported elsewhere [168, 169] was prepared by A. MacEachern. The bromo– and cyano– analogues (BrαT and CNαT) were a generous gift from Professor P. Morand; the details of their synthesis have been reported elsewhere [170]. 2,2'–Bithienyl, αB, (Aldrich) was recrystallized from hexane and then sublimed. The purity of the thiophene samples was judged to be in excess of 99% based on HPLC or capillary GC.

3.2.2. Ketones.

n–Butyrophenone, BUP, and isobutyrophenone were from Aldrich. Both were purified by passage over an alumina column followed by vacuum distillation. Benzophenone (Aldrich) was recrystallized from ethanol as was p–methoxyacetophenone (Aldrich). Xanthone (Fluka; puriss) was used as received.

3.2.3. Surfactants.

Sodium dodecyl sulfate (SDS) of "specially pure" grade from BDH and Brij–35 (Aldrich) were used without further purification. Sodium octyl sulfate (SOS) and sodium decyl sulfate (SDecS) were from Lancaster Synthesis and were recrystallized from ethanol prior to use. Dodecyltrimethylammonium bromide (DTAB) was from Sigma and was recrystallized several times from acetone. Cetyltrimethylammonium chloride (CTAC) and bromide (CTAB) were from K&K Laboratories and were precipitated from the 50% commercial solution with acetone. The crystals were washed with anhydrous ether and vacuum dried.

3.2.4. Solvents and gases.

Organic solvents were from Aldrich, Fisher or BDH and were of the highest quality commercially available. They were used as received. Water was of conductivity grade (resistance ≥ 18MΩ/cm$^2$) and was prepared by passing distilled water through a Sybron/Barnstead Nanopure II system. $D_2O$, MSD Isotopes, was used as received.

The only gases used in these studies were $N_2$ and $O_2$. These were both Union Carbide products of high purity (≥ 99%).

3.2.5. Micellaneous reagents.

Di–tert–butylperoxide, BOOB, (MCB Reagents) was passed over an alumina column immediately prior to use. 1,3–Pentadiene (Aldrich) was distilled before use. Pyrene was a zone refined product from Princeton Organics and was recrystallized from ethanol prior to use. Di–6–heptenoyl peroxide was prepared according to literature procedures [171, 172]. 1–Hexene and 1–methylcyclopentane were both from Aldrich and were used as received. Methyl viologen dichloride, $MV^{+2}$, was an Aldrich product and was recrystallized twice from ethanol while tetracyanoethylene, TCNE, (Aldrich) was used as received.

Inorganic salts were from BDH or Fisher and were of reagent grade. They were used as received.

3.3. General techniques.

3.3.1 Laser flash photolysis experiments.

Experiments involving reaction of Vitamin E (EOH) in homogeneous solution were performed in 7x7 mm$^2$ cells made of Suprasil quartz tubing. The concentration of ketone reagents used was approximately $10^{-3}$M in each case (i.e., benzophenone, p–methoxyacetophenone, xanthone) while the concentration of BOOB was typically

about 20% by volume. Aliquots of EOH stock solution were added to reagent solutions via Hamilton microlitre syringes. The samples were rendered oxygen free by bubbling with oxygen–free nitrogen for about 10 minutes. Experiments designed to determine kinetic isotope effects on the reaction of EOH with a reactive species (BOOB or ketone) were carried out in benzene or in 10% $H_2O$ in acetonitrile. In the former case the exchange of the hydroxy hydrogen of EOH for deuterium was facilitated by washing the benzene used several times with $D_2O$. This was true both of the benzene used to prepare the EOH stock and the reagent solution. In the case of "wet" acetonitrile 10% $D_2O$ was used in place of $H_2O$ to exchange the hydroxyl hydrogen.

When experiments were carried out in micellar media the phenols were added to 2mL aqueous solutions containing 0.1 to 0.2M surfactant. The exceptions to this were CTAB (0.07M surfactant) and SOS (0.5M surfactant). The phenol concentrations were typically $1.5x10^{-3}$M to $2.5x10^{-3}$M and the samples also contained 0.021M n–butyrophenone. Again the samples were contained in 7x7 $mm^2$ Suprasil tubes but were now sonicated briefly and deaerated by prolonged (1/2 h) bubbling with nitrogen. A somewhat different procedure was used in the case of BHT (see Chapter 4).

In experiments in which NaCl was to be included it was weighed and added prior to injection of the organic reagents. Other salts were added to micellar solutions at lower concentrations than NaCl and this was done by injecting aliquots of an aqueous stock solution of the salt with a microlitre syringe.

If the pH was to be controlled the following procedure was followed. The flash photolysis sample was prepared as indicated above. In addition a "dummy" sample of identical composition but much larger volume (20mL) was prepared. The pH of the dummy solution was adjusted to the desired level by injecting aliquots of HCl or NaOH stock solution. The volume of acid or base added to the dummy solution would then be a multiple of the volume needed to adjust the pH of the actual sample to the same level as that of the dummy. A similar approach was used to set the pH of certain

samples used in fluorescence experiments (section 3.3.3). In all of these experiments the pH was monitored with a digital pH meter (Canlab).

Temperature control was afforded by flowing nitrogen gas through a copper heat exchange coil which could either be warmed by a variable resistor or cooled by immersion in liquid nitrogen. The samples, which were surrounded by a double quartz wall temperature jacket, were allowed to equilibrate for 5 to 10 minutes once the desired temperature had been reached. The temperature was monitored by a Pt thermometer.

The magnetic field source was a "home made" magnet with a power supply which allowed for continuous variation of the field strength from ~20G (residual field when no current was supplied to the magnet) to 5.4kG. For "zero field" experiments (in fact the Earth's magnetic field) the magnet was removed from the vicinity of the sample holder. The field strength was calibrated with a gaussmeter which had been previously calibrated against the magnetic field of an ESR spectrometer. In certain experiments conventional horseshoe and stirring magnets were used. The sample holder, optical table, optical bench and mounts used near the sample compartment were built of non–magnetic materials.

Experiments involving reactions of thiophenes in homogeneous solution were performed in 7x7 $mm^2$ Suprasil tubes. The sample volumes were typically 2 mL and sample gas concentrations were adjusted by bubbling with oxygen free nitrogen (deaerated) or with high purity oxygen (oxygen saturated). We note that some of the very long triplet lifetimes recorded in this work may occasionally have been limited by the ability to remove last traces of oxygen employing this deaeration technique. Thiophene concentrations were typically between 20 and 100μM. Concentrations of $MV^{+2}$ and TCNE never exceeded 5mM in homogeneous solution.

The experimental conditions for our thiophene studies in micellar solution were very similar to those described for homogeneous samples. However the samples were

generally sonicated briefly and also bubbled with nitrogen longer. In addition it was necessary to employ up to 0.04M $MV^{2+}$ in micellar systems to compensate for the decreased ability of $MV^{2+}$ to quench thiophene triplets resulting from compartmentalization and reduced mobility (see Chapter 5).

Both phenol and thiophene samples were irradiated with the pulses from a Molectron UV–24 nitrogen laser or, less frequently, from an excimer laser operated at 308 nm. The transient decay traces (100 or 400 data points) were averages of 10 (occasionally 20) laser shots with suitable background or fluorescence correction. In some cases the full laser dose was attenuated by placing an appropriate neutral density filter in front of the laser beam. The sample kinetics were monitored at or near the $\lambda_{max}$ of the species of interest: the neutral phenoxyl radical; the thiophene radical cation; the methyl viologen radical cation. In the case of the phenoxyl radicals the monitoring wavelength had to be sufficiently long so as to avoid interference due to absorption by the n–butyrophenone biradical.

Transient absorption spectra were recorded with an E.G.&G. Series III OMA as described above. A typical experiment involved the collection and averaging of 1 to 5 cycles with suitable luminescence and background correction.

The use of static samples (as opposed to a flow system) lead to only minor ($\leq$ 10%) overall substrate conversion during the course of these LFP experiments. This was determined by comparison of the UV–vis spectra before and after the laser experiment; these spectra were obtained with a Hewlett–Packard 8451 diode array spectrometer.

### 3.3.2 Treatment of kinetic laser flash photolysis data in micellar solution.

In contrast to homogeneous solution where kinetic data could be analyzed in terms of either (pseudo–) first order or second order kinetics, transient decay data in micelles was generally found to be at least biexponential (see Chapters 4 and 5). As a

result a more sophisticated data analysis was desirable. Our transient decay data was fit to a function of the form

$$\Delta OD(t) = A_{fast}\exp\left(-k_{obs}t\right) + A_{slow}\exp\left(-k_{slow}t\right) \qquad (3.2)$$

where ΔO.D.(t) is the transient optical density as a function of time at the monitoring wavelength, $A_{fast}$ is the initial optical density associated with the fast decay component, $A_{slow}$ is the initial optical density associated with the slow component, $k_{obs} = k_{gem} + k_{-}$ is the observed rate constant of the fast component and $k_{slow}$ is the observed rate constant of the slow component. $A_{slow} + A_{fast}$ should equal the experimentally observed maximum transient optical density at zero time. The time window examined in our work typically covered about 10 lifetimes of the fast component ($k_{obs}$) and 0.1 to 0.3 lifetimes for the slow component. The latter does not necessarily follow first order kinetics. Although the value of $k_{slow}$ could vary significantly between one fitting of a given set of data and another fitting of the same data, the more important parameters $k_{obs}$, $A_{fast}$ and $A_{slow}$ were found to be very reproducible.

The data were fit using a Fortran 77 program. Only two initial parameters had to be selected in order to carry out the fit, namely $(k_{obs})^{-1}$ and $(k_{slow})^{-1}$. In order to improve the accuracy of the fit the transient decay data files contained 400 data points. Figure 3.2 shows an example of a typical data file and fit file for the system EOH + BUP in SDS. The figure shows the weighted residuals for the fit as calculated by the fitting program. From the essentially random distribution of the residuals, as well as from visual inspection, it is clear that the quality of the fit is quite good. It should be pointed out that the data obtained at intermediate field strengths like 1.5kG is more difficult to fit than data from zero field. This is so because at intermediate field the distinction between the fast and slow components is not as well established as at zero field.

3.3.3. Steady state fluorescence and single photon counting experiments.

In this study a number of experiments were carried out using the excited singlet state of pyrene as a probe of the micellar environment [4]. The experiments essentially involved measuring the pyrene fluorescence intensity or time–resolved decay profile as a function of experimental conditions. In particular monitoring the variation of the fluorescence parameter with added concentrations of either Trolox or $MV^{2+}$.

In the steady state experiments the fluorescence spectrum of pyrene in aqueous solutions of SDS was recorded between 350 and 460nm. The samples, containing about 50μM pyrene, were excited at 334nm. The fluorescence was determined by integrating the emission spectrum between 355 and 455nm. The variation in emission intensity as a function of quencher concentration at surfactant concentrations between 0.05M and 0.25M was determined. The concentration of Trolox never exceeded 9mM while that of $MV^{2+}$ never exceeded 2mM. The sample solutions were prepared in a manner similar to that described for the flash photolysis samples and pH control was afforded using the same dummy sample technique mentioned earlier. Samples were deaerated by bubbling with oxygen free nitrogen.

The emission data were recorded using a Perkin–Elmer LS–5 Luminescence Spectrophotometer equipped with a PE 3600 data station which provided data storage and hard copy facilities. Typical instrument settings were: slits (excitation = 10nm, emission = 3nm); scan speed = 60nm/min. Neutral density filters were generally needed to bring the pyrene emission on scale.

The lifetime of excited singlet pyrene in the absence or presence of quenchers was determined using the PRA single photon counting instrument described above. The samples used were identical to those used in the steady state experiments. The excitation wavelength was 334nm and emission above 375nm was collected by placing a 375nm cut–off filter before the emission PMT. This was necessary to reduce

interference from scattered light. Typically 10000 counts were collected in the maximum channel (time = 0). To avoid "pulse pile up" problems the excitation iris was adjusted so that the average number of detected emission photons per excitation was low. The instrument response function was obtained by scattering the excitation beam (400nm) from a suspension of Silicalite in water. A black cloth was placed over the sample compartment in all single photon experiments in order to avoid leaks of room light.

3.3.4 Micellar association constants.

The association constant, K, for association of a quencher, Q, with the micellar pseudo–phase can be defined in terms of the equilibrium

$$Q + M \rightleftharpoons Q_M \qquad (3.3)$$

where M represents a micelle and $Q_M$ is a micellized quencher molecule. The value of $K = ([Q_M]/[Q]\,[M])$ can be determined by the method of Encinas and LIssi [173]. In our experiments we used quenching of singlet pyrene by either Trolox or methylviologen as a probe in order to determine a value of K for each of these latter two substrates.

Briefly, the underlying principle of the Encinas–Lissi method is that the ratio of pyrene fluorescence intensity in the absence of quencher to that in the presence of quencher, $I_o/I_Q$, which is observed in a steady state fluorescence experiment depends only on the mean occupation number, $n_Q$, of the quencher in the micellar pseudo-phase. This relationship is assumed to be independent of the mechanism or efficiency of quenching. In practice, Stern–Volmer plots for the quenching of pyrene singlet ($\lambda_{ex}$ = 340 nm) by Trolox or methylviologen were determined at several SDS concentrations. The values of [Q] required to give the same value of $I_o/I_Q$ at each micelle concentration were determined by taking horizontal "cuts" through the Stern–

Volmer plots. These quencher concentrations were then plotted against micelle (not surfactant) concentration for the various $I_0/I_Q$ selected according to the equation

$$[Q] = \frac{n_Q}{K} + n_Q[Mic] \qquad (3.4)$$

where [Q] is the bulk concentration of Q needed to give a particular $I_0/I_Q$ value at the micelle concentration [Mic]. K and $n_Q$ can then be obtained form the slope and intercept of the plots.

3.3.5. Measurement of the critical micelle temperature.

The critical micelle temperature, cmt, of SDS in the presence of various concentrations of NaCl was determined by monitoring the frequency of the symmetric $-CH_2-$ of the surfactant's alkyl chain close to $2855cm^{-1}$. The frequency of this vibration is temperature dependent. The samples, 0.25M SDS plus the desired NaCl concentration in $D_2O$, were placed in an infrared cell with $CaF_2$ windows. The sample was placed in the thermostated cell holder of the FTIR spectrometer (Digilab FTS–15, $2cm^{-1}$ resolution) and cooled to $5^0C$. Spectra in the frequency region corresponding to the $CH_2$ stretch were recorded for about 40 temperatures up to about $70^0C$. This process was under the control of a computer which recorded a spectrum, incremented the temperature, waited for the temperature to equilibrate and then recorded another spectrum. The temperature was monitored by a copper–constantan thermocouple contacting the edge of the cell window. The details of this system have been published elsewhere [174–176].The basic experimental data are plots of the –CH2– stretching frequency versus temperature and these show a sudden break at the cmt due to a rapid increase in the frequency. The cmt value can be simply read off the plot. These experiments were kindly performed by Dr. H.L. Casal.

3.3.6. The 5–hexenyl radical clock.

The irreversible, unimolecular cyclization of the 5–hexenyl radical is a well known radical clock [177] and as such can be used to determine the rate constant of a reaction that competes with the cyclization. In these experiments we reacted a phenol, ArOH, with the 5–hexenyl radical in competition with its cyclization according to the following scheme

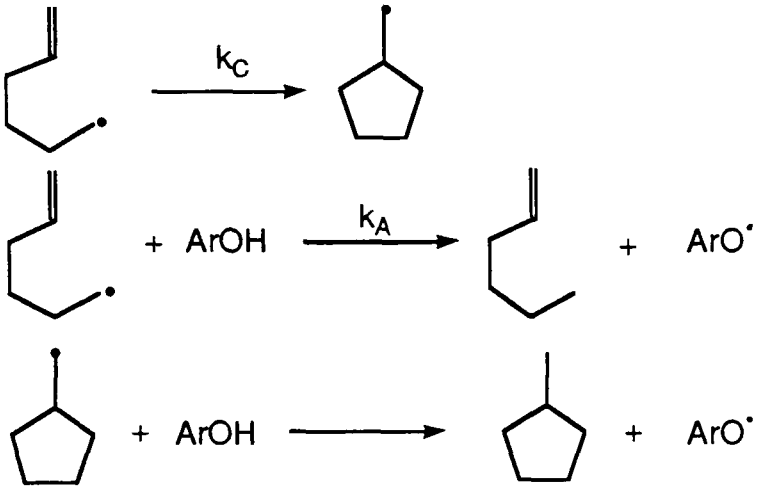


(3.5)

The rate constant, $k_A$, is readily calculated from a plot of

$$\frac{[1\text{–HEXENE}]}{[\text{METHYLCYCLOPENTANE}]} = \frac{k_A}{k_C}[\text{ArOH}] \qquad (3.6)$$

since $k_C$ is well known. At $70^0$C, the temperature at which these experiments were carried out, $k_C = 1.1 \times 10^6 s^{-1}$ [178].

The experimental procedure was as follows. An aliquot of ArOH stock solution at the desired phenol concentration in benzene was added to an NMR tube to which a ground glass vacuum joint had been attached. Next an aliquot of neat diheptenoyl peroxide was added to the ArOH solution at a concentration about 1/5 that of the phenol. The sample was then frozen in liquid nitrogen,connected to a vacuum line and

degassed by a series of freeze–pump–thaw cycles. After degassing the NMR tube was sealed and placed in an oil bath thermostated at $70^0$C. This was repeated for several more ArOH concentrations. The samples were left at $70^0$C for 5 days. This is sufficient time for most of the peroxide to decompose at this temperature. At the end of the 5 days the tubes were opened and 2μL aliquots injected onto the 1/8" x 30', 20% Carbowax 20M column of a Varian 6000 G.C. The injection temperature was $200^0$C while the detector temperature was $300^0$C. The vertical sensitivity was set to $10^{-9}$ arbitrary units. The oven temperature was increased from $60^0$C to $220^0$C at a rate of $20^0$C/minute. The oven was held at $220^0$C for 40 minutes in order to remove residual reagents. Under these conditions 1–hexene (I) appeared at 5.71 minutes and 1–methylcyclopentane (II) appeared at 6.87 minutes. These retention times were verified against authentic samples of these two products. The areas under the peaks for I and II were then used to calculate the product ratio [I]/[II].

# CHAPTER 4. THE KINETIC BEHAVIOUR OF KETYL–ARYLOXY TRIPLET–DERIVED RADICAL PAIRS.

## 4.1 Introduction.

Of the large number of neutral radical pairs which are subject to magnetic field effects in a micellar environment, few involve species other than carbon centered radicals [106]. In fact when this project was initiated only one report of field dependent decay kinetics involving a non-carbon centered radical was to be found in the literature [86]. We were therefore interested in investigating further the kinetic behaviour of micellized non-carbon centered radical pairs in the absence and presence of an external magnetic field. It was felt that hydrogen abstraction from a phenol by an excited triplet ketone to yield a triplet ketyl–aryloxy radical pair would be a likely candidate for such a study.

The hydroxyl –O–H bond of certain phenols is rather weak[179] so that the hydrogen atom can be readily abstracted giving rise to a phenoxyl radical. This property is reflected in the fact that phenols are employed as chain–breaking antioxidants (for reviews see [179, 180]) both in commercial and biological applications. In particular, a number of undesirable chemical effects such as aging of rubber [181] and deterioration of fats and oils [182, 183] can be attributed to the autoxidation of the lipids from which these materials are composed. The autoxidation of lipids (also known as lipid peroxidation) is a chain reaction involving the intermediacy of peroxyl radicals, ROO•, as the chain-carrier. Lipid peroxidation has also been suggested to play a role in several biological and medical phenomena such as inflammation [184], cell membrane damage [183, 185] and carcinogenesis [186, 187] as well as diseases of the aged such as Alzheimer's [188], Parkinson's [189] and artherio–sclerosis [189]. There is some evidence to suggest the latter set of ailments develop with age because the

bodies' antioxidant defenses become less effective [190] thus reducing resistance to "oxidative stress" [189].

The "antioxidant defenses of the human body" consist of a variety of preventative and chain breaking antioxidants. Among the latter is Vitamin E (Chart 3.1). Vitamin E (EOH), actually (2R, 4'R, 8'R)-α–tocopherol, is the major lipid soluble chain-breaking antioxidant in human blood [191, 192]. EOH owes its antioxidant activity to its ability to efficiently trap peroxyl radicals yielding the rather unreactive Vitamin E phenoxyl, EO• [193].

$$ROO^{\bullet} + EOH \longrightarrow ROOH + EO^{\bullet} \qquad (4.1)$$

Once formed EO• is eventually destroyed by reaction with a second peroxyl radical,

$$ROO^{\bullet} + EO^{\bullet} \longrightarrow \text{Molecular Products} \qquad (4.2)$$

or, in certain cases, it may be regenerated by reaction with a water soluble reducing agent like ascorbate, $AH^-$ also known as Vitamin C [194]

$$EO^{\bullet} + AH^{-} \longrightarrow EOH + A^{-\bullet} \qquad (4.3)$$

Other phenolic antioxidants like the commercially useful 2,6–di–tert–butyl–4–methyl phenol (BHT) act on the same principle of trapping ROO• although they tend to be less reactive towards peroxyls than is EOH [167, 195].

The high antioxidant activity of phenols can be attributed to the fact that the SOMO of the product phenoxyl overlaps with the π system of the phenyl group, i.e., phenoxyls are resonance stabilized. The exceptionally high antioxidant activity of EOH is due to the fact that the p-type lone pair orbital on the ethereal oxygen of the second

ring also overlaps the SOMO plus phenyl – π system of orbitals so that the resonance is further extended. [166, 167] Thus the Vitamin E phenoxyl should be rather easy to generate. This is an important feature if EOH or another phenol is to be used in a magnetic field effect study since the criterion of rapid radical pair formation must be fulfilled.

The reactivity of EOH towards a number of different reactive species has been studied (see the review by Craw [196] for example). Most attention has focused on the kinetics of hydrogen abstraction from EOH by peroxyl radicals (reaction 4.1). The reaction typically proceeds with rate constants on the order of $10^6$ $M^{-1}$ $s^{-1}$ in organic solvents [196]. EO• can also be generated by reaction of Vitamin E with singlet oxygen[197] and superoxide radical anion [198, 199]. However, from the point of view of magnetic field effects experiments the most promising means of generating EO• is via reaction with excited triplet ketones. The photoreduction of benzophenone triplet by Vitamin E proceeds with a rate constant approaching the diffusion controlled limit in acetonitrile [200]. Thus the intrinsic reactivity of nπ* carbonyl triplets towards EOH is very high. This is also true of many other phenols [201]

In addition to their rapid reactions with nπ* ketone triplets Vitamin E and other phenols have a number of other advantages that recommend them for use in magnetic field effect experiments of the type we are considering. The absorption spectra of EO• and many other phenoxyls are well established [194, 201–204]. The $\lambda_{max}$ of these species is generally found between 400 and 450nm. In addition the absorption spectra are rather distinctive in shape and have reasonably large extinction coefficients at $\lambda_{max}$ and are thus readily detectable and identifiable. Further, many carbonyl triplets (and ketyls) are only weakly absorbing in the 400 to 450 nm range [205]. Finally Vitamin E is known to be strongly associated with the SDS micellar pseudo–phase at $40^0C$[206] Although less strongly associated with SDS than EOH several simpler

phenols, including BHT, have been reported to reside predominantly in the micellar environment [206].

From the foregoing discussion we may conclude that reaction of a $n\pi^*$ ketone triplet with Vitamin E or other phenols is probably a suitable route to a micellized triplet radical pair involving a non–carbon centered radical. In order to make an informed choice as to which ketone would be most useful in this type of study we initially decided to investigate the reaction of EOH with several different ketones in homogeneous solution. In addition the kinetics of the reaction of the Vitamin E with alkyl radicals has only been roughly estimated [207] while the reaction of EOH with alkoxyl radicals has not been studied at all.

The influence of micellar dimensions on radical pair behaviour is another area which has received little attention. Several reports in the literature suggest that $k_{gem}$ and k–, as well as the efficiency of cage reaction, are dependent upon micellar size (see Chapter 2). Of these studies, the effects of micellar size has been examined in a systematic way only for k– and for the cage effect [48, 137]. The micellar volume was controlled by altering the surfactant chain length, by adding NaCl or a long chain alcohol. Although $k_{gem}$ has been largely ignored in the studies noted above, there is ample evidence in the literature to suggest that it too is influenced by micellar dimensions (see Chapter 2). Thus a second goal of this study is to examine more thoroughly the influence of micellar size on triplet radical pair behaviour especially on $k_{gem}$.

In summary, the first section of this chapter is an examination of the reactivity of Vitamin E and several related phenols towards various species in organic solvents. The latter parts of the chapter deal with the kinetic behaviour of triplet aryloxyl–ketyl pairs in a micellar environment.

## 4.2. Results.

4.2.1. Reactivity of Vitamin E and Related Phenols in Homogeneous Solution.

*Reaction with ketone triplets:*

The reactivity of EOH towards several aromatic ketone triplets was examined under homogeneous conditions. In each case laser excitation led to efficient formation of the triplet ketone which was rapidly quenched by EOH. Consider the case of benzophenone (K) as an example. The steps that may be involved in the the reaction mechanism are:

$$K \xrightarrow{h\nu} \xrightarrow{ISC} K^* \qquad (4.4a)$$

$$K^* \longrightarrow K \qquad (4.4b)$$

$$K^* + EOH \longrightarrow KH^\bullet + EO^\bullet \qquad (4.4c)$$

$$K^* + EOH \longrightarrow K + EOH^* \qquad (4.4d)$$

$$K^* + EOH \longrightarrow K + EOH \qquad (4.4e)$$

The last three reactions can contribute to EOH quenching of K* and their rate constants can be summed to give an overall quenching rate constant, $k_q$. The benzophenone triplet state, K*, has a $\lambda_{max}$ at 525 nm but also absorbs beyond 600 nm. The benzophenone ketyl, KH•, absorbs strongly at 545 nm. Thus the absorptions of these two species can interfere with one another when they are both present in the sample. In order to study the quenching of K* by EOH one may monitor the triplet state at 600 nm. At this wavelength K* absorbs weakly but KH• is essentially transparent.

In the absence of EOH the decay of triplet benzophenone at 600 nm was subject to minor second order contribution. This could be eliminated by working with lower ketone concentrations and by attenuating the laser dose by the use of neutral density filters. Under our experimental conditions (3mM ketone) the observed decay of K* at 600nm followed pseudo- first order kinetics both in the absence and presence of

EOH. The experimentally observed pseudo- first order rate constant, $k_{obs}$, can be related to $k_q$ by the relation

$$k_{obs} = k_0 + k_q[EOH] \qquad (4.5)$$

Where $k_o$ is the decay rate constant of triplet benzophenone in the absence of EOH (i.e. decay via reaction 4.4b) . Thus a plot of $k_{obs}$ versus [EOH] should be linear with slope $k_q$. Figure 4.1 shows such a plot for the triplet benzophenone EOH system in benzene. Values of $k_q$ obtained in this study are reported in Table 4.1 along with rate constants for the reaction of Vitamin E with several other ketone triplets. In each case the samples were excited with nitrogen laser pulses. The monitoring wavelengths used are given in the Table.

The rate constants of Table 4.1 approach the diffusion controlled limit indicating that the deactivation of aromatic ketone triplets is a very rapid process. This is true even for p-methoxyacetophenone the triplet state of which has $\pi\pi^*$ character [208]. The high reactivity of $\pi\pi^*$ triplets toward EOH is confirmed by the xanthone results. In fact the rate constants are greater for the $\pi\pi^*$ triplets than for the $n\pi^*$ triplet. For xanthone $k_q$ is essentially solvent independent although the configuration of the triplet state changes from $n\pi^*$ in non–polar solvents to $\pi\pi^*$ in polar solvents. In the case of benzophenone and p–methoxyacetophenone (PMAP) inclusion of a hydrogen bonding reagent (methanol) seems to slightly reduce the value of $k_q$. No such effect is observed for triplet xanthone.

The transient absorption spectrum observed following laser excitation of benzophenone in benzene corresponds to that of the benzophenone triplet [205]. When 1.2mM EOH is added the triplet spectrum is replaced by the transient spectrum shown in Figure 4.2b. This spectrum was recorded 900 ns after the laser pulse and clearly shows bands near 425 nm that are due to the Vitamin E phenoxyl [194] as well as bands near 545 nm due to the benzophenone ketyl [209]. Normally one would be able

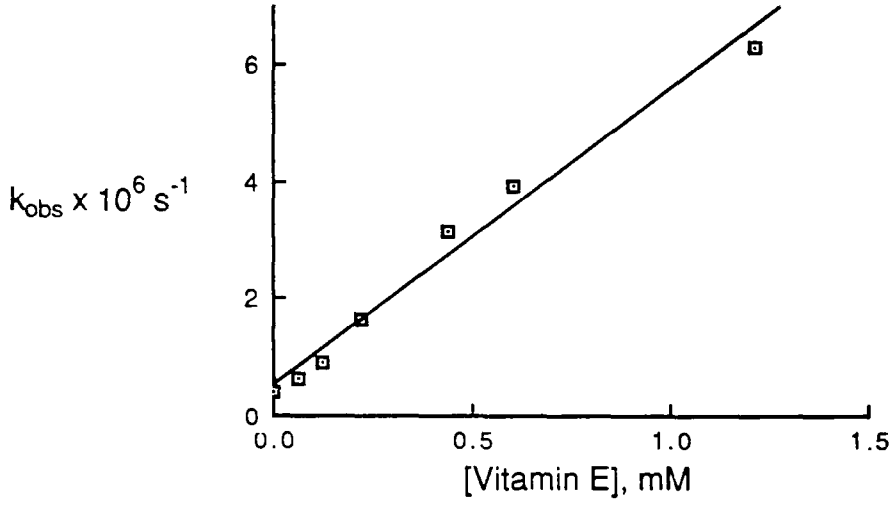


Figure 4.1. Quenching plot for the reaction of Vitamin E with triplet benzophenone in benzene. Data obtained at 600 nm. [Benzophenone] = 2mM.

Table 4.1. Rate constants for the reaction of Vitamin E with aromatic ketone triplets at 300K.

| Substrate | Solvent | $k_q$, $10^{9}$[a] $M^{-1}s^{-1}$ | $\lambda_{mon}$ nm |
|---|---|---|---|
| Benzophenone | $C_6H_6$ | 5.1±0.6 | 600 |
| | $C_6H_6$ + 1.3M $CH_3OH$ | 3.7±0.4 | 600 |
| PMAP | $C_6H_6$ | 5.9±0.2 | 370 |
| | $C_6H_6$ + 1.3M $CH_3OH$ | 3.2±0.4 | 370 |
| Xanthone | $C_6H_6$ | 5.7±1.6 | 603 |
| | $C_6H_6$ + 1.3M $CH_3OH$ | 6.0±0.8 | 603 |
| Butyrophenone[b] | $C_6H_6$ | 3.3±1.2 | 425 |

(a) Errors as ±2σ.

(b) Real error may be significantly greater than indicated here.

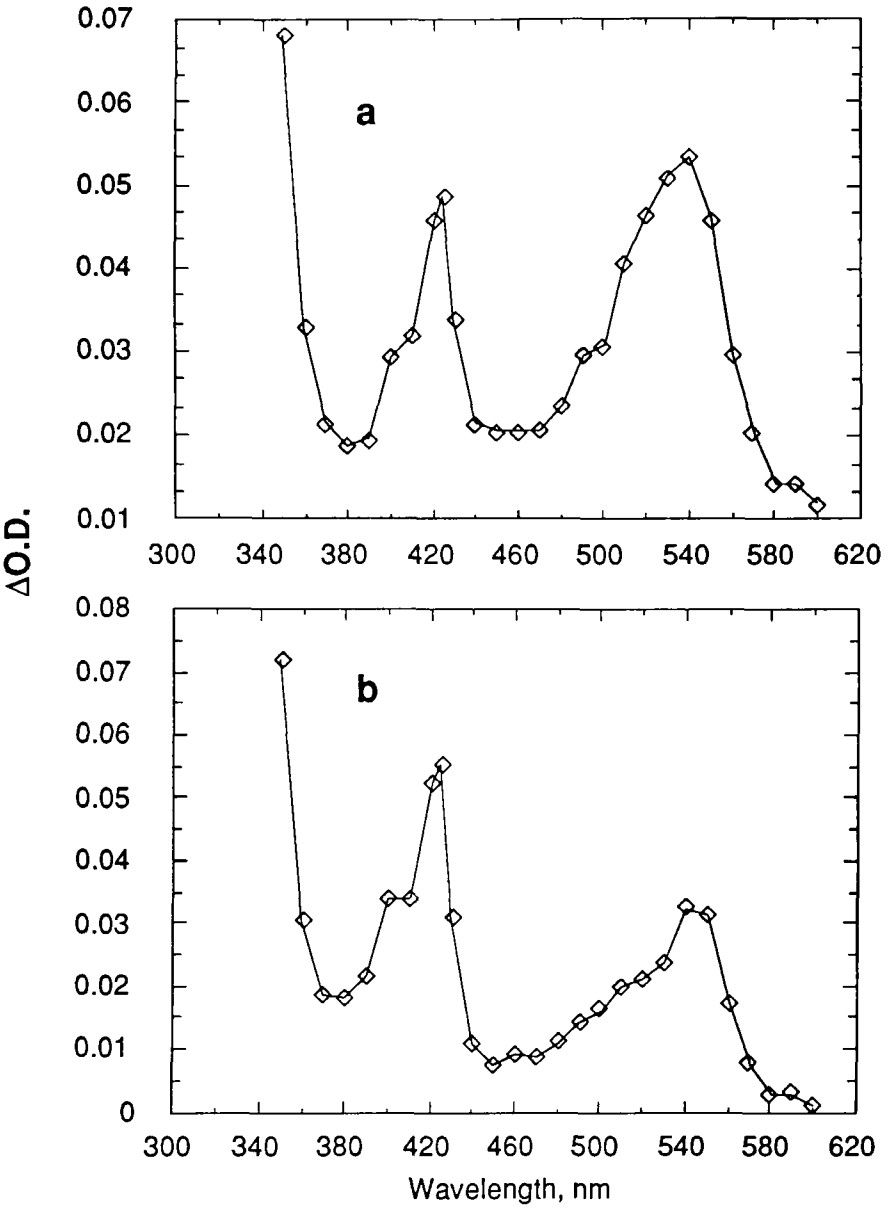


Figure 4.2. Transient absorption spectra recorded in nitrogen saturated benzene in the presence of 3mM benzophenone and 1.2mM EOH 120ns (a) and 900ns (b) after the laser pulse.

to obtain a value of $k_q$ by monitoring the EO• growth rate constant as a function of Vitamin E concentration. However in the benzophenone/EOH there is sufficient benzophenone triplet signal at 425 nm to cause an initial "jump" to be superimposed n the observed growth signal. Even so the growth rate constant monitored at 425 nm in the presence of EOH is comparable to that for triplet benzophenone decay monitored at 600 nm. This point is also evident if one compares Figure 4.2a and 4.2b. The former, recorded 120 ns after the laser, shows signals due to EO• and triplet benzophenone. The second part of the Figure, recorded 900 ns after the laser, shows that the triplet has completely decayed leaving the ketyl and that the concentration of EO• has increased. These results show conclusively that triplet quenching of benzophenone by EOH leads to the Vitamin E phenoxyl.

It is possible to shed some light on the relative importance of the various quenching mechanisms (reaction 4.4c,d,e) contributing to the EOH mediated deactivation of the benzophenone triplet using a technique proposed by Das et al [201]. The maximum end of pulse optical density (top OD) of the benzophenone triplet at 545 nm was measured for a sample containing 0.041 M benzophenone in benzene. This top OD value was compared to the top OD at 545 nm for an optically matched sample containing the same ketone concentration but with sufficient Vitamin E to quench about 95% of the triplets. The transient absorption at 545 nm in the latter case should be primarily due to the benzophenone ketyl radical. We found that at 545nm the ratio top OD triplet/top OD ketyl = 2.69±0.11 using 24% of the available nitrogen laser dose. Using the literature value of 2.36 for the ratio of extinction coefficients for the benzophenone triplet and ketyl [210, 211, 212] we find that 88±4% of quenching events lead to generation of ketyl radicals. In view of the uncertainty in the literature extinction coefficient values, as well as the uncertainty of our measured top OD ratio, the efficiency of radical formation should not be considered different from 100%. This

result implies that energy transfer from triplet benzophenone to EOH (reaction 4.4d) makes a negligable contribution to triplet quenching.

We have also examined deuterium isotope effects on the rate constants for the reactions of the ketone triplets with EOH. The exchange of the hydroxylic hydrogen of EOH was achieved by replacing $H_2O$ with $D_2O$ in the acetonitrile system and by saturating benzene with $D_2O$. The results are summarized in Table 4.2. For the three ketones studied there was only a very modest decrease in the value of $k_q$ in the deuterated system as expected for rates that approach the diffusion controlled limit.

The influence of hydrogen bonding on $k_q$ was examined using the $\pi\pi^*$ triplet of PMAP as the hydrogen acceptor. The configuration of this triplet is the same regardless of the solvent polarity [208]. The results of this study are summarized in Table 4.3 . The value of $k_q$ for EOH is subject only to a small decrease under conditions in which the phenoxyl hydrogen is subject to hydrogen bonding. This agrees with the data in Table 4.1. By contrast, the $k_q$ value for phenol is highly sensitive to hydrogen bonding changing by a factor of 42 between benzene and acetonitrile containing 10% $H_2O$. The value of $(0.41\pm0.06)\times10^9$ $M^{-1}s^{-1}$ found in acetonitrile reflects the fact that spectrograde acetonitrile will contain some water unless it has been carefully and recently dried.

We have also examined the reactivity of EOH towards the triplet state of n-butyrophenone (BUP) in benzene. Samples containing 0.021M BUP, with or without EOH, were irradiated at 337 nm. In the absence of EOH the triplet–triplet absorption spectrum of BUP could be detected as a rather weak, broad band with $\lambda_{max}$ at about 360nm. The top $\Delta$ O.D. under these conditions was only 0.009 at 360nm 50ns after laser excitation. The lifetime of triplet BUP is controlled by the Norrish type II reaction (see section 4.2.3) and was found to be 90ns in deaerated benzene.

When EOH is added to a solution of 0.021 M BUP in deaerated benzene the spectrum of $EO^{\bullet}$ is readily detectable. The observed spectrum is in excellent

Table 4.2. Kinetic isotope effects on the reactivity of Vitamin E at 300K.

| Substrate | Solvent | $k_H/k_D$[a] |
|---|---|---|
| Benzophenone | $C_6H_6$ | 1.09 |
| PMAP | $C_6H_6$ | 1.19 |
| Xanthone | $C_6H_6$ | 1.12 |
| t–BuO•[b] | $C_6H_6$ | 1.31 |
| | 10% $H_2O$ in $CH_3CN$ | 2.69 |

(a) $k_H$ values in Table 4.1.

(b) $k_H$ value in Table 4.5.

Table 4.3. Effect of hydrogen bonding on the reactivity of Vitamin E and phenol towards p–methoxyacetophenone triplet at 300K.

| Solvent | $k_q x 10^9$ $M^{-1}s^{-1}$(a) | |
|---|---|---|
| | EOH | PhOH |
| $C_6H_6$ | 5.9±0.2 | 5.4±0.3 |
| $H_2O$ saturated $C_6H_6$ | 5.0±0.2 | 0.41±0.06 |
| $CH_3CN$ | 4.8±0.3 | 0.13±0.01 |

(a) Errors as ±2σ.

agreement with that reported for EO• in the literature [194]. Because of the short lifetime of triplet BUP and because of interference with the detection of the triplet signal due to the strongly absorbing EO• it is difficult to measure a reliable rate constant for the reaction.

$$BUP^{*} + EOH \longrightarrow BTK + EO^{\bullet} \qquad (4.6)$$

by monitoring the decay kinetics of $BUP^{*}$ (Here BTK represents the butyrophenone ketyl radical). However, the EO• kinetics measured at 425 nm exhibit a rapid growth of the phenoxyl radical immediately after the laser pulse. For example, the growth rate constant was $3.1 \times 10^{7}$ $s^{-1}$ at 1.9mM EOH. This rate constant increased systematically with [EOH] and a plot of $k_{obs}$ for the growth process versus [EOH] (equation 4.5) yields a rate constant of $(3.3 \pm 1.2) \times 10^{9}$ $M^{-1}s^{-1}$ for reaction 4.6. It should be noted that the scatter in this plot was rather large due to the fact that the observed growth lifetimes are not much larger than the duration of the laser pulse. Thus the errors on our value of $k_q$ for reaction 4.6 may in fact be substantially larger than those indicated above. Nonetheless our data clearly shows that quenching of triplet BUP by EOH in homogeneous solution leads to good yields of EO• at a rate approaching diffusion control.

*Reaction with t–BuO• :*

In addition to its reaction with ketone triplets, the reactivities of EOH and several structurally related phenols (Chart 3.1) towards the tert-butoxyl radical (t–BuO•) have been examined. To the best of our knowledge this is the first report of the reaction of EOH and its model compounds (Chart 3.1) with an alkoxy radical.

The photodecomposition of di–tert–butylperoxide (BOOB) by pulses from the nitrogen laser was used as a source of t–butoxyl. This radical is known to readily abstract the phenoxyl hydrogen of phenols in competition with the pseudo–first order

decay of t–butoxyl [203]. The latter involves β – scission of t–BuO• or reaction with the solvent.

Nitrogen laser irradiation of samples containing 20% BOOB plus phenol in organic solvent lead to readily detectable transient absorptions in the 400 to 450 nm region. Figure 4.3 shows the absorption spectrum obtained when EOH was used as the hydrogen donor. R7912 detection was employed in this experiment. The spectrum closely resembles those of other phenoxyl radicals [194, 201–204] as well as reported spectra of the α–tocopheroxyl radical [194]. As a result we assign this transient to the Vitamin E phenoxyl radical. There was a slight solvent dependence of this spectrum with $\lambda_{max}$ = 425 nm in BOOB/methanol and 420nm in BOOB/$C_6H_6$. It is worth noting that the resolution of this spectrum (± 2nm) is superior to these published earlier for the same species.

Phenoxyl radicals for the Vitamin E model compounds CRM, FUR and Trolox were generated in a similar manner to that just described for EOH. Table 4.4 lists the $\lambda_{max}$ values for all of these radicals. In general the spectra are quite similar to those of EO• and other phenols.

Kinetic data pertaining to the reaction of EOH and the other phenols with t–BuO• were obtained by monitoring the various systems at the $\lambda_{max}$ of the respective phenoxyl radicals. In each case the hydrogen abstraction reaction

$$\text{t–BuO}^{\bullet} + \text{ArOH} \xrightarrow{k_{4.7}} \text{t–BuOH} + \text{ArO}^{\bullet} \qquad (4.7)$$

was easily followed by monitoring the growth of the ArO• signal (Figure 4.4). The growth process followed pseudo- first order kinetics in each case and plots of $k_{obs}$ (a growth rate constant ) versus [ArOH] were linear with slopes corresponding to $k_{4.7}$. Values of these rate constants, recorded at the phenoxyl's $\lambda_{max}$, are reported in Table

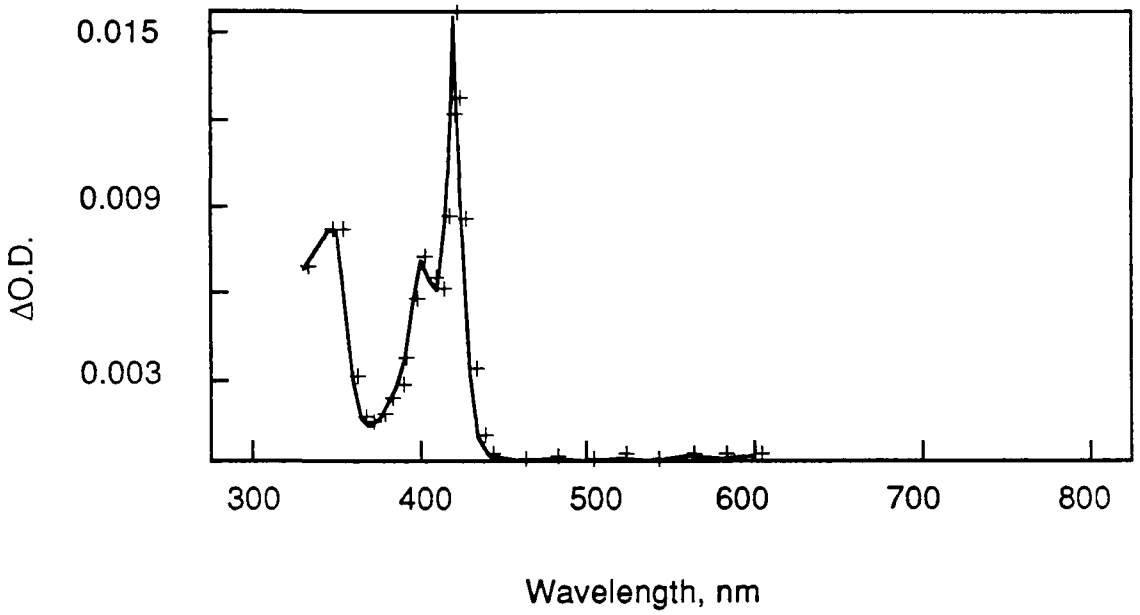


Figure 4.3. Absorption spectrum of the Vitamin E phenoxyl radical in nitrogen saturated 1:1 BOOB:benzene. Recorded 450 ns after laser excitation. [EOH] = 2.9mM.

Table 4.4. $\lambda_{max}$ values for phenoxyl radical absorption in homogeneous solution at 300K.

| Phenol | Solvent | $\lambda^{max(a)}$ nm |
|---|---|---|
| 35D | 1:1 BOOB:$C_6H_6$ | 425, 410 |
| BHT | 1:1 BOOB:$C_6H_6$ | 400, 380 |
| CRM | 1:1 BOOB:$C_6H_6$ | 420,403 |
| FUR | 1:1 BOOB:$C_6H_6$ | 420, 405 |
| EOH | 1:1 BOOB:$C_6H_6$ | 420, 403 |
| | 45% BOOB in $CH_3OH$ | 426, 404 |
| Trolox | 30% BOOB in $C_6H_6$ | 422, 403 |
| | 0.2M DTAC[(b)] | 430, 410 |

(a) Phenoxyls formed via reaction with t–BuO•.

(b) Phenoxyl formed via reaction with triplet BUP.

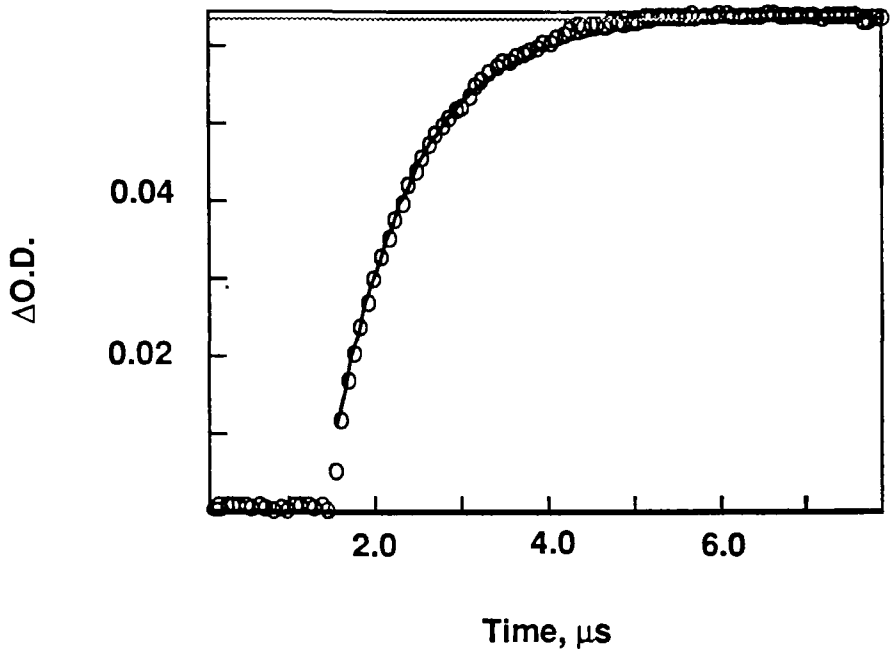


Figure 4.4. Growth of the Vitamin E phenoxyl radical recorded at 425 nm in 20% BOOB in benzene. [EOH] = 3.5mM.

Table 4.5. Rate constants for hydrogen abstraction from selected phenols by the t–butoxyl radical at 300K.

| Phenol | Solvent | $k_{4.7}$, $10^9$ $M^{-1}s^{-1}$[a] |
|---|---|---|
| EOH | 1:1 BOOB:C6H6 | 3.8±0.5 |
| | 10% H2O + 10% BOOB in $CH_3OH$ | 0.66±0.06 |
| Trolox | 1:3 BOOB:$C_6H_6$ | 3.4±0.2 |
| BHT | 2:1 BOOB:$C_6H_6$ | 0.12[b] |
| CRM | 1:1 BOOB:$C_6H_6$ | 4.2±0.4 |

(a) Errors as ±2σ.

(b) From reference [203].

4.5. As was the case with the reaction between EOH and ketone triplets the rate constant for reaction 4.7 approaches diffusion controlled in benzene. However in 10% $H_2O$ / acetonitrile the value of $k_{4.7}$ is much lower.

*Reaction with 5–hexenyl.*

We have carried out a preliminary study of the reactivity of EOH towards the alkyl radical 5– hexenyl. The experiment was carried out in benzene at 70$^0$C and the phenol concentration was always at about 5 times excess over the concentration of the radical precursor, bis–5–heptenoyl peroxide. Figure 4.5 show a plot of the ratio of the integrated G.C. peak area for 1–hexene to that
for methylcyclopentane versus the phenol concentration. Plot 4.5a is for EOH as hydrogen donor while plot 4.5b is for BHT as hydrogen donor. From the slopes of these plots, and taking $1.1 \times 10^6 s^{-1}$ for the cyclization rate constant of 5–hexenyl in benzene at 70$^0$C [178], we obtained the following rate constant for hydrogen abstraction from the phenols by the alkyl radical: $(1.7 \pm 0.2) \times 10^6$ $M^{-1}s^{-1}$ for EOH; $(3.3 \pm 0.2) \times 10^4$ $M^{-1}s^{-1}$ for BHT. To the best of our knowledge the former is the most precise value of the rate constant for hydrogen abstraction from EOH by an alkyl radical available to date.

4.2.2. Reactivity of Vitamin E in micellar solution.

In order to more effectively judge the usefulness of the various ketones examined as sources of the Vitamin E phenoxyl, the hydrogen abstraction reaction (reaction 4.4c) was studied in micelles of dodecyltrimethylammonium chloride (DTAC) via laser flash photolysis. In these experiments the concentration of EOH was generally kept below 2 mM since there is evidence that high concentration of alcohol substrates, especially these with long alkyl chains, tend to cause swelling of micelles[213]. This is also true of phenols [214] . The ketone concentrations were comparable to those used in the homogeneous solution experiments.

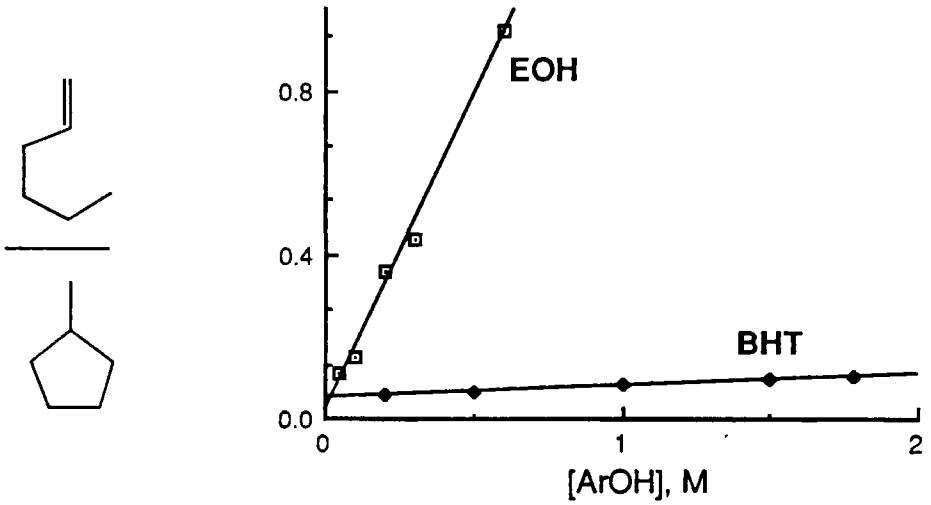


Figure 4.5. Plot of relative yields of unrearranged to rearranged product versus phenol concentration for hydrogen abstraction by 5–hexenyl in benzene at 70$^{0}$C.

Nitrogen laser excitation of 5mM benzophenone in 0.4M DTAC led to a weak but detectable triplet–triplet absorption spectrum of the ketone. The optical density of this spectrum at its $\lambda_{max}$ (525nm) was only 0.013 immediately after the laser pulse. Several hundred nanoseconds after the laser pulse there was a very weak ($\Delta OD < 0.003$) spectrum which appeared to be due to a mixture of the benzophenone triplet and ketyl radical. Under these conditions the triplet decayed via first order kinetics with a lifetime of 370ns as measured at 525nm and 425 nm. There is a weak, long-lived residual absorption at both of these wavelengths which accounts for only 4% of the top optical density observed. This may be attributed to exit from the micelle of ketyl radicals formed in the reaction of triplet benzophenone with the surfactant [54, 55].

When EOH is added to the system the situation changes somewhat. It is clear from spectral measurements that EOH quenches triplet benzophenone since in the end of pulse $\Delta$O.D. of the ketone triplet is reduced to 0.008 in the presence of 1.1mM EOH from 0.013 in the absence of the phenol. Again it is difficult to judge the extent of ketyl formation due to the weakness of the signals in the 500 to 600 nm region, although there is a shoulder at 550nm which is absent when no hydrogen donor is present. This may well be due to benzophenone ketyl absorption. In addition there is an increase in the optical density at 425 nm when EOH is present. The $\Delta$O.D. at this wavelength increased from 0.005 to 0.022 upon increasing the EOH concentration from zero to 2.8mM. The spectrum in this latter region, although weak, approximates that of the Vitamin E phenoxyl. No significant change in the triplet lifetime was observed at 525 nm however the kinetics at this wavelength are expected to be a complex mixture of triplet decay plus ketyl formation and decay [54, 55]. These mixed kinetics may mask the triplet decay.

In summary, we see that in a micellar environment triplet benzophenone abstracts a hydrogen atom from EOH leading to the phenoxyl radical. Further the reaction seems to be quite rapid. At least there is no grow in period for the signal

monitored at 425 nm (Figure 4.6). On the other hand there may be some interference from triplet benzophenone when measuring decay kinetics at 425 nm. This would be more of a problem at the lower EOH concentrations at which we prefer to work. In addition the fact that the escape fraction is only 4% means that the error in this quantity may be rather large. Since the value of escape fraction is used to calculate k– (see Chapter 2) a larger value of this parameter would be desirable if possible.

PMAP and xanthone triplets are also not ideal hydrogen abstractors for a magnetic field effect experiment involving EOH. In particular the ketone triplet absorptions interfere strongly with the kinetics observed at 425 nm in both cases. For example, the triplet absorption signal of PMAP in 0.3M DTAC in the presence of 3.8mM EOH did not decay completely until nearly 3μs after excitation. The kinetics of this same sample measured at 425 nm are also revealing. In the absence of EOH the PMAP triplet decays by first order kinetics and the absorption signal returns to pre-excitation baseline level. In the presence of EOH the observed decay trace resembles that of Figure 4.6 except that the residual is larger - about 10% at all EOH concentrations tested. However the observed rate constant of the fast component continues to increase with added Vitamin E up to the highest phenol concentration tested - 3.8 mM EOH. This fact, along with the spectral evidence, indicates that triplet PMAP interferes with the observation of $EO^{\bullet}$ kinetics even up to rather high concentrations of the phenol. A similar situation exists for the xanthone – Vitamin E – DTAC system. In particular, the value of the observed rate constant for the fast decay component measured at 425 nm continues to increase with EOH concentration at least up to 1mM EOH which was the highest Vitamin E concentration tested. In addition the escape fraction was only about 3% at this EOH concentration.

In micellar solution containing 0.021 M BUP the triplet state of this ketone decays by first order kinetics. We found the triplet lifetime to be 140 ns in 0.2M DTAC and 160 ns in 0.2 M SDS. In both cases the signals were measured at 365 nm. When

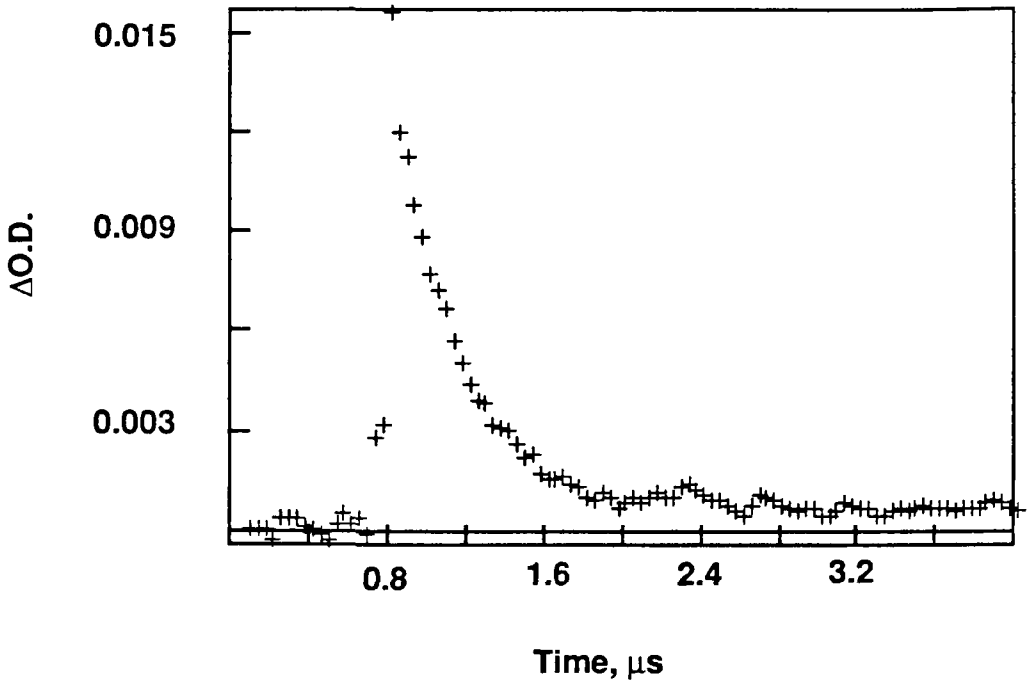


Figure 4.6. Deacy trace monitored at 425 nm in the presence of 5.5 mM bezophenone and 1.1mM Vitamin E in 0.4M DTAC.

1.6 mM EOH was added to the DTAC system the lifetime, monitored at 425 nm, increased slightly to 185 ns but the top ΔO.D. increased from 0,0055 to 0.025. Furthermore the end of pulse spectrum corresponds to that of the Vitamin E phenoxyl and there is no sign of a growing in period for the signal. Another promising feature is that the escape fraction was about 10% for BUP plus EOH in DTAC. Thus it would seem that the BUP triplet reacts efficiently with EOH in a micellar environment to form EO•. Further, there seems to be essentially no interference with the determination of the EO• kinetics by BUP species such as the triplet or the enol derived from the BUP biradical. We therefore conclude that the BUP triplet state is the most promising of the ketone triplets tested for use in a magnetic field effect experiment involving EOH.

4.2.3. Magnetic field effects on the decay of ketyl–aryloxyl radical pairs in micellar solution.

*The n-butyrophenone technique:*

Results obtained in the previous two sections suggested that the triplet state of n-butyrophenone (BUP) would be most useful for generating ketyl-aryloxyl triplet radical pairs in a micellar environment. In fact 0.021 M BUP was used as the hydrogen abstractor in practically all the experiments reported in the remainder of this chapter.

As indicated previously triplet BUP decays via the Norrish type II reaction in the absence of hydrogen donors [215–218], i.e.

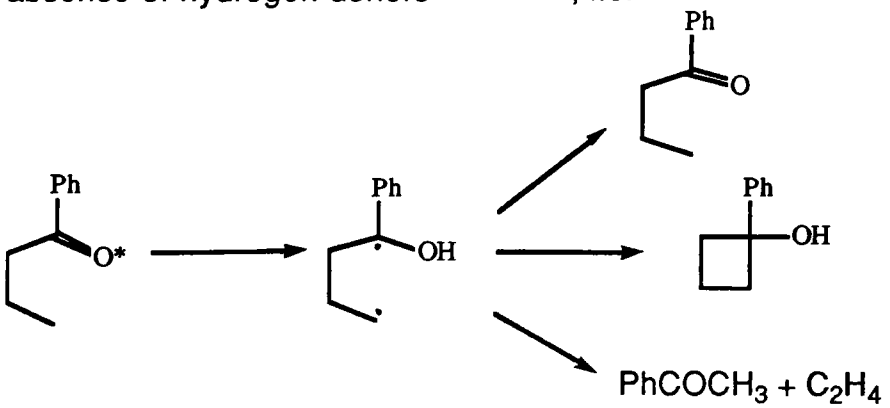

The triplet lifetime is about 100 ns in organic solvents and in micelles (*vide supra*). The biradical is also expected to have a lifetime of about 100 ns [219–221], for example, the biradical from γ–methylvalerophenone has $\tau_B$ = 92 ns in SDS micelles [50]. The lifetimes of Norrish type II biradicals are known to be insensitive to γ–alkyl substitution[219–221]. In any event, hydrogen abstraction from phenols by type II biradicals is not expected to be very rapid and hence not to be a significant source of phenoxyl radicals in the 100 ns time scale [201]. In the presence of phenols a considerable fraction of the BUP triplets undergo photoreduction (reaction 4.9) in

$$PhCOC_3H_7^* + ArOH \longrightarrow PhC^{\bullet}(OH)C_3H_7 + ArO^{\bullet} \qquad (4.9)$$

competition with reaction 4.8, This is supported by our own results with EOH in organic solvents and micelles as well as literature reports of the reactivity of EOH and other phenols towards nπ* ketone triplets [200, 201]. The interesting feature of this competition is that reaction 4.8 effectively becomes a "countdown" clock for reaction 4.9. In other words, any BUP triplets initially formed in phenol–free micelles may take a considerable time before they migrate to a phenol–occupied micelle. For example, for the isomeric isobutyrophenone triplet the exit rate from SDS micelles is only $1.6 \times 10^{6} s^{-1}$ [222]. In the absence of reaction 4.8, and at the relatively low phenol concentrations at which we work, the formation of phenoxyl radicals would therefore incorporate a slow component that would interfere with the study of radical pair decay. In effect this is likely the problem with using PMAP or xanthone as hydrogen abstractors for EOH except that the slow growth in these cases is probably masked by the fact that the ketone triplets have significant absorption in the EO• spectral region. By using BUP the ketone triplets that do not react with a phenol in the original micelle are able to decay rapidly and so have only a short lifetime.

In the case of BHT the technique described above led to complications. These were due to the production of only relatively weak signals and to the monitoring wavelength (400 nm) used. As a consequence both the BUP triplet and the acetophenone enol produced in reaction 4.8 caused interference. To minimize these problems we used 0.021M isobutyrophenone in place of BUP and added sufficient 1,3–pentadiene to reduce the triplet lifetime of the former to about 40 ns. Thus only those ketone triplets formed in phenol–occupied micelles will generate phenoxyl radicals.

*Characteristics of the decay traces and their analysis.*

Figure 4.7 shows decay traces obtained for the EO• – butyrophenone ketyl (BTK) triplet radical pair in SDS at various magnetic fields. Under our experimental conditions the formation of the radicals was much faster than their decay (*vide supra*). The chromophore monitored was that due to the phenoxyl radical and the decay traces, even at zero field, were always composed of a fast and a slow component. Spectral studies (Figure 4.8) showed that the species monitored was the same at short and long times, with only the intensity of the signal being different at different times following excitation. The spectrum agrees well with that reported for EO•[194] as well as with our own measurements in homogeneous solution.

Analysis of the "zero" field traces is straightforward. For this purpose we use the model developed previously for the photoreduction of benzophenone in micelles[54,55]. Scheme 4.1 illustrates the mechanistic model used. According to this model the rate constant for the fast decay, $k_{obs}$, will be given by

$$k_{obs} = k_{gem} + k- \qquad (4.10)$$

where $k_{gem}$ and k– are as defined previously. By fitting the decay traces with the biexponential function discussed in Chapter 3 we are able to obtain values of $k_{obs}$ as well as the values of $A_{fast}$ and $A_{slow}$, the optical densities associated with the fast and

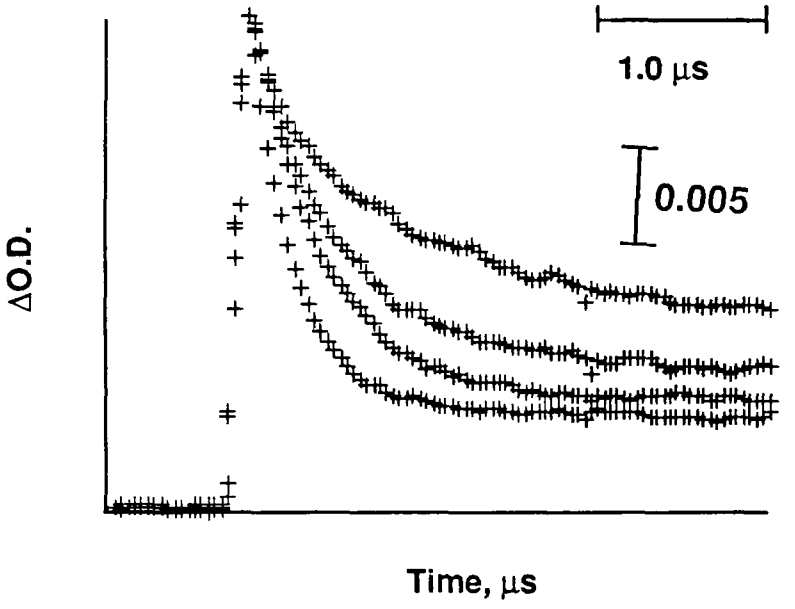


Figure 4.7. Magnetic field effect on the Vitamin E phenoxyl–butyrophenone ketyl radical pair in 0.2M SDS. From the bottom: 0 G; 100 G (stirring magnet); 500 G (horseshoe magnet); 1400 G. [EOH] = 1.5mM, [butyrophenone] = 0.021M, monitored at 425 nm.

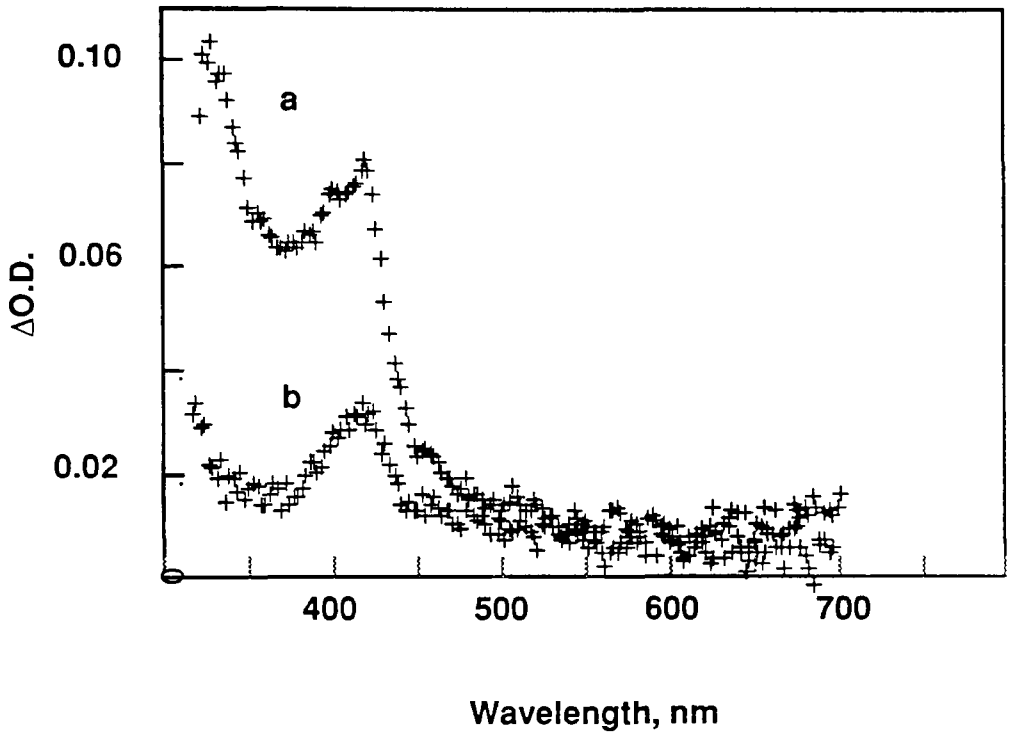


Figure 4.8. Transient absorption spectra of Vitamin E phenoxyl radical in SDS obtained at 200 ns (a) and 2.0 μs (b) after 308 nm laser excitation using OMA detection. Gate = 20 ns, [EOH] = 1.5 mM, [butyrophenone] = 0.021M.

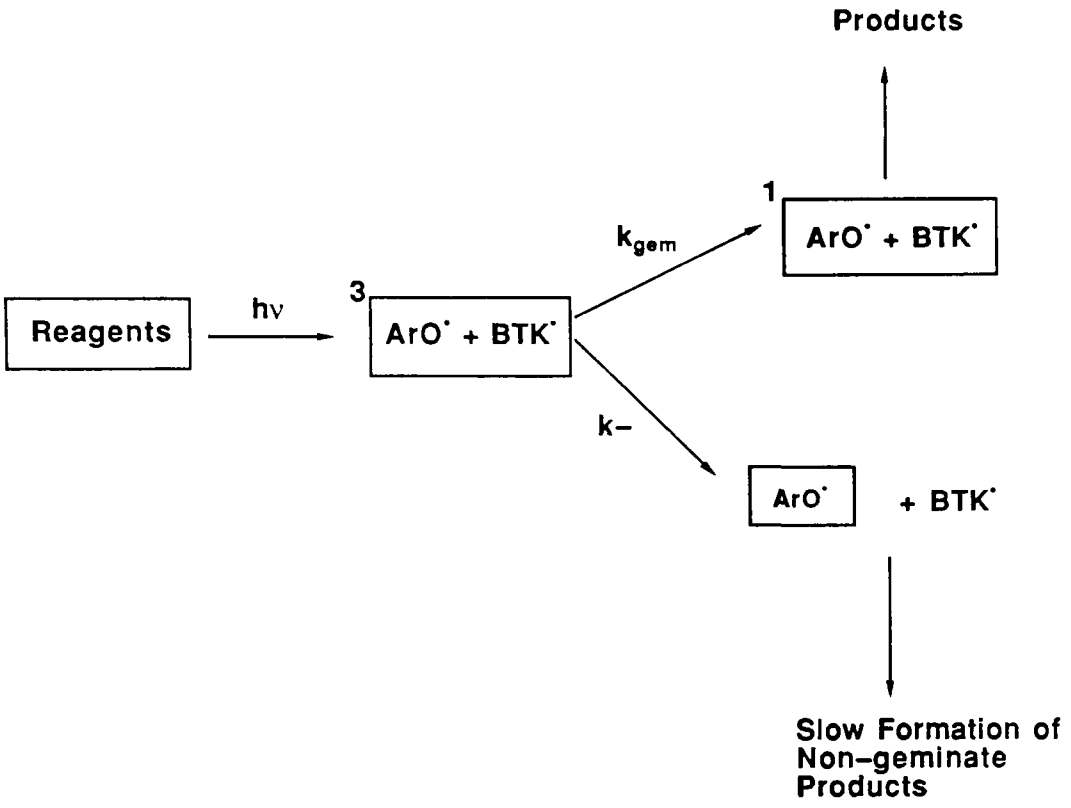
Products
1
ArO• + BTK•
kgem
Reagents
hν
3
ArO• + BTK•
k–
ArO•
+ BTK•
Slow Formation of
Non-geminate
Products

Scheme 4.1.

slow decay components, respectively. The escape fraction, or % escape, can then be determined from the relation.

$$\% \text{ Escape} = 100\left(\frac{A_{slow}}{\text{top } \Delta O.D.}\right) \qquad (4.11)$$

Once % escape and $k_{obs}$ are known, separate values of $k_{gem}$ and k– can be obtained as indicated in Chapter 1. For example, by fitting the zero field trace of Figure 4.7 in this manner we obtained % escape = 20%, k– = $7.7 \times 10^5 s^{-1}$, and $k_{gem} = 2.0 \times 10^6 s^{-1}$.

It should be noted while a double exponential provided an adequate fit to the kinetic data in all cases (see Figure 3.2, for example) this cannot be taken as a critical test of the mechanism of Scheme 4.1. In the presence of an external magnetic field, we would only anticipate this type (i.e., biexponential) behaviour if the interconversion among the triplet sublevels were fast on our time scale. This may or may not be the case. Multiexponential fits of transient absorption data are not as reliable as those obtained from luminescence (for example, single photon counting) [223], largely because the data are not as precise nor are they monitored over a comparable number of lifetimes. Our present results were, however, more than adequate to determine reproducible values of k–, $k_{gem}$, and the % escape at each field value.

The values of $k_{obs}$ for the $EO^{\bullet}$ – BTK system in SDS follow a characteristic pattern in which they decrease at low fields (usually < 1000 G) and start increasing again at higher fields (see figure 4.9a). This effect has been discussed before [54, 55]. It is simply due to a decrease of $k_{gem}$ from $T_+$ and $T_-$ at low fields, which blends with the decay process. Ideally, intersystem crossing would be totally shut off from $T_+$ and $T_-$ at high fields. In such a situation the kinetic behaviour of the fast component would be the same as that recorded at zero field. That is, if no $T_+ <-> T_o$ or $T_- <-> T_o$ interconversion takes place, the fast component at high field would be fully accounted for by the decay due to $T_o$, which is assumed to be field independent. Naturally, the value of $A_{fast}$ at

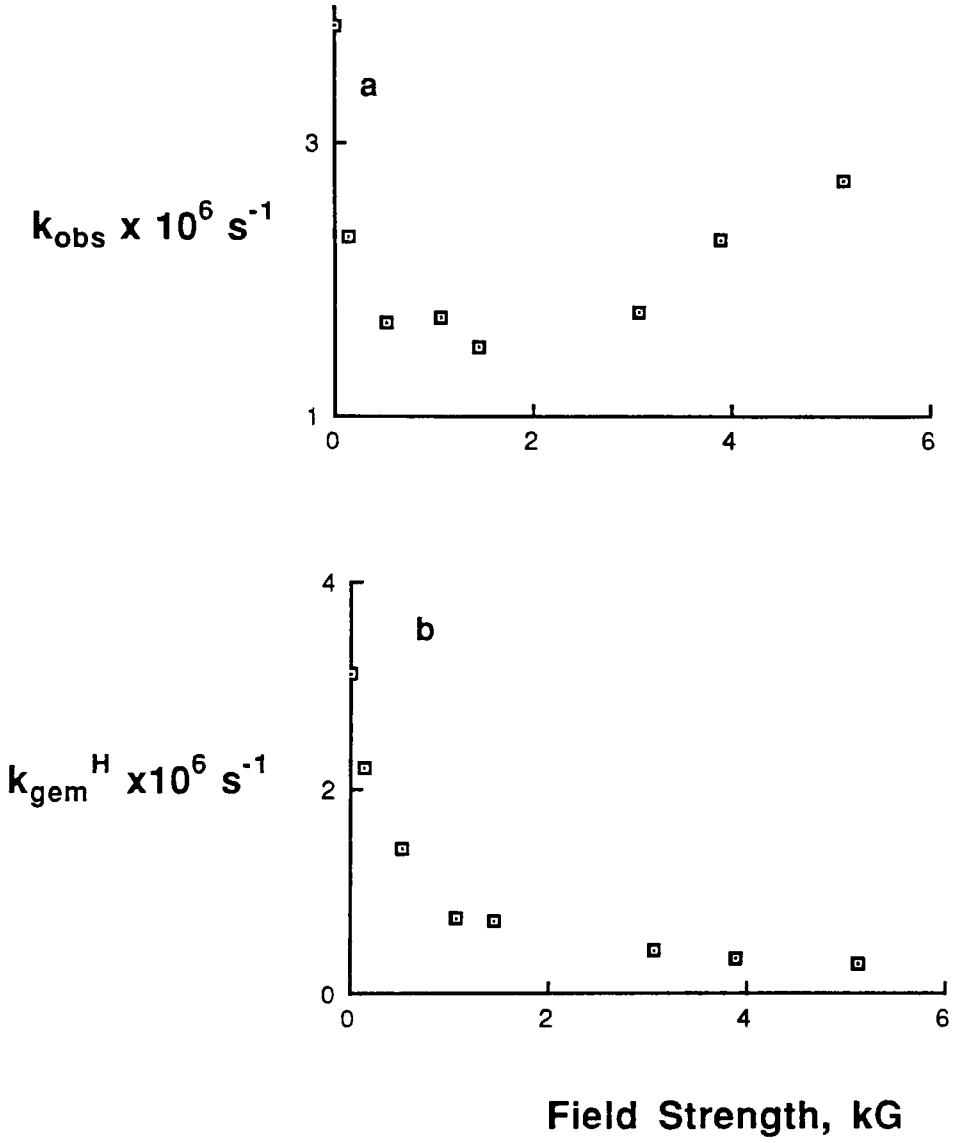


Figure 4.9. Variation of $k_{obs}$ and $k_{gem}^{H}$ with magnetic field strength for the Vitamin E phenoxyl–butyrophenone ketyl radical pair in 0.11M SDS. $k_{obs}$ (a), $k_{gem}^{H}$ (b).

high fields is much smaller than at zero field (ideally 1/3). Experimentally, the expected evolution of $k_{obs}$ is observed, but the full recovery is not realized by fields up to 5kG (Figure 4.9 a).

The plot of Figure 4.9 a should be compared to that of Figure 4.9 b in which an overall rate constant, $k_{gem}^{H}$, is plotted as a function of field strength. The value of $k_{gem}^{H}$ is based on the assumption that k– is field independent, i.e.

$$k_{gem}^{H} = \frac{k-}{(\%\ \text{escape})^{H}} - k- \qquad (4.12)$$

The value of $k_{gem}^{H}$ is that which would lead to the observed % escape if k- were field independent and if $k_{gem}$ was the same for all triplet sublevels (or if these were in rapid equilibrium). The plots of $k_{obs}$ and $k_{gem}^{H}$ clearly show that there is no rapid $T_{\pm}$ <–> $T_o$ interconversion in the EO• – BTK system at high fields. If this were not so $k_{obs}$ at high fields would not tend back towards the value of $k_{obs}$ at zero field but would rather follow a trend similar to that of $k_{gem}^{H}$.

Values of % escape, k– and $k_{gem}$ (at zero field) for the EO• – BTK system in a variety of different surfactants are reported in Table 4.6. The table also lists values of these parameters for several other phenoxyl–BTK systems. Our % escape values are subject to absolute errors of ca. 4 – 5 %. Values of escape of around 10% therefore have close to 50% relative error, and naturally this error is also incorporated into the values of the rate constants. Thus, systems such as DTAB/EOH are subject to rather large errors at zero field. Data in SDS were significantly more reproducible than in the other micelles, with errors in the % escape being closer to ± 2-3%.

Escape fractions were determined by equation 4.11. A representative plot is shown in Figure 4.10. All other plots showed similar features. The field required to achieve half the maximum change was usually around 500–800 G.

Table 4.6. Geminate reaction and escape data for various surfactant–phenol combinations.

| Surfactant | Phenol | $k_{gem}$ $x10^6$ $s^{-1}$ | k– $x10^6$ $s^{-1}$ | % escape 0 G | % escape 5000 G |
|---|---|---|---|---|---|
| SDS (0.15M) | 35D | 3.0 | 2.2 | 43 | 72 |
| | EOH | 2.0 | 0.77 | 20 | 72 |
| | CRM | 3.7 | 0.97 | 21 | 76 |
| | FUR | 2.7 | 1.4 | 34 | 68 |
| | BHT[a] | 2.0 | 0.63 | 24 | 62 |
| | Trolox[b] | 3.0 | 1.1 | 25 | 73 |
| CTAB (0.06M) | EOH | 0.94 | 0.15 | 15 | 57 |
| | CRM | 1.3 | 0.22 | 14 | 67 |
| | FUR | 1.4 | 0.36 | 21 | 57 |
| CTAC (0.13M) | 35D | 2.6 | 2.6 | 50 | 76 |
| | EOH | 0.94 | 0.26 | 22 | 64 |
| | CRM | 1.8 | 0.20 | 10 | 67 |
| | FUR | 2.0 | 0.60 | 23 | 61 |
| Brij–35 (0.1M) | 35D | 2.7 | 2.7 | 50 | 65 |
| | EOH | 1.9 | 0.51 | 19 | 65 |
| | CRM | 1.8 | 0.66 | 27 | 57 |
| | FUR | 2.1 | 1.4 | 35 | 49 |
| DTAB (0.16M) | EOH | 3.3 | 0.42 | 11 | 70 |
| | CRM | 4.0 | 0.53 | 12 | 70 |
| | FUR | 3.0 | 0.66 | 18 | 61 |

(a) Using isobutyrophenone; see text.
(b) At pH 4.

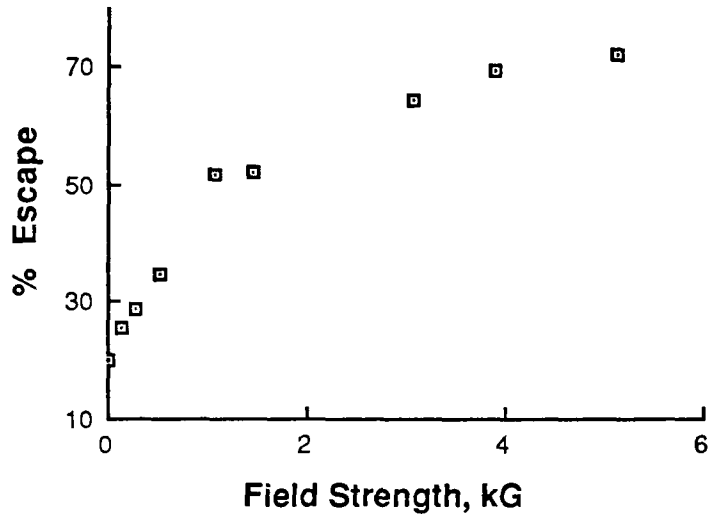


Figure 4.10. Variation in % escape with magnetic field strength for the Vitamin E phenoxyl–butyrophenone ketyl radical pair in 0.2M SDS.

Finally, it should be pointed out that the rate constants measured for the decay of phenoxyl–ketyl radical pairs in micelles (Table 4.6) are independent of the phenol concentration used. While the data reported in the table was obtained at 1.5mM phenol, increasing 35D or EOH to 6 mM, CRM to 12 mM, and FUR t0 14 mM lead to values of $k_{gem}$, k– and % escape which were within experimental error equal to those given in Table 4.6.

4.2.2 The influence of Cu(II) on the $EO^{\bullet}$– BTK system.

Addition of the paramagnetic salt $CuSO_4$ to the EOH–BUP–SDS system at concentrations not exceeding 5 mM has a profound effect on the high field decay behaviour. In the same concentration range, Cu(II) has only a marginal effect at zero field. For example, Figure 4.11a shows zero field decay traces at 425 nm for a sample containing 2.5 mM EOH plus 0.021 M BUP in 0.15 M SDS at zero and 2.2 mM Cu(II). The top ΔO.D. is insensitive to Cu(II). The value of $k_{obs}$ at these two metal ion concentrations were $3.2 \times 10^6$ $s^{-1}$ and $3.6 \times 10^6$ $s^{-1}$, respectively. The % escape values were 22% and 20%. Thus $k_{gem} = 2.5 \times 10^6$ $s^{-1}$ and k– = $0.71 \times 10^6$ $s^{-1}$ in the absence of Cu(II) while kgem = $2.9 \times 10^6$ $s^{-1}$ and k– = $0.74 \times 10^6$ $s^{-1}$ at 2.2 mM Cu(II).

At an applied field of 5 kG the situation is very different (Figure 4.11b). The presence of Cu(II) at 2.2 mM reduces the extent of escape from 74 % (no Cu(II)) to 37 % (2.2 mM Cu(II)) although it has essentially no influence on top Δ O.D. nor on $k_{obs}$. A similar type of effect on the high field behaviour of the triplet 1,4–naphthosemiquinone–SDS alkyl radical pair in the presence of paramagnetic lanthanides has been reported by Hayashi [85]. In this latter study the magnetic field effect could be fully suppressed at ion concentrations which had no influence on the zero field behaviour.

Finally, k– is effectively independent of [Cu(II)] in the concentration range studied. We note, however, that preliminary experiments at higher copper ion

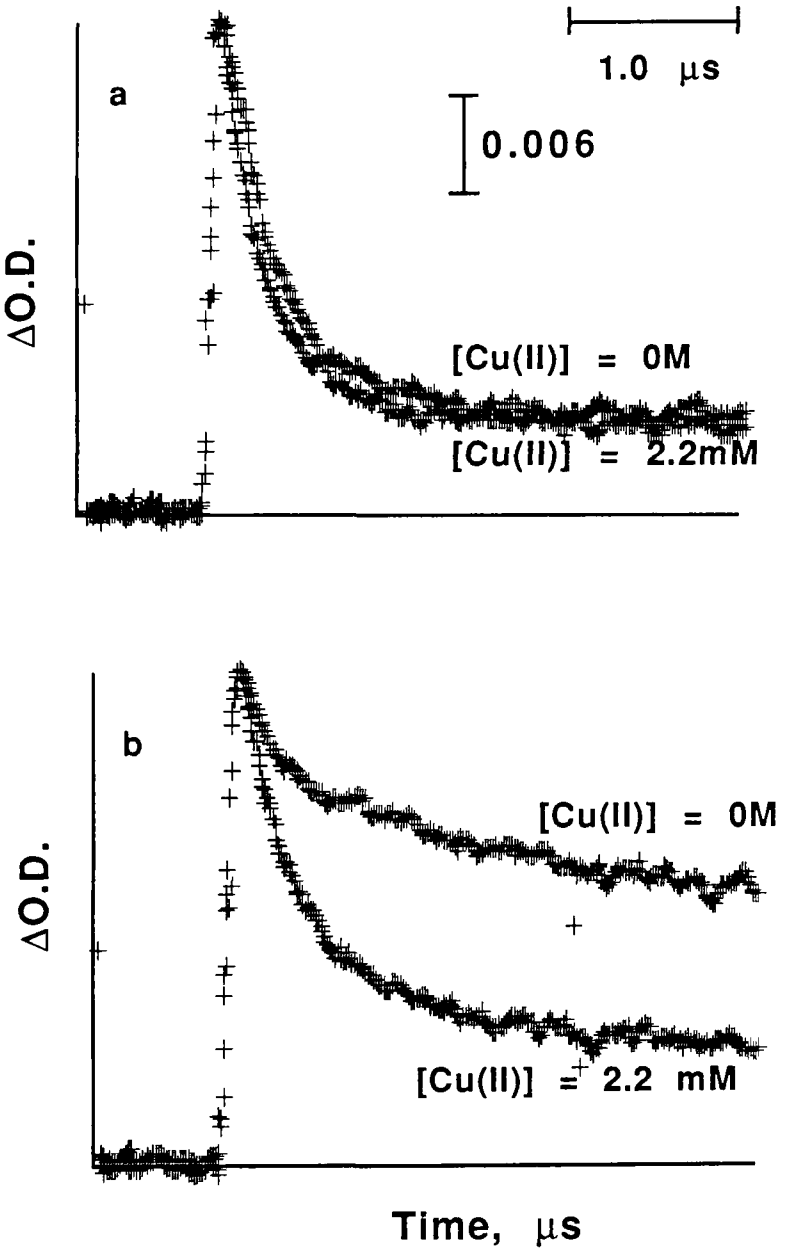


Figure 4.11. Decay of the Vitamin E phenoxyl at 425 nm in 0.2M SDS in the presence and absence of Cu(II) at 0 G (a) and 5000 G (b). [EOH] = 1.5mM, [butyrophenone] = 0.021M, [Cu(II)] as indicated. Top ΔO.D. = 0.03, same time scale for both.

concentrations showed that k– increased linearly with [Cu(II)] suggesting that reactions between the ion and exiting radicals may indeed take place although we did not observe any spectral evidence for BTK–Cu(II) complexes.

4.2.3 Trolox in micellar solution.

Trolox (Chart 3.1) is a popular, water soluble Vitamin E model compound[167,224–228]. Although often used as an antioxidant in model autoxidation systems involving micelles there seems to be little information available about the kinetics of Trolox interaction with micelles. As a result we have carried out a number of preliminary experiments in an attempt to gain some insight into these kinetic processes.

*Fluorescence:*

Figure 4.12 shows Stern–Volmer plots for quenching of pyrene monomer fluorescence by Trolox in methanol (4.12a) and in SDS at pH 4 (4.12b). The samples contained $5x10^{-6}$ M pyrene and were excited at 334 nm. The emission intensities were determined as described in Chapter 3. In the SDS experiments the solution pH was adjusted using the "dummy" technique outlined in the Experimental Chapter.

The Stern–Volmer constant, $k_q\tau$, for Trolox quenching of singlet pyrene was determined to be 977 ± 40 $M^{-1}$ in deaerated methanol. The lifetime of pyrene singlet in the absence of Trolox was determined to be 475 ns by single photon counting. Thus Trolox deactivates pyrene singlet with rate constant $k_q = 2.1x10^9$ $M^{-1}s^{-1}$ in homogeneous solution.

Figure 4.12b shows Stern–Volmer plots for the Trolox – pyrene system at various SDS concentrations at pH 4. There is obviously a strong contribution from static quenching. It is possible to calculate the association constant of Trolox with SDS under these experimental conditions using the method of Encinas and Lissi [173]

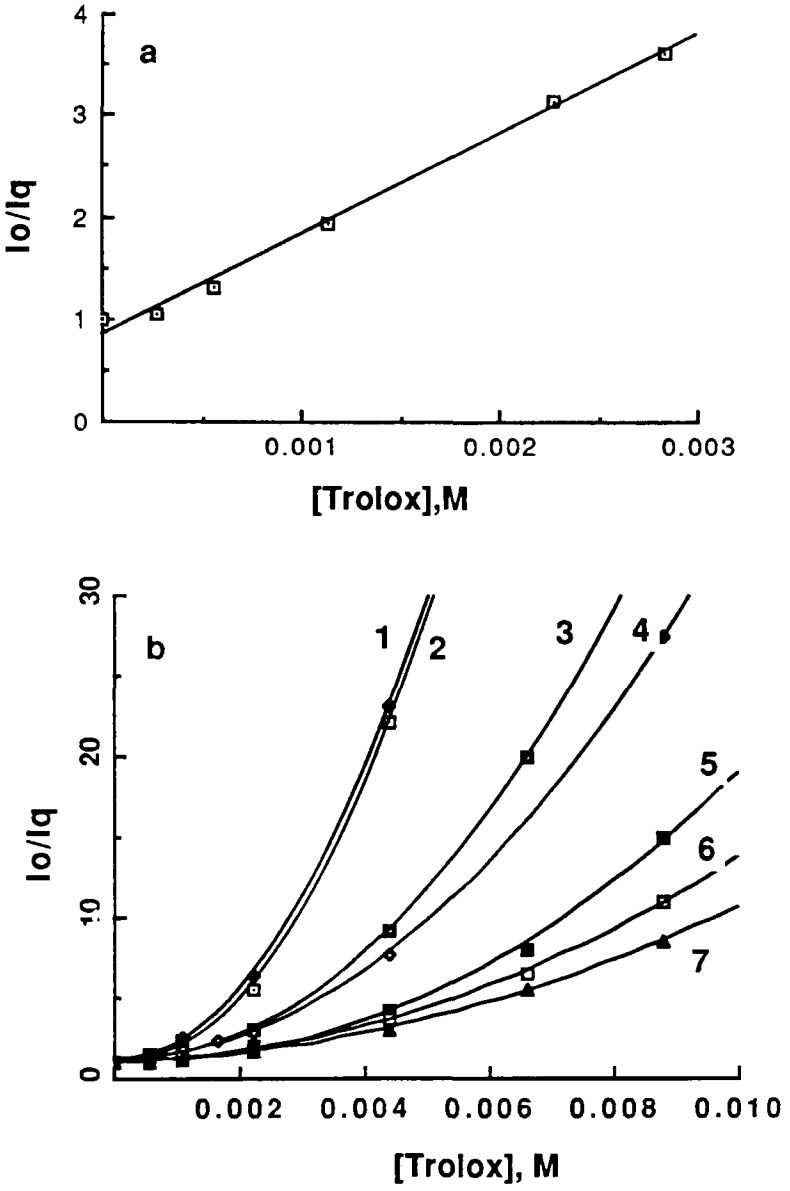


Figure 4.12. (a) Quenching of pyrene fluorescence by Trolox in methanol. (b) Quenching of pyrene fluorescence by Trolox in SDS at pH 4. [SDS]: 0.02M (1); 0.05M (2); 0.10M (3); 0.144M (4); 0.17M (5); 0.20 (6); 0.25M (7).

described in Chapter 3. Our data gives a mean association constant of 2374± 254 $M^{-1}$. Thus there is extensive association of Trolox with SDS at pH 4.

In aqueous SDS at pH 4 Trolox is by and large associated with the micellar pseudo–phase. At this pH a solution of 1.5 mM Trolox and 0.021 M BUP in 0.30M SDS show behaviour which is very similar to that of the EOH– BUP pair following nitrogen laser excitation. In the absence of an external field the % escape is 25%, $k_{gem}$ = $3.0x10^6s^{-1}$ and k– = $1.1x10^6s^{-1}$ as monitored at 430 nm. When an external magnetic field of 5 kG was applied the % escape increased to 73%. Essentially the same results were obtained at 0.01 M Trolox.

If the pH is altered the situation changes dramatically. Figure 4.13 shows % escape at zero field for the Trolox–BUP system as a function of pH in 0.3 M SDS solution. This figure is essentially a titration curve and the inflexion point is approximately pH 6.5. It seems that the $pK_a$ value of Trolox is not known. The figure shows that the water solubility of Trolox increases sharply between pH 5.5 and 7.

4.2.4. Influence of Micellar Dimensions on the decay of the $EO^{\bullet}$ –BTK triplet radical pair.

*Effect of added electrolyte:*

It is a well known characteristic of SDS that the micellar aggregation number and micellar volume increase upon addition of counter ions [4, 13]. In Figure 4.14a is shown a plot of $k_{gem}$ for the $EO^{\bullet}$–BTK system versus 1/N where N is the aggregation number of SDS. Each point represents a different NaCl concentration between zero and 0.6M. The N data were obtained from a number of literature sources [229–232]. Clearly there is a good correlation between the two sets of data. Figure 4.14b shows similar plot based on 1 / k–. In this case the overall trend is similar to that of the $k_{gem}$ data. Figure 4.15 shows values of k– plotted against 1/r where r is the mean hydrodynamic radius of SDS. The r values are from the literature [16, 233, 234] and

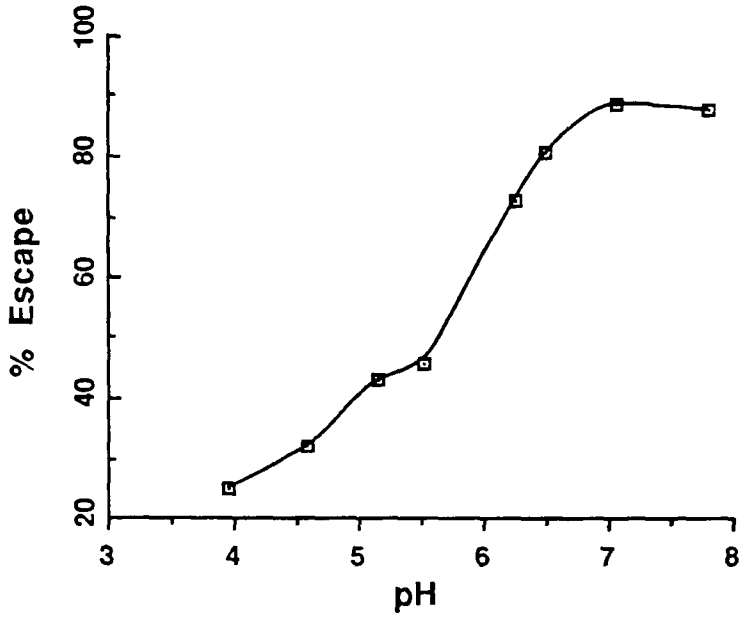


Figure 4.13. % Escape as a function of pH for the Trolox phenoxyl–butyrophenone ketyl radical pair in 0.15M SDS. [Trolox] = 0.01M; [butyrophenone] = 0.021M.

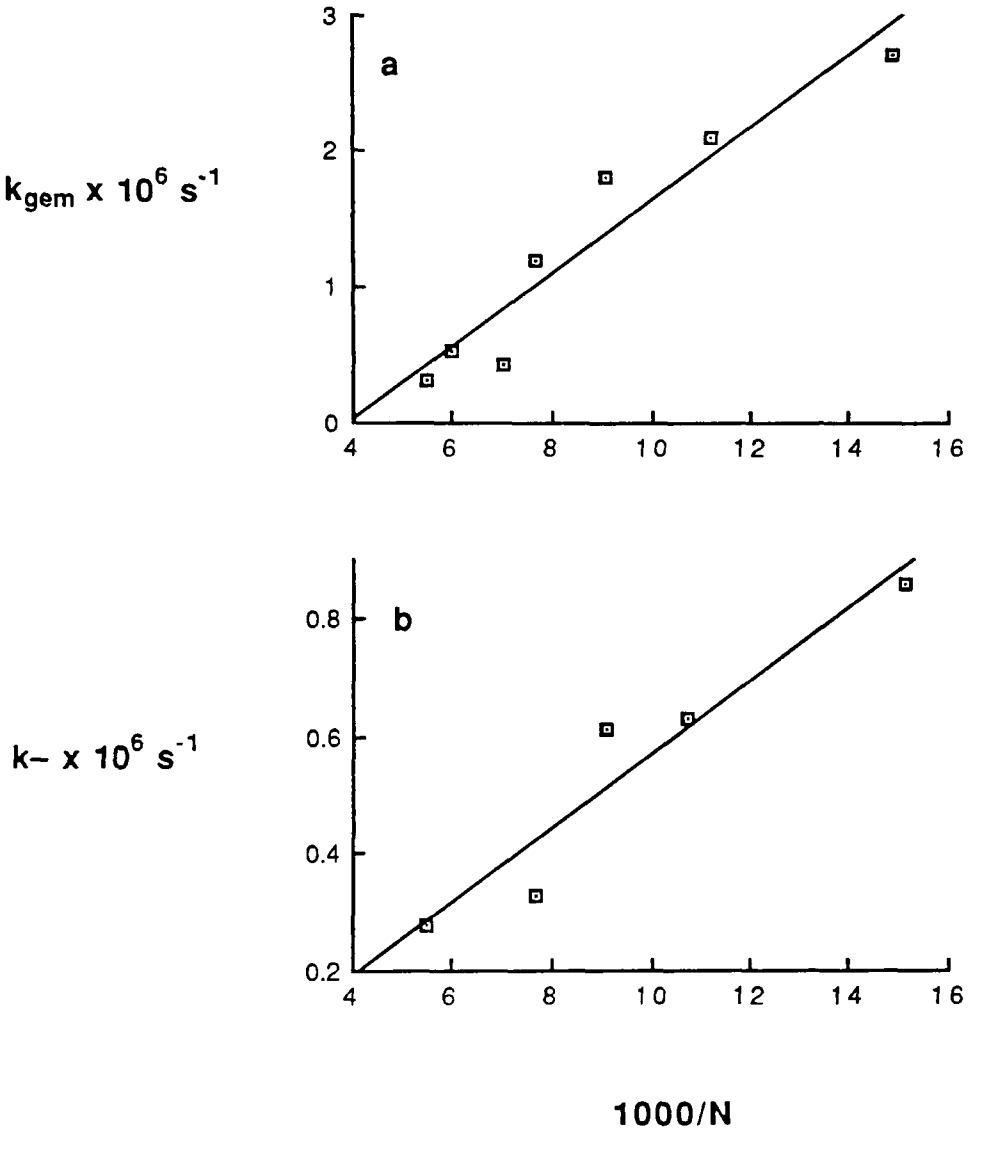


Figure 4.14. Variation in $k_{gem}$ (a) and k– (b) with the reciprocal of SDS aggregation number for the Vitamin E phenoxyl–butyrophenone ketyl radical pair. The points represent different [NaCl] between 0 and 0.6M NaCl. [EOH] = 2.5mM, [butyrophenone] = 0.021M, [SDS] = 0.15M.

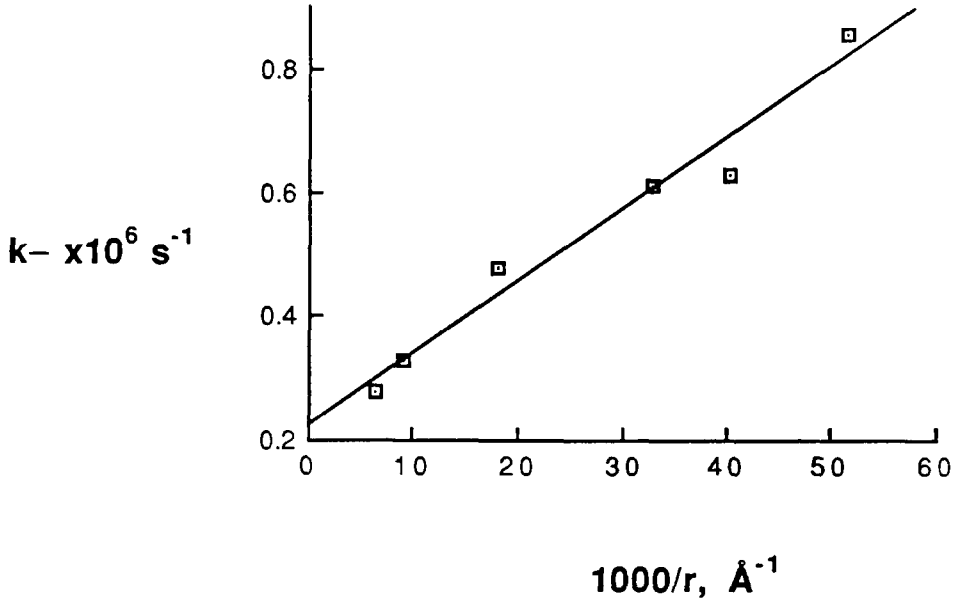


Figure 4.15. Variation in k– for the Vitamin E phenoxyl–butyrophenone ketyl radical pair with the reciprocal of the mean hydrodynamic radius of SDS. Each point represents a value of [NaCl] between 0 and 0.6M. [EOH] = 2.5mM, [butyrophenone] = 0.021M, [SDS] = 0.15M.

each point represents a different value of NaCl concentration. Selected values of $k_{gem}$ and k– in SDS at room temperature in the presence of several different concentrations of NaCl are given in Tables 4.7 and 4.8.

*Effect of surfactant chain length:*

Tables 4.7 and 4.8 report values of $k_{gem}$ and k– for the EO•–BTK triplet radical pair in SDS and in the $C_{10}$ analogue, sodiumdecylsulfate (SDecS). From these data it seems that changing the length of the surfactant's hydrocarbon chain, and therefore the micellar dimensions, has an effect on the rate constants, which parallels other variables (i.e., electrolytes or temperature), which also influence the micellar size.

*Effect of temperature:*

a) Exit rate constants.

At zero magnetic field the decay of the EO•–BTK triplet radical pair shows a pronounced temperature dependence in SDS and SDecS. For example Figure 4.16 shows the decay of the phenoxyl radical measured at 425 nm at $6^0$C (4.16a) and $69^0$C (4.16b) for a sample containing 2.5 mM EOH and 0.021M BUP in 0.15 M SDS. The details of this temperature dependence can also be influenced by additions of NaCl. At all temperatures (5 to $85^0$C) and salt concentrations (0 to 0.5M NaCl) examined we have been able to calculate $k_{gem}$ and k–. In this section we present our k– results.

Arrhenius plots based on k– are linear over the entire temperature range examined and at the three NaCl concentrations examined (see Figure 4.17). This is true for both SDS and SDecS. Table 4.9 presents the Arrhenius parameters for exit processes involving this particular radical pair. The activation energies shown are within experimental error of each other although there appears to be a trend towards larger Ea values in larger micelles.

b) Geminate rate constants.

Figure 4.18 shows Arrhenius plots based on $k_{gem}$ for the EO•–BTK system in SDS at 0, 0.25 and 0.5 M NaCl (4.18a, 4.18b and 4.18c, respectively). Similar plots of

Table 4.7. Values of $k_{gem}$ under various conditions of micellar aggregation.

| Surfactant | [NaCl] M | $k_{gem}$ $x10^6$ $s^{-1}$ | |
|---|---|---|---|
| | | $20^0C$ | $80^0C$ |
| SDecS | 0.0 | 3.4 | 6.2 |
| | 0.25 | 2.9 | 6.3 |
| | 0.50 | 2.2 | 6.2 |
| SDS | 0.0 | 2.5 | 5.6 |
| | 0.25 | 1.6 | 5.3 |
| | 0.5 | 0.31 | 5.6 |

Table 4.8. Values of k– under various conditions of micellar aggregation.

| Surfactant | [NaCl] | k– | |
|---|---|---|---|
| | M | $20^0$C | $80^0$C |
| SDecS | 0.0 | 1.1 | 6.2 |
| | 0.25 | 0.75 | 6.3 |
| | 0.50 | 0.64 | 4.5 |
| SDS | 0.0 | 0.72 | 5.2 |
| | 0.25 | 0.43 | 4.5 |
| | 0.50 | 0.27 | 4.9 |

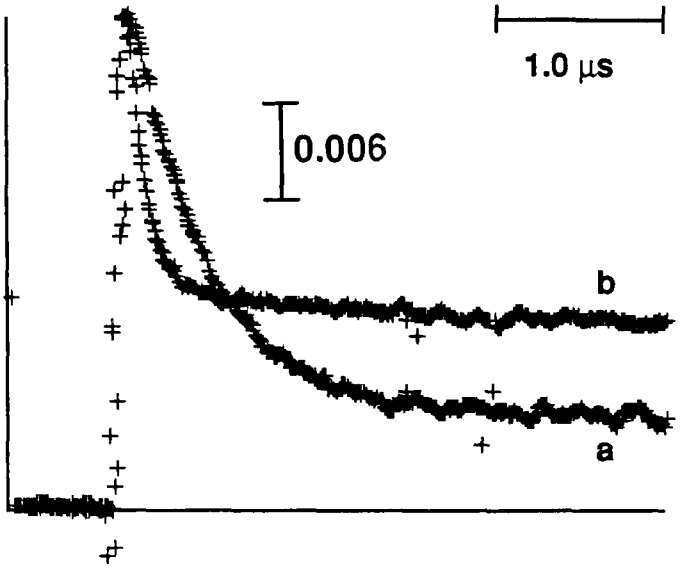


Figure 4.16. Kinetic traces for the decay of the Vitamin E phenoxyl radical at 425 nm recorded in SDS at 6C (a) and 69C (b). [EOH] = 2.5 mM, [butyrophenone] = 0.021M, [SDS] = 0.15M.

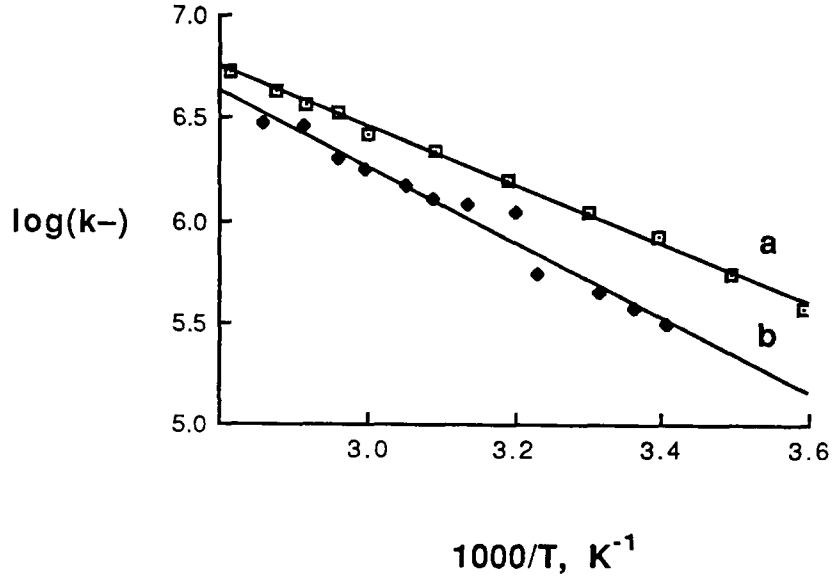


Figure 4.17. Arrhenius plots based on k– for the Vitamin E phenoxyl–butyrohpenone ketyl radical pair in 0.15M SDS in the presence of 0 M (a) and 0.5M (b) NaCl.

Table 4.9. Activation parameters for BTK ketyl radical exit from SDS and SDecS.

| Surfactant | [NaCl] M | Ea kcal/mol | Mean kcal/mol | logA $s^{-1}$ |
|---|---|---|---|---|
| SDecS | 0.0 | 5.5±0.8 | | 10.2±0.6 |
| | 0.25 | 6.1±1.2 | 5.8±0.3 | 10.5±1.0 |
| | 0.50 | 5.9±0.6 | | 10.3±0.4 |
| SDS | 0.0 | 6.5±1.8 | | 10.7±1.2 |
| | 0.25 | 7.0±1.0 | 7.3±1.0 | 10.9±0.8 |
| | 0.50 | 8.4±1.4 | | 11.7±1.0 |

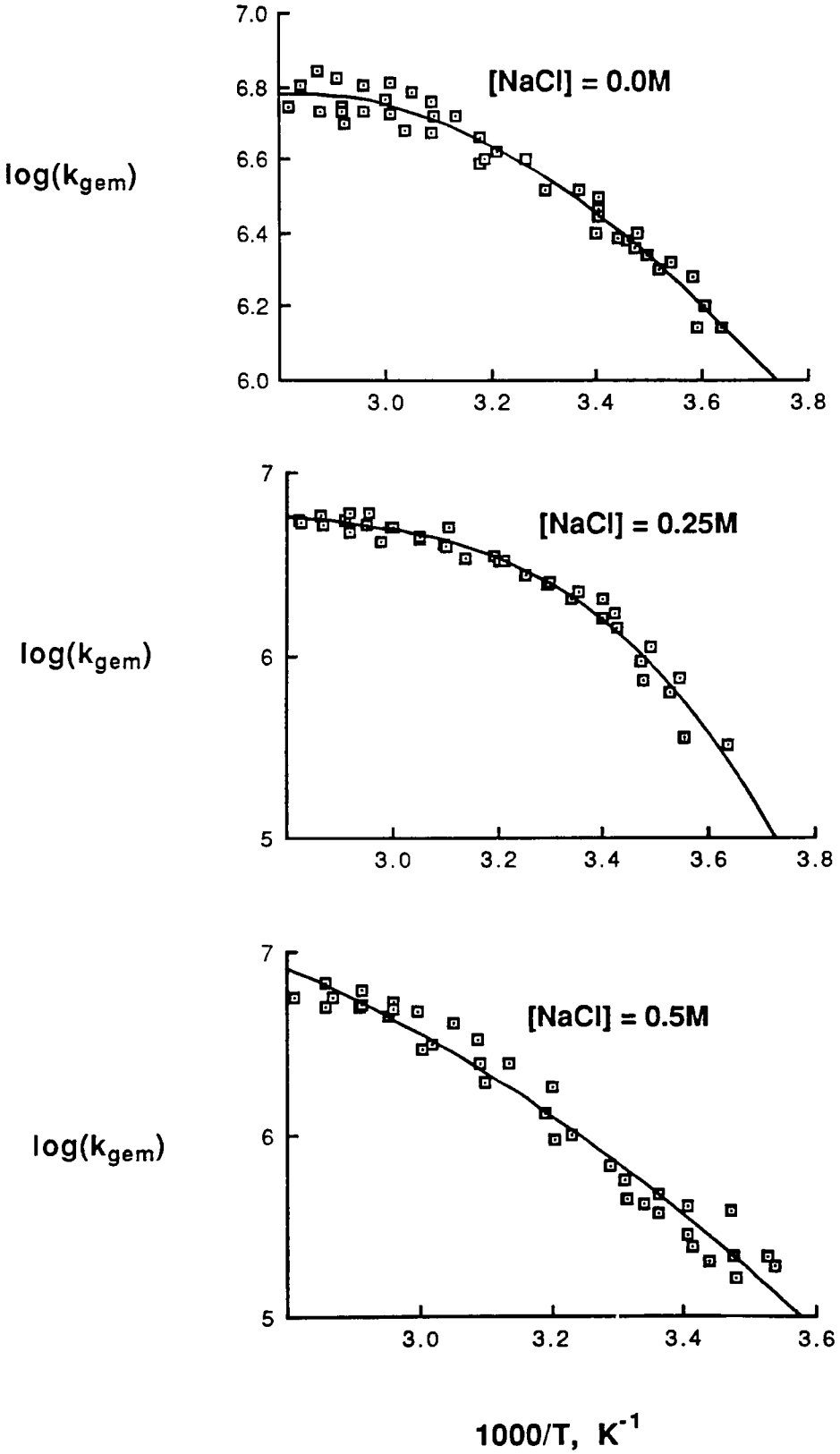


Figure 4.18. $k_{gem}$ Arrhenius plots for the $EO^{\bullet}$/BTK pair in 0.15M SDS at various [NaCl].

Table 4.10. "Break" temperatures and critical micelle temperatures (cmt) for SDS at various [NaCl].

| [NaCl] M | Break Temperature $^0C$ | cmt $^0C$ |
|---|---|---|
| 0.0 | 25–30 | 16[a], 15[b] |
| 0.25 | 35–40 | 24[c] |
| 0.50 | 60–65 | 26[c] |

(a) 0.069M SDS; reference [235].

(b) 0.20M SDS; reference [235].

(c) 0.15M SDS; by FTIR.

log $k_{gem}$ versus 1/T for SDecS show qualitatively similar behaviour. In contrast to the k– data, these $k_{gem}$ Arrhenius plots show significant curvature as well as an influence of salt concentration.

Table 4.10 gives values of the temperature ranges over which the $k_{gem}$ values for the SDS system seem to reach a plateau (Figure 4.18). The table also presents values of the critical micelle temperature (cmt) obtained from the literature [235] and from FTIR measurements carried out at NRCC (see Chapter 3). It would seem that there is not a correlation between the temperatures at which the plateau behaviour of $k_{gem}$ commences and the values of cmt. This suggests that the curvature in the Arrhenius plots of Figure 4.18 is probably not due to a phase change. However, it should be noted that an accurate estimate of the "plateau" temperatures is difficult to obtain from the plots of Figure 4.18 because the change of slope is poorly defined. In spite of this, it is clear that at high temperatures $k_{gem}$ becomes largely independent of the salt concentration (see also Table 4.7).

## 4.3 Discussion.

### 4.3.1 Homogeneous solution.

#### 4.3.1.1 Reactions of EOH with triplet ketones.

Our study of the reactivity of EOH towards aromatic ketone and aryl alkyl ketone triplets shows that, for the most part, vitamin E behaves as a typical phenol. For example, the near diffusion controlled rate constants [200, 201] for the triplet quenching yielding the phenoxyl radical, the fact that $n\pi^*$ and $\pi\pi^*$ triplets show comparable reactivities towards EOH [201] and the rather high ketyl yield of the quenching process[200, 201] are all characteristic of the photoreduction of triplet ketones by phenols. With respect to the last point, the ketyl yield is not reflected in the overall yield of products formed upon photoreduction of $n\pi^*$ ketone triplets by phenols [200, 236–238]. In fact the quantum yield of benzophenone disappearance due to photoreduction

by EOH has been estimated to be less than 0.1 in 1:1 acetonitrile:water [200]. These results indicate that the triplet quenching reaction leading to ketyl (reaction 4.4c) is reversible and leads to regeneration of the starting materials.

While it is clear that hydrogen abstraction leading to a ketyl radical and a phenoxyl radical is the dominant decay pathway for triplet benzophenone, this is not reflected in the deuterium isotope effect measured for this reaction. The measured effect of 1.09 is very small but is in line with the isotope effects measured for benzophenone with other phenols in wet acetonitrile which were found to be about 1.2 to 1.4 [201]. In contrast to Das's work we also found only a marginal isotope effect on the rate constant for quenching of PMAP and xanthone triplets ($\pi\pi^*$ under our experimental conditions) by Vitamin E. While our isotope effect values were about 1.2 (Table 4.2) Das et al. reported a value of 3.9 for quenching of triplet p–methoxypropiophenone by phenol. In fact for reactions with rate constants as high as those measured here (Table 4.1) it is not surprising that a very low isotope effect is observed [162, 239]. In fact, for diffusion controlled reactions no isotope effect is to be expected.

The data in Table 4.3 shows that the reactivity of phenol towards quenching of triplet PMAP in 10% $H_2O$/acetonitrile is almost 37 times lower than that of EOH in the same solvent. Such a large difference in reactivity towards hydrogen abstraction involving EOH versus other phenols is certainly not without precedent. For example, the rate constant for hydrogen abstraction from EOH by the poly(peroxystyryl)peroxyl radical at $30^0$C in 1:7 chlorobenzene:styrene has been reported to be $329 \times 10^4 M^{-1}s^{-1}$ [167] while the rate constant for hydrogen abstraction from 2,4,6–trimethylphenol by the same radical is just $8.5 \times 10^4$ $M^{-1}s^{-1}$ in the same solvent at the same temperature. In the PMAP experiments described here both phenols are subject to hydrogen bonding in 10% $H_2O$/acetonitrile so the difference in rate constants probably reflects an intrinsic difference in reactivity of these phenols towards the $\pi\pi^*$

triplet. This reactivity difference appears to vanish in benzene where no hydrogen bonding is possible. Since the phenolic –OH group is no longer hydrogen bonded in this latter solvent it is now more available for hydrogen abstraction. On the other hand, the reaction of EOH with triplet PMAP is nearly diffusion controlled even in a hydrogen bonding solvent, so one cannot expect to see its rate constant value increase when hydrogen bonding is eliminated. In other words, the similarity of the rate constant for EOH and phenol in benzene does not imply that these species are equally reactive in this solvent, merely that both reactions have reached the diffusion controlled limit. The fact that EOH is extremely reactive to triplet PMAP even in a hydrogen bonding solvent suggests that this reaction involves a transition state where hydrogen transfer is not as developed as is the case with phenol as hydrogen donor. The very modest isotope effect observed for the reaction of EOH with PMAP in benzene supports this view. By contrast, Das has reported an isotope effect of 3.9 on the quenching of p–methoxypropiophenone triplet by phenol in benzene [201]. These results suggest that the mechanism of $\pi\pi^*$ triplet quenching by EOH may be substantially different from the mechanism for other phenols. It may be that the transition state for the quenching reaction is dominated by charge transfer rather than by hydrogen transfer. A similar explanation has been offered by Das to explain the small deuterium isotope, $k_H/k_D$ = 1.2, observed for phenol quenching of triplet benzophenone in benzene [201]. In the EOH/PMAP case the contribution of charge transfer must be even greater than with phenol/benzophenone since the latter system does show a marked reduction in rate constant in hydrogen bonding solvents.

4.3.1.2 Reaction of EOH and related phenols with the t–butoxyl radical and with the 5–hexenyl radical.

*t–Butoxyl:*

As was the case for its reaction with triplet ketones, many aspects of the reaction of EOH with the t–butoxyl radical resemble those for the reaction of other phenols with this radical [203]. Again, the reaction rate constant is near diffusion controlled in non–polar solvents (Table 4.5) and the reaction yields the Vitamin E phenoxyl as indicated by the observed absorption spectrum (Figure 4.3). The reaction rate constant is, however, somewhat smaller than for the reaction of EOH with benzophenone. Similar results were obtained for BHT, FUR and CRM.

Das has reported similar behaviour in his studies of the rates of hydrogen abstraction from simple phenols by t–BuO• and triplet benzophenone [201, 203]. The higher reactivity of the triplet ketone towards phenols was attributed to the involvement of charge transfer in the transition state; a contribution which is lacking in the case of the alkoyl radical. In these respects EOH and several related compounds behave as typical phenols [203].

In contrast to simple phenols such as phenol and p–methoxyphenol which show deuterium isotope effects of 3.6 to 4.8 [203] in the reaction with t–BuO•, Vitamin E shows only a small effect of 1.31 in benzene. However, the reaction rate constant for EOH as substrate is typically 2 to 12 times larger than the rate constants for the simpler phenols. Thus, the isotope effect may be limited by the rapidity of the reaction in the case of Vitamin E. At any rate, it is clear from the transient spectra obtained (Figure 4.3, Table 4.5) that the reaction of t–BuO• with EOH and related phenols does lead to hydrogen abstraction from the phenolic –OH group.

The reduced rate constant for the t–BuO•/EOH system observed in 10% $H_2O$/acetonitrile may reflect the increased hydrogen bonding power of this solvent system compared to that of benzene. At first glance this explanation seems unlikely because of the lack of hydrogen bonding effects on the reaction of EOH with the PMAP triplet. However this insensitivity of EOH/PMAP to hydrogen bonding probably reflects the contribution of charge transfer to the transition state for quenching in this system as

discussed above. By comparison the reactivity of t–BuO• towards phenols is thought to be primarily determined by the bond energy of the ArO–H site [203]. Thus one would expect the latter reaction to be sensitive to environmental changes which influence the phenolic hydrogen.

It should be noted that the possibility of hydrogen abstraction from EOH by products of the β–scission of t–BuO• in wet 10% $H_2O$/acetonitrile [240]

$$(CH_3)CO^{\bullet} \longrightarrow {}^{\bullet}CH_3 + (CH_3)_2CO \qquad (4.13)$$

is quite small. The value of the rate constant for the reaction of methyl radicals with EOH is not likely to be greater than about $10^6$ $M^{-1}s^{-1}$ (see below for 5–hexenyl results) at room temperature. Thus reactions of methyl will contribute little, if at all, to the rate constants reported in Table 4.5.

Figure 4.4 shows that the transient Δ O.D. of EO• reaches a plateau after 750 ns or so. Our data shows that the EO• lifetime is on the order of hundreds of microseconds which agrees with the low reactivity of EO• as well as with the reported value of 3 ms[194] for its lifetime in a water/acetone/isopropanol mixture. Similar long lifetimes were estimated for CRM and FUR.

*5–hexenyl:*

As pointed out in the introduction to this chapter, only approximate values of the rate constant for hydrogen abstraction from EOH by alkyl radicals have been reported[207, 241]. In particular room temperature pulse radiolysis of deaerated cyclohexane solutions containing EOH lead to formation of the cyclohexanyl radical, $C_6H_{11}$•. Under these conditions Simic et al. reported that they were unable to observe the EO• signal and attributed this to the rate constant for the reaction

$$C_6H_{11} + EOH \longrightarrow C_6H_{12} + EO^{\bullet} \qquad (4.14)$$

being too low to be detectable by their system, i.e. $< 10^5$ $M^{-1}s^{-1}$. The same technique gave $k < 10^2$ $M^{-1}s^{-1}$ for BHT in cyclohexane [207]. By contrast, our results using 5–hexenyl as the hydrogen abstractor were $(1.7 \pm 0.2)x10^6$ $M^{-1}s^{-1}$ for EOH and $(3.3 \pm 0.4)$ $x10^4$ $M^{-1}s^{-1}$ for BHT at $70^0C$ in benzene. At present we are unable to explain this discrepancy between our values and those of Simic. There are two other points that should be noted. While the ratio, $k_{EOH}/k_{BHT}$, of our 5–hexenyl rate constants is 52 the same ratio for poly(peroxy styryl)peroxyl as hydrogen abstractor is $k_{EOH}/k_{BHT}$ = $3.2x10^6$ $M^{-1}s^{-1}$ / $1.4x10^4$ $M^{-1}s^{-1}$ = 229 [167]. This difference may arise because access of the –OH group of BHT, which is sterically hindered, to the abstracting radical centre will be reduced in the case of the polymer radical as compared to the case of a simple alkyl radical like 5–hexenyl. Finally, we note that the hydrogen abstraction occurring in these experiments is certainly from the phenolic –OH group rather than from, say, the alkyl chain of EOH. In support of this we note that rate constants for abstraction of even a tertiary hydrogen by methyl radical are on the order of 60 $M^{-1}s^{-1}$ at $25^0C$ [27] which is much lower than the rate constants observed in this study.

4.3.2. Micellar solution.

Our preliminary study of the reactivity of EOH towards several ketone triplets in micellar solution points to n–butyrophenone as the most promising for use in magnetic field effect experiments. This is based on the observation that photoreduction of BUP by Vitamin E leads to "instantaneous" formation of EO• and that BUP derived transients are so weakly absorbing at 425 nm that they do not interfere with detection of EO• (and therefore radical pair) kinetics at this wavelength. The same is true for the other phenols tested except BHT. As indicated previously, an alternate technique was used in experiments involving the latter phenol. The practicality of these techniques is

borne out by our successful completion of the magnetic field study described in the results section of this chapter.

In addition, we should like to point out that the use of a triplet like that of BUP, the lifetime of which is limited by intramolecular reaction, in experiments of this type is quite novel. The intramolecular reaction essentially acts as a "clock" for the hydrogen abstraction reaction in micelles in the sense that if the hydrogen abstraction does not take place in < 100 ns, the BUP triplet will no longer be available. That is to say the "clock" will "run out" on the hydrogen abstraction. Since the exit of ketone triplets from micelles is much slower than the duration of the triplet state there will be no slow growth of the phenoxyl signal due to the diffusion of the triplet from a micelle containing no phenol to one which does contain a phenol. By use of this clock technique one can ensure that the criterion of rapid radical pair formation (i.e., rapid on the time scale of radical pair decay) is fact fulfilled. It is reasonable to suppose that such a clock might also be useful in studies of radical pair kinetics in micelles involving hydrogen donors other than phenols. In order for the technique to be applicable in a given case the reaction of the hydrogen donor with the triplet must be intrinsically rapid.

4.3.2.1 Interpretation of exit rates.

*Kinetic data in the absence of electrolytes and at room temperature:*

Scheme 4.1 shows exit of the ketyl radical from the micelle as the only escape process. In fact, the experimental values of k– include all escape modes, that is, all processes by which the geminate character is destroyed while the chromophore of interest (i.e., phenoxyl) is preserved. In practical terms this means exit of either radical (i.e., phenoxyl and or ketyl) from the micelle in which they were originally formed. The top segment in Table 4.6 illustrates the values of k– obtained in SDS micelles for the different phenols (Chart 3.1). The more hydrophobic phenols, particularly EOH, will

yield phenoxyl radicals that will tend to remain in the micelle in which they were initially formed. Such systems lead to ~ 20% escape at zero field and k– values (which must be dominated by exit of the BTK radical) of ca. $0.8 \times 10^6 s^{-1}$. It is worth noting in this context that an escape rate constant of this magnitude is entirely consistent with the exit rate constants of triplet ketone exit from SDS micelles under similar experimental conditions [222].

Exit rates for the BTK–EO• pair in CTAC and CTAB micelles were $0.2 \times 10^6$ and $0.15 \times 10^6$ $s^{-1}$, respectively. Reduced exit rates with increased micellar size have been documented in the literature [54, 55, 143]; this is nicely illustrated by comparison of the CRM or FUR data in CTAB and DTAB, which leads to exit rates from 50 to 100% faster in the latter.

Interestingly, k–(FUR) > k–(CRM) in all the micelles studied. This suggests that even a minor structural change can have a fairly pronounced effect on k–. Presumably the smaller heterocyclic ring in FUR makes the non–phenolic oxygen more accessible thus leading to increased hydrophilicity. Note that the exit rate constant for Trolox is quite similar to that for FUR. While Trolox is nominally water soluble it should be kept in mind that the data for Trolox in Table 4.6 was obtained at pH 4; a value at which the acid group of Trolox is protonated thereby reducing its water solubility. By contrast at pH 7.8, a value at which Trolox is largely in the anionic form, the value of k– is close to $3 \times 10^6 s^{-1}$ based on a % escape value of 88% (Figure 4.13).

*Influence of added electrolyte:*

As indicated earlier the dimensions of SDS and other sodium–n–alkyl sulfate micelles increase with increasing concentrations of added counterion. Turro et al. have systematically examined the effect of adding alkali metal chlorides to SDS solutions upon the exit rate constant for benzyl radicals [137]. These authors found that k– varied inversely with changes in surfactant aggregation number such that at high electrolyte levels the exit rate constant is reduced. It was concluded that factors which

influence micellar volume also influence k–. Our k– data (Figure 4.14b, Table 4.8) appear to be in agreement with Turro's conclusion.

Further support for the view that micellar size influences k– comes from the work of Steiner's group [142] on the decay kinetics of the thionine radical–aniline radical cation pair in reversed micelles of AOT as well as the work of Scaiano on the benzophenone/cyclohexadiene system in SDS [54, 55]. In the former system the micellar volume was adjusted by changing the water content of the reversed micelles and k– was found to vary as 1/r, where r is the radius of the water pool. This indicates that it is the ratio of surface area to volume that controls the exit rate for this system.

While the value of k– for several radicals and radical ions increases in smaller micelles this cannot be considered general behaviour for reagent exit. For example the exit rate constant for m–dicyanobenzene from SDS [230] and for exit of pyrene from alcohol swollen SDS [213, 242] increases as salt is added although the effect is quite modest for the benzene derivative. It would seem, then, that the variation in k– with salt concentration may depend on the nature of the exiting species as well as on the presence of co–solubilized material.

The details of the variation of k– with electrolyte will no doubt also depend on the mechanism by which the solubilite actually escapes from the micelle. For example, pyrene is highly hydrophobic. It has been suggested that pyrene "exits" a micelle due to fragmentation of the micelle into submicellar aggregates which carry the pyrene molecule from one micelle to another [213, 242–244]; that is, pyrene migrates due to fragmentation–coagulation of the micelles [245, 246]. Fragmentation–coagulation rates are enhanced, rather than inhibited, by the presence of alcohols and electrolytes[243–248].

*Influence of surfactant chain length:*

Table 4.8 reports k– values for the EO•–BTK system in SDS and its $C_{10}$ analogue, SDecS. From these data it seems clear that increasing the hydrocarbon

chain length results in a reduction in k–. Turro has reported a similar effect on the value of k– for benzyl radicals in a variety of sodium–n–alkyl sulfate micelles [137]. This work also reported a good correlation between cage effect and micellar volume (i.e. the greater the volume the larger the cage effect). We would like to make a similar comparison of rate constants to micellar volume using literature values of micellar radius to calculate the micellar volume.

Values of mean hydrodynamic radii for SDS and SDecS have been reported at 0.1 and 0.2 M NaCl [16, 249]. Since no radius data at 0.25M NaCl seems to be available we will use the 0.2 M NaCl data to discuss the rate constants we have measured at 0.25 M NaCl. At 0.25 M NaCl, sodium–n–alkyl sulfate micelles are expected to still be essentially spherical [16] particularly for shorter chain length surfactants. Thus by taking $r_{SDS}$ = 25 Å and $r_{SDecS}$ = 20 Å at 0.25 M NaCl, and assuming spherical micelles, we find that the ratio of volumes, $V_{SDS}/V_{SDecS}$, is equal to 2.0. At this same electrolyte concentration the ratio of k– values for SDecS versus SDS is 1.7. This suggests that micellar volume is indeed the factor controlling the exit rate constant. Unfortunately the situation is not so straightforward since the ratio of SDS to SDecS surface areas at 0.25 M NaCl is 1.6 (again assuming spherical micelles) which is also close to the rate constant ratio. Thus for the EO•–BTK radical pair it is not clear which is more important in controlling the exit rate; micellar volume or surface area. In fact, as shown in Figure 4.15b there is an excellent correlation between k– and 1/r as well. It seems we must conclude that our k– data is of insufficient precision to distinguish which of the several micellar size parameters (volume, surface area or the ratio of surface area to volume) is responsible for the observed variation in the rate constant.

*Influence of temperature:*

It is clear from Figure 4.17 that temperature changes have a marked effect upon the exit rate constant, k–, of the EO• – BTK radical pair from SDS. The Arrhenius plots

of Figure 4.17 and the Arrhenius parameters of Table 4.9 are the basic results describing the effect of temperature on exit rates in the EO• – BTK system.It would appear that ours is the first attempt to study the impact of temperature on exit processes involving micellized triplet radical pairs.

Consider the activation energy. For SDS the activation energy for exit is 6.5 ± 1.8 kcal / mol at zero NaCl while for SDecS it is 5.5±0.8 kcal/mol. DeSchryver and co–workers have measured an activation energy of 5.7 kcal/mol [230] for exit of m–dicyanobenzene from SDS which compares well with our SDS value. Thus our Ea values are reasonable for exit of a polar but uncharged species from this particular micelle. Although m–dicyanobenzene is probably not an especially good model for a ketyl radical, to the best of our knowledge no reports of exit activation energies for radicals from micelles are available.

How does the ketyl radical exit? Three mechanisms for exit from ionic micelles have been discussed in the literature: diffusion of a reactant from the micelle and into the aqueous phase [239, 250–253]; collision and partial penetration of two micelles accompanied by reagent exchange [254–256]; fragmentation in to submicellar aggregates containing the reagents followed by coagulation [245, 246]. The latter two processes are expected to be accelerated at high salt concentrations because of decreased intermicelle repulsion (collision mechanism) and increased micellar polydispersity (fragmentation – coagulation mechanism) under these conditions. Since our k– values decrease with increasing salt concentration we can rule out the involvement of either of these two mechanisms. This leaves us with direct exit of the ketyl into the bulk aqueous phase.

The reaction between butyrophenone triplet and EOH probably occurs near the surface of the micelle since vitamin E and other phenols are known to locate their hydroxyl group near the hydrocarbon – water interface in aqueous solutions of micelles and vesicles [257–259]. Ketones (and presumably ketyl radicals) also reside

near the Stern layer of micelles [222, 260]. Thus escape processes in this radical pair need not include substantial diffusion through the micellar interior although the lifetime of the geminate pair (Table 4.6 and 4.7) may be sufficiently long to provide ample opportunity for the entire micelle to be explored. For example, pyrene, another very hydrophobic substrate, has been reported to require only about 10 ns to travel from the inner core of SDS to the surface region and approximately 50 ns to explore the micellar surface. [261].

Even so, diffusion through the Stern layer into the bulk phase seems to be the most likely exit route for the EO$^{\bullet}$ – BTK pair. One may imagine, however, that Ea reflects an energy barrier to the exiting radical (almost certainly to be the ketyl in this case) diffusively crossing the micelle – water interface. We note that the trend in the Ea values of Table 4.9 is towards larger values in larger micelles which is consistent with the reduction in k– in larger micelles. Intuitively, if diffusion itself is not the main factor, one would expect some kind of proportionality with the frequency with which the ketyl "hits" the micellar surface. This would mean that k– $\alpha$ 1/r. The fact that our k– values do correlate well with 1/r is consistent with this view although we can not rule out the involvement of other factors, such as micellar volume, based on our data (*vide supra*). Note also that while the trend in Ea values with micelle size seems clear (see the mean values given in Table 4.9), the individual values are in fact within experimental error of one another.

Another interesting observation is that the Arrhenius pre – exponential factor is rather small for ketyl exit from both surfactants. This indicates that the exit process is accompanied by a decrease in entropy. When the ketyl radical is associated with the micellar pseudo – phase it is located in a less polar, more hydrocarbon like environment than it would encounter in the bulk phase. In such an environment the entropy of the system should be relatively high compared to the system entropy when the ketyl is in the aqueous phase. When the ketyl, which is not highly water soluble,

enters the aqueous phase it may cause the surrounding water molecules to become highly oriented in the same manner that water molecules become oriented to accommodate a hydrocarbon molecule [8, 11, 26]. In the hydrocarbon case the orientation of water is so extreme as to cause formation of a cavity in which the hydrocarbon sits. The overall process is associated with a substantial decrease in entropy. It may well be that our observation of decreased entropy in the transition state for ketyl exit from SDS and SDecS reflects similar ordering of water which must take place in order that exit may occur. Rate constants for entry of hydrophobic substrates into micelles are typically on the order of diffusion controlled [4]. This implies an early transition state for entry and therefore a late transition state for exit. In other words, the transition state probably puts BTK almost in the water. This would be consistent with the rather small Arrhenius A factors observed here.Thus we can imagine that the activation energy arises in part because of the need to order water molecules so that BTK can be solubilized in the aqueous phase.

In order to gain more insight into what factors influence the energetics of ketyl exit we can make an estimate of the contributions of enthalpy of activation and entropy of activation to the value of Ea by noting that [262]

$$Ea \sim \Delta H^{\neq} + RT \qquad (4.15)$$

and that

$$k_{-} = \frac{kT}{h}\exp\left(\frac{\Delta S^{\neq}}{R}\right)\exp\left(\frac{-\Delta H^{\neq}}{RT}\right) \qquad (4.16)$$

where $\Delta H^{\neq}$ is the activation enthalpy, $\Delta S^{\neq}$ is the activation entropy, k is Boltzmann's constant, h is Planck's constant and R is the gas constant. Using these equations in conjunction with the data in Tables 4.8 and 4.9 the room temperatures values of $\Delta H^{\neq}$

and $\Delta S^{\neq}$ presented in Table 4.11 were obtained. These data show several points. First of all $\Delta G^{\neq}$ (and therefore Ea) is dominated by the $\Delta H^{\neq}$ term even at the highest temperature examined. As was the case with Ea, the trend in $\Delta H^{\neq}$ values is towards smaller energy barriers in smaller micelles. The opposite trend is observed for $\Delta S^{\neq}$. $\Delta S^{\neq}$ becomes more positive in larger micelles. The fact that the $\Delta H^{\neq}$ term dominates the $T\Delta S^{\neq}$ term and that the former becomes larger in larger micelles is consistent with a reduction in k– with increasing micelle size.

The data of Table 4.11 also clearly show that exit is associated with a decrease in entropy. Again, this is consistent with a restructuring of water at the exit transition state. For transfer of hydrocarbon from bulk hydrocarbon to water the contribution of the entropy term ($T\Delta S$ in this case rather than $T\Delta S^{\neq}$) to $\Delta G$ for the overall transfer process actually dominates the overall free energy change. For example $\Delta G$ (transfer) for n–butane is + 5.9 kcal / mol to which the entropic term contributes 85% at $25^0C$ [11]. In the case of BTK we should keep in mind that the exiting species is somewhat polar so that less restructuring of water molecules may be required to solubilize BTK compared to a hydrocarbon like n–butane. Even so, based on the average $\Delta H^{\neq}$ and $\Delta S^{\neq}$ values (Table 4.11), the entropy term contributes 29% to the $\Delta G^{\neq}$ value for SDS and 42% for SDecS at room temperature.

It is also interesting to compare the $\Delta S^{\neq}$ value of the $EO^{\bullet}$–BTK system to that for separation of a reaction pair in the absence of hydrophobic effects. For example the $\Delta S^{\neq}$ term associated with dissociation of pyrene excimer in cyclohexane has been reported to be +15 cal/K mol [263]. This value reflects the entropy change when a pair of non–polar molecules reach the transition state for exit from a solvent cage into a bulk hydrocarbon solvent. This should be compared with the values of between –12 and –9 cal/K mol obtained in our systems. These latter values reflect the entropy change when a pair of (more–or–less) non–polar radicals reach the transition state for exit from a micellar super cage into a bulk aqueous medium. The large difference both

Table 4.11. Enthalpy, entropy and free energy of activation for exit of BTK from SDecS and SDS at 298K.

| Surfactant | [NaCl] M | $\Delta H^{\neq}$ kcal/mol | Mean kcal/mol | $\Delta S^{\neq}$ cal/K mol | Mean cal/K mol | $\Delta G^{\neq(a)}$ kcal/mol |
|---|---|---|---|---|---|---|
| SDecS | 0.0 | 4.9±0.7 | | −13.2 | | |
| | 0.25 | 5.5±1.1 | 5.2±0.3 | −11.9 | −12.6±0.7 | 9.0 |
| | 0.50 | 5.3±0.5 | | −12.8 | | |
| SDS | 0.0 | 5.9±1.6 | | −10.6 | | |
| | 0.25 | 6.4±0.9 | 6.7±1.0 | −9.9 | −9.1±2.1 | 9.4 |
| | 0.50 | 7.8±1.3 | | −6.7 | | |

(a) Based on the mean values of $\Delta H^{\neq}$ and $\Delta S^{\neq}$ at 298K.

in the magnitude and sign of $\Delta S^{\neq}$ between these two systems is a clear reflection of the hydrophobic effect.

Our Arrhenius data suggest that the value of k– for the EO•–BTK system may well be controlled by the energetics of crossing the micelle–water interface. The good correlation of k– with 1/r suggests that the probability of the ketyl encountering the micellar surface is also important. The variation of k– with micellar size probably arises because of changes in the enthalpy of activation and the probability of reaching the micellar surface with micellar size. The question then arises as to why does $\Delta H^{\neq}$ get larger as the micelle gets larger. Since BTK is uncharged its binding to the micelles must be largely hydrophobic in nature. Thus one may think of $\Delta H^{\neq}$ as the energy required to overcome this hydrophobic binding energy in order to bring the ketyl radical to the transition state for exit. If, on the average, the ketyl resides in a more "oil" like environment in a larger micelle it will be more strongly associated with the micelle and the energy barrier to be overcome will be larger. In fact literature data indicates that the association constant for many (but not all) hydrophobic substrates with micelles is greater in larger micelles [4, 13]. The value of the association constant, K, is even linked to the exit rate constant since $K = k_+/k-$ where $k_+$ is the entry rate constant. Variations in K between different hydrophobic solubilites arises primarily from changes in k– since the value of $k_+$ is almost always close to diffusion controlled [4]. Thus a large association constant generally implies a small value of k–.

To summarize, our data seems to suggest that the observed changes in k– with micellar size in the EO•–BTK system arise because of changes in the enthalpy of activation with micellar size and because of differences in the probability that the ketyl will encounter the micellar surface. The negative $\Delta S^{\neq}$ values associated with the exit process indicate that exit probably requires restructuring of the arrangement of water molecules in order to obtain the transition state which in turn implies that the transition state for exit of non–ionic species from SDS and SDecS occurs when the exiting

reagent is nearly in the water. These results also imply that exit of the ketyl (i.e. loss of geminate radical pair character) does in fact involve exit of the ketyl from the micelle and into the bulk aqueous phase. This is supported further by the fact that k– decreases as [NaCl] increases. Such an increase is consistent with neither a collision–exchange mechanism nor with a fragmentation–coagulation mechanism for loss of geminate character.

4.3.2.2. Magnetic field effects on escape efficiencies.

The dependence of % escape on field strength show for the EO•–BTK system in SDS (Figure 4.10) is typical of those observed in this study. As already mentioned, values of $H_{1/2}$ were in the 500 to 800 G range. This type of behaviour has conventionally been interpreted in terms of the reduced ability of isotopic hyperfine couping to facilitate $T_{\pm}$ <–> S intersystem crossing at fields which are significant compared to the hfc interaction energy [9, 39, 54, 69, 76, 81, 98–100, 106, 138]. Weller and co-workers have derived the following expression for the half field value to be expected in radical pair systems showing hfc mediated magnetic field effects [111]

$$H_{1/2} = \frac{2(H_1^2 + H_2^2)}{H_1 + H_2} \qquad (4.17)$$

where the $H_i$ are given by

$$H_i = \left( \sum_j I_{ij}(I_{ij} + 1)\, a_{ij}^2 \right)^{1/2} \qquad (4.18)$$

Here the $H_i$ are the hyperfine interactions between the nuclear spins, $I_j$, and the unpaired electron spin on each radical (i = 1 or 2). The hyperfine interaction is governed by the magnitude of the isotropic hfc constants $a_{ij}$. Using these two equations and literature data we can estimate a theoretical $H_{1/2}$ value for the EO• –

BTK system. $a_{ij}$ values for EO• were taken from the ESR work of Mukai [264], Niki [265] and Ingold [167]. This data yields an average value of 11.6 G for $H_{EO•}$.

We were unable to find ESR data for the n–butyrophenone ketyl radical. However the Landolt – Börstein compilation provided data for several related alkyl aryl ketyls: 2–phenyl–2–hydroxyethyl [266–268]; 3 – phenyl –3 – hydroxy propyl [267–269]; the ketyl formed upon photo reduction of phenyl isopropyl ketone [267–269]. For these ketyl radicals equation 4.20 gives $H_i$ values of 22.7 G, 12.9 G and 8.6 G, respectively. Using these values as well as 11.6 G for HEO• gives $H_{1/2}$ values of 37.8 G, 24.5 G and 20.6 G for the EO• / 2 – phenyl –2 hydroxy ethyl, EO• / 3 – phenyl – 3 hydroxypropyl and EO•/phenylisopropyl ketyl radical pairs, respectively. It is clear that the $H_{1/2}$ value predicted for a hfc mediated magnetic field dependence in the EO• – BTK pair should be much smaller than the value we have observed in our experiments which is close to 800 G. Thus inhibition of isotropic hfc mediated intersystem crossing by the applied magnetic field can only make a small contribution to the observed magnetic field effect on the % escape of the EO• – BTK pair. While this contradicts the conclusion of much of the pre – 1984 literature on magnetic field effects in micelles (see for example, the work of Scaiano [54, 55, 69], the work of Tanimoto which has recently been reviewed[81] and reviews by Turro [9, 39, 76, 98–100, 138] and Steiner [106]) it is in line with the proposals of more recent work from several groups namely of Hayashi[83,86], Steiner[44, 97, 142] and Levin [123, 148–152, 270]. In a very recent article Turro et al [94] have also attributed the magnetic field dependence of $k_{gem}$ for triplet benzylic radical pairs at fields between 100 and 500 G in CTAC to spin relaxation. The magnetic field dependence below 100 G was attributed to the hfc mechanism.

The latter authors have all proposed that it is the spin relaxation mechanism that accounts for the magnetic field dependence of the systems they have examined. Invariably they attribute this conclusion to the fact that a magnetic field dependence of % escape or $k_{gem}$ is observed at fields well above those at which a hfc mediated field

dependence should be saturated. Based on our calculated $H_{1/2}$ values for EO• – ketyl pairs we are probably being generous if we attribute an isotropic hfc interaction energy as large as 100 G to radical pairs of this type. This implies that applied fields in excess of 100 G should cause a Zeeman splitting of $T_{\pm}$ from $T_0$, S that is too large to allow hfc $T_{\pm}$ <–> S interconversions to continue to be effective. We therefore suggest that in our system the observed magnetic field dependence of % escape at fields above 50 to 100 G is probably due to a reduction in the rate of $T_{\pm}$ <–> S spin relaxation. As pointed out in the results section (Figures 4.8 and 4.9) our data provides no evidence for efficient $T_{\pm}$ <–> $T_0$ interconversions in the EO•–BTK system in the presence of applied fields.

Normally hfc mediated spin state interconversion is considered to be much more rapid than that brought about by spin relaxation [32, 77, 91, 106, 271–273] in homogeneous solutions of moderate viscosity (~ 1 cP). Spin relaxation is so slow that it can't compete with hfc as a spin conversion mechanism in the lifetime of a typical solvent cage. However, in the more constrained micellar environment radical pair geminate lifetimes are much longer. If the external field strength exceeds that of the hyperfine field, which it will do above ~100 G in our case, the rate of hfc mediated $T_{\pm}$ $\leftrightarrow$ S processes will drop below that of spin relaxation interconversion. Since the radical pairs may still retain their geminate character because of the "supercage" effect of the micelle, spin relaxation will have the opportunity to become the dominant intersystem crossing process at moderate fields. Note that at zero field the rate of hfc intersystem crossing is still expected to far exceed that of the relaxation process. One may therefore envisage a series of events where the EO• – BTK radical pair intersystem crossing is controlled by hfc at zero field but the rate of which rapidly drops over field strengths between zero and $\leq$ 100 G resulting in an initial increase in % escape. At higher fields, spin relaxation is responsible for EO• – BTK transitions from $T_{\pm}$ to S and there are essentially no $T_{\pm} \leftrightarrow T_0$ interconversions. The rate of spin

relaxation is also field dependent so % escape continues to increase until the effect saturates at rather high fields.

As a final comment we note that an interesting feature of the magnetic field dependence of % escape is the rather high slope of plots such as that in Figure 4.10. This is a characteristic that may have considerable implication for biological studies. Among these, it should be noted that photo initiated free radical processes will have very different consequences if they are studied in the presence of magnetic fields (NMR, EPR, magnetic stirrers) than in the absence of these fields. For purposes of illustration, trace b in Figure 4. 7 has been obtained by using a regular (11/2 in.) stirring magnet. We note that the magnet was not in the sample but actually external to both sample and sample compartment.

4.3.2.3 Geminate kinetics.

Perhaps the single most striking feature of our $k_{gem}$ data is the apparent dependence of this rate constant on micellar size. In particular, $k_{gem}$ is smaller in larger micelles. This type of behaviour has been noted previously for other radical pair systems both in normal [54, 55] and in reversed micelles [44, 142]. Our own results show, for example, that for the EO•–BTK pair $k_{gem}$ is $0.94 \times 10^6$ $s^{-1}$ in CTAB and $3.3 \times 10^6$ $s^{-1}$ in the smaller DTAB. Similarly, for FUR –BTK the value of $k_{gem}$ is twice as large in DTAB as in CTAB (Table 4.6). Table 4.7 shows that $k_{gem}$ for EO•–BTK is about twice as large in SDecS as in SDS at 0.25 M NaCl. We have already seen (section 4.3.2.2) that the volume (and surface areas) ratio of SDS to SDecS is about 2. Likewise, typical aggregation numbers for $C_{12}$ surfactants (e.g., SDS, DTAC, DTAB) are around 60, while for $C_{16}$ surfactants (e.g., CTAC,CTAB) they are around 100[6,242,250,253,274–276]. Thus on the basis of numbers of $CH_2$ and $CH_3$ groups in the micellar hydrophobic region, the $C_{16}$ micelles will be about twice as large as the

$C_{12}$ micelle. These rough size estimates agree with the observed changes in $k_{gem}$ on going from SDecS to SDS to CTAC.

In addition to having different sizes $C_{12}$ and $C_{16}$ micelles also differ in polarity, with the latter being less polar as judged by pyrene fluorescence [4]. In our case differences in $k_{gem}$ between $C_{12}$ and $C_{16}$ micelles are more likely to reflect size differences than polarity differences since, in general, biradicals bearing ketyl sites show larger lifetimes in polar solvents [41]. In fact, a radical pair confined to a micelle can be regarded as a biradical, the ends of which are prevented from diffusing apart by a phase boundary rather than by a connecting molecular frame.

Further evidence that our $k_{gem}$ values in some way reflect micellar dimensions is offered by the good correlation of the variation in SDS aggregation number as a function of [NaCl] with the variation in $k_{gem}$ with [NaCl] (Figure 4.14a). The same type of trend is seen in the $k_{gem}$ data for SDecS (Table 4.7). However, while $k_{gem}$ (SDS) < $k_{gem}$ (SDecS) at each [NaCl], the ratio $k_{gem}$ (SDecS)/$k_{gem}$ (SDS) is not constant with salt concentration. While this ratio is roughly constant at zero and 0.25 M NaCl (1.4 and 1.8, respectively) it jumps dramatically on going to 0.5 M NaCl where its value is 7.1. It is well known that SDS undergoes a transition from spherical to rod like micelles (or aggregates) at about 0.5 M NaCl [4]. Below this concentration the aggregation number increases slowly with salt while close to and above this concentration the aggregation number grows dramatically. The same type of behaviour occurs for other sodium–n–alkyl sulfate micelles but the concentration of salt needed to bring about the sphere–to–rod transition increases as the surfactant chain length decreases [16]. Thus we attribute the sudden jump in the $k_{gem}$ (SDecS)/$k_{gem}$(SDS) ratio at 0.5 M NaCl to SDecS micelles not yet having begun to transform from spheres to rods at this salt concentration while the SDS micelles have begun to do so.

Temperature variation also results in changes in the aggregation number of sodium–n–alkyl sulfate micelles [15, 16, 229, 234, 277–279]. In particular the micelles

achieve a minimal, spherical configuration at higher temperatures and begin to grow in size as the temperature is reduced. The growth effect is more pronounced at increased salt concentrations. At salt concentrations between zero and 0.6M the micellar aggregation number and the mean hydrodynamic radius both become independent of temperature at high temperature. The Arrhenius plots based on $k_{gem}$ which are shown in Figure 4.18 seem to follow a similar trend. Again there seems to be dependence of $k_{gem}$ on micellar size reflected in this data. To further verify the size dependence of $k_{gem}$ upon changing temperature we have plotted values of $k_{gem}$ and N (the aggregation number) as a function of temperature (Figure 4.19). There is clearly a complementary relationship between these sets of data. In these Figures the N data at zero and 0.25M NaCl is from Miller's paper [229] while that at 0.5M NaCl is taken from the work of Briggs [234].

As was noted above there is literature precedent for a dependence of $k_{gem}$ on micellar size. The kinetics of other types of reaction have also been shown to correlate with micellar dimensions. For example, the intramicellar rate constants for quenching of probe fluorescence by a wide variety of quenchers shows a dependence on aggregation number in SDS as well as in DTAC and CTAC [4]. Theoretical models have predicted that this should be so, both in spherical and cylindrical aggregates, regardless of whether the reaction is diffusion or activation controlled .

In addition to the fluorescence studies, other examples of the dependence of reaction rates on aggregate size are available. The pseudo – first order rate constant for bromination of trans – stilbene in SDS water/decanol mixtures is an example [280]. An effect of micellar size was also reported for the dimerization efficiency of phenyl radicals generated upon photolysis of diphenyl mercury. The biphenyl yield was larger in smaller micelles [281].

A closer analogy to the system we are studying is that of triplet biradicals. The lifetimes of triplet biradicals containing an acyl and a benzyl terminus have been

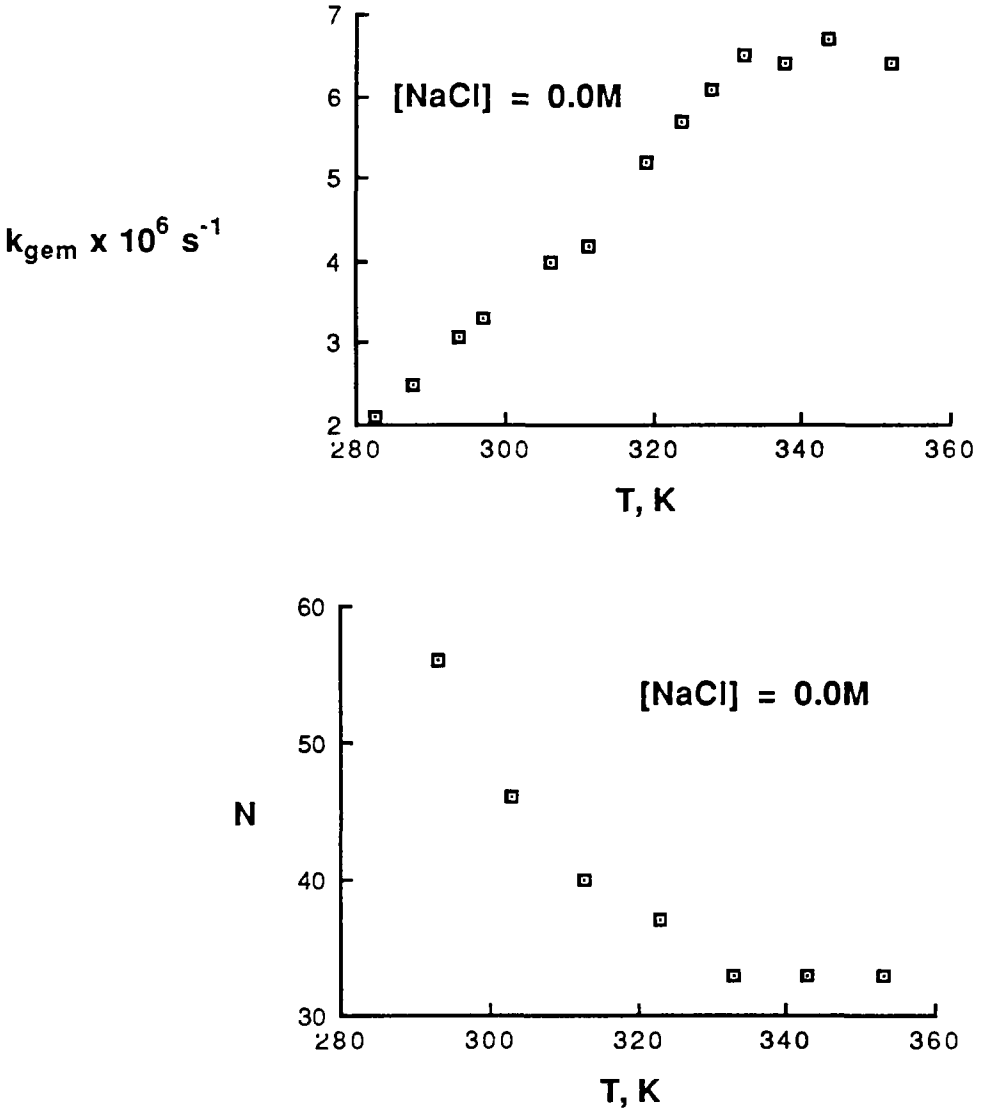


Figure 4.19a. Variation of $k_{gem}$ and SDS aggregation number with temperature in the absence of added electrolyte. [EOH] = 2.5mM, [butyrophenone] = 0.021M, [SDS] = 0.15M.

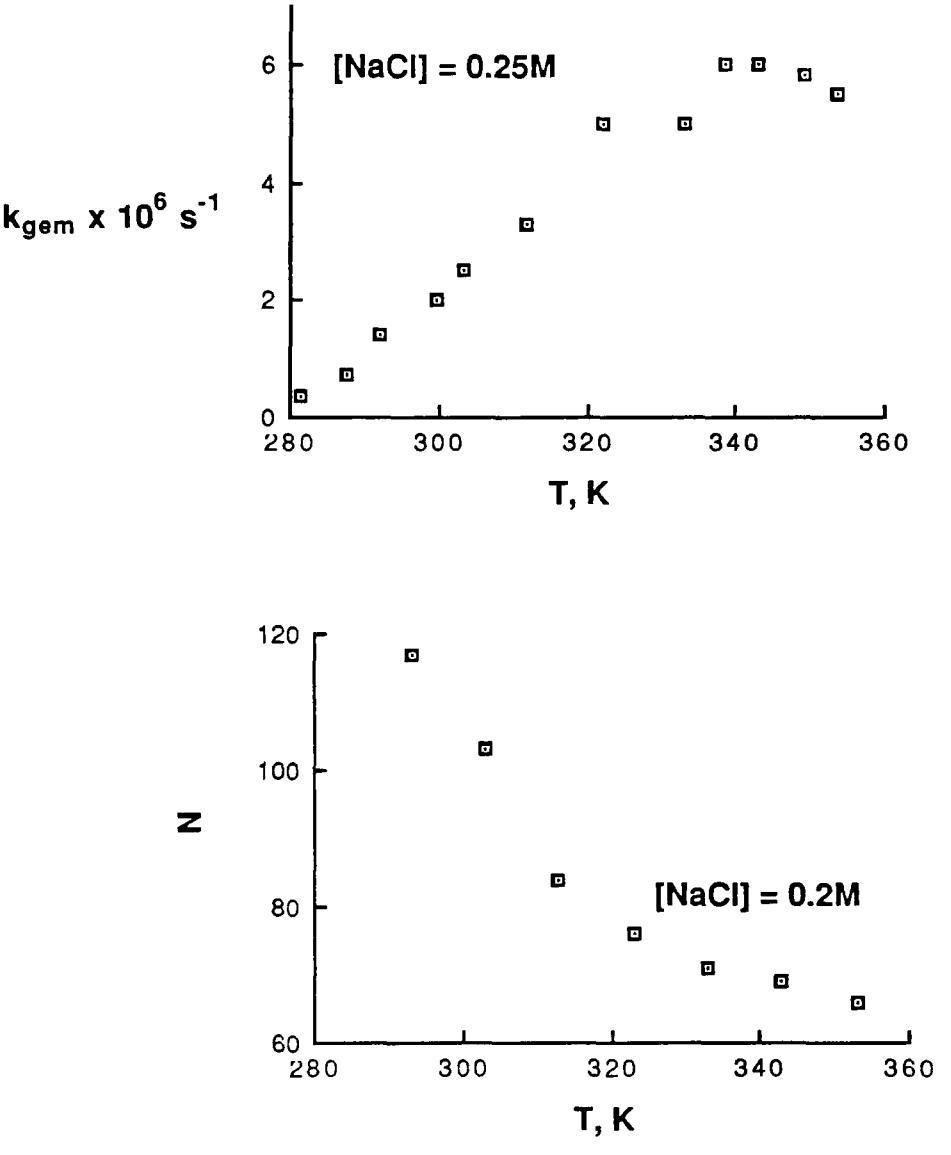


Figure 4.19b. Variation of $k_{gem}$ and SDS aggregation number with temperature in the presence of 0.25M NaCl. Other conditions as for Figure 4.19a.

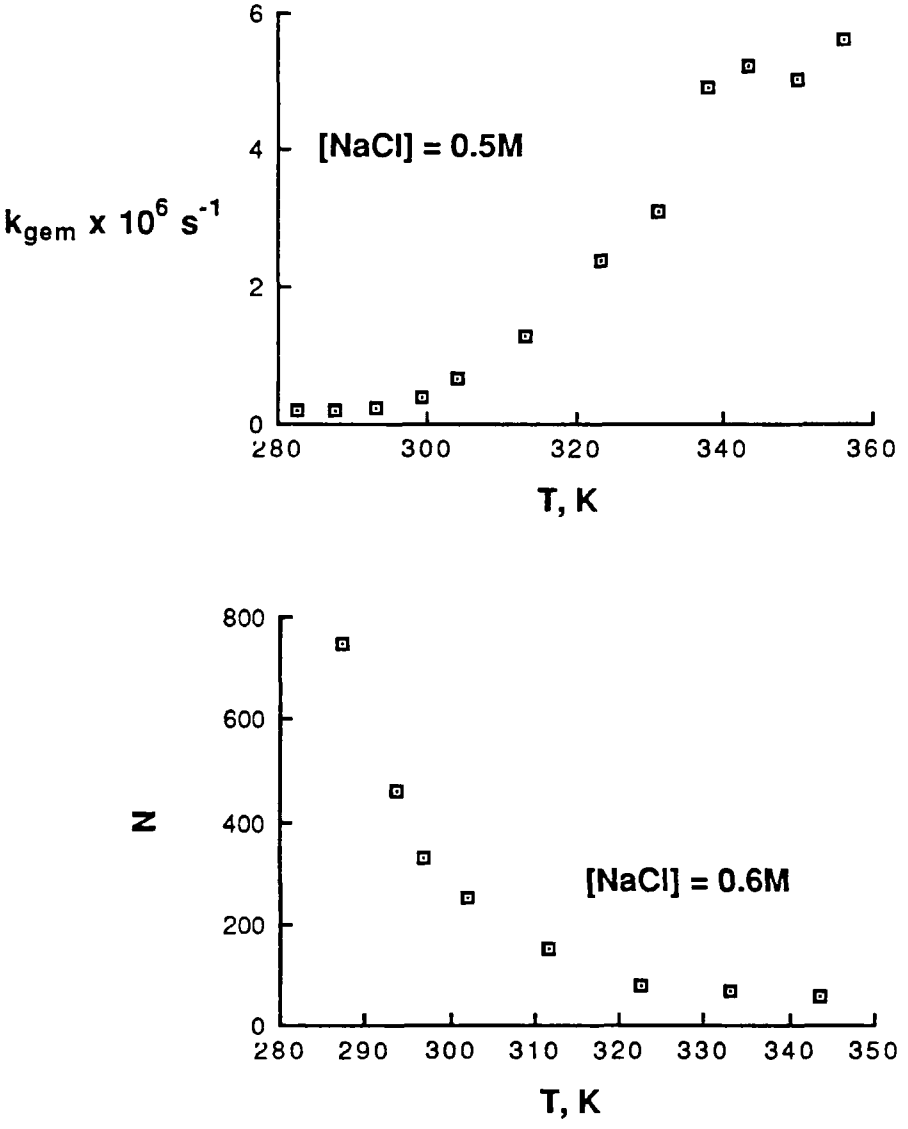


Figure 4.19c. Variation of $k_{gem}$ and SDS aggregation number with temperature in the presence of 0.5M NaCl. Other conditions as for Figure 4.19a.

shown to vary with chain length [282–285] as have lifetimes of biradicals with two benzylic centers [125]. In both cases the lifetime increases with increasing methylene chain length. An effect of terminus proximity has also been reported for the triplet lifetimes of biradicals formed via the Norrish Type II reaction [41, 42] although no concensus has been reached with regards to whether distance, or other parameters such as biradical configuration, controls the lifetimes in these systems. Thus there seems to be ample precedent in the literature for size effects of the type we observe on our $k_{gem}$ values.

The question then arises as to why $k_{gem}$ should vary with micellar dimensions. Analysis of the $k_{gem}$ data should be carried out in light of knowledge about the factors that control the lifetimes of flexible triplet biradicals in solution since such biradicals are analogous to triplet radical pairs in micelles. Two questions are critical. First, to what extent is diffusional motion (as opposed to intersystem crossing) an important factor in determining the rates of geminate processes in the absence of a magnetic field. Second, if intersystem crossing is important, what type of interactions determine the magnitude of $k_{gem}$. Most available evidence suggests that triplet biradical lifetimes are intersystem crossing controlled [41–43, 286] although for long chain species chain dynamics may become important [125, 284, 285, 287]. Most authors working in the field of triplet pair behaviour in micelles have also associated the zero field value of $k_{gem}$ with radical pair intersystem crossing [9, 39, 54, 55, 69, 76, 81, 98–100, 106, 138] and in most cases the intersystem crossing process was said to be determined by hyperfine coupling. As we have seen hfc can only be effective as a radical pair intersystem crossing mechanism when the radical centers are sufficiently separated so that the exchange interaction is close to zero. This implies that if $k_{gem}$ is determined by the rate of hfc its value should, if anything, increase in larger micelles since the radical separation will be greater on the average. This is contrary to our observation.

Another possibility is that $k_{gem}$ is intersystem crossing controlled but determined by spin – orbit coupling (SOC) rather than by hfc. The rate of SOC is known to vary exponentially with separation between the unpaired electrons in such a way that the rate increases as the electrons approach each other more closely [28]. In fact this is believed to be the source of the observed variation in the triplet lifetimes of several biradicals with methylene chain length since these lifetimes are generally held to be SOC controlled [43].

While attributing the value of $k_{gem}$ to SOC mediated intersystem crossing would qualitatively explain our zero field variation of this rate constant with micellar dimensions, we must point out that SOC mediated processes are at best only weakly dependent on the strength of an applied magnetic field. This is in contrast to our $EO^{\bullet}$ – BTK results which show a very pronounced magnetic field effect on % escape and on $k_{gem}$. Thus it would appear that trying to explain our $k_{gem}$ data in terms of SOC mediated intersystem crossing is also unsatisfactory.

Yet a third possible approach to explaining our $k_{gem}$ data would be to attribute its value to the rate of radical diffusion. Several authors have suggested that their observed values of $k_{gem}$ are diffusion controlled for radical pairs in micelles [44, 83, 89] so such a suggestion is not without precedent. If $k_{gem}$ is diffusion controlled it means that the rate of radical pair intersystem crossing is significantly faster than the rate of radical reencounter at zero field.

A number of theoretical models have been presented to describe the kinetics of diffusion controlled fluorescence quenching kinetics in micelles [288–292]. Although these models are at various degrees of sophistication and treat several different modes of diffusion (i.e. on the surface, in the interior, etc) they all indicate that the probability of a diffusion controlled reaction, and therefore the rate constant for the reaction, will decrease in larger micelles. This seems instinctively reasonable since the frequency of encounter will be reduced in larger micelles. If we ascribe to the view

that $k_{gem}$ is diffusion controlled it is clear that its value should depend on micellar dimensions. In addition, a large magnetic field effect is not precluded if $k_{gem}$ is diffusion controlled. In fact as the field strength is increased the (hfc or spin relaxation mediated) intersystem crossing rate will decrease and a magnetic field effect will be observed when the intersystem crossing rate drops below the rate of diffusional reencounter. Furthermore, the fact that $Cu^{2+}$ has little effect on $k_{gem}$ at zero field while at the same time suppressing the magnetic field effect on the $EO^{\bullet}$ – BTK pair, is consistent with a diffusion controlled $k_{gem}$. If $k_{gem}$ is diffusion controlled at zero field its value will be insensitive to paramagnetic effects. This of course assumes that $Cu^{2+}$ suppresses the magnetic field effect because of its paramagnetic nature and not simply because it traps exiting ketyl radicals thereby reducing the observed exit yield.

There have been two earlier reports of non–linear Arrhenius plots for reactions approaching diffusion control in SDS. Zana [242] has observed a curved Arrhenius dependence of the pseudo–first order rate constant for pyrene excimer formation while Emert has reported a similar effect for the intramolecular excimer formation of methylene linked arene chromophores in SDS [293]. In both cases the levelling off of the Arrhenius plots at high temperature was attributed to an enhanced rate of excimer dissociation compared to the decay rate of excimer fluorescence. In both of these studies the activation energies calculated from the linear regions of the plots were between 4 and 6 kcal/mol. The activation energy for the variation in $k_{gem}$ with T in the linear range of Figure 4.18a is also about 4 kcal/mol. Thus the value of Ea calculated on the basis of $k_{gem}$ from the data in the temperature dependent region of Figure 4.18a is comparable to that for a diffusion controlled reaction in an SDS micelle.

If, as we propose, the variation in $k_{gem}$ with salt, chain length and temperature is largely due to changes in micellar size with these parameters, the activation energy calculated from Figure 4.18a is in fact an apparent activation energy that arises mainly from changes in the rate constant due to changes in micellar size as the temperature is

altered [242, 294, 295]. We therefore replotted the $k_{gem}$ data in the form of $\log(Nk_{gem})$ versus 1/T where $Nk_{gem}$ is the rate constant adjusted for the micellar volume. The aggregation number data we have used in these plots was taken from papers by Miller and Briggs [229, 234] as before. Figure 4.20 shows a corrected Arrhenius plot for the EO•–BTK system in SDS at zero NaCl. It is clear that $Nk_{gem}$ is only weakly dependent on 1/T. The activation energy derived from this plot is 0.9±0.4 kcal/mol while Ea is 1.9±1.6 kcal/mol and 2.5±1.1 kcal/mol at 0.25M and 0.5M NaCl, respectively. Thus we see that when the variation of $k_{gem}$ with T is adjusted for changing micellar volume the calculated activation energy is quite small. The mean activation energy for the three salt concentrations tested is just 1.8±0.8 kcal/mol. It should be noted that because of the errors intrinsic in the values of $k_{gem}$, the fact that the rate constants were measured over a rather narrow temperature range, the fact that the N data was not obtained under conditions identical to ours and because the experimental slopes are so small, the actual errors in the three Ea values may be substantially larger than the statistical error limits given above.

The activation energy of 4 kcal/mol given by Zana [242] for pyrene excimer formation in SDS was adjusted for changes in micellar volume. It is associated with the diffusion of the pyrene in the micellar environment. It is clear that for the EO•–BTK system the activation energy is about one half of Zana's value. This suggests that $k_{gem}$ might in fact be associated with intersystem crossing. The reasons for this are: (1) the lifetimes of triplet biradicals (intersystem crossing controlled) show activation energies on the order of zero to 1 kcal/mol [296]; (2) if the EO•–BTK $k_{gem}$ value were diffusion controlled we would probably expect it to show a larger Ea than the pyrene system. This last point arises because of the long hydrocarbon tail of EO• which probably acts somewhat like an anchor cable reducing the diffusion of this radical.

There are two additional arguments against associating $k_{gem}$ solely with the rate of intramicellar diffusion. First of all, a wide variety of measurements of the rate

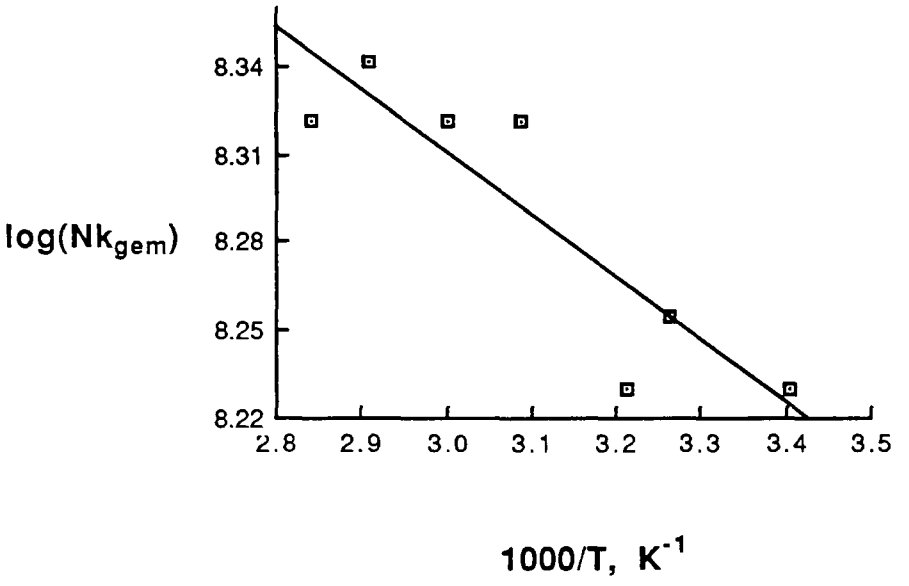


Figure 4.20. Arrhenius plot based on values of the product $Nk_{gem}$ recorded for the Vitamin E phenoxyl–butyrophenone ketyl radical pair in 0.15M SDS in the absence of NaCl.

constant, $k_q$ , for intramicellar quenching of fluorescent probes by neutral and charged species show that the value of $k_q$ for this diffusion controlled process falls between 1x $10^7$ and 8 x$10^7$ $s^{-1}$ in SDS [4]. That is about ten times the value of $k_{gem}$ which we observe in our systems. In addition fluorescence quenching studies indicate that a hydrophobic species like pyrene can explore the entire micellar domain of SDS in about 50 ns [261]. These results suggest that during the lifetime of the $EO^{\bullet}$ – BTK pair in SDS at room temperature, about 500ns (see Table 4.6), there is sufficient time for numerous reencounters of the radical pair. Even if one takes 4x$10^7$ $s^{-1}$ as an average value for the intramicellar value of $k_{diff}$ and assumes that the radical pairs have sufficient time to reach spin – state equilibrium (i.e. 1/4 of the radical pairs are singlets), the expected value for the observed rate constant will be ~ 1.0x$10^7$ $s^{-1}$ which is still 5 times greater than our observed values. In addition if $k_{gem}$ is not diffusion controlled at room temperature it is less likely to be so at elevated temperatures. The second argument against $k_{gem}$ being strictly diffusion controlled is the fact that a number of neutral triplet radical pairs exhibit kinetic isotope effects on $k_{gem}$ as well as isotope enrichment (see the review by Steiner [106] for examples). These effects arise because of an enhanced rate of geminate reaction in systems labelled with a nuclei which has greater hfc than does the proton. Examples of such nuclei are deuterium and $^{13}C$.

In addition to the curved Arrhenius plots observed in SDS, non–linear Arrhenius behaviour has also been observed for the decay of the triplet biradicals formed upon photolysis of long chain 2–phenylcycloalkanones in organic solvents[285]. In this case the decay rate constant became independent of temperature in the high temperature regime and the curvature of the plots became more pronounced as the chain length increased. The authors attributed the curvature to a change in rate determining step from chain dynamics at low temperatures to intersystem crossing at higher temperatures. We feel that there is no need for us to invoke this type of

explanation to rationalize our $k_{gem}$ data in light of the fact that most of the temperature variation we see in the rate constant in fact results from changes in micellar volume.

The low activation energies we observe suggest that $k_{gem}$ is intersystem crossing controlled at zero field. However it is also clear that $k_{gem}$ varies inversely with micellar dimensions as one would expect for a diffusion controlled reaction. How then are we to reconcile these apparently contradictory conclusions? We suggest that indentifying $k_{gem}$ at zero field with *either* a diffusion controlled *or* intersystem crossing controlled rate constant is an oversimplification. This oversimplification arises because of the tendency to view $T_{\pm}$, $T_0$ and S as pure, unmixed spin states. While triplet born radical pairs will indeed be initially formed in pure triplet $T_{\pm}$, $T_0$ states, these states will mix with the S state once the exchange energy, 2J, has been reduced to the level of the hfc interaction energy by radical pair separation [106, 297]. This mixing occurs at about $10^8$ $s^{-1}$ [32] which is much more rapid than the rate of geminate decay ($10^6$ $s^{-1}$). This means that at zero field a "triplet" radical pair is not a pure triplet but rather a predominantly triplet pair with some singlet character [106, 297].

Radical pairs must achieve a small encounter distance in order to undergo (geminate) reaction since radical–radical reaction is a contact process. Only that fraction of (mixed) radical pairs which can access the singlet surface at the time of encounter will lead to closed shell geminate products. Thus the partners of a given mixed, but largely triplet, radical pair may have to undergo numerous collisions with each other before a collision occurs in which the singlet character of the pair is emphasized at the reactive encounter distance. That is to say, the observed geminate reaction rate constant is related to the product of the frequency of reencounter of the geminate partners ($k_e$) with the fraction of singlet character in the mixed radical pair ($f_S$) [106, 297] i.e.,

$$k_{gem} \alpha k_e x f_S \qquad (4.19)$$

It should be noted that in this equation $k_{gem}$ still represents the experimentally determined geminate decay rate constant. The only difference is that we now interpret it in a different manner than before.

The reencounter frequency, $k_e$, is expected to be a function of the reciprocal of the micellar volume and of the value of the mutual diffusion coefficient for the two radicals involved. This comes from the work of Gosele et al. [288, 289] who have shown that the probability that a reagent, A, has not undergone diffusion controlled bimolecular reaction in a micelle after a time period, t, under conditions in which both reagents A and B are free to diffuse is given approximately by

$$P_A \cong \exp\left(-4\pi D r_{AB}\left(\frac{1}{V_M}\right)t\right) \qquad (4.20)$$

Here D is the mutual diffusion coefficient, $r_{AB}$ is the reactive encounter radius, $V_M$ is the micellar volume available for diffusion and t is time. Since by definition every encounter in a diffusion controlled reaction leads to reaction, the probability that A will react within a given time, $1-P_A$, is equal to the encounter probability. From this we can see that $P_A$ will increase when D decreases and when $V_M$ increases. $1-P_A$ will therefore decrease when D decreases and when $V_M$ increases. Since $1-P_A$ equals the encounter probability for a diffusion controlled reaction we would expect the encounter frequency to vary in the same way.

Our temperature dependence data shows that most of the variation in $k_{gem}$ with this parameter comes from changing the micellar volume. This supports the view that micellar microviscosity changes are not of central importance in determining changes in $k_{gem}$. One would expect the same to be true for changing the NaCl concentration or surfactant chain length since, in either of these cases, the micellar environment remains largely hydrocarbon like. In other words our data suggests that the D term in equation 4.20 is not is not as important as the $1/V_M$ term since diffusion and micellar

size factors will influence $k_{gem}$ via $k_e$. Following this line of reasoning $k_e \alpha 1/V_M$ for the EO•/BTK system.

The fraction of singlet character, $f_S$, is also expected to show a dependence on micellar size. In particular as the micelle becomes larger the average radical separation can become greater. This would lead to a reduction in the average value of the exchange energy, $2J_{av}$, since $J_{av}$ drops off exponentially with increasing radical separation [28]. As a result the T/S energy gap at zero field will be smaller in a larger micelle and this will result in greater T/S mixing. That is, the larger the micelle the greater the degree of singlet character to be expected in the radical pairs. Our $k_{gem}$ values clearly decrease with increasing micellar size which shows that the $k_e$ term dominates the $f_S$ term in setting the value of $k_{gem}$. This is so because an increase in $f_S$ (i.e. larger micelles) would favour geminate reaction and therefore increase $k_{gem}$.

In the discussion of the previous paragraph we have assumed that the radical centers not only can be but in fact are subject to larger average separations in a larger micelle. There is excellent experimental evidence for this in the time–resolved ESR data of Closs obtained for benzophenone ketyl–surfactant radical pairs in SDS and SDecS [297]. This work showed that $J_{av}$ = –5.3 MHz (1.9G) in SDecS and –3.4 MHz (1.2G) in SDS where the less negative number implies smaller $J_{av}$. This same type of decrease in $J_{av}$ was observed when NaCl was added to the benzophenone/SDS system.

We have seen that the quantum mechanical picture of radical pair behaviour tells us that a given radical pair will have mixed T and S character. The geminate recombination rate constant is therefore related to the product $k_e f_S$. In the EO•/BTK system it would seem that the degree of radical centre separation (i.e. micellar volume) has a greater influence on $k_e$ than does micellar microviscosity.There is also clear evidence that radical centres are, on the average, further apart in large micelles. We

therefore conclude that the size variation in $k_{gem}$ at H = 0 arises due to a reduction in the frequency of radical pair reencounter in larger micelles.

In many previous studies of "triplet" radical pair kinetics in micelles models like that shown in Scheme 4.1 have been used. It would seem that such schemes are oversimplified in the sense that they represent the behaviour of pure triplet and singlet radical pairs. Scheme 4.2 presents an alternative view which we feel is somewhat more realistic. The curly braces are intended to emphasize the mixed nature of the geminate radical pair spin states. The use of the superscripts 3 and 1 is intended only to indicate that the mixed radical pair is primarily expressing either its T or S character under the indicated conditions of the exchange interaction. As before, boxes are used to represent micelles. When the radical pair is written EO•••BTK it is meant to represent a situation where the partners are sufficiently separated so that J is low. When J is high ( written as EO•,BTK) the radicals are in close contact. Only those close encounters in which the singlet character is expressed will lead to geminate reaction. $f_T$ and $f_S$ represent the degree of triplet and singlet character in the separated (low J) radical pair. These fractions will determine what fraction of the collisions between the radicals are effective in bringing about geminate reaction. Note that throughout this discussion the terms encounter radical pair and separated radical pair are used in a relative sense. Both types of pairs still reside within the micellar environment. A separated pair is not one that has undergone exit but rather one which is separated by distances greater than the reactive encounter distance.

It should also be pointed out that a model like that outlined here does not preclude the observation of isotope enrichment and of magnetic isotope effects on radical pair kinetics. Rather increased hfc due to, say, $^{13}C$ labelling will result in more effective T/S mixing and therefore to greater singlet character in a triplet born radical pair (i.e. higher $f_S$). This will result in enhanced geminate reaction.

Scheme 4.2.

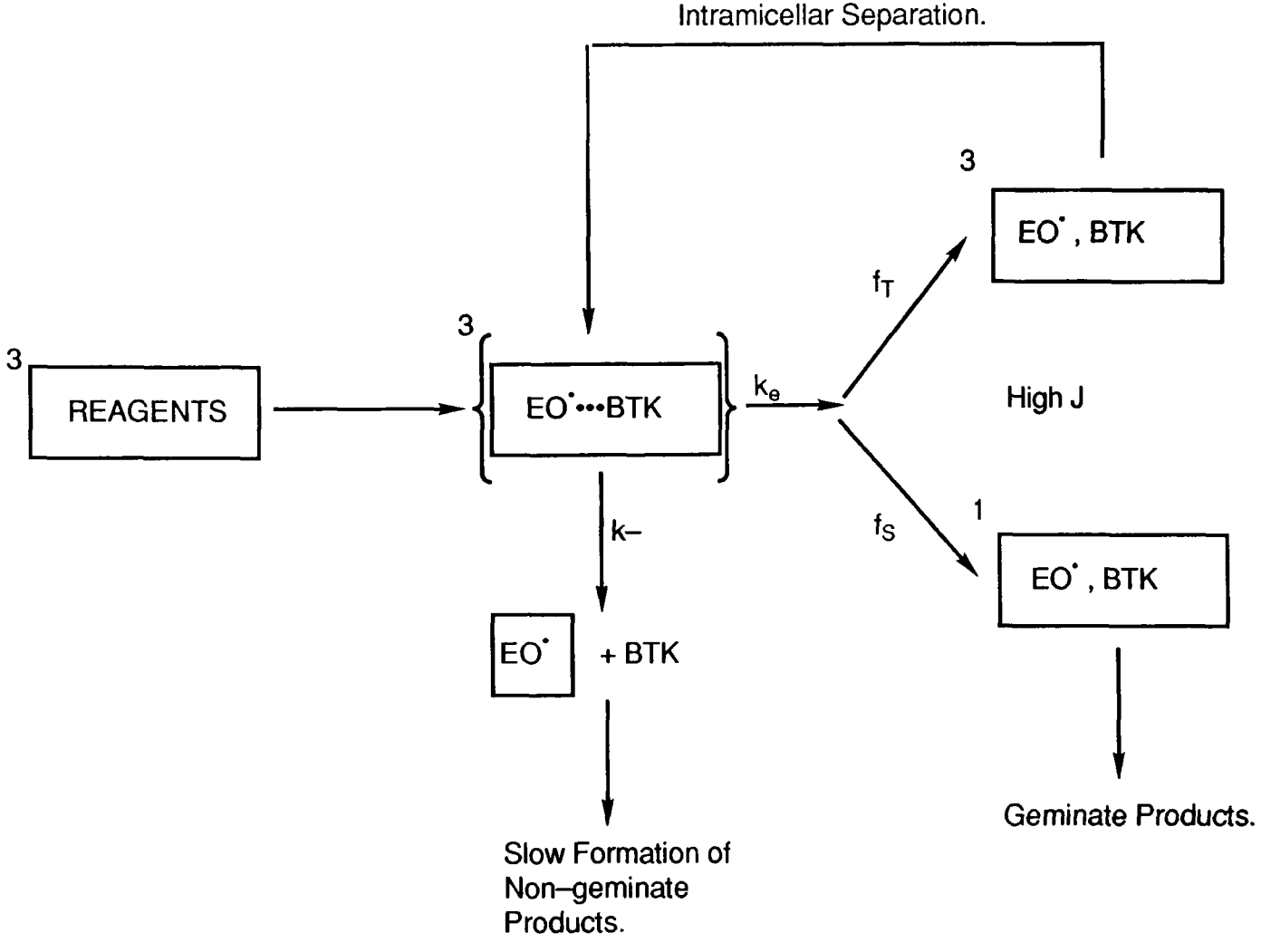
Intramicellar Separation.
3
EO•, BTK
$f_T$
3
3
REAGENTS
EO••••BTK
$k_e$
High J
k–
$f_S$
1
EO•, BTK
EO•
+ BTK
Geminate Products.
Slow Formation of
Non–geminate
Products.

At this point a brief comment about the influence of the duration of the intramicellar encounter "complex" (i.e. EO•,BTK) seems suitable. Even if the micellar environment causes a "triplet" radical pair to be held at the encounter distance for a relatively long period of time after a given collision, this radical pair will not undergo geminate reaction. The reason is that at such small separations J is quite large compared to hfc so that a given "triplet" collision cannot evolve into a "singlet' collision. Of course, if a given collision is dominted by "singlet" character the duration of the encounter complex is irrelevant since the encounter will result in rapid geminate reaction.

At this point a comment concerning micellar microviscosity is in order. The value of SDS microviscosity under a given set of experimental conditions seems to be a matter of some controversy (see Kalyanasundaram's monograph [4]). In particular, some data indicate that microviscosity decreases on increasing micellar dimensions [4] while other data suggests the opposite [298, 299]. This discrepancy may indicate that such changes are indeed rather small. Because of the lack of concensus as to the microviscosity of SDS at room temperature in the absence of additives, let alone as to the way microviscosity depends on experimental conditions, we feel it is probably useless to try and explicitly incorporate microviscosity considerations in our model at this time.

Is it possible to fit the observation of magnetic field effect into our proposed model? The answer is yes. In fact, for a radical pair with small J there is no doubt that the magnetic field effect arises because of the reduced ability of $T_{\pm}$ to access the singlet surface at high fields. However in light of our model we should now describe this as a reduction in the ability of $T_{\pm}$ to undergo hfc mediated mixing with S at high fields because of the increased Zeeman splitting. That is, at high fields $T_{\pm}$ become pure triplet spin states and therefore cannot undergo "singlet" collisions. Geminate reaction will therefore be inhibited. This is illustrated in Figure 4.21a for a single

radical pair under conditions of low J. The various spin states are in fact energy broadened somewhat because of the range of hyperfine interactions they are subject to in a radical pair containing many coupling nuclei.

Each of the triplet sublevels will have an observed rate constant ($k_{T0}$, $k_{T\pm}$) associated with its decay. Although these individual sublevel rate constants may not be obtainable one can qualitatively predict how they will change with applied field strength for a situation corresponding to that in Figure 4.21a. This variation is shown in Figure 4.22. To a first approximation $k_{T0}$ is unaffected. $k_{T+}$ begins to drop off as soon as the field strength is increased and eventually reaches an asymptotic value. The field required to effectively shut off $T_+/S$ mixing will be somewhat higher in a system in which $T_+$ and S are broadened than would be the case if there was no broadening.

The $T_-$ level's decay rate constant will initially increase due to improved energy matching with S. $k_{T-}$ will reach a maximum at fields near 2J. Here 2J refers to the exchange energy for *one* radical pair at a fixed separation. Above this field, energy matching will be reduced and $k_{T-}$ will also drop off and eventually become negligible compared to $k_{T0}$. As was the case with $T_+$, higher fields are required to shut off $T_-$ when the spin sublevels are broadened by hfc. This analysis predicts that the observed rate constant at high fields ($k_{T0}$) should be essentially the same as that at zero field provided that triplet sublevel interconversions are slow compared to the rate of $T_0$ decay at high field. In addition, it is clear that exponential decay cannot be expected at intermediate fields especially because different kinetic behaviour is expected for each triplet sublevel for every radical pair in the ensemble of pairs at intermediate fields.

We can also relate the % escape to the values of the $k_{T0}$, $k_{T\pm}$. That is

$$\% \text{ Escape} = \sum_i \frac{1}{\text{Abundance}_i} x \frac{k-}{k_i} \qquad (4.21)$$

where k– is the exit rate constant and "Abundance" refers to the population of each of the triplet sublevels. The sum is over the i rate constants $k_{T0}$, $k_{T\pm}$. Thus as the $k_i$ are reduced, % escape will increase.

In reality the situation is more complex than described here. For a solution of triplet–born radical pairs in, say, SDS a more realistic energy level diagram is that shown in Figure 4.21b (hfc broadening not shown). In such a solution there is an ensemble of radical pair separations and therefore of J values and $T_0$/S splittings. Thus one can only talk in terms of an average splitting energy, $2J_{av}$. In a smaller micelle, SDecS for example, $2J_{av}$ will be larger than in SDS resulting in a reduction in the average degree of singlet character in the radical pair ensemble.

For a system like that depicted in Figure 4.21b, radical pairs with large separations (low J) will exhibit magnetic field effects at relatively low field strengths while those with small separations (large J) will exhibit magnetic field effects even at fairly high fields. This may in part contribute to the fact that we observe a magnetic field dependence on % escape up to fields near 1kG. That is, at higher fields radical pairs with large J experience T_/S mixing which initially enhances geminate reaction . As the field is increases still further mixing is inhibited again. As a result one might expect to see a magnetic field dependence at fields well above those at which mixing of $T_0$/S in radical pairs with J close to $J_{av}$ should be shut off. This is depicted figuratively in Figure 4.22. Here the value of $2J_{av}$ represents the average $T_0$/S energy gap for the radical pair ensemble. However there is also a range of relevant 2J values ($2J_{relevant}$) which reflects the range of T/S energy gaps over which the system may be expected to display a magnetic field dependence.

Figure 4.10 shows that the greatest influence of the applied field on % escape occurs at relatively low fields for the EO•/BTK pair. In light of the low $J_{av}$ values obtained by Closs for the benzophenone ketyl–surfactant radical pair [297] this should be taken to mean that those radical pairs having separations at or near the ensemble's


a) High field, isolated radical pair.


b) High field, ensemble of radical pairs.

Figure 4.21. Relative spin sublevel energy separations at high field under conditions of low J. (a) Isolated radical pair, (b) Ensemble of radical pairs.

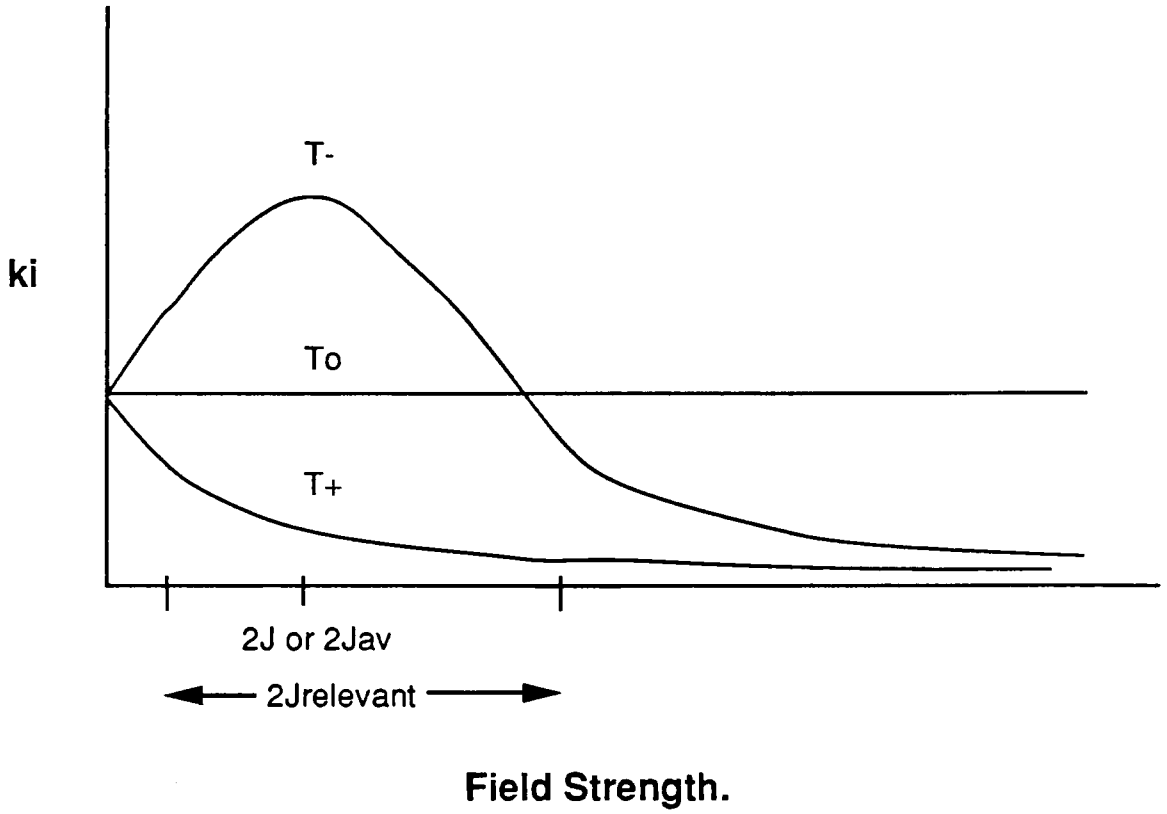


Figure 4.22. Qualitative behaviour of the decay rate constants for individual triplet sublevels of a radical pair with low exchange energy.

average separation (i.e. those with low J) contribute most to the field dependence of the EO•/BTK system.

Radical pairs at or near the average separation making the greatest contribution to the observed magnetic field effect would also explain why the magnetic field dependence of Figure 4.10 shows no minimum corresponding to improved $T_-/S$ mixing at some field value. For the average radical pair the relative energies of the four spin states will be approximately as shown in Figure 4.21a. In such a system $T_-/S$ mixing (and therefore reduced % escape from this sublevel) would occur at energies quite close to $2J_{av}$.That is, $T_-/S$ mixing would occur at such low energies that the hfc interaction would still be effectively mixing $T_+$, $T_0$ and S as well as $T_-$ and S. As a result, on the average the improved $T_-/S$ mixing would have little influence on the average degree of singlet character in the radical pair ensemble.

To summarize, we have reported the first detailed study of the kinetic behaviour of triplet ketyl–aryloxyl radical pairs in micelles in the presence and absence of external magnetic fields. In doing so we have developed a novel approach to generating triplet radical pairs by hydrogen abstraction, namely by the use of a triplet ketone the lifetime of which is limited by intramolecular reaction.

We have also made the first detailed study of the influence of micellar size on the rate constant for geminate reaction as well as the first examination of the influence of temperature on triplet radical pair decay kinetics. We have found that $k_{gem}$ can be interpreted as either intersystem crossing controlled rate constant or a diffusion controlled rate constant at zero field depending at which set of data one looks. We have proposed that this apparent contradiction can be removed by viewing $k_{gem}$ as a rate constant that depends on both the reencounter frequency of the radical pair and its singlet character. At fields in excess of about 100 G spin relaxation may play a role in determining the value of $k_{gem}$.

In addition to our $k_{gem}$ results, our k– data show that the radical pair loses its geminate character because of exit of the ketyl from the micelle into the aqueous phase. Our estimates of the activation energy for this process are the first that have been reported.

Finally we should point out that our model is consistent with all of our observations except the influence of Cu(II). We would expect a paramagnetic species like Cu(II) to have a greater effect on the zero field value of $k_{gem}$. Why it does not is not clear at the present time although it is worth noting that it may not be sufficient to to view this system as a radical pair plus paramagnetic "bystander". Rather it is more like a three unpaired electon system in which the unpaired spins may be coupled to one another.

# CHAPTER 5. GENERATION, CHARACTERIZATION AND KINETIC BEHAVIOUR OF THIOPHENE RADICAL CATIONS IN HOMOGENEOUS AND MICELLAR ENVIRONMENTS.

## 5.1. Introduction.

Alpha–terthienyl (αT) is a secondary plant metabolite [300] which has been the subject of considerable interest over the past ten years because of its phototoxicity and possible insecticidal applications.[301–303] Chart 3.2 shows the structure of αT and of several synthetic analogues which have been examined in the present study.

It is now well established that the lowest triplet states of αT and its derivatives are excellent singlet oxygen sensitizers, [170, 303–308] and their energy transfer characteristics have been studied in some detail. [170, 307, 309] It is believed that the phototoxicity of αT *in vivo* is a direct result of its ability to generate singlet oxygen. [170, 308, 310]

In contrast, little is known about the electron donor/acceptor behaviour of excited thiophenes. Preliminary results indicate that thiophene triplets (αT for example) are excellent electron donors but poor electron acceptors. [307, 309] In addition, ground state thiophenes form weak charge transfer complexes with some electron acceptors [311] and can be electrochemically polymerized to form electrically conducting films of polythiophene; [312–314] the proposed initiator in these polymerizations is the radical cation of the parent thiophene. [315, 316] In spite of the possible intermediacy of thiophene radical cations ($T^{+\bullet}$) in this polymerization process, relatively little is known about $T^{+\bullet}$. The information that is available is mainly ESR data which shows that for the radical cation of the parent thiophene, $C_5H_4S^{+\bullet}$, the unpaired electron density resides in a π molecular orbital which lies on either side of the sulfur atom and has a node which runs through the sulfur atom. [317–319]

As indicated in Chapters 1 and 2, relatively little attention has been paid to magnetic field effects involving micellized radical ion pairs. It was therefore of interest to study such a system in some detail. In light of the rapid reaction of triplet thiophenes with electron acceptors and the fact that thiophenes are quite hydrophobic [320, 321] it was felt that this class of compound would be a likely source for a radical cation that would be useful in such a study. Naturally, it is essential that the homogeneous solution characteristics of $T^{+\bullet}$ be determined prior to investigation of the system in a micellar environment. Thus, this Chapter is divided into two parts; the first examines triplet thiophene electron transfer in organic solvents while the second is concerned with the same reaction in micelles including magnetic field effects.

## 5.2. Results.

### 5.2.1. Homogeneous solution.

*Triplet state characterization.*

The triplet state of α–bithienyl, αB, is the only one of those listed in Chart 3.2 which has not been characterized in the literature. [170, 307, 309] Nitrogen laser excitation of αB in deaerated acetonitrile leads to the formation of an intense, long–lived absorption with $\lambda_{max}$ at 370nm. This transient is formed within the duration of the laser pulse and is readily quenched by oxygen ($k_{O2} = (2.1\pm0.2)\times10^{9}M^{-1}s^{-1}$), but not by 1,3–octadiene ($k_{OCD} << 10^{4}M^{-1}s^{-1}$). The transient lifetime, extrapolated to zero laser dose is 27μs under our experimental conditions. We assign this intermediate to the lowest triplet state of αB. Figure 5.1 shows a comparison of the triplet spectra for αB and αT and the corresponding values of $\lambda_{max}$ have been included in Table 5.1.

At high laser doses the decay of this species exhibits a substantial second order contribution. This type of behaviour is not uncommon and is attributable to triplet–triplet annihilation. The inefficiency of 1,3–octadiene quenching suggests that the triplet energy of αB is less than 58kcal/mol, as expected. [309]

*Formation and characterization of thiophene radical cations.*

The triplet states of αB, αT and the bromo– and cyano– derivatives of αT are readily quenched by good electron acceptors such as methyl viologen ($MV^{+2}$) and tetracyanoethylene (TCNE). In each case quenching rate constants were determined by monitoring the decay of the thiophene triplet state as a function of acceptor concentration. The decays follow pseudo–first order kinetics with a rate constant, $k_{obs}$, that can be related to the rate constants of interest according to equation 5.1

$$k_{obs} = k_o + k_q[\text{quencher}] \qquad (5.1)$$

where $k_0$ is the reciprocal of the triplet thiophene lifetime in the absence of quencher and $k_q$ is the bimolecular rate constant for the quenching reaction. In the case of $MV^{+2}$ it was also possible to follow the reaction by monitoring the formation of the reduced form, $MV^{+\bullet}$, at either 603 or 390nm. [219] Representative plots are shown in Figure 5.2 and the corresponding rate constants are listed in Table 5.2. These rate constants typically approach diffusion control. Reactions 5.2 and 5.3 show the processes responsible for the quenching where T is used to represent any of the thiophenes of Chart 3.2.

$$^3T + TCNE \longrightarrow T^{+\bullet} + TCNE^{-\bullet} \qquad (5.2)$$

$$^3T + MV^{+2} \longrightarrow T^{+\bullet} + MV^{+\bullet} \qquad (5.3)$$

Reaction 5.2 can also be monitored by observing the growth of $T^{+\bullet}$. For example, a plot of the growth rate constant of $\alpha T^{+\bullet}$ at 650nm as a function of TCNE concentration yields a rate constant for the electron transfer reaction of $(2.3\pm0.6)\times10^{10}M^{-1}s^{-1}$, *vide infra*.

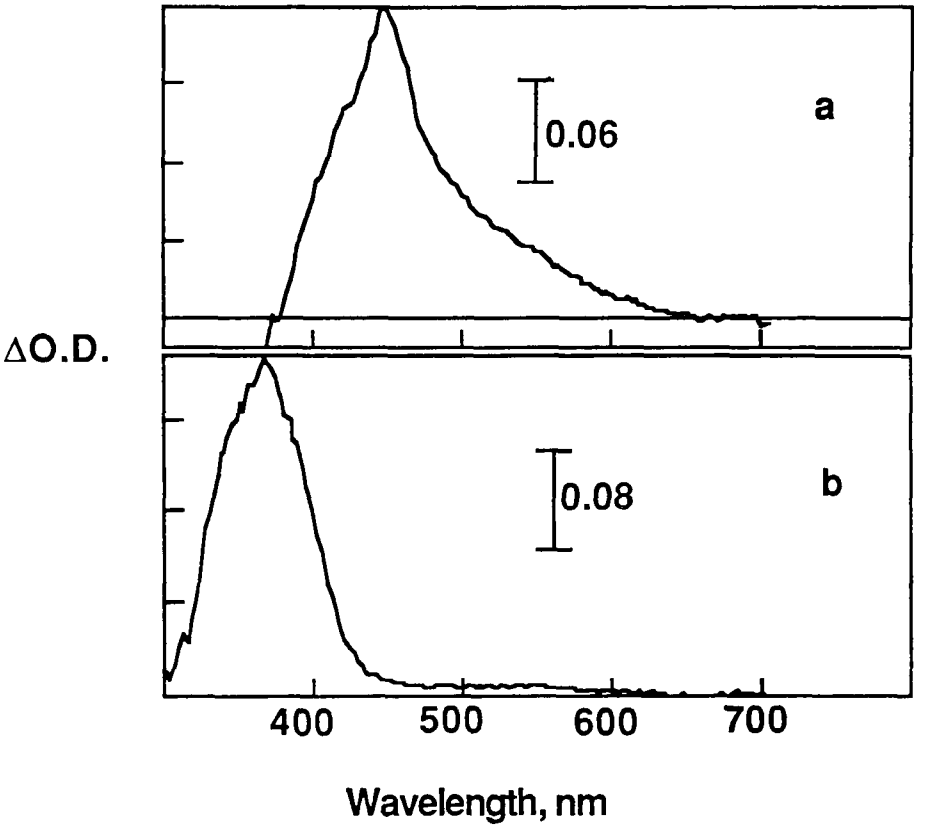


Figure 5.1. Triplet–triplet absorbtion spectra of 50μM αT (a) and 0.6mM αB (b) in nitrogen saturated acetonitrile 500 and 100 ns after the laser pulse and at 24 and 100% of the full laser dose, respectively. Top ΔO.D. = 0.19 (a) and 0.29 (b).

Table 5.1. Spectroscopic data for the triplet states and radical cations from thiophenes, and efficiencies of electron transfer to oxygen in acetonitrile.

| Substrate | $\lambda_{max}$[a] | | $\lambda_{isosbestic}$[a] | $\Psi_{R.C.}$[b] |
|---|---|---|---|---|
| | Triplet | Cation | | |
| αT | 450[c] | 530 | 500 | ≤ 0.01 |
| CNαT | 493[d] | 536 | 523 | 0.03 |
| BrαT | 465[d] | 550 | 523 | 0.04 |
| αB | 370 | 420, 580 | 405 | 0.06 |

(a) In nanometres.

(b) Measured at the isosbestic point, see text.

(c) In methanol, from reference [309].

(d) In methanol, from reference [310].

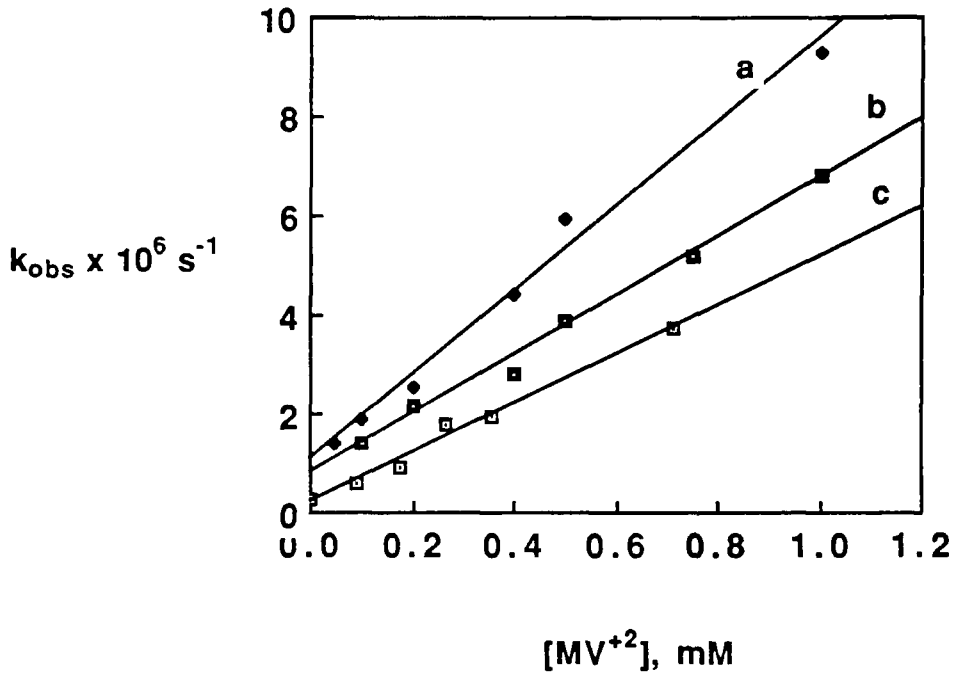


*Figure 5.2. Quenching plots for the reaction of* $MV^{+2}$ with thiophene triplets in methanol: (a) αB, monitoring the growth of $MV^{+\bullet}$ at 603 nm; (b) BrαT, monitoring the growth of $MV^{+\bullet}$ at 603 nm; (c) CNαT, monitoring triplet decay at 420 nm.

Table 5.2. Rate constants for quenching of thiophene triplets by electron acceptors.

| Thiophene | Acceptor | Solvent | $k_q$, $10^{9}$[a] $M^{-1}s^{-1}$ | $\lambda_{max}$ nm |
|---|---|---|---|---|
| αT | $MV^{+2}$ | $CH_3OH$ | 6.8±0.3[b] | 450 |
| | $MV^{+2}$ | 1:9 $H_2O$:$CH_3CN$ | 5.5±0.4 | 450 |
| | TCNE | $CH_3CN$ | 23±6 | 650 |
| αB | TCNE | $CH_3CN$ | 16±4 | 425 |
| | TCNE | $CH_3CN$ | 28±4 | 600 |
| | $MV^{+2}$ | $CH_3OH$ | 8.5±0.5 | 603 |
| CNαT | $MV^{+2}$ | $CH_3OH$ | 5.0±0.6 | 420 |
| BrαT | MV+2 | $CH_3OH$ | 5.9±0.6 | 603 |
| | TCNE | $CH_3CN$ | 16±2 | 650 |

(a) Errors as ±2σ.

(b) From reference [309].

Figure 5.3 illustrates the time evolution of the transient spectra of a sample consisting of 50μM αT and 0.1mM TCNE in deaerated acetonitrile. It is clear that the decay of αT triplet is accompanied by the formation of a new transient with $\lambda_{max}$ at 530nm. The figure shows data obtained when both species (i.e., $\alpha T^{*}$ and $\alpha T^{+\bullet}$) are present (top) and once the decay of the triplet is complete (bottom). We assign the band at 530nm to $\alpha T^{+\bullet}$ formed in reaction 5.4

$$\alpha T^{*} + TCNE \longrightarrow \alpha T^{+\bullet} + TCNE^{-\bullet} \qquad (5.4)$$

In principle, it is possible to follow the progress of reaction 5.4 by monitoring the decay of the αT triplet at or near its $\lambda_{max}$. However, overlapping absorptions due to $\alpha T^{+\bullet}$ and $TCNE^{-\bullet}$ also occur at this wavelength. In the present case it seemed preferable to monitor the reaction at 650nm by following the growth of $\alpha T^{+\bullet}$. At this wavelength the signals are somewhat weaker, but are not complicated by the extensive spectral overlap that characterizes other spectral regions.

For the other thiophenes tested, at acceptor concentrations sufficient to quench over 90% of the triplets and at delays (following laser excitation) to allow for the triplet decay, the spectra observed are those of the corresponding radical cations produced in reactions 5.2 and 5.3. The new transients decay with second order kinetics, which we attribute to reverse electron transfer, for example, in the $MV^{+2}$ system:

$$MV^{+\bullet} + T^{+\bullet} \longrightarrow MV^{+2} + T \qquad (5.5)$$

In the case of $MV^{+2}$ as acceptor the signals from its reduced form, $MV^{+\bullet}$, are sufficiently intense that they can be readily observed in the presence of the various thiophene cation radicals. Figure 5.4 illustrates this for the αT system. In the case of TCNE as an acceptor the system is much cleaner and for practical purposes leads to

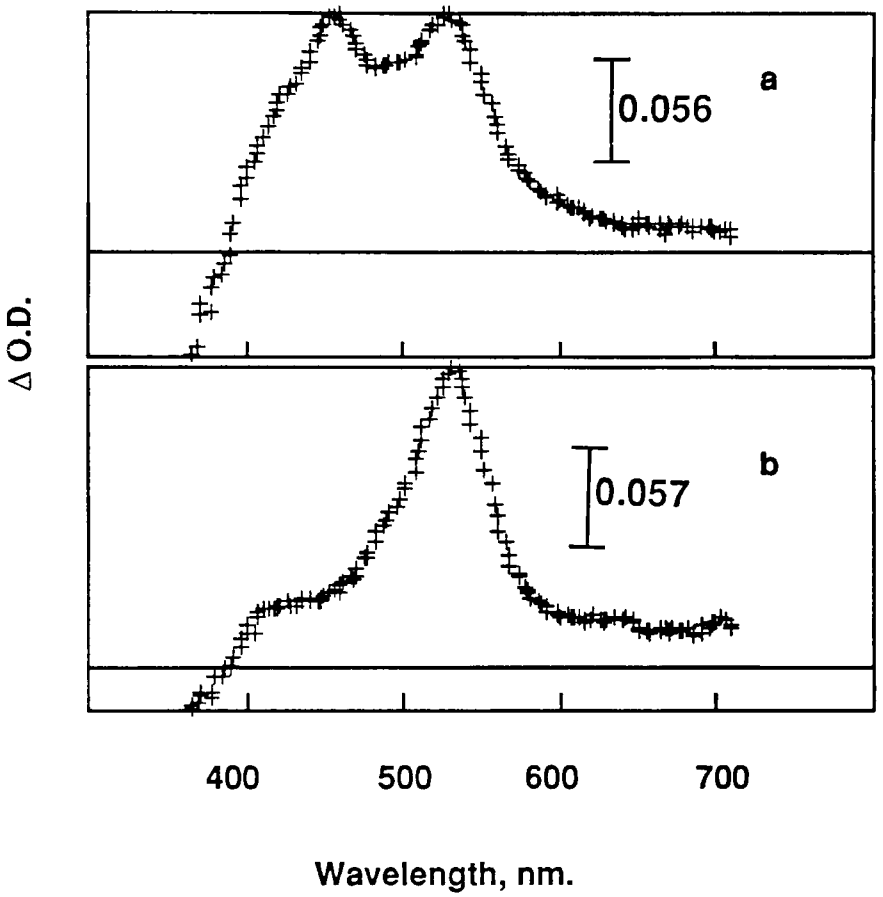


Figure 5.3. Transient spectra recorded in the presence of 50μM αT and 0.1M TCNE in acetonitrile: (a) 200ns after laser, top ΔO.D. = 0.14; (b) 5μs after laser, top ΔO.D. = 0.17. Both spectra recorded at 40% of full laser dose.

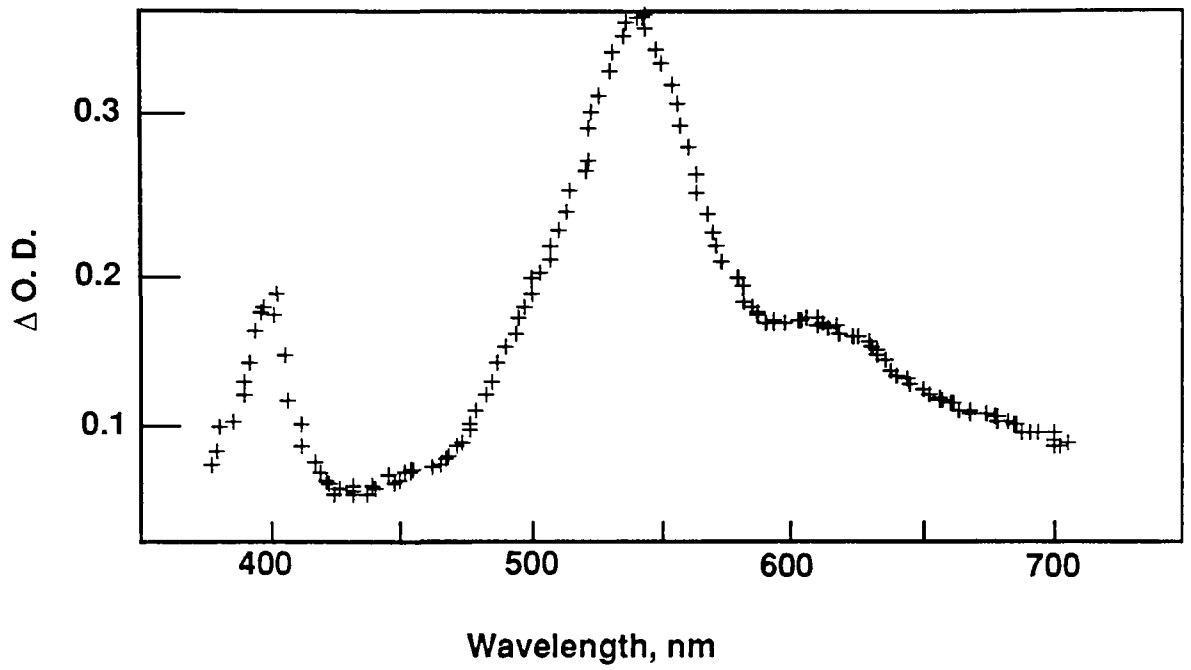


Figure 5.4. Transient spectrum recorded in the presence of 50μM αT and 4mM $MV^{+2}$ in methanol 500ns after excitation.

spectra of just the thiophene radical ions. The TCNE radical anion produced in reaction 5.2 has a relatively weak absorption in the spectral region of interest ($\lambda_{max}$ 435nm; $\varepsilon_{435}$ = 7100$M^{-1}cm^{-1}$ in dichloromethane [322, 323]). Only in the case of $\alpha B^{+\bullet}$ can we expect some spectral interference (*vide infra*). The reader may note that the absorption mentioned above for $TCNE^{-\bullet}$ is not really a "weak" one, however, it is in relative terms and in comparison with the thiophene radical cations that this description applies. Figure 5.5 shows the spectra of $CN\alpha T^{+\bullet}$ and $\alpha B^{+\bullet}$ in acetonitrile. The spectra of the radical cations from the three thiophene trimers (i.e., $\alpha T^{+\bullet}$, $Br\alpha T^{+\bullet}$, $CN\alpha T^{+\bullet}$) are very similar. The corresponding $\lambda_{max}$ values are listed in Table 5.1.

The spectrum of $\alpha B^{+\bullet}$ (Figure 5.5) shows two bands (420 and 580nm), which decay with identical kinetics and are therefore attributed to the same intermediate. Figure 5.6 shows the decay monitored at 540nm for a sample of 50μM CNαT and 4mM TCNE in acetonitrile. The transient decays with second order kinetics and a first half–life of 0.73μs. Saturation of this solution with oxygen does not reveal any quenching of the $CN\alpha T^{+\bullet}$ signal in the time scale of our experiments (10ns to 200μs), thus supporting the assignment of the 536nm band to $CN\alpha T^{+\bullet}$ and showing our ability to detect the radical cation in the presence of oxygen (*vide infra*). Corresponding results were obtained for each of the thiophene radical cations studied.

As in the case of $MV^{+\bullet}$, we attribute the decay shown in Figure 5.6 to the back electron transfer, i.e.

$$T^{+\bullet} + TCNE^{-\bullet} \longrightarrow T + TCNE \qquad (5.6)$$

The fact that the decay of these intermediates can be attributed to back electron transfer is supported by the very low conversion (< 10% as judged by UV spectroscopy) observed upon prolonged irradiation of the samples. In agreement with this observation, we find that the decay traces return to the pre–excitation baseline

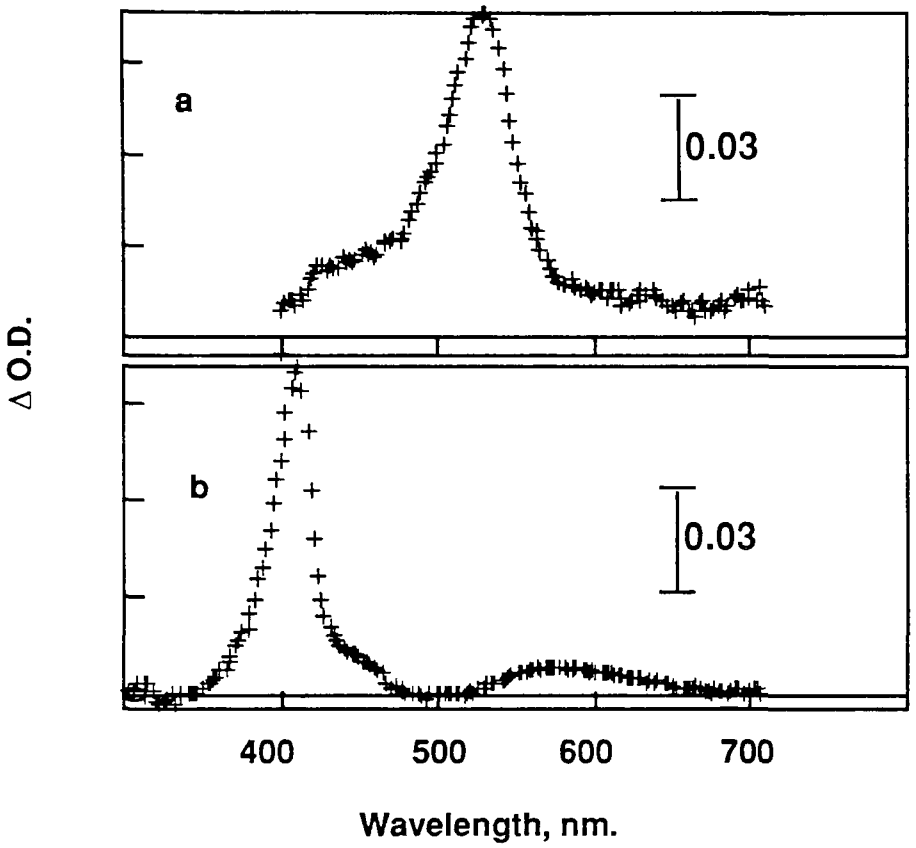


Figure 5.5. (a) Spectrum of CNαT radical cation recorded in the presence of 50μM CNαT and 4mM TCNE in nitrogen saturated acetonitrile 2μs after the laser pulse. Top ΔO.D. = 0.11. (b) Spectrum of the αB radical cation recorded in the presence of 100μM αB and 12mM TCNE in nitrogen saturated acetonitrile 120ns after the laser pulse. Top ΔO.D. = 0.13.

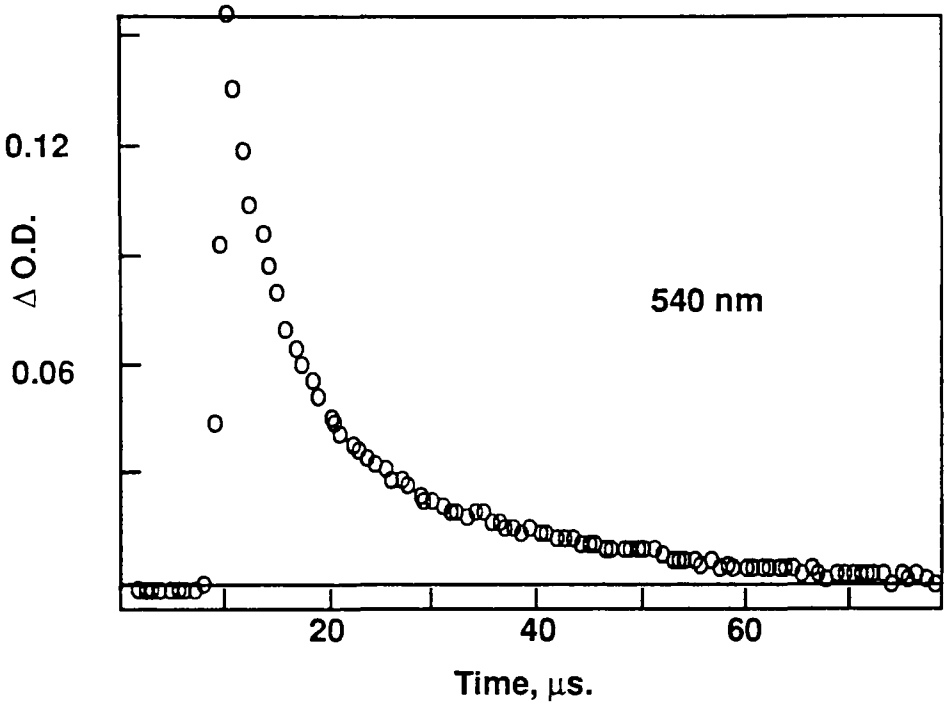


Figure 5.6. Decay trace for the CNαT radical cation in the presence of 50μM CNαT and 4mM TCNE in nitrogen saturated acetonitrile.

level, showing that no overall change in optical properties takes place. The same type of behaviour has been reported previously for the $\alpha T/MV^{+2}$ system. [309]

Table 5.3 reports values of the kinetic parameter, $k_{5.6}/\varepsilon_T{}^{+\bullet}$, for the back electron transfer reaction 5.6. $\varepsilon_T{}^{+\bullet}$ is the molar extinction coefficient for $T^{+\bullet}$ at the $\lambda_{max}$ of the radical cation. If an independent value of $\varepsilon_T{}^{+\bullet}$ can be obtained we can calculate the back electron transfer rate constant, $k_{5.6}$. In fact our data do allow independent evaluation of $\varepsilon_T{}^{+\bullet}$ and the procedure for obtaining it will be illustrated for the case of $\alpha T^{+\bullet}$.

From Figure 5.4 it is clear that $MV^{+\bullet}$ and $\alpha T^{+\bullet}$ can be simultaneously detected in deoxygenated solution. Since the extinction coefficient of $MV^{+\bullet}$ is well known [324] it should be possible to evaluate $\varepsilon_{\alpha T}{}^{+\bullet}$ if the degree of spectral overlap can be estimated. Consider the observed optical densities at two wavelengths, $\lambda_1$ and $\lambda_2$, where $\lambda_2$ is $\lambda_{max}$ for $\alpha T^{+\bullet}$. Then

$$\Delta OD^1 = (C_{MV+\bullet}\varepsilon^1_{MV+\bullet}) + (C_{\alpha T+\bullet}\varepsilon^1_{\alpha T+\bullet}) \qquad (5.7a)$$

$$\Delta OD^2 = (C_{MV+\bullet}\varepsilon^2_{MV+\bullet}) + (C_{\alpha T+\bullet}\varepsilon^2_{\alpha T+\bullet}) \qquad (5.7b)$$

Where $C_{MV+\bullet}$ and $C_{\alpha T+\bullet}$ are the transient concentrations of $MV^{+\bullet}$ and $\alpha T^{+\bullet}$, respectively, and the superscripts refer to the wavelengths. Since each quenching event leads to one $MV^{+\bullet}$ and one $\alpha T^{+\bullet}$, $C_{MV+\bullet} = C_{\alpha T+\bullet}$. Also, define $P=\varepsilon_{1\alpha T+\bullet} / \varepsilon_{2\alpha T+\bullet}$. Using these latter two conditions and equation 5.7 we can derive that

$$\varepsilon^2_{\alpha T+\bullet} = \frac{\Delta OD^2\varepsilon^1_{MV+\bullet} - \Delta OD^1\varepsilon^2_{MV+\bullet}}{\Delta OD^1 - \Delta OD^2 P} \qquad (5.8)$$

Using this approach we are able to estimate that $\varepsilon\alpha_{T+\bullet} = 29000\ M^{-1}cm^{-1}$ at 530 nm. From this we obtain a value of $k_{5.6} = 2.6\times10^{10}\ M^{-1}s^{-1}$ in acetonitrile. These values, along with the corresponding values for αB, CNαT and BrαT are presented in Table 5.3. The final values are all very similar and not unreasonable in view of the

Table 5.3. Values of $k_{5.6}/\varepsilon_T{}^{+\bullet}$ measured at 300K in acetonitrile.

| Thiophene | $k_{5.6}/\varepsilon_T{}^{+\bullet}$(a) cm $s^{-1}$ | $\varepsilon_T{}^{+\bullet}$(b) $M^{-1}$ $cm^{-1}$ | $k_{5.6}$, $10^{10}$ $M^{-1}$ $s^{-1}$ |
|---|---|---|---|
| αT | $9.1 \times 10^5$ | 29 000 | 2.6 |
| αB | $2.7 \times 10^6$ | 15 900(c) | 4.3 |
| CNαT | $9.1 \times 10^5$ | 59 100 | 5.4 |
| BrαT | 1.5x106 | 42 210 | 6.3 |

(a) At $T^{+\bullet}$ $\lambda_{max}$ in a 0.7 cm path.

(b) At $T^{+\bullet}$ $\lambda_{max}$.

(c) May be subject to interference by TCNE radical anion.

Coulombic attraction that will tend to favour the back reaction in the case of TCNE as an acceptor.

Note that there is an apparent discrepancy between the ΔO.D. values at 530 and 398 nm shown in Figure 5.4 when one considers the relative extinction coefficients of $\alpha T^{+\bullet}$ and $MV^{+\bullet}$ at these wavelengths ($\varepsilon_{MV+\bullet}$ = 33000 $M^{-1}$ $cm^{-1}$ at 398 nm[324]). This is readily explained since the ground state of αT absorbs significantly at 398 nm which results in an apparent reduction of the $MV^{+\bullet}$ signal due to bleaching by the αT ground state.

With hindsight, it is not clear why $\alpha T^{+\bullet}$ was not observed in earlier work from this laboratory, [309] although it should be noted that this earlier work involved the use of $MV^{+2}$ concentrations substantially smaller than those used in the present study.

Before closing this section it is worth commenting on the possibility that ground state complexes may be involved in the photoreactions studied. αB and TCNE are known to form a change transfer (CT) complex with $\lambda_{max}$ 650 nm in acetonitrile [311]. However, the complex is a rather weak one, with an equilibrium constant for association, $K_{CT}$, of only 2.39 $M^{-1}$. Thus, under our experimental conditions ([αB] ~ 0.1 mM and [TCNE] ~ 12 mM) we would typically expect to form ~ 2.9 μM complex. Since the extinction coefficient of the complex at 650 nm is 660 $M^{-1}cm^{-1}$ we would expect an absorbance of ca. $1.3 \times 10^{-3}$ in a 0.7 cm cell. Such a small ground state signal is not expected to introduce any interference in our measurements.

There seems to be no literature on CT complexation between αT and TCNE, but the $\lambda_{max}$ for the CT complex between TCNE and 2 – methylthiophene is at 410 nm while that for the complex between TCNE and 5,5'–dimethyl–2,2' dithiophene is at 750 nm [311]. Although this effect of increased conjugation may not be as dramatic on going from a thiophene dimer to a trimer as it is as going from monomer to dimer, we suspect that any CT complex band in the αT/TCNE system will be at a long enough wavelength so as not to interfere in our measurements.

In the case of the $\alpha T/MV^{+2}$ system we examined the UV–VIS spectra between 220 and 720 nm using 50 μM αT and concentrations of $MV^{+2}$ of up to 44 mM in $CH_3OH$. The αT absorbance at 350 nm was not modified by addition of $MV^{+2}$ and no new absorption bands were detected. Our study, therefore, does not provide any evidence for significant complexation between αT and $MV^{+2}$ in the ground state.

*Oxygen quenching of triplet thiophenes:*

Characterization of $\alpha T^{+\bullet}$ and the other thiophene radical cations should allow one to estimate the contribution of the following reaction

$$T^{*} + O_2 \longrightarrow T^{+\bullet} + O_2^{-\bullet} \qquad (5.9)$$

to the oxygen quenching of thiophene triplets. Oxygen quenching of triplet states leading to significant yields of superoxide is not unprecedented. For example, triplet rose bengal undergoes rapid oxygen quenching with about 75% of the quenching events leading to singlet oxygen and about 20% to superoxide [325]. For the related xanthene dyes tetrabromo – and tetraiodo fluorescein, Gandin et al [326] have reported that the singlet oxygen quantum yield, $\Phi_\Delta$, is also about 75% of $\Phi_T$. In the context of the rose bengal results it is not unreasonable to expect that the yield of superoxide for these fluorescein compounds may also be the balance between the singlet oxygen yield and the intersystem crossing efficiency. In light of these reports we feel that a direct measurement of the superoxide yield arising from reaction 5.9, although this is expected to be small, is nonetheless desirable.

In order to address the question of superoxide yields, we carried out oxygen quenching studies of the thiophene triplets in acetonitrile, a system where $T^{+\bullet}$ is readily detectable, long lived and not quenched by oxygen. As already indicated, laser excitation of nitrogen saturated solutions of T (50μM) in acetonitrile leads to the readily detectable triplet–triplet absorption spectra of these substrates. When the same

solutions are saturated with oxygen the resulting spectra, employing OMA detection, show no clear evidence of the presence of $\alpha T^{+\bullet}$ nor of $CN\alpha T^{+\bullet}$ at 1μs after excitation and only very weak signals for $Br\alpha T^{+\bullet}$ and $\alpha B^{+\bullet}$. At this time delay the decay of the thiophene triplets is complete in each case.

We repeated the experiments described above by following the triplet thiophene decay kinetics in oxygen saturated acetonitrile monitoring at wavelengths (see Table 5.1) where $T^*$ and $T^{+\bullet}$ have an isosbestic point. The decay traces showed a very small residual in each case. If one monitors the same systems at the $\lambda_{max}$ of the respective $T^{+\bullet}$, where detection is biased in favour of the radical cations, a residual of somewhat greater intensity is observed. The spectra of these residuals were monitored using R7912 "point–by–point" detection rather than the OMA (as the sensitivity of the former is superior) and were found to be in agreement with those of the corresponding thiophene radical cations, $T^{+\bullet}$.

The residual absorptions just discussed can be used to obtain quantitative values for the fraction of triplet quenching events, $\Psi_{R.C.}$, that lead to $T^{+\bullet}$, and therefore to $O_2^{-\bullet}$ (reaction 5.9) . The transient concentrations of $T^*$ and $T^{+\bullet}$, $C_T$ and $C_{T+\bullet}$, are related via the simple relation

$$C_{T^*}\Psi_{RC} = C_{T+\bullet} \tag{5.10}$$

or

$$\frac{\Delta OD_{T^*}}{\varepsilon_{T^*}}\Psi_{RC} = \frac{\Delta OD_{T+\bullet}}{\varepsilon_{T+\bullet}} \tag{5.11}$$

Since the data is obtained at the isosbestic wavelength, $\varepsilon_{T^*} = \varepsilon_{T+\bullet}$. Thus

$$\Psi_{RC} = \frac{\Delta OD_{T+\bullet}}{\Delta OD_{T^*}} \tag{5.12}$$

The values of $\Psi_{R.C.}$ obtained using this approach are listed in Table 5.1. While it is evident that electron transfer is a minor process in all cases, it is also clear that in some systems, αB in particular, it is not an insignificant process.

5.2.2. Generation and decay of radical ion pairs in surfactant solution.

Figure 5.7 show decay traces (monitored at 540 nm) for a deaerated sample of 100 μM αT and 40 mM $MV^{+2}$ in 0.15 M SDS at room temperature, measured in the absence and presence of a magnetic field (*vide infra*). The chromophore monitored under these conditions is largely the thiophene radical cation. While at 540 nm there may be some contribution from $MV^{+\bullet}$, its contribution to the absorption at this wavelength does not exceed 30%. At any rate, since the decay observed can be attributed to back electron transfer in the $\alpha T^{+\bullet}$ / $MV^{+\bullet}$ pair (reaction 5.6), it should make no difference which radical ion (or mixture) is monitored.

The zero field trace of Figure 5.7 consists of two kinetic components: a rapid initial decay followed by a low intensity, long - lived residual absorption. As in other systems involving micellar reactions of radical pairs, we attribute the fast decay fraction to geminate processes, and the residual absorption to escape processes leading to separation of the radical pair. Under these conditions the fast decay, which behaves monoexponentially, corresponds to the sum of rate constants for geminate and escape processes i.e.

$$k_{obs} = k_{gem} + k- \qquad (5.13)$$

where these rate constants are as defined previously. The escape fraction and the individual values of $k_{gem}$ and k– can be obtained from the experimental decay traces by use of the same technique as was applied to the EOH – BUP system (see Chapter 3). A summary of results is given in Table 5.4 and Scheme 5.1 illustrates the mechanism proposed. Note that we have used a scheme similar to that proposed in

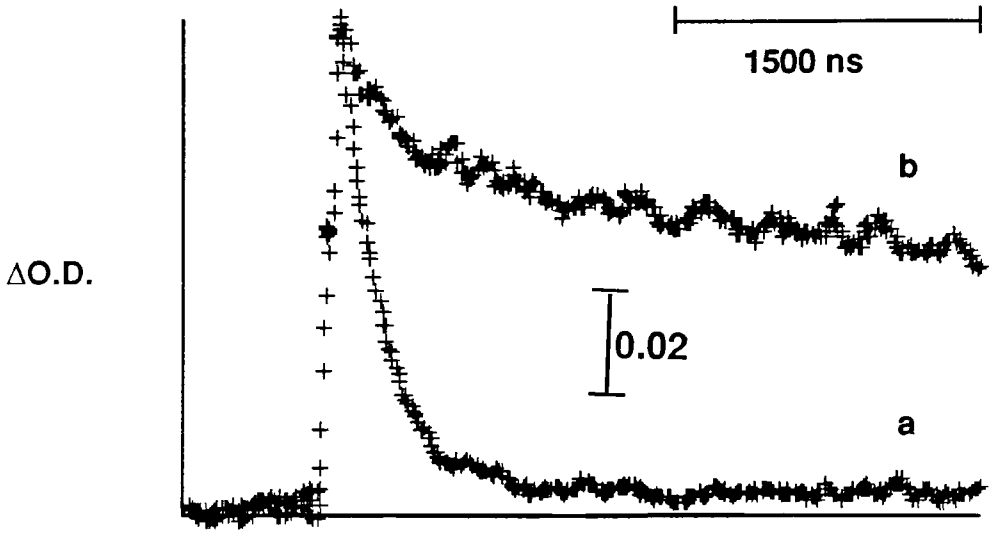


Figure 5.7. Decay traces recorded at 540nm in the presence of 96μM αT, 40mM $MV^{+2}$ and 0.15M SDS at zero (a) and 5kG (b) applied magnetic field. The top ΔO.D. is 0.11 for both traces.

Table 5.4. Geminate reaction and escape data for various thiophene–surfactant combinations.

| Surfactant | Thiophene | kgem | k– | % Escape | |
|---|---|---|---|---|---|
| | | $x10^6\ s^{-1}$ | | 0 G | 5 kG |
| 0.15M SDS | αT | 4.7 | 0.21 | 4.3 | 71 |
| | CNαT | 3.6 | 0.23 | 6.0 | 68 |
| | BrαT | 7.9 | 0.19 | 2.4 | 7.9 |
| 0.5M SOS | αT | 11.6 | 2.6 | 18 | 79 |
| | CNαT | 8.6 | 1.8 | 18 | 74 |

Scheme 5.1.

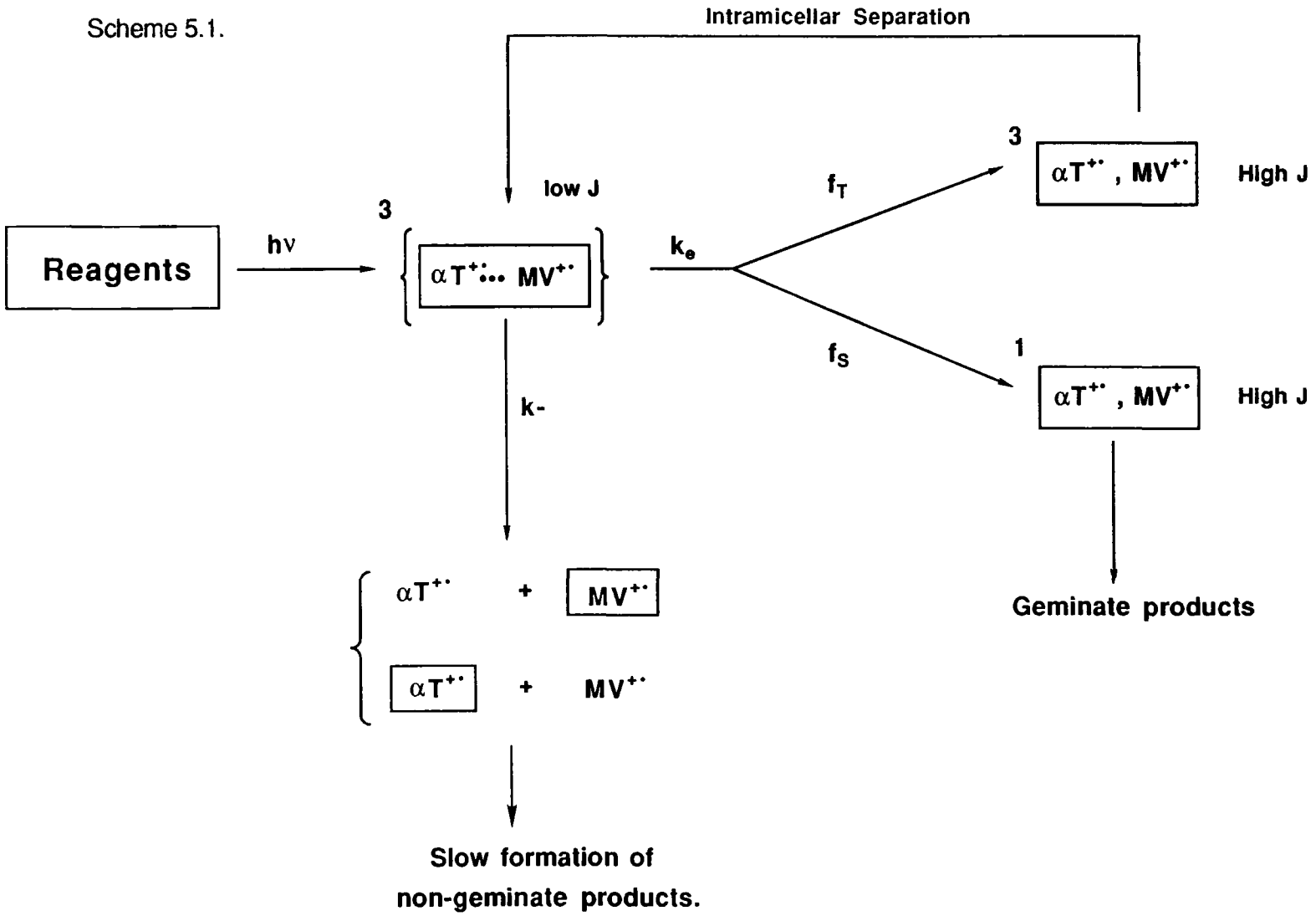
Intramicellar Separation
Reagents
hν
3
low J
αT+• ... MV+•
kₑ
f_T
3
αT+• , MV+•
High J
f_S
1
αT+• , MV+•
High J
k-
αT+• + MV+•
αT+• + MV+•
Geminate products
Slow formation of
non-geminate products.

Chapter 4 to emphasize the mixed nature of the radical pair spin states. For example, in the $\alpha T^{+\bullet}$ / $MV^{+\bullet}$ pair only ca. 4% of the pairs undergo separation suggesting that the highly charged negative micelle efficiently keeps the pair together for the time required for geminate processes to occur. We note that values of k– based on such small residual absorption (see Figure 5.7) may have a rather large relative error (as much as 50% for 5% escape), although this drops rapidly when the escape fraction increases. Several experiments were also carried out in micelles sodium octyl sulfate (SOS) and the results have also been included in Table 5.4.

Application of magnetic fields leads to an increase in the residual absorption (and therefore escape) observed. Figure 5.8 illustrates this effect for the $\alpha T^{+\bullet}$ / $MV^{+\bullet}$ system; quite clearly the system reaches a plateau at fields over 1–2 k G. The field required to achieve one half of the maximum effect ($H_{1/2}$) is only 130 G in this system. In this particular case escape increases from 4.3% at zero field to 71% at 5.2 kG. The yield of radical ions (as measured by the absorbance immediately following the laser pulse) was not affected by application of magnetic fields, indicating that the triplet state processes that precede radical formation are field independent.

We interpret the magnetic field effects as resulting from a slow–down of geminate reaction from the T+ and T– triplet sublevels of the radical. We further suggest (*vide infra*) that once a radical ion pair collision which emphasizes the singlet character of the pair occurs the pair reacts rapidly to generate products and/or regenerate the starting materials. At intermediate fields (at $H_{1/2}$, for example) the decay is complex and the fast component cannot be readily explained as a monoexponential component of the decay. As discussed for the EOH – BUP system (Chapter 4) this is an indication that interconversion among the various triplet sublevels in the $\alpha T^{+\bullet}$ / $MV^{+\bullet}$ system is slow in the time scale of our experiment [54, 55]

In contrast to the results for $\alpha T$ and $CN\alpha T$, the $Br\alpha T/MV^{+2}$ system shows little sensitivity of the % escape to application of an external magnetic field (Table 5.4).

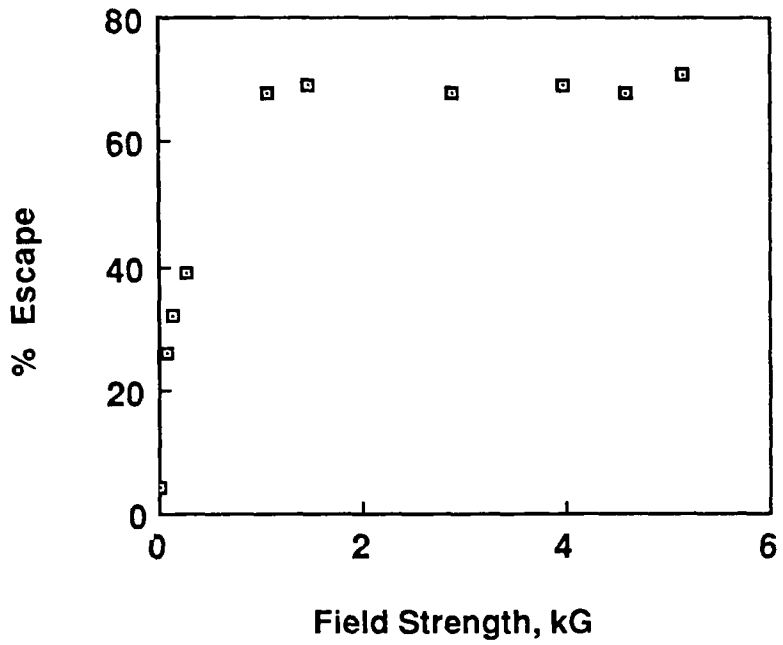


Figure 5.8. Variation in % escape with magnetic field Strength for the $\alpha T^{+\bullet}/MV^{+\bullet}$ radical cation pair in 0.15M SDS. [$\alpha$T] = 100$\mu$M; [$MV^{+2}$] = 40 mM.

However, $k_{obs}$ did vary with field strength (Figure 5.9). In these latter experiments the escape fraction was always so low (< 11%) that we preferred to report $k_{obs}$ rather than $k_{gem}$ since the value of the former is almost exclusively determined by the latter. As is clear from Figure 5.9 field effect on the geminate rate constant for this system saturates at relatively low fields ($H_{1/2}$ ~ 150 G). The $k_{gem}$ value at zero field was $7.9 \times 10^6$ $s^{-1}$ but that at high fields was only $4.3 \times 10^6$ $s^{-1}$, i.e. about 1/2 the zero field value. By contrast for αT, the values of $k_{gem}$ at zero and 5kG were $4.7 \times 10^6$ $s^{-1}$ and $4.0 \times 10^6$ $s^{-1}$, respectively.

In order to carry out reliable kinetic studies in systems such as those illustrated in Figures 5.8 and 5.9, it is important to generate the radical ion pair in a time much shorter than its decay lifetime. This normally requires moderately high concentrations of electron acceptor. By contrast, at low concentrations (2 mM $MV^{+2}$ in the presence of αT/SDS, for example) there was a noticeable growth period for $\alpha T^{+\bullet}$; in addition, triplet αT could be detected several microseconds after excitation. This may be a reflection of the fact that for 0.15 M SDS and 2mM $MV^{+2}$, 35% of the micelles would not have any $MV^{2+}$ associated with them (assuming a Poisson distribution) even if all the methyl viologen was associated with the micelles. This serves to illustrate the difficulties that can arise when the "clock" technique (see Chapter 4) cannot be used to generate the desired radical pair. At higher $MV^{+2}$ concentrations the appearance of $\alpha T^{+\bullet}$ became instantaneous in our time scale and the residual absorbance decreased from a value of 24% at 2.3 mM (largely due to αT triplet, not escape) to about 5% at 15 mM $MV^{+2}$. The latter value was essentially independent of further changes in the $MV^{+2}$ concentration up to the highest value tested, 40 mM. Under these conditions ([SDS] = 0.15M) we can estimate that about 0.038 M $MV^{+2}$ will be associated with the micellar pseudo - phase taking 2400 $M^{-1}$ as the association constant, K, of the $MV^{+2}$ with SDS. Based on these values, we can safely assume that all triplet thiophenes will find one or more acceptors in the same micelle; we therefore attribute the "instantaneous"

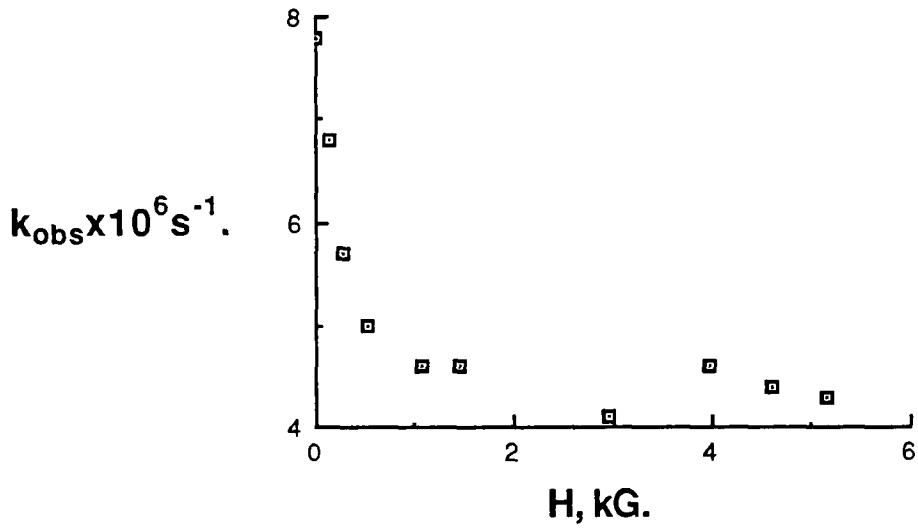


Figure 5.9. Variation in kobs with field strength for the Br$\alpha T^{+\bullet}$/$MV^{+\bullet}$ radical cation pair in 0.15M SDS. [Br$\alpha$T] =100$\mu$M; [$MV^{+2}$] = 40 mM.

formation of $\alpha T^{+\bullet}$ (or $T^{+\bullet}$ in general) to the efficient quenching of the triplet at high acceptor concentrations.

The value of K for $MV^{+2}$ quoted above is the average of several literature values ranging between 844 and 4590 $M^{-1}$ [327–329]. These values seem rather low when one compares them to typical equilibrium constants for the association of dications such as $Cu^{+2}$ (10,000 M-1 to 60,000 M-1), $Ni^{+2}$(10,900 M-1) or $Pb^{+2}$ (27,700) with SDS [250, 252]. We therefore attempted to measure K for $MV^{+2}$ using the pyrene probe technique of Encinas and Lissi [173] described in Chapter 3.

The usefulness of the Encinas/Lissi method is rather limited in the two extreme cases where K is very small (quencher is fully dissolved in the aqueous phase) or very large (quencher is fully associated with the micellar environment). In the former case the observed quenching behaviour will be independent of micelle concentration while in the latter case increasing [Mic] merely dilutes the fully micellized quencher. When this condition holds $I_0 / I_Q$ should be directly proportional to [Mic]. At either of these two extremes the technique will not provide accurate quantitative but will indicate that the quencher is strongly associated with one phase or the other.

For the $MV^{+2}$/SDS system with pyrene as a probe we have determined values of K ranging between 9000 $M^{-1}$ and 14,000 $M^{-1}$ Further, a plot of Io / IQ versus [Mic] at a fixed $MV^{+2}$ concentration was linear with a slope close to unity. The results should be interpreted to mean that $MV^{+2}$ is quantitatively associated with SDS although these K values cannot be regarded as accurate. Nonetheless, our results indicate that earlier reports substantially underestimated the value of K. This finding is borne out by laser flash photolysis measurements of the exit rate constant for $MV^{+\bullet}$ discussed below.

## 5.3 Discussion.

The long lived triplet states of all the thiophenes in this study are readily quenched by good electron acceptors such as $MV^{+2}$ and TCNE. Quenching leads to the thiophene radical cations which show strong absorptions in the 530 - 550 nm region for trimer systems and at 420 nm for αB. In homogeneous solution the radical ions are generated efficiently and decay by essentially diffusion controlled recation to regenerate the starting materials.

Our results also rule out any role of reaction 5.9 accounting for more than 1% of the absorbed light dose in the oxygen quenching of αT triplet and for more than 10% of the absorbed dose in oxygen quenching of triplet thiophenes generally in acetonitrile as solvent. While our results clearly show that electron transfer from triplet thiophenes to oxygen will make only a minor contribution to the *in vitro* photoactivity of the thiophene, this does not rule out the possible involvement of an electron transfer process *in vivo*. A relay mechanism, analogous to that exemplified by the reaction of $MV^{+\bullet}$ with $O_2$ to yield superoxide [324], is one such possibility. Even so, the most likely explaination for αT phototoxicity remains its ability to generate singlet oxygen in high yield. This result is in agreement with work by Bakker et al. [304] who showed that mannitol benzoate, superoxide dismutase or catalase had little effect on αT photooxidations of glucose–6–phosphate dehydrogenase, suggesting that activated species such as $OH^{\bullet}$, $O_2^{-\bullet}$ and $H_2O_2$ are not involved. Singlet oxygen quenchers such as $NaN_3$, histidine and methionine did protect and similar *in vivo* protection of yeast cells was observed by Arnason et al. [330]

Analysis of the behaviour of radical ion pairs in micellar systems presents several interesting features and sheds some light regarding the type of interactions that determine the kinetics of geminate processes.

It is worth noting that the values of k– show a clear dependence on micellar size at room temperature. As noted previously similar effects have been observed in the case of neutral radicals, as well as in reversed micelles. The values of k– incorporate

the rate constants for all processes that lead to the separation of the radical ion pair, and therefore to loss of its geminate character. In our case this means the sum of the exit rate constants for $MV^{+\bullet}$ and $T^{+\bullet}$. The fact that these values are rather small (see Table 5.4) in spite of the evident hydrophilicity of these species is a reflection of the Coulombic interactions that tend to keep the cations associated with the anionic micelles. Interestingly, if we assume that k– represents an upper limit for the exit rate constant for $MV^{+\bullet}$, and that the association rate constant is controlled by diffusion (i.e., ~ $1x10^{10}$ $M^{-1}$ $s^{-1}$ for diffusion in water), then the equilibrium constant for $MV^{+\bullet}$ association with an SDS micelle must exceed 50,000 $M^{-1}$. We find it unlikely that the association value for $MV^{+\bullet}$ would be so much higher than the value for $MV^{+2}$ suggested in the literature, and are therefore inclined to believe that the highest values discussed above represent a lower limit for the true value. Such high values for the equilibrium constants simply mean that for practical purposes the $MV^{+2}$ and $MV^{+\bullet}$ ions are quantitatively associated with the micelles in SDS surfactant solutions. This quantitative association may be in part responsible for the wide variation in K literature values.

In the systems described herein the exit process probably does not involve migration from the oil phase to the water, but rather release from the micellar surface and into the aqueous phase. The values of k– are probably remarkable only in the large change observed on going from the $C_8$ to the $C_{12}$ micelle.

Analysis of the $k_{gem}$ values should be carried out in the light of our knowledge of the factors that control the lifetimes of flexible triplet biradicals in solution [41–43, 125] as well as the lifetimes of neutral radical pairs (see Chapter 4). A recent extensive review on magnetic field effects also provides insight into the key elements for this discussion [106]. In our examples we can reasonably assume that the radical ion pair moves on the surface of the micelle rather than in the micellar environment. Two questions are of prime importance. First, to what extent is diffusional motion (as

opposed to spin motion is an important factor in determining the rates of geminate processes in the absence of magnetic fields. Second, if spin evolution is important, what types of interactions determine the magnitude of $k_{gem}$. Most reports on the subject have assumed that $k_{gem}$ is controlled by intersystem crossing (see Chapter 2); however, a recent report by Turro [94] as well as work by Hayashi [83], Levin [149] and Steiner [44] has suggested that the rate constants for geminate decay in the absence of magnetic fields are determined by diffusional motion of the radicals within the micelles for several different radical pairs.

We propose that the reactive decay, as measured by $k_{gem}$, of the radical ion pairs studied here is controlled by the product of $k_e$ and $f_S$ (see Chapter 4) rather than by either intersystem crossing or diffusive reencounters. In support of this we note that the value of $k_{gem}$ for BrαT is nearly twice that for αT. It is hard to see how substitution by bromine could possibly enhance the rate of diffusion; in contrast it is straightforward to associate heavy atom substitution with an increase in the rate constant of triplet–singlet intersystem crossing. Thus the mechanisms proposed by Turro for benzylic radicals [94] and by Hayashi, Levin and Steiner for their systems cannot be generalized to the case of radical cation pairs. It is worth noting that a similar increase in the observed decay rate constant upon bromine substitution has been observed for biradicals containing benzyl radical centres. [331]

The zero field values of $k_{gem}$ are systematically higher for the smaller micelles (Table 5.4). While a decrease in spin orbit coupling mediated intersystem crossing would account for this behaviour because of the increased time averaged separation of radical centers in larger micelles, this explanation is not consistent with the large magnetic field effect observed in the αT and CNαT systems. However, as described in Chapter 4, the value of $k_{gem}$ should also depend on the frequency of reencounter and therefore vary inversely with micellar volume.

The effect of magnetic fields on the yield of radicals that exit (Table 5.4) is considerably reduced in the case of heavy atom substituted radical pairs; thus application of a 5kG field in the case of αT changes the escape yield from 4 to 71% (SDS micelles). By contrast, in the case of BrαT the the yield changes from 2.4 to just 7.9%. This result is not likely to be associated with changes in polarity of the thiophene donor, since the results for CNαT are virtually identical to those for αT. Similar heavy atom effects have been reported in other systems [44, 48, 70, 151] and have been attributed to a change in mechanism from hfc to spin orbit coupling [48, 70] or to the increased contribution of spin rotational relaxation to $T_{\pm}$ –> S (and $T_{\pm}$ <–> $T_0$) interconversion in the presence of heavy atoms [44]. As indicated before, in the case of αT we believe the interconversion between triplet states to be a slow process in the time scale of $k_{gem}$. If this condition is preserved in the presence of a field, we expect that at a sufficiently high field the $T_{\pm}$ intersystem crossing channels will be shut off, while for $T_0$ the competition between escape and intersystem crossing will remain essentially unaffected. It is straightforward to estimate that for all the SDS systems in Table 5.4 escape will saturate at about 70% if the above conditions are met. This is indeed the case for αT and CNαT, but not for BrαT. We suggest that in the case of BrαT the criterion of slow interconversion between triplet sublevels is not met.

In the limit of fast triplet sublevel interconversion the situation is quite different from that described in the previous paragraph. Here even if intersystem crossing from $T_{\pm}$ is completely shut off, these sublevels could still "leak" into the singlet manifold via conversion to the $T_0$ level. In the limit $k_{gem}$ would be reduced to one third (assuming equal initial populations of $T_{\pm}$ and $T_0$) of its value at zero field since at high field the statistical weight of $T_0$ (the state that actually undergoes intersystem crossing) would be 1/3. Under these conditions the escape yield would go up to about 7% for BrαT. When one takes into account that this applies only in the high field, fast sublevel

interconversion limit, and that k– carries considerable error, the value is entirely consistent with the escape yield of 7.9% observed experimentally.

To test the applicability of these considerations to the present system we fit the decay traces for the αT and Br αT systems in SDS at zero and 5 k G applied field. In all cases a good fit was obtained. By assuming k– to be field independent it was possible to calculate $k_{gem}$ both at high and low fields. For αT these values are $4.7 \times 10^6$ $s^{-1}$ at zero field and $4.0 \times 10^6$ $s^{-1}$ at 5 k G while for BrαT $k_{gem}$ was found to be $7.9 \times 10^6$ s-1 at zero field but only $4.3 \times 10^6$ $s^{-1}$ at high field, i.e. about one half the zero field value. These data support our view of slow triplet sublevel interconversion in the case of αT and fast interconversion in the BrαT system since, as already mentioned, if spin state interconversion were rapid compared to intersystem crossing we would expect $k_{gem}$ (H>>0) to be substantially smaller than $k_{gem}$ (H = 0). If spin state interconversion were slow, the value of $k_{gem}$ at zero and high fields should be approximately equal.

What is the source of this rapid interconversion between triplet sublevels in the BrαT$^{+\bullet}$ / MV$^{+\bullet}$ radical ion pair? One possible explanation is similar to that offered by Ulrich and Steiner [44]. These authors write the rate constant for spin relaxation mediated spin state interconversion in a radical pair, $k_{rel}$ ,as

$$k_{rel} = k_{AHF} + k_g + k_{SR} \qquad (5.14)$$

where $k_{AHF}$ is the anisotropic hyperfine coupling term, $k_g$ is the term arising due to anisotropy of the g - factor and $k_{SR}$ is the spin - rotational coupling term. The former two rate constants are field dependent while the latter is not. As a result $k_{rel}$ can never be less than $k_{SR}$. Significant magnetic fields will be observed when $k_{SR}$ is comparable to, or smaller than, $k_{gem}$ (H=0) assuming the rate constant for $T_0$ to S interconversion is field independent. When $k_{SR}$ is substantially larger then $k_{gem}$ (H=0) there will be rapid spin state interconversion so that even at high fields $T_{\pm}$ will be able to "leak" into

$T_0$. The magnetic field will then be less effective at inhibiting $T_\pm \rightarrow S$ intersystem crossing.

The magnitude of $k_{SR}$ is related to the value of the longitudinal relaxation time, $T_1$, of the radical which is subject to increased spin – orbit coupling in the presence of a heavy atom ($\alpha T^{+\bullet}$ in this case). The value of $T_1^{-1}$ can be increased substantially in the presence of a heavy atom [32]. Thus one would expect bromine substitution of the $\alpha T$ moiety to increase $k_{SR}$. Presumably the increase in the value of this rate constant is sufficient to make the rate of triplet sublevel interconversion at high field comparable to the rate of intersystem crossing thus effectively suppressing the magnetic field effect.

Note that an increase in $k_{SR}$ implies an increase in the rate of $T_\pm$ –> S as well as of $T\pm$ <–> $T_0$ transitions. If the rate of the former process was to remain comparable to the rate of $T_0$ –> S at high fields one would not expect the observed value of $k_{gem}$ to reach a plateau since the Zeeman effect on $T_\pm$ continues to increase with the field strength. However Figure 5.9 clearly shows that the value of $k_{gem}$ becomes field independent by 1 k G for the Br$\alpha$T system. This means that direct $T_\pm$ –> S transitions are not important in this system at high fields. We may therefore conclude that the reduction in the magnetic field effect for the Br$\alpha$T system is due solely to the effect of the heavy atom upon the rate of $T_\pm$ <–> $T_0$ interconversion.

Finally, a comment on the magnitude of the $H_{1/2}$ values obtained in this study is in order. For both the $\alpha$T and CN$\alpha$T systems $H_{1/2}$ is about 130 G. This value is much lower then that observed for the $EO^\bullet$ – BTK system. While no ESR data seem to be available for $\alpha T^{+\bullet}$ or $\alpha B^{+\bullet}$ such data can be found for the radical cation of thiophene itself. Using this data [318] as well as ESR data for $MV^{+\bullet}$ [332] it was possible to calculate that the $H_{1/2}$ value for the thiophene radical cation / $MV^{+\bullet}$ pair should be about 16 G using Weller's equations [111]. While this value is a factor of 8 different from our experimental value it is in much better agreement with experiment than was the case for the $EO^\bullet$ – BTK system where the discrepancy was a factor of 40. Part of the

discrepancy in the present case may be due to the fact that the unpaired electron will be substantially more delocalized in $\alpha T^{+\bullet}$ than is $C_5H_4S^{+\bullet}$ [333] so that more nuclei will couple to the electron in the former case. Thus we expect that αT's contribution to the hfc interaction will be greater than that of $C_5H_4S$. If so a larger value of $H_{1/2}$ would be calculated for the $\alpha T^{+\bullet}/MV^{+\bullet}$ system than for the $C_5H_4S^{+\bullet}/MV^{+\bullet}$ system. The low experimental $H_{1/2}$ as well as the points just discussed make it not unreasonable to suggest that the magnetic field effect in the αT and CNαT systems arises because of the hfc mechanism.

To summarize, thiophene triplet states are good electron donors and readily lose an electron to yield the rather long - lived, intensely absorbing radical cations in the presence of a suitable acceptor. Electron transfer to oxygen accounts for only a small fraction of total quenching events observed during the interaction of triplet thiophenes with ground state oxygen. The major decay path of the thiophene radical cations appear to be reverse electron transfer to regenerate starting materials. In micellar solution our data suggest that the rate of geminate reaction in the absence of an applied field is in fact determined by both intersystem crossing and radical pair reencounter. Considering the low $H_{1/2}$ value for these systems it seems likely that the observed magnetic field effects are dominated by the hfc mechanism at least for αT and CNαT.

The fact that we only observed a small magnetic field effect in the BrαT system appears to be indicative of rapid spin state conversion of this radical pair, even at high field strengths. We have rationalized this finding using arguments proposed by Ulrich and Steiner, namely that enhanced rates of spin rotational coupling at high field provide efficient $T_{\pm} <-> T_0$,S transitions. Our data also suggest that $T_{\pm} <-> S$ transitions are not important at 5 kG. These data suggest that it may be spin relaxation effects which dominate the kinetics behaviour of the BrαT system at high fields.

Finally our data provide yet another example of a radical pair the kinetics of which depend on micellar dimensions. From the point of view of our interpretation of $k_{gem}$ it would seem that such size dependence should be considered normal behaviour for triplet born radical and radical ion pairs in micelles.

# CHAPTER 6. FINAL COMMENTS AND NEW DIRECTIONS.

Although the focus of intense research since the early 1970s, the influence of magnetic fields on a wide range of chemical systems is a subject that continues to hold the interest of scientists. [106] Prior to 1984 it seemed that a reasonably detailed picture was available by which one could understand the impact of applied fields on radical pair behaviour in micelles. In particular, zero field geminate decay kinetics were attributed to hfc mediated intersystem crossing and the observed magnetic field effects to a reduction in the (hfc) intersystem crossing rate because of Zeeman splitting of the triplet sublevels at higher fields. However with the work of Hayashi, Levin and Steiner, which suggested that $k_{gem}(H=0)$ could be diffusion controlled and that spin relaxation might play a role in causing magnetic field effects, this pleasant situation seems to no longer exist. It is within this context that the $k_{gem}$ results of the present study have their meaning. Before discussing the $k_{gem}$ data a brief comment will be made concerning exit processes.

The exit data presented here for the EO•–BTK system clearly show that k– has an inverse dependence on micellar size. While the rate constant values are insufficiently precise to decide which micellar parameter (volume, surface area or the ratio of surface area to volume) k– correlates with, one would not be surprised if the surface area to volume ratio were to be most important. This is reasonable since the BTK ketyl is uncharged and is therefore likely to access the micellar core for at least part of the time it is resident in the micellar environment. In terms of obtaining a quantitative correlation between k– and micellar size, it would be advantageous if micellar size data could be obtained under experimental conditions which more closely match those used in the present study.

Our exit data also suggests that ketyl escape is via diffusion of this species out of the micelle and into the bulk aqueous phase rather than via either fragmentation–coagulation or collision followed by reagent exchange. The measured activation parameters for exit are comparable to those for other diffusional processes in micelles and the reduction in entropy at the exit transition state probably reflects the restructuring of water which is needed to accommodate the escaping hydrophobic species. It would be of interest to obtain exit activation parameters for charged species such as $\alpha T^{+\bullet}$ and $MV^{+\bullet}$. One might expect the activation energy to be higher for such species since they are subject to electrostatic attraction to the surface of anionic micelles like SDS. Measurements of this type might be able to shed some light on a somewhat surprising interpretation in the literature regarding the nature of the binding of $MV^{+2}$ to anionic micelles. Whitten [327, 328] has reported that the association of the quite water soluable $MV^{+2}$ with SDS is largely due to the hydrophobic interaction. If the activation energy for exit of a system like thiophene–methyl viologen were to significantly larger than that for the phenoxyl–ketyl system it would argue strongly against $MV^{+2}$ being hydrophobically bound to SDS. In addition, the value of $\Delta S^{\neq}$ is not expected to be as negative for the thiophene system as that for the phenol–ketyl system since $\alpha T^{+\bullet}$ and $MV^{+\bullet}$ are substantially more hydrophillic than BTK. One might imagine that it is therefore possible to solubilize such substances in water with less rearrangement of the water structure than is the case with more hydrophobic reagents.

Perhaps the most interesting result to come out of the $EO^{\bullet}$–BTK study is the observation that $k_{gem}$ depends on micellar size at zero field. It is evident that practically the entire temperature dependence of $k_{gem}$ arises form changes in micellar volume. When this is corrected for, the activation energy for the geminate decay process is quite small as would be expected if $k_{gem}$ were primarily determined by intersystem crossing. These apparently contradictory results become more compatible when one adopts the view that triplet derived radical pairs in fact posses some degree

of singlet character and that the rate constant for geminate reaction is related to the product of the radical pair reencounter frequency with this degree of singlet character. At any rate, our data provide two additional examples of micellar size dependent geminate decay kinetics and in fact suggests that such behaviour is to be expected regardless of the chemical nature of the triplet derived radical pair under investigation.

The only result we have that conflicts with the model we are proposing is the lack of an appreciable effect of Cu(II) on the zero field kinetics of the EO•–BTK pair. While the data presently available does not allow one to explain this discrepancy one may suggest alternative approaches to examining the influence of changing the magnetic environment of the EO•–BTK pair at zero applied field. One possibility would be to use a bromine substituted phenol in place of 3,5–dimethylphenol. If, as was observed for the αT system, this lead to an increase in $k_{gem}$ at zero field then one would feel confident that there is something special about the interaction of Cu(II) with this radical pair.. A second approach would be to compare the $k_{gem}$ value of EO•–BTK with that for the radical pair formed following photoreduction by EOH of the triplet of a $^{13}C$ labelled BUP. The $^{13}C$ label should be at the carbonyl carbon to be most effective. Since the hyperfine coupling constants of $^{13}C$ are substantially greater than those for hydrogen the rate of hfc mediated intersystem crossing at zero field should be larger in the $^{13}C$ case as opposed to the case where only hydrogen nuclei contribute to hfc. If the $k_{gem}$ value increased in a $^{13}C$ labelled system it would again be good evidence that the results obtained with Cu(II) reflect more than just a simple paramagnetic interaction between the metal ion and the radical pair.

Another consideration is that perhaps the EO•/BTK/Cu(II) system should not be regarded as a (predominately) triplet radical pair with a paramagnetic "bystander" at all. The system actually consists of three unpaired electrons which probably interact as a coupled system. Thus the overall spin state of the three electron system may be (predominately) doublet or quartet rather than triplet. One may imagine that if spin flips

of the Cu(II) electron is rapid the "radical pair" (i.e. the EO•/BTK electrons) spin state, which is coupled to that of the ion, will quickly lose its spin memory. If such a situation exists it may not be surprising that little effect of Cu(II) is observed on the zero field kinetics of EO•/BTK. While this is merely speculation at this point it may be an idea that is worth further examination.

The fact that bromination of αT increases the rate of geminate decay in the thiophene–methyl viologen radical cation pair is also compatible with the model of triplet derived radical pairs presented here. Both this system and the aryloxyl–ketyl systems exhibit large magnetic field effects which preclude spin orbit from being an important source of intersystem crossing at zero field. However while the low $H_{1/2}$ value of the $\alpha T/MV^{+2}$ system suggests that magnetic field effects arise via the hfc mechanism in this case, the large $H_{1/2}$ value for EO•–BTK combined with the large difference between this value and that calculated from Weller's equation indicates that a different magnetic field effect mechanism may well be operating in the latter case. The most likely candidate for the EO•–BTK pair is spin relaxation. This may also be important for $Br\alpha T/MV^{+2}$ since our data suggests that rapid spin state interconversion is operative in this pair even at 5kG applied field.

A set of experiments that might prove interesting in light of the proposal that transitions between spin states continue to be rapid even at high field for $Br\alpha T/MV^{+2}$ would be to measure $k_{gem}(H=0)$ and the magnetic field effect on %escape for a series of halogen substituted αTs, i.e. Cl– and IαT in addition to the bromo compound. One would then be able to see if the values of $k_{gem}$ and %escape did in fact correlate with the degree of spin orbit coupling in the radical pair which should increase with the atomic weight of the halogen atom. If $k_{gem}$ and %escape did show such a correlation it would be evidence for the validity of the Ulrich–Steiner arguments regarding suppression of magnetic field effects in the presence of heavy atoms.

An interesting question that arises from our EO•–BTK data as well as from the work of Hayashi, [83] Levin, [149] and Turro [94] is how fast is diffusion in a micelle? As we have seen fluorescence probe data indicates that the rate of intramicellar exploration is much larger than the rate of geminate decay typically observed for micellized radical pairs. However this data is generally obtained from systems that do not closely mimic radical pairs systems. A possible approach to getting a handle on this problem would be to try and investigate the decay kinetics of a micellized singlet radical pair. A possible system one might use in such a study is the diphenylmethyl radical pair. This pair can be generated in the singlet state upon photolysis of diphenylmethyldiphenylacetate (DMDA) [334]

$$^1Ph_2CH(CO)OC(H)Ph_2^* \longrightarrow {}^1[Ph_2(H)C^\bullet, {}^\bullet C(H)Ph_2] + CO_2 \qquad (6.1)$$

In their study of the photochemistry of DMDA under lamp photolysis conditions, Simmers et al. [334] have estimated that about 40% of the observed cleavage of the acetate is via the singlet. The majority of the cleavage reactions (about 90%) lead to diphenylmethyl radicals. However for reaction 6.1 to be useful for a study of the type we are proposing the fraction of acetate cleavage which proceeds via the triplet, and therefore leads to triplet radical pairs, must be suppressed. One possible approach would be to saturate the system with oxygen. The oxygen will quench the triplet acetate thus preventing the formation of triplet radical pairs. Of course $O_2$ can also trap the diphenylmethyl radicals generated via the singlet route ($k_{O2} = 6x10^8\ M^{-1}s^{-1}$ [163]) but it will only trap those radicals which have already lost their geminate character. In fact in homogeneous solution about 10% of the diphenylmethyl radicals recombine even under conditions of oxygen saturation. This has been attributed to the fraction of radicals which undergo in cage reaction [334]. It should be kept in mind that in cage reaction will be much more extensive in micelles than in an organic solvent. Thus it

should be possible to study the decay kinetics of singlet diphenylmethyl radical pairs even in the presence of oxygen. While these points indicate that some preliminary work must be done to evaluate the usefulness of the DMDA system for our purpose, it would seem that this approach is potentially quite informative.

In conclusion, the two radical pair systems studied in this thesis differ from each other, and also from the radical pair systems described in the literature, in terms of chemical structure. Even so, they behave in a similar fashion in the sense that both are subject to large magnetic field effects and decay by kinetics that depend on micellar dimensions. In these respects the two systems are quite similar to a number of radical pairs that have been studied previously. While it is possible to explain the magnetic field effect on the thiophene systems in terms of the conventional hfc model, this is not so for the phenol systems where a combination of hfc and spin relaxation must be resorted to. In terms of the size effect, we feel that the most promising approach to radical pair kinetics at zero field is to view such systems as having mixed spin state character. Finally, in light of the current debate in the literature over the importance (or not) of diffusion in influencing geminate reaction kinetics of triplet radical pairs in micelles, a more detailed theory of the combined effects of spin evolution and diffusion on intramicellar geminate decay is highly desirable.

## CLAIMS TO ORIGINAL RESEARCH.

1: The proposal of a new interpretation of the geminate decay rate constant for micellized triplet derived radical pairs, in terms of the product of radical re-encounter frequency and degree of singlet character.

2: The first systematic study of the influence of micellar size on the geminate decay kinetics of triplet derived radical pairs. The results of this study lead directly to the new proposal noted in item 1.

3: The first measurements of the activation parameters for exit of a ketyl radical from a micellar environment. These activation parameters have given substantial insight into the nature of the transition state associated with ketyl exit.

4: Development of a mild and simple technique for generating thiophene radical cations in polar organic solvents. This permitted the characterization of these species in terms of their optical absorption spectra and decay kinetics.

5: The finding that electron transfer from thiophene triplet states to ground state molecular oxygen is a rather inefficient process.

6: The first observations of magnetic field effects on the geminate behaviour of a radical cation pair in a micellar environment.

REFERENCES

(1) Gymer, R.G. *Chemistry in the Natural World*; D.C. Heath: Toronto, 1977.

(2) Manahan, S.E. *Environmental Chemistry*; Willard Grant Press: Boston, 1984.

(3) Gulotty, R.J.; Mets, L.; Alberte, R.S.; Fleming, G.R. *Applications of Fluorescence in the Biomedical Sciences*. Taylor, Waggoner, Murphy, Lanni and Birge ed. 1986 Alan R. Liss. New York.

(4) Kalyanasundaram, K. *Photochemistry in Microheterogeneous Systems*; Acedemic Press: New York, 1987.

(5) Ramanath, N.; Ramesh, V.; Ramamurthy, V., *J. Photochem.* **1985**,*31*, 75.

(6) Fendler, J.H.; Fendler, E.J. *Catalysis in Micellar and Macromolecular Systems*; Acedemic Press: New York, 1975.

(7) Bovey, F.A.; Winslow, F.H. *Macromolecules. An Introduction to Polymer Science*; Acedemic Press: New York, 1979.

(8) Tanford, C.B. *The Hydrophobic Effect: Formation of Micelles and Biological Membranes*; Wiley: New York, 1980.

(9) Turro, N.J.; Cox, G.S.; Paczkowski, M.A., *Top. Curr. Chem.* **1985**,*129*, 57.

(10) Turro, N.J., *US Patent* **1984**,*4 448 657*, .

(11) Israelachvili, J.N. *Intermolecular and Surface Forces With Applications to Colloidal and Biological Systems*; Acedemic Press: New York, 1985.

(12) Shaw, D.J. *Introduction to Colloid and Surface Chemistry*; Butterworths: Toronto, 1978.

(13) Lindmann, B.; Wennerstrom, H. Micelles. Amphiphilic Aggregation in Aqueous Solutions. 1980 Springer-Verlag. New York.

(14) von Bunau, G.; Wolff, T., *Adv. Photochem.* **1987**,*14*, 273.

(15) Missel, P.J.; Mazer, N.A.; Carey, M.C.; Benedek, G.B. *Solution Behavior of Surfactants*. Mittal and Fendler ed. 1982 Plenum. New York.

(16) Missel, P.J.; Mazer, N.A.; Benedek, G.B.; Carey, M.C., *J. Phys. Chem.* **1983**,*87*, 1264.

(17) Malsch, J.; Hartley, G.S., *Z. Phys. Chem.* **1934**,*A170*, 321.

(18) Dill, K.A.; Flory, P.J., *Proc. Natl. Acad. Sci. USA* **1981**,*78*, 676.

(19) Fromherz, P., *Chem. Phys. Lett.* **1981**,*77*, 460.

(20) Menger, F.M., *Acc. Chem. Res.* **1979**,*12*, 111.

(21) Wishima, A., *J. Phys. Chem.* **1963**,*67*, 2079.

(22) Watanabe, K.; Ferrario, M.; Klien, M.L., *J. Am. Chem. Soc.* **1988**,*92*, 819.

(23) Casal, H.L., *J. Am. Chem. Soc.* **1988**,*110*, 5203.

(24) Kalyanasundaram, K.; Thomas, J.K., *J. Am. Chem. Soc.* **1977**,*99*, 2039.

(25) Dong, D.; Winnik, M.A., *Photochem. Photobiol.* **1982**,*35*, 17.

(26) Franks, F. *Water. A Comprehensive Treatise*; Plenum: New York, 1975.

(27) Ingold, K.U. *Free Radicals*. Kochi ed. 1973 Wiley Interscience. New York.

(28) Turro, N.J. Benjamin-Cummings: Don Mills, 1978.

(29) Kerr, J.A. *Free Radicals*. Kochi ed. 1973 Wiley Interscience. New York.

(30) Sheldon, R.A.; Kochi, J.K., *J. Am. Chem. Soc.* **1970**,*92*, 4395.

(31) Griller, D.; Ingold, K.U., *Acc. Chem. Res.* **1976**,*9*, 13.

(32) Molin, Y. *Spin Polarization and Magnetic Effects in Radical Reactions*; Elsevier: New York, 1984.

(33) Noyes, R.M., *J. Am. Chem. Soc.* **1955**,*77*, 2042.

(34) Noyes, R.M., *J. Am. Chem. Soc.* **1956**,*78*, 5486.

(35) Koenig, T.; Fischer, H. *Free Radicals*. Kochi ed. 1973 Wiley Interscience. New York.

(36) Francks, J.; Rabinowich, E., *Trans. Farad. Soc.* **1934**,*30*, 120.

(37) Rabinowich, E.; Wood, W.C., *Trans. Farad. Soc.* **1936**,*32*, 1381.

(38) Lowery, T.H.; Richardson, K.S. *Mechanism and Theory in Organic Chemistry*; Harper and Row: New York, 1981.

(39) Turro, N.J., *Pure Appl. Chem.* **1981**,*53*, 259.

(40) Barltrop, J.A.; Coyle, J.D. *Excited States in Organic Chemistry*; Wiley: New York, 1975.

(41) Scaiano, J.C., *Acc. Chem. Res.* **1982**,*15*, 252.

(42) Wilson, R.M. *Organic Photochemistry*. Padwa ed. 1985 Marcel Dekker. New York.

(43) Johnston, L.J.; Scaiano, J.C., *Chem. Rev.* **1989**,*In Press*, .

(44) Ulrich, T.; Steiner, U.E.; Schlenker, W., *Tetrahedron* **1986**,*42*, 6131.

(45) Quinkert, G.; Opiyz, K.; Wiersdorff, W.W.; Weinlich, J., *Tetrahed. Lett.* **1963**,1863.

(46) Engle, P.S., *J. Am. Chem. Soc.* **1970**,*92*, 6074.

(47) Robbins, W.K.; Eastman, R.H., *J. Am. Chem. Soc.* **1970**,*92*, 6077.

(48) Turro, N.J.; Weed, G.C., *J. Am. Chem. Soc.* **1983**,*105*, 1861.

(49) Selwyn, J.C.; Scaiano, J.C., *Can. J. Chem.* **1981**,*59*, 663.

(50) Scaiano, J.C.; Selwyn, J.C., *Photochem. Photobiol.* **1981**,*34*, 29.

(51) Sakaguchi, Y.; Nagakura, S.; Hayashi, H., *Chem. Phys. Lett.* **1980**,*72*, 420.

(52) Sakaguchi, Y.; Nagakura, S.; Minoh, A.; Hayashi, H., *Chem. Phys. Lett.* **1981**,*82*, 213.

(53) Sakaguchi, Y.; Hayashi, H.; Nagakura, S., *J. Phys. Chem.* **1982**,*86*, 3177.

(54) Scaiano, J.C.; Abuin, E.B., *Chem. Phys. Lett.* **1981**,*81*, 209.

(55) Scaiano, J.C.; Abuin, E.A.; Stewart, L.C., *J. Am Chem. Soc.* **1982**,*104*, 5673.

(56) Turro, N.J.; Chow, M.F.; Chung, C.J.; Tanimoto, Y.; Weed, G.C., *J. Am. Chem. Soc.* **1981**,*103*, 4574.

(57) Tanimoto, Y.; Itoh, M., *Chem. Phys. Lett.* **1981**,*83*, 626.

(58) Tanimoto, Y.; Udagawa, H.; Itoh, M., *J. Phys. Chem.* **1983**,*87*, 724.

(59) Turro, N.J.; Mattay, J., *Tetrahed. Lett.* **1980**,*21*, 1799.

(60) Turro, N.J.; Mattay, J., *J. Am. Chem. Soc.* **1981**,*103*, 4200.

(61) Turro, N.J.; Tung, C.H., *Tetrahed. Lett.* **1980**,*21*, 4321.

(62) Baretz, B.H.; Turro, N.J., *J. Am. Chem. Soc.* **1983**,*105*, 1309.

(63) Turro, N.J.; Kraeutler, B., *J. Am. Chem. Soc.* **1978**,*100*, 7432.

(64) Turro, N.J.; Kraeutler, B.; Anderson, D.R., *J. Am. Chem. Soc.* **1979**,*101*, 7435.

(65) Scaiano, J.C., *J. Photochem.* **1973**,*2*, 81.

(66) Chilton, J.; Giering, L.; Steel, C., *J. Am. Chem. Soc.* **1976**,*98*, 1865.

(67) Hayahsi, H.; Sakaguchi, Y.; Nagakura, S., *Chem. Lett.* **1980**,1149.

(68) Lougnot, D.; Jacques, P.; Fouassier, J.P., *J. Photochem.* **1981**,*17*, 75.

(69) Scaiano, J.C.; Lougnot, D.J., *J. Phys. Chem.* **1984**,*88*, 3379.

(70) Turro, N.J., *Tetrahedron* **1982**,*38*, 809.

(71) Lehni, M.; Schuh, H.; Fischer, H., *Int. J. Chem. Kinet.* **1979**,*11*, 705.

(72) Lunazzi, L.; Ingold, K.U.; Scaiano, J.C., *J. Phys. Chem.* **1983***87*, 529.

(73) Turro, N.J.; Gould, I.R.; Baretz, B.H., *J. Phys. Chem.* **1983**,*87*, 531.

(74) Atkins, P.W.; Lambert, T.P., *Chem. Soc., Ann. Reports* **1975**,*A72*, 67.

(75) Buchachenko, A.L., *Russ. Rev. Chem.* **1976**,*45*, 761.

(76) Gould, I.R.; Turro, N.J.; Zimmt, M.B., *Adv. Phys. Org. Chem.* **1984**,*20*, 1.

(77) Carrington, A.; McLachlan, A.D. *Introduction to Magnetic Resonance*; Chapman and Hall: London, 1967.

(78) Karplus, M.; Porter, R.N. *Atoms and Molecules*; W.A. Benjamin: Don Mills Ontario, 1970.

(79) Weller, A.; Staerk, H.; Treichel, R., *Farad. Discuss. Chem. Soc.* **1984**,*78*, 271.

(80) Tanimoto, Y.; Itoh, M., *Bull. Chem. Soc. Jpn.* **1986**,*59*, 3039.

(81) Tanimoto, Y.; Itoh, M., *Stud. Org. Chem.* **1987**,*31*, 257.

(82) Sakaguchi, Y.; Hayashi, H., *Chem. Phys. Lett.* **1982**,*87*, 539.

(83) Hayashi, H.; Nagakura, S., *Bull. Chem. Soc. Jpn.* **1984**,*57*, 322.

(84) Nagakura, S.; Hayashi, H., *Int. J. Quantum Chem.: Quantum Chem. Symp.* **1984**,*18*, 571.

(85) Sakaguchi, Y.; Hayashi, H., *Chem. Phys. Lett.* **1984**,*106*, 420.

(86) Sakaguchi, Y.; Hatashi, H., *J. Phys. Chem.* **1984**,*88*, 1437.

(87) Hayashi, H.; Sakaguchi, Y.; Tsunooka, M.; Yanagi, H.; Tanaka, M., *Chem. Phys. Lett.* **1987**,*136*, 436.

(88) Hayashi, H.; Sakaguchi, Y.; Kamachi, M.; Schnabel, W., *J. Phys. Chem.* **1987**,*91*, 3936.

(89) Levin, P.P.; Khudyakov, I.V.; Kuz'min, V.A., *Dokl. Akad. Nauk SSSR* **1986**,*288*, 661.

(90) Levin, P.P.; Kuz'min, V.A., *Izv. Akad. Nauk SSSR, Ser. Khim.* **1987**,2611.

(91) Brocklehurst, B., *J. Chem. Soc. Farad. Trans II* **1976**,*72*, 1869.

(92) Luders, K.; Salikov, K.M., *Chem. Phys.* **1987**,*117*, 113.

(93) Atkins, P.W.; Kivelsen, D., *J. Chem. Phys.* **1966**,*44*, 169.

(94) Turro, N.J.; Zimmt, M.B.; Gould, I.R., *J. Phys. Chem.* **1988**,*92*, 433.

(95) Sagdeev, R.Z.; Molin, Y.N.; Salikhov, K.M.; Leshina, T.V.; Kamila, M.A.; Shein, S.M., *Org. Mag. Res.* **1973**,*5*, 559.

(96) Sagdeev, R.Z.; Molin, Y.N.; Salikov, K.M.; Leshina, T.V.; Kamila, M.A.; Shein, S.M., *Org. Mag. Res.* **1973**,*5*, 603.

(97) Baumann, D.; Ulrich, T.; Steiner, U.E., *Chem. Phys. Lett.* **1987**,*137*, 113.

(98) Turro, N.J.; Krautler, B., *Acc. Chem. Res.* **1980**,*13*, 369.

(99) Turro, N.J.; Mattay, J.; Lehr, G.F., *ACS Symp. Ser.* **1982**,*117*, 19.

(100) Turro, N.J., *Proc. Natl. Acad. Sci. USA* **1983**,*86*, 609.

(101) Nagakura, S.; Hayashi, H., *Radiat. Phys. Chem.* **1983**,*21*, 91.

(102) Hayashi, H., *Scientific Papers of the Institute of Physical and Chemical Research (Japan)* **1986**,*80*, 87.

(103) Ohmine, I.; Yamashita, K.; Morita, N.; Okamoto, H.; Onoda, M.; Oshio, H.; Nagashima, U.; Mitani, T.; Ishiguro, S.; Nakamura, M. *Institute for Molecular Science. Annual Review*; Institute for Molecular Science (Japan): Kyoto, 1987.

(104) Schulten, K., *Festkoerperprobleme* **1982**,*22*, 61.

(105) Schulten, K., *BGA Schriften* **1986**,*3*, 133.

(106) Steiner, U.E.; Ulrich, T., *Chem. Rev.* **1989**,*89*, 51.

(107) Steiner, U., *Z. Naturforsch.* **1979**,*34a*, 1093.

(108) Steiner, U., *Ber. Bunsenges. Phys. Chem.* **1981**,*85*, 228.

(109) Ulrich, T.; Steiner, U.E.; Foll, R.E., *J. Phys. Chem.* **1983**,*87*, 1873.

(110) Nolting, F.; Staerk, H.; Weller, A., *Chem. Phys. Lett.* **1982**,*88*, 523.

(111) Weller, A.; Nolting, F.; Staerk, H., *Chem. Phys. Lett.* **1983**,*96*, 24.

(112) Nath, D.N.; Chowdhury, M., *Chem. Phys. Lett.* **1984**,*109*, 13.

(113) Petrov, N.K.; Fedotova, E.Y.; Frankevich, E.L., *Khim. Vys. Energ.* **1980**,*14*, 345.

(114) Tanimoto, Y.; Nishino, M.; Itoh, M., *Bull. Chem. Soc. Jpn.* **1985**,*58*, 3365.

(115) Hata, N.; Hokawa, M., *Chem. Lett.* **1981**,507.

(116) Hata, N., *Bull. Chem. Soc. Jpn.* **1985**,*58*, 1088.

(117) Hata, N.; Nishida, N., *Bull. Chem. Soc. Jpn.* **1985**,*58*, 3423.

(118) Hata, N., *Bull. Chem. Soc. Jpn.* **1986**,*59*, 2723.

(119) Khudyakov, I.V.; Prokof'ev, A.I.; Margulis, L.A.; Kuz'min, V.A., *Chem. Phys. Lett.* **1984**,*104*, 409.

(120) Margulis, L.A.; Khudyakov, I.V.; Kuz'min, V.A., *Chem. Phys. Lett.* **1985**,*119*, 244.

(121) Margulis, L.A.; Khudyakov, I.V.; Kuz'min, V.A., *Chem. Phys. Lett.* **1986**,*124*, 483.

(122) Kuz'min, V.A.; Levin, P.P.; Khudyakov, I.V., *Izv. Akad. Nauk SSSR, Ser. Khim.* **1987**,998.

(123) Kuz'min, V.A.; Levin, P.P.; Khudyakov, I.V., *Izv. Akad. Nauk. SSSR, Ser. Khim.* **1987**,437.

(124) Levin, P.P.; Khudyakov, I.V.; Kuz'min, V.A., *Izv. Akad. Nauk SSSR, Ser. Khim.* **1988**,520.

(125) Doubleday, C., Jr.; Turro, N.J.; Wang, J., *Acc. Chem. Res.* **1989**, *22*, 199.

(126) Boxer, S.; Chidsey, C.E.D.; Roelofs, M.G., *J. Am. Chem. Soc.* **1982**,*104*, 1452.

(127) Chidsey, C.E.D.; Kirmaier, C.; Holten, D.; Boxer, S.G., *Biochim. Biophys. Acta* **1984**,*766*, 424.

(128) Chidsey, C.E.D.; Takiff, L.; Goldstein, R.A.; Boxer, S.G., *Proc. Natl. Acad. Sci. USA* **1985**,*82*, 6850.

(129) Savdimaliev, R.M.; Voznyak, V.M., *Studia Biophys.* **1986**,*115*, 69.

(130) Goldstein, R.A.; Takiff, L.; Boxer, S.G., *Biochim. Biophys. Acta* **1988**,*934*, 253.

(131) Usui, S.; Nakamura, H.; Ogata, T.; Uehata, A.; Motonaga, A.; Matsuo, T., *Chem. Lett.* **1987**,1779.

(132) Morita, H.; Higasayama, I.; Yamaoka, T., *Chem. Lett.* **1986**,963.

(133) Morita, H., *Phys. Org Chem.* **1987**,*31*, 273.

(134) Hummel, K.; Schaller, R.; Mertl, M.G., *Polym. Bull. (Berlin)* **1987**,*17*, 369.

(135) Schaller, R.; Martl, M.G.; Hummel, K., *Eur. Polym. J.* **1987**,*23*, 259.

(136) Wintgens, V.; Scaiano, J.C., *Can. J. Chem.* **1987**,*65*, 2131.

(137) Turro, N.J., *Tetrahedron* **1987**,*43*, 1589.

(138) Turro, N.J., *Ind. Eng. Chem. Prod. Res. Dev.* **1983**,*22*, 272.

(139) Turro, N., J,, *Polymer Preprints* **1986**,*27*, 318.

(140) Turro, N.J.; Arora, K.S., *Macromolecules* **1986**,*19*, 42.

(141) Sakaguchi, Y.; Hayashi, H.; Murai, H.; I'Haya, J., *Chem. Phys. Lett.* **1984**,*110*, 275.

(142) Ulrich, T.; Steiner, U.E., *Chem. Phys. Lett.* **1984**,*112*, 365.

(143) Turro, N.J.; Zimmt, M.B.; Lei, X.G.; Gould, I.R.; Nitsche, K.S.; Cha, Y., *J. Phys. Chem.* **1987**,*91*, 4544.

(144) Herve, P.; Nome, F.; Fendler, J.H., *J. Am. Chem. Soc.* **1984**,*106*, 8291.

(145) Fendler, J.H., *CHEMTECH.* **1985**,686.

(146) Tanimoto, Y.; Takashima, M.; Itoh, M., *J. Phys. Chem.* **1984**,*88*, 6053.

(147) Tanimoto, Y.; Takashima, M.; Itoh, M., *Nippon Kagaku Kaishi* **1984**,1741.

(148) Levin, P.P.; Kuz'min, V.A., *Izv. Akad. Nauk SSSR, Ser. Khim.* **1986**,464.

(149) Levin, P.P.; Kuzman, V.A., *Izv. Akad. Nauk SSSR, Ser. Khim.* **1986**,*4*, 762.

(150) Kuz'min, V.A.; Levin, P.P., *Izv. Akad. Nauk SSSR, Ser. Khim.* **1986**,1421.

(151) Levin, P.P., *Izv. Akad. Nauk SSSR, Ser. Khim.* **1987**,1003.

(152) Levin, P.P.; Kuz'min, V.A., *Izv. Akad. Nauk SSSR, Ser. Khim.* **1988**,298.

(153) Turro, N.J.; Lei, X.; Goud, I.R.; Zimmt, M.B., *Chem. Phys. Lett.* **1985**,*120*, 397.

(154) Hayashi, H.; Sakaguchi, Y.; Mochida, K., *Chem. Lett.* **1984**,79.

(155) Turro, N.J.; Chung, C.J.; Jones, G., II, *J. Phys. Chem.* **1982**,*86*, 3677.

(156) Levin, P.P.; Kuz'min, V.A., *Dokl. Akad. Nauk SSSR* **1987**,*292*, 134.

(157) Tanimoto, Y.; Shimizu, K.; Udagawa, H., *Chem. Phys. Lett.* **1983**,*100*, 353.

(158) Tanimoto, Y.; Takayama, M.; Itoh, M.; Nakagaki, R.; Nagakura, S., *Chem. Phys. Lett.* **1986**,*129*, 414.

(159) Schlenker, W.; Ulrich, T.; Steiner, U.E., *Chem. Phys. Lett.* **1983**,*103*, 118.

(160) Grant, A.I.; McLaucchlan, K.A.; Nattrass, S.R., *Mol. Phys.* **1985**,*46*, 273.

(161) Hadel, L. *Handbook of Photochemistry*. Scaiano ed. 1989 CRC Press. Cleveland, Ohio.

(162) Scaiano, J.C., *J. Am. Chem. Soc.* **1980**,*102*, 7747.

(163) Scaiano, J.C.; Tanner, M.; Weir, D., *J. Am. Chem. Soc.* **1985**,*107*, 4396.

(164) Goldschmidt, C.R.; Ottolenghi, M.; Stein, G., *Isr. J. Chem.* **1970**,*8*, 2041.

(165) Rabek, J.F. *Experimental Methods in Photochemistry and Photophysics*; Wiley: Toronto, 1982.

(166) Burton, G.W.; Ingold, K.U., *J. Am. Chem. Soc.* **1981**,*103*, 6472.

(167) Burton, G.W.; Doba, T.; Grabe, E.; Hughes, L.; Lee, F.L.; Prasad, L.; Ingold, K.U., *J. Am. Chem. Soc.* **1985**,*107*, 7053.

(168) Phiologene, B.J.R.; Arnason, J.T.; Berg, C.W.; Duval, F.; Champange, D.; Taylor, R.G.; Leitch, L.C.; Morand, P., *J. Econ. Entomol.* **1985**,*78*, 121.

(169) Arnason, J.T.; Philogene, B.J.R.; Berg, C.; MacEachern, A.; Kaminski, J.; Leitch, L.C.; Morand, P.; Lam, J., *Phytochem.* **1986**,*25*, 1609.

(170) Scaiano, J.C.; MacEachern, A.; Arnason, J.T.; Morand, P.; Weir, D., *Photochem. Photobiol.* **1987**,*46*, 193.

(171) Staab, H.A., *Angew. Chem., Int. Ed. Eng.* **1962**,*1*, 351.

(172) Singer, L.A.; Kong, N.P., *J. Am. Chem. Soc.* **1966**,*88*, 5213.

(173) Encinas, M.V.; Lissi, E.A., *Chem. Phys. Lett.* **1982**,*91*, 55.

(174) Cameron, D.G.; Casal, H.L.; Mantsh, H.H., *J. Biochem. Biophys. Methods* **1979**,*1*, 21.

(175) Cameron, D.G.; Charette, G.M., *Appl. Spectrosc.* **1981**,*35*, 224.

(176) Cameron, D.G.; Kauppinen, J.K.; Moffatt, D.J.; Mantsh, H.H., *Appl. Spectrosc.* **1982**,*36*, 245.

(177) Griller, D.; Howard, J.A.; Marriott, P.; Scaiano, J.C., *J. Am. Chem. Soc.* **1980**,*103*, 619.

(178) Chatgilialoglu, C.; Ingold, K.U.; Scaiano, J.C., *J. Am. Chem. Soc.* **1981**,*103*, 7739.

(179) Ingold, K.U., *Spec. Publ. Chem. Soc.* **1971**,*24*, 285.

(180) Mahoney, L.R., *Angew. Chem., Int. Ed. Eng.* **1969**,*8*, 547.

(181) Scott, G., *Bull. Chem. Soc. Jpn.* **1988**,*61*, 165.

(182) Porter, N.A., *Acc. Chem. Res.* **1986**,*19*, 262.

(183) Burton, G.W.; Ingold, K.U., *Acc. Chem. Res.* **1986**,*19*, 194.

(184) Wefers, H.; Sies, H. *Oxy-Radicals in Molecular Biology and Pathology.* Liss ed. 1988 Acedemic Press. New York.

(185) Pascoe, G.A.; Reed, D.J., *Free Rad. Biol. Med.* **1989**,*6*, 209.

(186) McBrien, D.; Slater, T. *Free Radicals, Lipid Peroxidation and Cancer*; Acedemic Press: London, 1982.

(187) Dix, T.A.; Maenett, L.J., *Science* **1983**,*221*, 77.

(188) Harman, D. Free Radicals in Biology. Pryor ed. 1982 Acedemic Press. New York.

(189) Melhorn, R.J.; Cole, G., *Adv, Free Rad. Biol. Med.* **1985**,*1*, 165.

(190) Sohal, R.S.; Allen, R.G., *Adv. Free Rad. Biol. Med.* **1986**,*2*, 117.

(191) Burton, G.W.; Joyce, A.; Ingold, K.U., *Lancet* **1982**,*2*, 327.

(192) Burton, G.W.; Joyce, A.; Ingold, K.U., *Arch. Biochem. Biophys.* **1983**,*221*, 281.

(193) Burton, G.W.; Ingold, K.U., *J. Am. Chem. Soc.* **1981**,*103*, 6472.

(194) Packer, J.E.; Slater, T.F.; Wilson, R.L., *Nature* **1979**,*278*, 737.

(195) Burton, G.W.; Foster, D.O.; Perly, B.; Slater, T.F.; Smith, I.C.P.; Ingold, K.U., *Phil. Trans. R. Soc. London B* **1985**,*311*, 565.

(196) Craw, M.T.; Depew, M.C., *Rev. Chem. Intermed.* **1985**,*6*, 1985.

(197) Clough, R.L.; Yee, B.G.; Foote, C.S., *J. Am. Chem. Soc.* **1979**,*101*, 683.

(198) Sawyer, D.T.; Valentine, J.S., *Acc. Chem. Res.* **1981**,*14*, 393.

(199) Matsumoto, S.; M., M., *Tetrahed. Lett.* **1981**,*22*, 3649.

(200) Encinas, M.V.; Lissi, E.A.; Olea, A.F., *Photochem. Photobiol.* **1985**,*42*, 347.

(201) Das, P.K.; Encinas, M.V.; Scaiano, J.C., *J. Am. Chem. Soc.* **1981**,*103*, 4154.

(202) Land, E.J.; Porter, G.; Strachan, E., *Trans. Farad. Soc.* **1961**,*57*, 1885.

(203) Das, P.K.; Encinas, M.V.; Steenken, S.; Scaiano, J.C., *J. Am. Chem. Soc.* **1981**,*103*, 4162.

(204) Mukai, K.; Watanabe, Y.; Ishizu, K., *Bull. Chem. Soc. Jpn.* **1986**,*59*, 2899.

(205) Carmichael, I.; Hug, G.L., *J. Phys. Chem. Ref. Data* **1986**,*15*, 1.

(206) Castle, L.; Perkins, M.J., *J. Am. Chem. Soc.* **1986**,*108*, 6381.

(207) Simic, M.G.; Hunter, E.P.L. *Radioprotectors and Anticarcinogens.* Nygard and Simic ed. 1983 Acedemic Press. New York.

(208) Lutz, H.; Breheret, E.; Lindqvist, L., *J. Phys. Chem.* **1973**,*77*, 1758.

(209) Schuler, R.H.; Buzzard, G.K., *Int. J. Radiat. Phys. Chem.* **1976**,*8*, 563.

(210) Bell, J.A.; Linschitz, H., *J. Am. Chem. Soc.* **1963**,*85*, 528.

(211) Land, E.J., *Proc. Roy. Soc. London A* **1968**,*305*, 457.

(212) Bensasson, R.; Land, E.J., *Trans. Farad. Soc.* **1971**,*67*, 1904.

(213) Malliaris, A.; Lang, J.; Strum, J.; Zana, R., *J. Phys. Chem.* **1987**,*91*, 1475.

(214) Kandori, K.; McGreevy, R.J.; Schecter, R.S., *J. Phys. Chem.* **1989**,*93*, 1506.

(215) Wagner, P.J., *Acc. Chem. Res.* **1971**,*4*, 168.

(216) Wagner, P.J.; Kelso, P.A.; Zepp, R.A., *J. Am. Chem. Soc.* **1972**,*94*, 7480.

(217) Wagner, P.J.; Kemppainen, A.E., *J. Am. Chem. Soc.* **1972**,*94*, 7495.

(218) Grotewald, J.; Soria, D.; Previtali, C.M.; Scaiano, J.C., *J. Photochem.* **1972/1973**,*1*, 471.

(219) Small, R.D., Jr.; Scaiano, J.C., *J. Phys. Chem.* **1977**,*81*, 828.

(220) Small, R.D., Jr.; Scaiano, J.C., *Chem. Phys. Lett.* **1978**,*59*, 246.

(221) Bays, J.P.; Encinas, M.V.; Small, R.D., Jr., *J. Am. Chem. Soc.* **1980**,*102*, 727.

(222) Scaiano, J.C.; Selwyn, J.C., *Can. J. Chem.* **1981**,*59*, 2368.

(223) O'Connor, D.V.; Phillips, D. *Time-Correlated Single Photon Counting*; Acedemic Press: New York, 1984.

(224) Doba, T.; Burton, G.W.; Ingold, K.U., *J. Am. Chem. Soc.* **1983**,*105*, 6505.

(225) Doba, T.; Burton, G.W.; Ingold, K.U., *Biochem. Biophys. Acta*, **1985**, *835*, 298.

(226) Wayner, D.D.M.; Burton, G.W.; Ingold, K.U., *Biochim. Biophys. Acta* **1986**,*884*, 119.

(227) Wayner, D.D.M.; Burton, G.W.; Ingold, K.U.; Barclay, L.R.C., *Biochim. Biophys. Acta* **1987**,*924*, 408.

(228) Barclay, L.R.C.; Baskin, K.A.; Locke, S.J.; Schaefer, T.D., *Can. J. Chem* **1987**,*65*, 2529.

(229) Miller, D.; Klein, U.K.A.; Hauser, M., *Ber. Bunsenges. Phys. Chem.* **1980**,*84*, 1135.

(230) Croonen, Y.; Gelade, E.; van der Zegel, M.; van der Auweraer, M.; Vandendelessche, H.; DeSchryver, F.C., *J. Phys. Chem.* **1983**,*87*, 1426.

(231) DeSchryver, F.C. Proceedings of the 2nd Latin American Meeting on Photochemistry and Photobiology. **1988**, 9.

(232) Evans, D.F.; Evans, J.B.; Sen, R.; Warr, G.G., *J. Phys. Chem.* **1988**,*92*, 784.

(233) Mazer, N.A.; Carey, M.C.; Benedek, G.B. *Micellization, Solubilization and Microemulsions*. Mittel ed. 1977 Plenum. New York.

(234) Briggs, J.; Nicoli, D.F.; Ciccolello, R., *Chem. Phys. Lett.* **1980**,*73*, 149.

(235) Hayashi, S.; Ikeda, S., *J. Phys. Chem.* **1980**,*84*, 744.

(236) Turro, N.J.; Engel, R., *J. Am. Chem. Soc.* **1969**,*91*, 7113.

(237) Turro, N.J.; Engel, R., *Mol. Photochem.* **1969**,*1*, 143.

(238) Turro, N.J.; Lee, T.J., *Mol. Photochem.* **1970**,*2*, 185.

(239) Grieser, F., *Chem. Phys. Lett.* **1981**,*83*, 59.

(240) Paul, H.; Small, R.D., Jr.; Scaiano, J.C., *J. Am. Chem. Soc.* **1978**,*100*, 4520.

(241) Simic, M.G., *Mut. Res.* **1988**,*202*, 377.

(242) Malliaris, A.; Lang, J.; Zana, R., *J. Phys. Chem.* **1986**,*90*, 655.

(243) Lang, J.; Zana, R., *J. Phys. Chem.* **1986**,*90*, 5258.

(244) Lang, J.; Zana, R.; Candau, S., *Ann. di Chim.* **1987**,*77*, 103.

(245) Kahlweit, M., *Pure Appl. Chem.* **1981**,*53*, 2060.

(246) Kahlweit, M., *J. Colloid Interface Sci.* **1982**,*90*, 92.

(247) Lessner, E.; Teubner, M.; Kahlweit, M., *J. Phys. Chem.* **1981**,*85*, 3167.

(248) Kahlweit, M. *Physics of Amphiphiles, Micelles, Vesicles and Microemulsions.* Degiorgio and Corti ed. 1985 North-Holland. Amsterdam.

(249) Corti, M.; Degiorgio, V., *J. Phys. Chem.* **1981**,*85*, 711.

(250) Dederen, J.C.; van der Auweraer, M.; DeSchryver, F.C., *Chem. Phys. Lett.* **1979**,*68*, 451.

(251) Yekta, A.; Aikawa, M.; Turro, N.J., *Chem. Phys. Lett.* **1979**,*63*, 543.

(252) Dederen, J.C.; van der Auweraer, M.; DeSchryver, F.C., *J. Chem. Phys.* **1981**,*85*, 1198.

(253) Malliaris, A.; Lang, J.; Zana, R., *J. Chem. Soc. Farad. I* **1986**,*82*, 109.

(254) Atik, S.; Thomas, J.K., *Chem. Phys. Lett.* **1981**,*79*, 351.

(255) Atik, S.; Thomas, J.K., *J. Am. Chem. Soc.* **1981**,*103*, 3543.

(256) Zana, R.; Weill, C., *J. Phys., Lett.* **1985**,*46*, l-935.

(257) Eriksson, J.C., *Acta Chim. Scand.* **1966**,*20*, 209.

(258) Jacobs, J.J.; Anderson, R.A.; Watson, T.R., *J. Pharm. Pharmacol.* **1971**,*23*, 148.

(259) Perly, B.; Smith, I.C.P.; Hughes, L.; Birton, G.W.; Ingold, K.U., *Biochim. Biophys. Acta* **1985**,*819*, 131.

(260) Turro, N.J.; Liu, K.C.; Chow, M.F.C., *Photochem. Photobiol.* **1977**,*26*, 413.

(261) Jay, J.; Johnston, L.J.; Scaiano, J.C., *Chem. Phys. Lett.* **1988**,*148*, 517.

(262) Moore, W.J. *Physical Chemistry*; Prentice-Hall: Englewood Cliffs, New Jersey, 1972.

(263) Birks, J.B.; Lumb, M.D.; Munro, I.H., *Proc. Roy. Soc. London A* **1964**,*280*, 289.

(264) Mukai, K.; Tsuzuki, N.; Ishizu, K.; Ouchi, S.; Fukuawa, K., *Chem. Phys. Lipids* **1981**,*29*, 129.

(265) Tsuchiya, J.; Niki, E.; Kamiya, Y., *Bull. Chem. Soc. Jpn.* **1983**,*56*, 229.

(266) Wilson, R., *Can. J. Chem.* **1966**,*44*, 551.

(267) Wilson, R., *J. Chem. Soc. B* **1968**,1581.

(268) Paul, H.; Fischer, H., *Helv. Chim. Acta* **1973**,*56*, 1575.

(269) Wilson, R., *J. Chem. Soc. B* **1968**,84.

(270) Kuz'min, V.A.; Levin, P.P.; Khudyakov, I.V., *Izv. Akad. Nauk SSSR, Ser. Khim.* **1986**,479.

(271) Werner, H.J.; Schulten, Z.; Schulten, K., *J. Chem. Phys.* **1977**,*67*, 646.

(272) Haberkorn, R., *Chem. Phys.* **1977**,*24*, 111.

(273) Schulten, K.; Wolynes, P., *J. Chem. Phys.* **1978**,*68*, 3292.

(274) Roelants, E.; Gelade, E.; van de Auweraer, M.; Croonen, Y.; DeSchryver, F.C., *J. Colloid Interface Sci.* **1983**,*96*, 288.

(275) Roelants, E.; E., G.; Smid, J.; DeSchryver, F.C., *J. Colloid Interface Sci.* **1985**,*107*, 337.

(276) Malliaris, A.; Binana-Limbele, W.; Zana, R., *J. Colloid Interface Sci.* **1986**,*110*, 114.

(277) Mazer, N.A.; Benedek, G.B.; Carey, M.C., *J. Phys. Chem.* **1976**,*80*, 1075.

(278) Young, C.Y.; Missel, P.J.; Mazer, N.A.; Benedek, G.B.; Carey, M.C., *J. Phys. Chem.* **1978**,*82*, 1375.

(279) Missel, P.J.; Mazer, N.A.; Benedek, G.B.; Young, C.; Carey, M.C., *J. Phys. Chem.* **1980**,*84*, 1044.

(280) Labes, M.M.; Ramesh, V., *J. Am. Chem. Soc.* **1986**,*108*, 4643.

(281) Wolff, T., *J. Photochem.* **1982**,*18*, 269.

(282) Closs, G.L.; Miller, R.J., *J. Am. Chem. Soc.* **1981**,*103*, 3586.

(283) Caldwell, R.A.; Sakaguri, H.; Majima, T., *J. Am. Chem. Soc.* **1984**,*106*, 2471.

(284) Zimmt, M.B.; Doubleday, C., Jr.; Gould, I.R.; Turro, N.J., *J. Am. Chem. Soc.* **1985**,*197*, 6724.

(285) Zimmt, M.B.; Doubleday, C., Jr.; Turro, N.J., *J. Am. Chem. Soc.* **1986**,*108*, 3618.

(286) Caldwell, R.A., *Monograph* **1989**,*In Press*, .

(287) Zimmt, M.B.; Doubleday, C., Jr.; Turro, N.J., *J. Am. Chem. Soc.* **1985**,*107*, .

(288) Gosele, U.; Klein, U.K.A.; Hauser, M., *Chem. Phys. Lett.* **1979**,*68*, 291.

(289) Gosele, U., *Chem. Phys. Lett.* **1980**,*69*, 332.

(290) Tachiya, M., *Chem. Phys. Lett.* **1980**,*69*, 605.

(291) Hatlee, M.D.; Kozak, J.J.; Rothenberger, G.; Infelta, P.P.; Gratzel, M., *J. Phys. Chem.* **1980**,.

(292) Sano, H.; Tachiya, M., *J. Chem. Phys.* **1981**,*75*, 2870.

(293) Emert, J.; Behrens, C.; Goldenberg, M., *J. Am. Chem. Soc.* **1979**,*101*, 771.

(294) Van der Auweraer, M.; Dederen, J.C.; Gelade, E.; DeSchryver, F.C., *J. Chem. Phys.* **1981**,*74*, 1140.

(295) Van der Auweraer, M.; DeSchryver, F.C., *Chem. Phys.* **1987**,*111*, 105.

(296) Wagner, P.J., *Acc. Chem. Res.* **1989**,*22*, 83.

(297) Closs, G.L.; Forbes, M.D.E.; Norris, J.R., Jr., *J. Phys. Chem.* **1987**,*91*, 3592.

(298) Miyagishi, S.; Asakawa, T.; Nishida, M., *J. Colloid Interface Sci.* **1987**,*115*, 199.

(299) Miyagishi, S.; Matsumura, S.; Asakawa, T.; Nishida, M., *J. Colloid Interface Sci.* **1988**,*125*, 237.

(300) Bohlmann, F.; Burkhardt, T.; Zdero, C. *Naturally Occuring Acetylenes*; Acedemic Press: New York, 1973.

(301) Wat, C.K.; Prasad, S.K.; Graham, E.A.; Partington, S.; Arnason, T.; Towers, G.H.N.; Lam, J., *Biochem. Syst. Ecol.* **1981**,*9*, 59.

(302) Arnason, T.; Swain, T.; Wat, C.K.; Graham, E.A.; Partington, S.; Towers, G.H.N.; Lam, J., *Biochem. Syst. Ecol.* **1981**,*9*, 63.

(303) McLachlan, D.; Arnason, J.T.; Philogene, B.J.R.; Champangr, D., *Experimentia* **1982**,*38*, 1061.

(304) Bakker, J.; Gommers, F.J.; Nieuwenhuis, I.; Wynberg, H., *J. Biol. Chem.* **1979**,*253*, 1841.

(305) Gommers, F.J.; Bakker, J.; Wynberg, H., *Photochem. Photobiol.* **1982**,*35*, 615.

(306) Garcia, F.J.; Yamamoto, E.; Abramowski, Z.; Downum, K.; Towers, G.H.N., *Photochem. Photobiol.* **1984**,*39*, 521.

(307) Reyftmann, J.P.; Kagan, J.; Santus, R.; Morliere, P., *Phtotchem. Photobiol.* **1985**,*41*, 1.

(308) Foote, C.S., *ACS Symp. Ser.* **1987**,*339*, 36.

(309) Evans, C.; Weir, D.; Scaiano, J.C.; MacEachern, A.; Arnason, J.T.; Morand, P.; Hollebone, B.R.; Leitch, L.; Philogene, B.J.R., *Photochem. Photobiol.* **1986**,*44*, 441.

(310) Arnason, J.T.; Philogene, B.J.R.; Morand, P.; Scaiano, J.C.; Werstiuk, N., *ACS Symp. Ser.* **1987**,*339*, 255.

(311) Abu-Eittah, R.; Al-Sugeir, F., *Can. J. Chem.* **1979**,*57*, 2337.

(312) Yamamoto, T.; Sanechika, K.; Yamamoto, A., *J. Polym. Sci., Polym. Lett.* **1980**,*ED-18*, 9.

(313) Kossmehl, G.; Chatzitheoudorou, G., *Makromol. Chem. Rapid Commun.* **1981**,*2*, 551.

(314) Tourillon, G.; Garnier, F., *J. Electroanal. Chem.* **1982**,*135*, 173.

(315) Tourillon, G.; Garnier, F., *J. Electroanal. Chem.* **1984**,*161*, 51.

(316) Funt, B.L.; Lowen, S.V., *Synth. Metals* **1985**,*11*, 129.

(317) Shlotani, M.; Nagata, Y.; Tasaki, M.; Shoma, J.; Shida, T., *J. Phys. Chem.* **1983**,*87*, 1170.

(318) Ramakrishna Rao, D.N.; Symons, M.C.R., *J. Chem. Soc. Perkin II* **1983**,135.

(319) Davies, A.G.; Julia, L.; Yazdi, S.N., *Chem. Commun.* **1987**,929.

(320) MacEachern, A. M.Sc. Thesis, University of Ottawa, 1987.

(321) Kagan, J.; Bazin, M.; Santus, R., *J. Photochem. Photobiol. B: Biology* **1989**,*3*, 165.

(322) Webster, O.W.; Mahler, W.; Benson, R.E., *J. Am. Chem. Soc.* **1962**,*83*, 2501.

(323) Hilinski, E.F.; Masroui, J.M.; Kochi, J.K.; Rentzepis, P.M., *J. Am. Chem. Soc.* **1984**,*106*, 8071.

(324) Patterson, L.K.; Small, R.D., Jr.; Scaiano, J.C., *Radiat. Res.* **1977**,*72*, 218.

(325) Lee, P.C.C.; Rodgers, M.A.J., *Photochem. Photobiol.* **1987**,*45*, 79.

(326) Gandin, E.; Lion, Y.; van de Vorst, A., *Photochem. Photobiol.* **1983**,*37*, 271.

(327) Schmehl, R.H.; Whitten, D.G., *J. Am. Chem. Soc.* **1980**,*102*, 1938.

(328) Bonhila, J.B.S.; Forman, T.K.; Whitten, D.G., *J. Am Chem. Soc.* **1982**,*104*, 4215.

(329) Bertolotti, S.G.; Cosa, J.J.; Gsponer, H.E.; Hamity, M.; Previtali, C.M., *Can. J. Chem.* **1986**,*64*, 845.

(330) Arnason, T.; Chan, G.F.Q.; Wat, C.K.; Downum, K.; Towers, G.H.N., *Photochem. Photobiol.* **1981**,*33*, 821.

(331) Zimmt, M.; Doubleday, C., Jr.; Turro, N.J., *Chem. Phys. Lett.* **1987**,*134*, 549.

(332) Johnson, C.S., Jr.; Gutowsky, H.S., *J. Chem. Phys.* **1963**,*39*, 58.

(333) Waltman, R.J.; Bargon, J., *Can. J. Chem.* **1986**,*64*, 76.

(334) Simmers, S.B.; Hobbs, S.S.; Downs, D.J.; Hutt, T.J.; Degraff, B.A., *J. Photochem. Photobiol. A: Chemistry* **1988**,*41*, 347.